

The vertical structure of thickened bars in disk galaxies



Dissertation

zur
Erlangung des Grades
„Doktor der Naturwissenschaften“
der Fakultät für Physik und Astronomie
an der Ruhr-Universität Bochum

von
Giuseppe Agostino Aronica
aus
Altena (Westf.)

Bochum 2006

1. Gutachter: Prof. Dr. Ralf-Jürgen Dettmar
2. Gutachter: Priv. Doz. Dr. Susanne Hüttemeister

Datum der Disputation: 05.04.2006

To my parents

Contents

1	Introduction	11
1.1	Classification of galaxies	11
1.2	Bars in galactic disks	13
1.2.1	Galactic bars in observational astronomy	13
1.2.2	Theory and simulations of galactic bars	14
1.3	Bulges in disk galaxies	16
1.4	Boxy or peanut shaped structures in disk galaxies	18
1.5	Aim and outline of the thesis	21
2	Data	25
2.1	The galaxy sample	25
2.2	Observations	28
2.3	Wavelength ranges	30
2.4	Data Reduction	30
2.5	Calibration	31
2.6	Seeing and masking	31
2.7	Sources of errors in the data reduction	32
3	Morphological Analysis	35
3.1	Unsharp masking	36
3.1.1	Spatial filtering	36
3.1.2	Application to the galaxy sample	37
3.2	Radial surface brightness profiles	39
3.3	Results	41
3.3.1	Morphological structure	41
3.3.2	Orbital structure of bars and related morphological features	44
3.3.3	Structures in the surface brightness distribution	45
3.3.4	Photometry of barred galaxy simulations	48
3.3.5	Lenses and inner rings	49
3.4	Central regions of the galaxies	50
3.4.1	Central bulge region	51
3.4.2	Mechanisms shaping the inner central regions	55
3.4.3	Central nucleus	57
3.5	Conclusions	58
4	Vertical Structure	61
4.1	Fitting Functions	63

4.2	Fitting Technique and Parameters	66
4.2.1	Analysis methods of other studies	69
4.3	Results	73
4.3.1	The vertical surface brightness distribution (VSFBD)	74
4.3.2	Scaleheight	74
4.3.3	Shape of the VSFBD	76
4.3.4	Fitting the inner central region	79
4.3.5	Quantitative description of the VSFBD	82
4.3.6	The shape parameter in the Gauss–Hermite (GaHe) approach	86
4.3.7	Comparison with simulations of disk galaxies	86
4.3.8	Galactic components and the VSFBD	87
4.4	Conclusions	90
5	Summary and outlook	93
5.1	The bar–buckling scenario	93
5.2	The vertical structure of barred galaxies	94
5.3	The central regions of disk galaxies	96
5.4	Secular evolution in barred disk galaxies	97
5.5	Outlook	98
A	Alternative methods	101
A.1	Vertical analysis in simulated disks	101
A.2	Variance and Kurtosis	102
A.2.1	Varying the exponent of the variance and kurtosis	104
A.3	Perturbed distributions	104
B	Conversion of the Sérsic Law to Generalized Gaussians	111
C	Photometry of the sample galaxies	115
D	Results of the VSFBD fitting	131
	Abbreviations	163
	Bibliography	167
	Acknowledgments	175

List of Figures

1.1	The Hickson Compact Group 87 with a galaxy member showing a pronounced B/PS structure	20
3.1	Unsharp masking and folding	38
3.2	Minor axis extrema	44
3.3	Central regions of galaxies	56
4.1	Fitting results without masking along the major axis	80
	(a) Fitting results of the Generalized Gaussian (GGau) approach	80
	(b) Fitting results of the GGau approach	80
4.2	Fitting results with masking of 3'' along the major axis	81
	(a) Masking the innermost 3'' (GGau)	81
	(b) Masking the innermost 3'' (GaHe)	81
4.3	Fitting results with masking of 5'' along the major axis	84
	(a) Masking the innermost 5'' (GGau)	84
	(b) Masking the innermost 5'' (GaHe)	84
A.1	Vertical cut through a simulated, symmetrized disk	102
A.2	Kurtosis defined with varying exponents as a function of distributions	105
A.3	Perturbations present in the center of tested distributions	106
	(a) Unperturbed distribution	106
	(b) Distribution with a strong central perturbation	106
	(c) Distribution with a small central perturbation	106
A.4	Variance calculated in the case of perturbations in the center of distributions	107
	(a) Variance in the case of the maximal central perturbation	107
	(b) Variance in the case of a weaker central perturbation	107
A.5	Kurtosis calculated in the case of perturbations in the center of distributions	107
	(a) Kurtosis in the case of the maximal central perturbation	107
	(b) Kurtosis in the case of a weaker central perturbation	107
A.6	Perturbations of the original distributions due to the redistribution of particles from the center to the outer parts	108
	(a) Original distribution for $\lambda = 0.8$	108
	(b) Distribution with noise for $\lambda = 0.8$	108
	(c) Original distribution for $\lambda = 5.0$	108
	(d) Distribution with noise for $\lambda = 5.0$	108
A.7	Stability of the variance calculation under the influence of noise in the underlying distribution.	109
	(a) Analysis of the stability of variance calculation	109

	(b) Enlarged view of a part of (a)	109
A.8	Analysis of the stability of kurtosis calculation under the influence of noise in the underlying distribution.	109
	(a) Analysis of the stability of kurtosis calculation	109
	(b) Enlarged view of a part of (a)	109

List of Tables

2.1	Galaxy parameters	26
2.2	Bulge classifications	28
3.1	Mask size used for the unsharp masking of the NIR images	39
3.2	Morphological features observed in the unsharp masked images of the galaxy sample	42
3.3	Inner bulge region extension and comparison with the disk extension	53
4.1	The $\text{sech}(z)$ -distribution and isothermal-distribution in the region of the boxy or peanut shaped (B/PS) structure	78
4.2	The shape of the VSFBD in the inner central regions	83

Chapter 1

Introduction

Since the work of Hubble in 1926 on the nature of the objects formerly called nebulae, the picture about galaxies has been enriched dramatically. In the field of galaxy structure and galaxy dynamics a rough scheme has been established and the major part of studies dealing with galaxies are based on that picture. Especially astronomers working on the field of photometrical studies of galactic objects have developed a classification scheme based mainly on morphological arguments.

1.1 Classification of galaxies

A starting point of all classifications of galaxy morphology is the 'tuning fork scheme' proposed by Hubble in 1936. Its major criteria for the subdivision in three main classes of the scheme are: i) the value of the bulge-to-disk luminosity ratio (B/D) ii) the tightness of the spiral arm structure (if present) iii) the ratio of cold unprocessed interstellar material (simply called gas) to the luminous mass. That results in the categories of *ellipticals* (E), *lenticulars* (S0), and *spirals* (S). The spiral pattern is embedded in a stellar disk component so that the term spiral galaxy and disk galaxy are used as synonyms. Concerning the S0s and the spirals also a clear geometry can be observed. In those galaxies the disk component forms a symmetry plane with an additional symmetry axis perpendicular to the plane and traversing it in the center of the luminous disk component. Often the symmetry axis is called simply the 'z' axis of the system. Therefore, in disk galaxies, a distinction of the appearance of the object can be made based on the angle i between the line-of-sight (LOS) and the central plane of the galaxy. That angle i is called the inclination angle. Objects seen with an inclination angle of 0° , i.e., with the LOS along the z axis, are called 'face-on' systems, whereas objects seen at an inclination of $i = 90^\circ$ pointing to the edge of the stellar disk, are called 'edge-on' systems. The arrangement of the distinct categories was intended to be based on an evolutionary sequence with the ellipticals at the beginning and the spirals at the end of the sequence. Clearly, each class has also subclasses which lead to the denotation of the ellipticals with an additional number from 1 to 7 and in the case of the spirals with a letter from 'a' to 'd'. Lenticular galaxies are at an intermediate position between the elliptical and the spiral galaxies. Due to historical reasons based on first theoretical models (see below) the different spiral types are labeled 'early-type' and 'late-type' objects with the former type including S0 and the latter ones ranging until the Sd class. The spiral structure is observed preferentially in galaxies with a large stellar and gaseous disk because of the distinct physical environment

present in ellipticals and disk galaxies. In the case of the spirals a subdivision based on the presence or the absence of a bar component (denoted by the additional letter B following that one classifying the object as an spiral S) is adopted.

During the last decades new categories were added to the previously described ones and a general revision of the scheme has been done resulting in a parallel classification scheme. The new objects added consist in the largest ellipticals (cd) found typically in the center of clusters of galaxies. Further, along with the observations of irregular stellar systems still bearing the characteristics of a flat disk galaxy object, the new class Irr was added. With the improvement of the observational techniques also galaxies with a total brightness fainter than the galaxies known until that time were observed. Those galaxies have been grouped in the so called *dwarf* galaxy class comprising also elliptical objects and objects showing a spiral structure. In recent years finally spiral galaxies with a surface brightness (SFB) lower than that one of the disk galaxies known so far were discovered and labeled low surface brightness (LSB) galaxies.

The extended approach proposed in de Vaucouleurs (1959) still based on Hubble's scheme introduced a 3-dimensional structured view taking into account also the arm shape as the third dimension classification axis. Additionally a distinction between objects with no bar (SA), a weak bar (SAB), and a strong bar (SB) was made. In a further evolution of that scheme (de Vaucouleurs, de Vaucouleurs, & Corwin 1976) a quantitative parameter (T) spanning the entire classification from elliptical to irregular galaxies was introduced. The values range from -5 for the 'earliest' elliptical to 10 representing irregular late-type spirals.

One of the most important aims in extragalactic astronomy during the last decades was to give a physical fundament to the classification schemes which were in use. Clearly, that approach is founded on the assumption that the classification schemes stemming from a morphological approach do indeed reflect results of related physical processes. At the beginning it was thought that ellipticals would transform with time into disk galaxies with spirals. The mechanism underlying to this transformation was searched in the consumption of the cold gas through the formation of stars. As later studies showed the situation was the opposite as thought, in fact being the ellipticals the galaxies with less cold gas content than the late-type spirals. The investigations on that subject split into the area of research concerning ellipticals on one side and spirals on the other with the lenticulars as a link between both (see also below). On the path to find the physical bases also alternative classifications for disk galaxies were developed like for example the scheme proposed by van den Bergh (1960a,b,c) relating the morphology of the spiral arms to the luminosity of their parent galaxies. Finally, Morgan (1958, 1959, 1962) proposed a classification scheme based exclusively on the central concentration of light without taking into account the morphology of spiral arms (in contrast to the Hubble scheme).

The difficulties in achieving the aim of a physical consistent picture explaining the Hubble classification can be evidenced on the example of the lenticular galaxies. When that class was introduced by Hubble it was meant as an auxiliary link between elliptical objects and disk galaxies rather than a self-contained part. In fact already Matthews, Morgan, & Schmidt (1964) pointed out some inconsistencies with the classification of lenticulars as an own class. Further, in van den Bergh (1990) the author pointed to the fact, that the class of lenticulars comprises a number of objects with physically distinct type but exhibiting *superficial* morphological similarities. An argument reported by van den Bergh against the view of S0s as link between ellipticals and spiral disk galaxies of type Sa is the fact, that S0s are in the mean fainter than the neighboring Hubble-class objects. Similar problems arise when the

evolution proposed for the spiral galaxies from one end to the classification to the other end is investigated. At the present state it is thought that an evolution is possible from late-type objects to objects of earlier type, more precisely from the **Scd** to the **Sb** class. The mechanisms accomplishing this transformation require a bar component and an activity of the process on time scales of several times the rotational period of the structure. Such kind of evolution, which extends over several crossing times or rotational periods (10 – 100) is called 'secular evolution' (Pfenniger 1984). Compared to that time ranges the dynamical timescale involves ≈ 1 rotational period, i.e., in the case of a disk it spans a disk rotation. The precise mechanisms can be understood if the properties of bars are analyzed in more detail.

1.2 Bars in galactic disks

1.2.1 Galactic bars in observational astronomy

Contrary to the spiral structure visible in face-on disk galaxies the also visible bar component has received in the beginning less attention. During the last decades it has been shown that a huge fraction of the disk galaxies harbor a bar. Eskridge et al. (2002) have analyzed a statistically well defined sample of 186 disk galaxies from the Ohio State University Bright Spiral Galaxy survey. The authors find, in accordance to previous studies (Knapen 1999), that about 70% of the galaxies have bars or ovals. In Seigar & James (1998) the authors suggest, based on the results of their study, that possibly almost all disk galaxies do have a barred component. In fact, Grosbøl, Patsis, & Pompei (2004) find in a smaller sample (54 galaxies) of spirals barred objects with a frequency of about 90%.

The studies mentioned above are based on observational data acquired in the near-infrared (NIR) wavelength regime. That has several advantages compared to the optical wavelength regime. First, the dust obscuration of dust lanes and patches is strongly reduced in the NIR and hence all light emission originating in the stellar component of the galaxy can be observed (Buta & Block 2001). Second and equally important is the fact that the NIR light is the most direct tracer of the stellar mass and therefore it is a direct tracer of the gravitational potential of the galaxy (e.g., Hunt, Pierini, & Giovanardi 2004). Thus, that wavelength regime enables to study the 'backbone' of the spiral galaxies which is the old stellar population present for several 10^9 years (Buta & Block 2001). It is clear that star formation regions with a high fraction of high mass stars with a short 'lifetime' compared to the stars constituting the old stellar population do emit large amounts of light in the NIR regime. This could lead to problems since they do not trace the potential of the galaxy in such an ideal manner as the old stellar population does. However, the work of Rhoads (1998) has shown that the emission originating from young red supergiants (typically found in star forming regions) does not exceed that one of the old stellar population. Indeed, it constitutes only one third of it. Also James & Seigar (1999) report a significant amount of NIR light emission from associations of stars (like O and B star (OB) associations). That work shows that additionally to the stellar emission also emission from hot dust (600 – 1000K) contributes to the overall NIR brightness. However, those sources are spatially sharply confined avoiding a misinterpretation as being part of the structure contributing largely to the galactic potential.

Geometrically, bars can be described as biaxial or triaxial structures and can be considered as ellipsoids with two or three distinct symmetry axes. The major axis (MJA), which is the longest axis, measures always less than the diameter of the host galaxy. When the bar is seen in an edge-on galaxy with the LOS perpendicular to the bar's MJA, the bar is called

to be seen side-on. Otherwise, if the bar's MJA is aligned with the LOS and only the planar minor axis (MNA) is visible, it is called end-on. Although the geometry seems to be simple structured there are still debates about the measuring of the length of a bar. The same is true for the estimation of the prominence of the bar (e.g., the measuring of the apparent ellipticity as function of radius, Abraham, Merrifield, Ellis, Tanvir, & Brinchmann 1999). In general, the shape and length of bars varies from early-type to late-type galaxies with the shape being more rectangular in the early-type objects (e.g., Athanassoula 1990). Late-type galaxies show a less smooth surface brightness distribution (SFBD) due to the greater dust obscuration compared to early-types. Dust lanes present at the leading edges of the bar play an important role in understanding the dynamics of that rectangular structure. Indeed, they are visible in many barred galaxies as an almost straight line parallel to the MJA of the bar. Those lanes are formed by interstellar gas streaming further inwards to smaller galactocentric radii. This is due to the shape of the orbits in the bar component and the fact that contrary to stars gas can undergo dissipation. In fact, at the end of the bars the gas undergoes shocks and loses part of its kinetic energy (Athanassoula 1992; Athanassoula & Bureau 1999). Contrary to the high number of investigations focusing on the shape in the $x - y$ -plane visible in face-on galaxies, little is known about the vertical structure of a bar. According to Wakamatsu & Hamabe (1984) it should be a rather thin structure compared to the disk component (see also Chap. 1.2.2).

As the pattern speed Ω_P is an important parameter describing bars (see Chap. 1.2.2) several studies tried to address this field observationally. However, the difficulties encountered in such approaches prevented a build up of a large database of such pattern speeds (e.g., Tremaine & Weinberg 1984). A further parameter introduced by theory of bar formation is the ratio denoted R of the Corotation Resonance (CR) radius (see Chap. 1.2.2) to the length of the bar semi-major axis (R_{bar}), $R = R_{CR}/R_{bar}$. Based on that quantity a distinction between fast bars ($R \leq 1.4$) and slow bars ($R \geq 1.4$) is made (Debattista & Sellwood 2000). One of the most recent studies (Rautiainen, Salo, & Laurikainen 2005) reports that a large variety of bar pattern speeds is detected with a clear correlation between bar pattern speed and Hubble-type. Indeed, early-type galaxies tend to have fast bars ($R \approx 1.1$) whereas late-type galaxies tend to have slower bar components ($R \approx 1.7$).

Apart from the aspect of morphology in galactic disks bars are invoked to shape the innermost regions in spiral galaxies. Therefore, bars are proposed to be partially a good driver of fueling an active galactic nucleus at the center of galaxies (Bournaud & Combes 2002). A further observation which is made in this context is the fact that at the center, in addition to the large scale bar, a secondary bar is present. It is much smaller in size compared to the primary one and embedded in the larger one (Erwin 2004). The secondary bars are also centered around the galactic center but do not need to be aligned with it and can be even perpendicular to it.

1.2.2 Theory and simulations of galactic bars

In galactic stellar disks the density of stars throughout the whole galaxy potential is rather low so that the relaxation time is very high compared to the dynamical time scale, exceeding the Hubble-time. Therefore, the distribution of stars can be approximated by the description of a collisionless fluid and hence obeying dynamical equations like the Vlasov equation. However, it had become clear that, solutions for realistic, non-axisymmetric potentials could not be obtained exclusively by an analytical approach. To overcome this problem, orbits in the

given potentials have to be calculated numerically or N -body numerical simulations are used. Considering in a first step a 2-dimensional disk potential and small deviations of the test particles' circular motion, epicyclic motions about a guiding center which orbits with the speed Ω_C around the galactic center are introduced (Lindblad epicycles). If now a weak sinusoidal perturbation with a pattern of Ω_P is added, it is possible to describe the bar as the $m = 2$ (with m as the wavenumber) component of the Fourier decomposition of that perturbation. The particular solution of the resulting equations does lead to three resonance conditions which can be written as:

$$\Omega_P = \Omega_C \qquad \text{Corotation Resonance (CR)} \qquad (1.1)$$

$$\Omega_P = \Omega_C + \kappa/2 \qquad \text{Outer Lindblad Resonance (OLR)} \qquad (1.2)$$

$$\Omega_P = \Omega_C - \kappa/2 \qquad \text{Inner Lindblad Resonance (ILR)} \qquad (1.3)$$

with κ as the epicycle frequency. From the usage of the Jacobi Integral it can be seen that the bar has a negative angular momentum content. As a consequence, the loss of angular momentum strengthens the bar component instead of weakening it.

Studies focusing orbital structures of model potentials were able to give a theoretical ground to the observation that bar components were mostly within the surrounding disk. The work of Contopoulos (1980) showed that bar components end before or just at the CR radius. Further orbital calculations have show that several main families of periodic orbits can be grouped together. The principal family sustaining the bar component are the so called x_1 orbits elongated parallel to the bar ending within CR. Additionally, the x_2 orbits are elongated perpendicular to the bar and located inside the ILR. However, this orbits are not present in all barred structures since an ILR has to be present (see the definition). Since x_2 orbits are perpendicular to the bar structure, they can contribute to weaken the bar component. If present, the ILR can have an important role in the formation of inner rings due to the fact that infalling gas can be shocked at the edges of the x_2 orbit structure. A further result of the orbital calculations is that the different periodic orbits families change at each resonance (e.g., ILR and CR)

First numerical N -body simulations of spiral galaxies aimed to understand what the predominant spiral modes are and how they evolve. During this simulations it emerged that the stellar disk is in most cases unstable and forms a large scale stellar bar (e.g., Miller & Prendergast 1968; Hohl 1971). Soon after it was clear how to facilitate or inhibit the evolution of a bar instability inside the disk. As principle processes the evolution of the radial and vertical velocity dispersion inside the disk and the influence of the halo in which the disk is immersed could be identified. After the first studies using 3-dimensional simulations, (Hohl & Zang 1979; Combes & Sanders 1981) only few other numerical investigations dedicated much effort to the vertical structure of simulated disk galaxies. Until that time mostly the 2-dimensional approach was investigated because it was thought that the largest part of the physical processes are present in two dimensions whereas the vertical dimension would add only effects of higher order. As an argument for that approach the thin nature of spiral disks (compared to the radial extension) was invoked. Combes, Debbasch, Friedli, & Pfenniger (1990), Pfenniger & Friedli (1991) as well as Raha, Sellwood, James, & Kahn (1991) did reconsider the analysis of 3-dimensional models but in recent times only Athanassoula & Misiriotis (2002) have again payed much attention to that subject.

In the last years two main topics in numerical disk studies have gained more interest.

First, the fact that the halo used in the simulations, if implemented as 'living', i.e., consisting of simulated particles and not as a rigid potential, plays a crucial role in redistributing angular momentum within the disk. Before that, it was common wisdom that a heavy halo does stabilize the galactic disks against bar instabilities. The same result was found for the presence of a large spheroidal bulge component in the center of a disk. The difference of using a rigid halo potential and a halo formed by particles able to react to the dynamics in the inner parts of the disk was first reported by Debattista & Sellwood (2000). Athanassoula (2002) and Athanassoula (2003) analyzed that process in more depth and showed analytically and numerically that the halo particles can indeed — depending on the parameter set describing the halo — receive angular momentum from the bar stabilizing therefore the bar component. Further, depending on the extent and the central concentration of the central spheroidal bulge component, it is, contrary to the previous believe, not a stabilizing element of the disk against bar growth but can receive as well angular momentum and thus strengthening the bar instability. The amount of angular momentum transfer is strongly dependent on the extent of resonant regions and their density. This fact facilitates the understanding of the observed high bar frequency (see above).

A second strongly debated field is the stability of bars against Central Mass Concentrations (CMCs) in the galaxy, like super-massive black holes and/or compact massive central disks. Orbital-structure studies dealing with that field (Hasan & Norman 1990; Hasan, Pfenniger, & Norman 1993) showed that an increasing CMC (mass or concentration) destabilized the bar component. Also the first numerical studies described in Norman, Sellwood, & Hasan (1996) led the authors to claim that a CMC with a mass of about 5% of the total galaxy mass is sufficient for bar dissolution. Recently Shen & Sellwood (2004) and Athanassoula, Lambert, & Dehnen (2005) have refined their galactic disk simulations and reanalyzed a probable bar dissolution scenario under the influence of a CMC growth. That numerical studies point to a scenario where a CMC does not destroy the present bar at least to a CMC mass of a few percent. However, Bournaud, Combes, & Jog (2004) argue that it is not the CMC itself which does or does not weaken the bar but the loss of angular momentum to the bar component of gas when falling into the center (and possibly forming the CMC). That fact is then used as an argument for the possibility of a bar renewal. If the CMC is not the original source of bar weakening it means that a presence of it after bar dissolution does not inhibit a new bar instability. The question of bar dissolution and bar renewal is still debated, though. While Bournaud & Combes (2002) as well as Bournaud et al. (2004), and Bournaud, Combes, & Semelin (2005) argue strongly for a bar dissolution mechanism (with a subsequent new bar instability), the simulations of isolated disks discussed in Athanassoula (2002), Athanassoula (2003), and Athanassoula (2005) do not show any signs of bar dissolution. Currently no unequivocal observational signature for bar dissolution and bar renewal has been reported.

1.3 Bulges in disk galaxies

Among the categories defining the Hubble sequence the extent and prominence of the central component, the bulge, is used to classify the galaxies. The description of the bulge component is based almost completely on morphological criteria apart the important exception describing its dynamical conditions based on velocity dispersions. Indeed, bulge and disk components in a spiral galaxy can be distinguished rather fast due to their distinct morphologies. In the literature there are mainly two descriptions of the central component which can be used

as working definitions for bulge components: i) the steep central component of the surface brightness profile (SFBP) which is generally steeper and brighter than the inward extrapolation of the outer exponential disk (e.g., Carollo, Ferguson, & Wyse 1999) ii) the kinematically hot component of the galaxy recognized by the central peak in the velocity profile. Due to its spheroidal morphology and first kinematical studies, bulges have largely been considered as being simply small scale low luminosity ellipticals. Furthermore, the stellar kinematics of elliptical galaxies and bulges of the same luminosity fit well in the prediction of the rotational velocity based on isotropic oblate models (Davies, Efsthathiou, Fall, Illingworth, & Schechter 1983). Therefore, studies focusing on the photometry of the galaxy bulges use the de Vaucouleur-law ($R^{1/4}$ -law), originating from photometrical studies of elliptical galaxies, to describe the SFBD. Indeed, in a large amount of investigations a good agreement could be achieved with this assumption (see Kodaira, Watanabe, & Okamura 1986 and specially for bulges of early-type galaxies Carollo, Stiavelli, de Zeeuw, Seigar, & Dejonghe 2001). Thus, the same formation scenario for ellipticals and bulges was suggested.

Eggen, Lynden-Bell, & Sandage (1962) proposed a rapid formation through a dissipative monolithical gravitational collapse of a protogalactic gas cloud. Alternatively, Searle & Zinn (1978) suggested a formation dominated by mergers of smaller structures. In that context the $R^{1/4}$ -law has been interpreted as being the form for a SFBD profile describing a structure which evolved out of a clumpy collapse scenario (van Albada 1982). Besides the same formation scenarios also the formation periods were claimed to be similar. In that picture bulge and disk components of spiral galaxies would form consecutively with the bulge forming first. That should then be detectable in the stellar populations of the two galactic components. Investigations on stellar spectra of the Milky Way bulge and other bulges (Whitford 1978) did corroborate on a first sight that picture. Furthermore, color studies of bulges (e.g., Bothun & Gregg 1990) gave results similar to those of elliptical galaxies (e.g., Impey, Wynn-Williams, & Becklin 1986). However, with the improvement of the observational methods and wide spread usage of Charge Coupled Devices (CCDs) in observational astronomy, the arguments of such a view became less stringent.

Extended color studies on bulges in early-type spirals done by Peletier & Balcells (1996) revealed that there is a rather noticeably large range of colors. Furthermore, those studies suggested a much lower age difference between the bulge stars and the old disk stars. Apart from color studies the increasing number of photometrically studied spiral galaxies evidenced more and more cases where the bulge SFBD does not follow the 'classical' $R^{1/4}$ -law. A more general law for the description of a galaxies' SFBD was proposed by Sersic (1968) allowing a broader range of values for the exponent $1/n$ of the radial dependence. For $n = 4$ the usual $R^{1/4}$ -law is retrieved whereas $n = 1$ represents an exponential SFBD. Andredakis, Peletier, & Balcells (1995) did show that a large part of the investigated galaxies were not best fitted by a $R^{1/4}$ -law but by distributions with values of n ranging from 1 to ≈ 6 (see also Caon, Capaccioli, & D'Onofrio 1993, for a previous study). In addition, a clear trend is visible for different Hubble-types. Early-type galaxies tend to have higher n values than late-type objects. Hence, structural differences can be detected between bulges of different Hubble-types.

Kinematical investigations of bulge regions had already given a significant amount of evidence for a more differentiated view of the central structures of galaxies. The reviews of Kormendy (1993) and Kormendy & Kennicutt (2004) illustrate the arguments for such an approach. Considering the ratio of the averaged velocity dispersion to the maximum rotational velocity $V_R/\bar{\sigma}$ (or equivalently $\bar{\sigma}/V_R$), several bulges of disk galaxies have values pointing to a considerable amount of ordered to random velocities. This is in strong contrast to ellipti-

cals which have much lower ordered motion contribution since they are pressure supported systems. Indeed, some galaxies with a peculiar bulge shape, i.e., showing a rather box shape instead of a spheroidal morphology, do exhibit ordered motion up to values of z at which the disk contribution can be neglected. In Kormendy & Illingworth (1982) the authors report for the disk galaxy *NGC 4565*, which has a box shaped bulge, constant rotation velocities up to heights of about $z \simeq 30''$ above the plane of the disk. The fact that such a situation of constant rotational velocity with increasing z was observed in all galaxies showing a box shape, points to a scenario where the two properties are tightly connected. For the previously described velocity distribution the term 'cylindric rotation' was introduced. Since the bulge structures exhibiting (ordered) rotational motion have more disk-like kinematics than a typical spheroidal bulge signature dominated by random motions, Kormendy introduced the term 'pseudobulge' to indicate that difference. Hence, it is consequently more appropriate to label the central regions displaying a box shape 'box shaped structures', but not 'box shaped bulges'. This is likewise for other shapes of the central regions of disk galaxies deviating from the spheroidal morphology of 'classical bulges' (see Chapter 1.4).

In the last years a large number of observations have shown that a monolithical picture of bulge formation cannot be established but has to be replaced by a variety of evolutionary 'paths' which led to a special morphology and dynamical conditions. Among the observations (reviewed in Kormendy & Kennicutt 2004) are the detection of cold stellar disks in center of spiral galaxies (e.g., Carollo & Stiavelli 1998) as well as areas inside the central regions dominated by young stellar populations (e.g., Benedict et al. 2002). In a majority of the cases the presence and dynamical evolution of the bar seems to be an essential ingredient to shape the discussed galactic regions. Furthermore, such an evolutionary process allows a model where SBcd galaxies can evolve to galaxies with a SBb Hubble-type.

1.4 Boxy or peanut shaped structures in disk galaxies

Galaxies with a shape of the central region as described previously (Chap. 1.3) are not rare. In fact, several galaxies with such box shaped structure are well known since a long time (Sandage 1961). Parallel to the discovery of galaxies with a box shaped central structure also objects with a more complex bulge region were noted. Those galaxies were labeled peanut shaped (bulge) galaxies since the bulge region resembled a peanut when seen from the side (de Vaucouleurs 1974). Since the morphology of the bulge region is not clearly separated between box and peanut shaped but does show a smooth transition from one to the other the general expression of boxy or peanut shaped (B/PS) is used. As will be discussed later, this aggregation into one category is also most probably justified by the formation process proposed for both types. In some of the most prominent galaxies with a peanut structure (e.g., *IC 4767*, *ESO 597-G036*) the bumps seem to form an 'X'. Therefore, the B/PS structure is also often called X-structure.

An extensive statistical study of the occurrence of B/PS structures in disk galaxies was presented by Lütticke, Dettmar, & Pohlen (2000a). Based on the visual classification of optical images made available through the Digital Sky Survey 2 (DSS2) a sample of ≈ 1350 galaxies was analyzed. In order to investigate the influence of dust on the classification also a much lower number of NIR frames of the objects were inspected. It emerged that the possible presence of dust does almost not alter the classification obtained in the optical wavelength range. From their analysis it emerges that almost half ($\approx 45\%$) of all edge-on galaxies exhibit

a B/PS structure. Furthermore, it was shown that the occurrence of galaxies with a B/PS structure is equally distributed along the Hubble sequence of galaxies (Lütticke et al. 2000a). That fact implies that the underlying formation process have to be viable in all those galaxy types and that they are a fundamental stage in the formation/evolution of disk galaxies.

In order to explain such pronounced morphologies two main formation processes were proposed. The accretion scenario is based on an external process depending, besides on kinematical parameters, on the environment of the galaxy hosting a B/PS structure. Repeated accretion of satellite galaxies could provide the luminous material, the energy, and the amount of appropriate angular momentum to form such structures. Binney & Petrou (1985) constructed models based on a distribution function depending on a third integral of motion, in a addition to the energy and the angular momentum along the symmetry axis z . This third integral of motion favored indirectly the presence of orbits at a given height above the galactic plane. The authors argued that the accretion of satellite galaxies was best suited to populate particular regions of action space with a subsequent formation of the B/PS. However, a drawback of that scenario is its request of a very restricted parameter range of orbital energies and angular momenta of the satellite. That would drastically reduce the probability of such a formation event. Further, remaining satellite galaxies should be detectable but are not observed. The merger of two spiral galaxies of similar size, as also proposed by Binney & Petrou (1985), suffered the same problem of low probability.

The other approach is based on internal (disk driven) mechanisms of the galaxy hosting the B/PS structure. In analogy to the resonances induced by the bar in the plane of the galaxy, vertical resonances can lift material from small z heights to higher values. That mechanism, called 'resonance heating', was discussed by, e.g., Pfenniger (1984, 1985) as well as Pfenniger & Friedli (1991) and Combes et al. (1990). Further, early 3-dimensional N -body simulations of disk galaxies showed a B/PS structure when viewed edge-on under a large variety of conditions (e.g., initial mass distributions, Combes & Sanders 1981; Combes et al. 1990). Raha et al. (1991) reported on similar results of their simulations pointing to the occurrence of a vertical bar instability, called fire-hose or buckling instability (Toomre 1966; Fridman & Poliachenki 1984; Araki 1985). The bar-buckling instability evolves on a dynamical time scale contrary to the resonant heating mechanism evolving on a secular time scale. Subsequent numerical studies based on N -body simulations could reproduce those results and enrich the bar thickening scenario with additional details about, e.g., the evolution of the buckling process (Athanasoula & Misiriotis 2002; Martinez-Valpuesta, Shlosman, & Heller 2005). In addition, extensive orbital structure studies done by Skokos, Patsis, & Athanasoula (2002a,b) and Patsis, Skokos, & Athanasoula (2002b, 2003) have shown for a 3-dimensional bar potential a large wealth of orbit families which, when sufficiently populated by stars, can well sustain the B/PS structures visible in edge-on galaxies.

Despite the fact, that the evolution of a B/PS structure is not necessarily bound to the occurrence of the bar-buckling instability, it can still be used as a fundament for the understanding of the B/PS structure formation (Martinez-Valpuesta et al. 2005). This is due to the much longer formation times for a B/PS structure through resonant heating. The frequent observation of pronounced B/PS structures in edge-on disk galaxies of all Hubble-types does point to an efficient formation process as the bar-buckling mechanism is. Further, the frequent occurrence is an argument against the claims of investigations dealing with N -body simulations that the formation of a B/PS structure does destroy the underlying bar as suggested by Raha et al. (1991). More recent studies of Martinez-Valpuesta et al. (2005) report indeed a weakening of the bar but not its dissolution.



Figure 1.1: *The shown compact group of galaxies (Hickson Compact Group 87) harbors a galaxy with a pronounced B/PS structure. In the lower left corner an extended edge-on galaxy is visible being easily distinguished from the other ones due its departure from a simple spheroidal or circular morphology. Along the galactic plane of that object (ESO 597-G036) an extended disk component with a dust lane seen edge-on can be observed. That galaxy is part of the sample used in this work. In the central region, above and below the plane of the galaxy, a peanut shape can be detected formed by the underlying X-structure. This image illustrates well the complex structure of the central regions of galaxies with a B/PS structure. The image is a composite of frames originating from four different cameras with one having a different spatial resolution than the other ones. Therefore the upper right corner has an extended dark region. The image is made available by the Hubble Heritage project: "NASA and The Hubble Heritage Team (STScI/AURA)"*

The orbital calculations described above also illustrate in a transparent way, that only a part of the bar is thickened and not the entire bar. That is in agreement with observations of galaxies, where, due to the inclination angle, the B/PS structure and the bar are simultaneously visible, proving thus the smaller spatial extension of the B/PS region compared to the bar extent. Such examples are *NGC 4762* (Wakamatsu & Hamabe 1984) and *NGC 4442* described in Bettoni & Galletta (1994). A strong observational support for the proposed formation scenario was presented by Bureau & Freeman (1999) using ionized gas kinematics. They showed convincingly that in 17 galaxies with a B/PS morphology in the central regions, 14 harbored also a bar. For the same sample Chung & Bureau (2004) presented additional kinematical data based on stellar absorption lines. Also in that case a large part of galaxies with a B/PS morphology did unveil the presence of a bar in the disk (22 out of 24 galaxies). Furthermore, the study of Bureau & Athanassoula (2005), based on methods used frequently in observational astronomy and applied to simulated disk galaxies, revealed a strong resemblance in important features commonly observed in galaxies with a B/PS structure (see Lütticke et al. 2000a). Indeed, the disk-driven formation scenario does explain in a relatively elementary way the different morphologies of B/PS central regions as already Combes et al. (1990) and Pfenniger & Friedli (1991) pointed out. Galaxies with a peanut shaped central region are oriented towards the observer with a LOS angle ϕ , measured relatively to the bar MJA, of $\phi \geq 80^\circ$ (determined in Lütticke, Dettmar, & Pohlen 2000b, based on simulations of galactic disks). The box shape is still visible at much lower values. Due to the rectangular shape of the bar, in cases where it is oriented with a LOS angle of $\phi = 0^\circ$, only the planar minor axis is observable. Such an angle ϕ results in a round morphology for the central regions. In Athanassoula & Misiriotis (2002) an illustrative example for such an end-on viewed bar is presented. All the above mentioned observations and self-consistent models give a coherent picture of B/PS structure formation in the light of bar driven disk evolution and are consequently a benchmark for all other competing models. Therefore, the present study will use that formation scenario as the fundamental one and investigate if the properties of the galaxies analyzed here are in agreement with it.

The proposed close connection of galaxies with a B/PS structure and a bar component in those galaxies, makes them furthermore to interesting objects for the deeper understanding of galactic secular evolution. Indeed, it is not only the peculiar morphology of those objects requesting a profound analysis but also the underlying processes at work on dynamical and secular timescales.

1.5 Aim and outline of the thesis

The previously presented studies (especially Bureau & Freeman 1999 and Chung & Bureau 2004) do point to a scenario where a large majority of the disk galaxies harboring a B/PS structure do contain a bar which suffered bar-buckling. However, the presence and observation of a bar in galaxies with a B/PS structure is essential for the bar-buckling mechanism but does still not provide a connection between both structures. Therefore, the present study addresses the morphology and the structure of the B/PS structure searching for correlations corroborating the assumed formation scenario. Simulations and orbital calculations of objects with potentials resembling galactic disks with a bar component have revealed a large variety of morphological substructure (Athanassoula 2005). Taking into account the appropriate conditions and modifications for an analysis of observable astronomical objects, an investigation

of a large galaxy sample can give a concise insight if such substructure is not an artefact of the simulations. Furthermore, it gives a deeper insight in the vertical structure of the galaxy which is important for the complete understanding of the bar–buckling mechanism. Indeed, a detailed investigation of edge–on disk galaxies can give a great contribution to the knowledge about the vertical structure. The near–infrared K_n –band data used in this thesis allows a nearly unobscured view on the edge–on disk and the B/PS structure. In order to have quantitative parameters to characterize the VSFBD, a fitting approach, as done in studies investigating disk scalelengths, will give the possibility to verify predictions made by the different formation models. Also in this case NIR data is ideally suited since it is a tracer of the stellar component shaping the galactic potential. The numerical studies as well as the theoretical ones dealing with stellar orbits in disk galaxies did not present any precise assertion concerning the shape and scale characteristics of the VSFBD in the region of the B/PS structure. Nevertheless, it can be supposed that in a bar–buckling scenario the scaleheight of the B/PS structure is amplified compared to that one present in regions undisturbed of dynamical processes changing the vertical structure. The aim of the thesis is thus to give a functional description describing the VSFBD leading to a parameterization of the observed morphology. An additional aspect in such an approach is the analysis of different functional distributions since there is no clear description of the VSFBD in disks of galaxies, yet. Further, of special interest is the relation between the characteristics of the bar and those of the outer disk regions. It is up to now not clear if the vertical structure of the bar is qualitatively different from that of the unperturbed disk. Both approaches, the morphological analysis and the quantitative investigation of the VSFBD using model distributions are used in the present study. During the development of the analysis methods best suited to achieve the described aims, special attention is also paid to the aspect of using them (easily) also in the field of the analysis of N –body simulations. It is of advantage to have a toolbox with which observational astronomy as well as numerical astronomic research can work equally well. This leads to a major comparability of the results of both fields and therefore to a more effective proceeding in understanding the physics driving galaxy formation and evolution.

Since it is aimed to study the correlation of a bar and a B/PS component it is important to have both edge–on disk galaxies displaying a B/PS structure as well as some basic information about the bar leading to such a structure. This has been accomplished through the usage of the sample on which the important investigations of Bureau & Freeman (1999) and Chung & Bureau (2004) are based. In Chapter 2 the sample is presented and further information about the applied data reduction methods is given. A separate focus is put on the masking of other astronomical objects like stars which can disturb severely the description of the VSFBD through a functional approach. The morphological investigation presented in this study (Chapter 3) is primarily based on profiles measuring the SFB along the radial extent. This comprises cuts along the MJA of the galaxy as well as profiles obtained by summing up all SFB contribution present above and below the galactic plane. Further, unsharp masking is described, which is the other approach used here in analyzing the substructure present in the disk galaxies. Unsharp masking has been used already in astronomical contexts but has not yet been applied to edge–on galaxies. Additionally the method was implemented in such a way that it is also applicable on numerical simulations (Chap. 3.5). An overview of all the galaxies with their SFB is given in Appendix C. The quantification of characteristics of the VSFBD is discussed in Chapter 4. First, possible functional shapes used to describe the VSFBD in previous studies are presented and discussed if they are suited for the purposes of this study. A special emphasis was put on the different aspects influencing the development of the fitting

process used here. Although the aim of a compatibility of the analysis process for observed galaxies and that ones obtained by numerical simulations was set, it become evident that a complete compatibility is not achievable. This problem is discussed in more detail in **Appendix A**. The results of the vertical fitting process are discussed, paying attention to the variations present and to the correlation of the obtained values with the presence of distinct galactic components. All diagrams resuming the fitting results obtained during the fitting process are collected and shown in **Appendix D**. The equivalence of the family of functions proposed by Athanassoula & Misiriotis (2002) and also used in this study with that one commonly used in bulge parameterizations (Sersic 1968) is shown in **Appendix B**. Finally, in **Chapter 5** the results discussed in the previous chapters are summarized and put into the general context of bulge and galaxy formation. Additionally some propositions for further projects are given resulting from the conclusions presented at the end as well as questions emerged during the study of the morphology and vertical structure of the disk galaxies. Special emphasis is put there on the investigations of N -body simulations in order to reproduce best the physics involved in galaxy structure formation.

Chapter 2

Data

2.1 The galaxy sample

The galaxy sample used for this thesis is identical to that one studied in the study of Bureau & Freeman (1999) and Chung & Bureau (2004). It consists of 30 edge-on spiral galaxies ranging from early-type (*S0*) to late-type (*Sc*) spiral galaxies. Those galaxies were selected basically on their morphology aiming primarily to have a differentiated base of objects harboring a B/PS structure (24 objects). A smaller part without that structure (6 objects), respectively showing a spheroidal bulge, was chosen to serve as a control sample to the former ones (see Tab. 2.2). In the previously mentioned studies the sample was assembled under the aspect of investigating the vertical structure in spiral galaxies and its evolution and confirmation of the presence of a bar, through spectroscopical techniques, in galaxies with a B/PS structure. Both studies proofed that the sample galaxies with a B/PS structure indeed harbored a bar.

As described in Chapter 1.5, it is an aim of this thesis to deepen the understanding of the correlation between the bar-buckling mechanism and the formation of a B/PS structure. In order to investigate in detail the morphology of the B/PS structure and the VSFBD, imaging in the NIR wavelength regime is used. The results can then subsequently be related in a consistent way to the results of the previous two studies which provided an independent proof that the galaxies harbor a bar. Furthermore, when a bar is present its length can be estimated roughly by the kinematical data presented in Bureau & Freeman (1999) and Chung & Bureau (2004). Additional selection criteria included the visibility on the southern hemisphere ($\delta \lesssim 15^\circ$), the size of the bulge (larger than $0'.6$), and a galaxy diameter of $D_{25} \lesssim 7'$. Only the last selection criterion is specific to the observation mode carried out for the data set used. It ensured that quick imaging was possible when using the instrument available for this study. Restriction to the bulge size was necessary to accomplish the investigations for bar signatures based on spectroscopy and described in Bureau & Freeman (1999).

All galaxies are contained in the large survey compiled by Lütticke et al. (2000a) which was intended as a database for galaxy samples defined by their bulge morphology. Comparing the classifications of both studies, 4 galaxies ($\approx 13\%$ of the sample) do not have the same classification, which is due to the classification method (visual inspection of Digital Sky Survey (DSS) images of the galaxies) lacking an automated procedure. Despite that drawback, the number of objects of which the classification disagrees is rather low. General properties of the galaxies are listed in Tab. 2.1 whereas Tab. 2.2 summarizes the classification by Bureau & Freeman (1999) and Lütticke et al. (2000a).

Table 2.1: *General parameters of sample galaxies*

Galaxy	R.A. ^a (J2000)	Dec. ^a (J2000)	Type ^b	B_T^a (mag)	D_{25}^a (arcmin)	V_{vir}^a (km s ⁻¹)	M_B^c ^a (mag)	Gal. extinc. ^c (mag)
(1)	(2)	(3)	(4)	(5)	(6)	(7)	(8)	(9)
<i>NGC 0128</i>	00 29 15.1	+02 51 50	S0 pec	12.7	2.81	4220	-21.4	0.010
<i>ESO 151-G004</i>	00 56 07.3	-53 11 28	S0 ⁰	14.7	1.31	7456 ¹	-20.4 ¹	0.009
<i>NGC 1032</i> [¶]	02 39 23.6	+01 05 38	S0/a	12.7	3.46	2660	-20.7	0.013
<i>NGC 1381</i>	03 36 31.7	-35 17 43	SA0	12.7	2.63	1545	-19.2	0.005
<i>NGC 1596</i>	04 27 37.8	-55 01 37	SA0	12.0	3.89	1229	-19.3	0.004
<i>NGC 1886</i>	05 21 48.2	-23 48 36	Sab	13.8	3.23	1545	-19.2	0.009
<i>NGC 2310</i>	06 53 53.8	-40 51 46	S0	12.6	4.16	943	-18.6	0.039
<i>ESO 311-G012</i>	07 47 34.0	-41 27 07	S0/a?	12.4	3.71	894	-20.0	0.141
<i>NGC 2788A</i>	09 02 40.2	-68 13 38	Sb	13.6	2.88	3793	-21.5	0.037
<i>IC 2531</i>	09 59 55.4	-29 37 02	Sb	12.9	6.76	2312	-21.6	0.030
<i>NGC 3203</i>	10 19 34.4	-26 41 53	SA(r)0+?	13.0	2.81	2265	-19.9	0.025
<i>NGC 3390</i>	10 48 04.4	-31 32 02	Sb	12.8	3.46	2680	-21.5	0.029
<i>NGC 3957</i> [¶]	11 54 01.5	-19 34 09	SA0 ⁺	13.0	3.09	1615	-19.0	0.017
<i>NGC 4469</i>	12 29 28.0	+08 44 59	SB(s)0/a?	12.4	3.46	674	-17.8	0.007
<i>NGC 4703</i> [¶]	12 49 18.9	-09 06 30	Sb	14.0	2.45	4450	-21.1	0.014
<i>NGC 4710</i>	12 49 38.9	+15 09 57	SA(r)0 ⁺	11.9	4.89	1434	-19.8	0.011
<i>PGC 44931</i>	13 01 49.5	-08 20 10	Sbc	14.2	2.81	3810	-21.1	0.017

NOTE: Units of right ascension are hours, minutes, and seconds, and units of declination are degrees, arcminutes, and arcseconds.

^aParameters from Lyon–Meudon Extragalactic Database (LEDA)

^bMorphological classifications from Jarvis 1986, de Souza & Dos Anjos 1987, Shaw 1987, and Karachentsev, Karachentseva, & Parnovskij 1993.

^cParameters from NASA Extragalactic Database (NED)

¹Redshift (V_{hel}) and absolute B magnitude from Chung & Bureau 2004

[¶]Galaxy belonging to the original control sample of Bureau & Freeman 1999

continued on next page

Tab. 2.1 *continued*

Galaxy	R.A. ^a (J2000)	Dec. ^a (J2000)	Type ^b	B_T ^a (mag)	D_{25} ^a (arcmin)	V_{vir} ^a (km s ⁻¹)	M_B^c ^a (mag)	Gal. extinc. ^c (mag)
(1)	(2)	(3)	(4)	(5)	(6)	(7)	(8)	(9)
<i>ESO 443-G042</i>	13 03 29.9	-29 49 36	Sb	13.9	2.88	2808	-20.6	0.031
<i>NGC 5084</i> [¶]	13 20 16.8	-21 49 38	S0	11.5	10.71	1664	-20.9	0.043
<i>NGC 5746</i>	14 44 55.9	+01 57 17	SAB(rs)b?	11.4	6.91	1800	-21.8	0.015
<i>IC 4767</i>	18 47 41.6	-63 24 20	S pec	14.3	1.51	3300	-19.5	0.032
<i>NGC 6722</i>	19 03 39.6	-64 53 41	Sb	13.5	2.88	5525	-22.2	0.021
<i>NGC 6771</i>	19 18 39.6	-60 32 46	SA(r)0 ⁺ ?	13.6	2.34	3978	-20.5	0.022
<i>ESO 185-G053</i>	20 03 00.4	-55 56 53	SB pec	14.3	1.23	4276	-20.0	0.025
<i>IC 4937</i>	20 05 17.9	-56 15 20	Sb	14.8	1.86	2136	-18.6	0.020
<i>ESO 597-G036</i>	20 48 15.0	-19 50 58	S0 ⁰ pec	15.2	0.87	8645	-20.7	0.029
<i>IC 5096</i>	21 18 21.8	-63 45 42	Sb	13.6	3.16	2907	-20.7	0.011
<i>NGC 7123</i> [¶]	21 50 46.4	-70 19 59	Sa	13.6	2.51	3478	-20.3	0.010
<i>IC 5176</i> [¶]	22 14 55.3	-66 50 56	SAB(s)bc?	13.4	4.36	1494	-19.6	0.011
<i>ESO 240-G011</i>	23 37 50.5	-47 43 37	Sb	13.4	4.89	2626	-21.0	0.005

NOTE: Units of right ascension are hours, minutes, and seconds, and units of declination are degrees, arcminutes, and arcseconds.

^aParameters from Lyon–Meudon Extragalactic Database (LEDA)

^bMorphological classifications from Jarvis 1986, de Souza & Dos Anjos 1987, Shaw 1987, and Karachentsev, Karachentseva, & Parnovskij 1993.

^cParameters from NASA Extragalactic Database (NED)

¹Redshift (V_{hel}) and absolute B magnitude from Chung & Bureau 2004

[¶]Galaxy belonging to the original control sample of Bureau & Freeman 1999

2.2 Observations

The observations were done by M. Bureau at the 2.3m telescope at the Siding Spring Observatory (SSO), Australia, between January 1996 and March 1997 over 8 runs for a total of 24 nights . The SSO Cryogenic Array Spectrometer/Imager (CASPIR) was used for all observations. Its Santa Barbara Research (SBRC) CRC463 256×256 InSb detector array ($30\mu\text{m}$ pixels) covered a field-of-view (FOV) of $128'' \times 128''$. It was used in direct imaging mode with a pixel scale of 0.5 arcsec and a NIR K_n -band filter (central wavelength $2.165\mu\text{m}$, width $0.33\mu\text{m}$; see Chap. 2.3)

For the observations the following strategy was adopted: The galaxies were observed at a minimum on one night to increase the probability of observing under photometric conditions, allowing a photometric calibration. Using the instrument rotator, the array rows were always aligned (and centered) on the galaxy major axis. At the beginning and at the end of each night dome flatfields were recorded to account for the pixel-to-pixel sensitivity variations. Since the NIR sources are often much fainter than the broadband sky background and since the sky background is variable on temporal as well as spatial scales, accurate sky signal removal is required. This is accounted for by taking exposures of the sky background repeatedly between two scientific exposures with an time interval of about 4 to 5 minutes. Under typical background brightness conditions ($12.0 - 13.0 K_n \text{ mag/arcsec}^{-2}$) the observations were always background limited (the typical photometric zero-point offset at K_n was $\approx 20.5\text{mag}$). The exposure time for the scientific frames (except standard stars), as for the sky frames, was 60s.

Table 2.2: *The classification of the galaxy bulges and the presence of a bar derived from different studies are listed. The first classification follows the scheme adopted by Lütticke, Dettmar, & Pohlen (2000a) whereas the second one is taken from Bureau & Freeman (1999). Further the presence of a bar signature is listed. The results of the method using gas PVDs as well as stellar kinematics are shown.*

Galaxy BC	Bulge Class ^a	DSS	Gas PVD ^b	Stellar Kinematics ^c
(1)	(2)	(3)	(4)	(5)
<i>NGC 0128</i>	1.0	Peanut	Bar	Bar
<i>ESO 151-G004</i>	1.0	Peanut	Bar	Bar
<i>NGC 1032</i> [¶]	4.0	Spheroidal	Axisymmetric	No bar
<i>NGC 1381</i>	2.0	Boxy	—	Bar
<i>NGC 1596</i>	4.0	Boxy	—	Bar
<i>NGC 1886</i>	1.0	Peanut	Bar	Bar

^a1: peanut-shaped bulge; 1.5: bulge boxy-shaped on one side and peanut-shaped on the other;

2: box-shaped bulge; 3: bulge is close to box-shaped, not elliptical; 4: elliptical bulge

^bBureau & Freeman 1999; Galaxies where no conclusion could be drawn have no entry in the column.

^cChung & Bureau 2004; Galaxies, whose kinematic signature does not meet all criteria set up for a bar signature in Chung & Bureau 2004, are classified as harboring probably a bar ("Bar?")

[¶]Galaxy belonging to the original control sample of Bureau & Freeman 1999

continued on next page

Tab. 2.2 *continued*

Galaxy BC (1)	Bulge Class ^a (2)	DSS (3)	Gas PVD ^b (4)	Stellar Kinematics ^c (5)
<i>NGC 2310</i>	2.0	Boxy	—	Bar
<i>ESO 311-G012</i>	2.0	Boxy	—	Bar
<i>NGC 2788A</i>	1.0	Peanut	Bar	Bar
<i>IC 2531</i>	1.0	Peanut	Bar	Bar
<i>NGC 3203</i>	3.0	Boxy	—	Bar
<i>NGC 3390</i>	2.0	Boxy	Accretion	Bar?
<i>NGC 3957</i> [¶]	3.0	Spheroidal	Axisymmetric	Bar
<i>NGC 4469</i>	1.0	Peanut	Axisymmetric	Bar
<i>NGC 4703</i> [¶]	4.0	Spheroidal	Axisymmetric	Bar
<i>NGC 4710</i>	1.5	Boxy	Bar	Bar
<i>PGC 44931</i>	1.0	Peanut	Bar	Bar
<i>ESO 443-G042</i>	1.0	Peanut	Bar	Bar?
<i>NGC 5084</i> [¶]	4.0	Spheroidal	Accretion	No bar
<i>NGC 5746</i>	1.0	Peanut	Bar	Bar
<i>IC 4767</i>	1.0	Peanut	—	Bar
<i>NGC 6722</i>	1.0	Peanut	Bar	Bar
<i>NGC 6771</i>	1.0	Peanut	Bar	Bar
<i>ESO 185-G053</i>	2.0	Peanut	—	Bar
<i>IC 4937</i>	1.0	Peanut	Bar	Bar
<i>ESO 597-G036</i>	1.0	Peanut	Accretion	Bar
<i>IC 5096</i>	4.0	Boxy	Bar	Bar
<i>NGC 7123</i> [¶]	4.0	Spheroidal	Accretion	Bar?
<i>IC 5176</i> [¶]	4.0	Spheroidal	Axisymmetric	No bar
<i>ESO 240-G011</i>	4.0	Boxy	Bar	Bar

^a1: peanut-shaped bulge; 1.5: bulge boxy-shaped on one side and peanut-shaped on the other;

2: box-shaped bulge; 3: bulge is close to box-shaped, not elliptical; 4: elliptical bulge

^bBureau & Freeman 1999; Galaxies where no conclusion could be drawn have no entry in the column.

^cChung & Bureau 2004; Galaxies, whose kinematic signature does not meet all criteria set up for a bar signature in Chung & Bureau 2004, are classified as harboring probably a bar ("Bar?")

[¶]Galaxy belonging to the original control sample of Bureau & Freeman 1999

Large part of the galaxies in the sample have a spatial extension well beyond the size of the FOV. Therefore, it was necessary to mosaic those galaxies with 2 to 5 mosaic frames depending on the individual size of the galaxy. Registering of the mosaic frames was made possible by realizing an overlap region of 50 pixels between adjacent mosaic frames. Additionally a dithering pattern of 8 pixels parallel or perpendicular to the galaxy major axis was introduced to account for cosmoics or bad pixels. The mosaic and sky exposures were grouped to a cycle of five integrations after which a dark current and a bias exposure was recorded. Summing up all exposures each galaxy image has an exposure time of 40 minutes. During each night at least three IRIS (Infrared Imaging Spectrograph) photometric standard stars for photometric calibration were observed, if possible. The observation of the standard stars was distributed over the whole night to allow to correct for the airmass.

2.3 Wavelength ranges

The NIR light is a perfect tracer for the intermediate to old stellar population in spiral galaxies. As discussed in Chap. 1.2 the contribution of these stellar populations dominate the luminosity of a spiral galaxy and originates from the stellar part which also dominates the mass distribution of the galaxy. Therefore, mapping the NIR light of a galaxy traces equivalently the mass distribution of the galaxy. The mapping of the mass distribution by NIR light is also the case for bars, since bars are largely build up by old population stars (see Chap. 1.2). Furthermore the mass-to-light ratio is almost independent of metallicity and age in the NIR K -band (de Grijs, Peletier, & van der Kruit 1997) which makes the estimation of masses and the investigation of its gravitational potential more reliable. For this reasons the usage of a NIR images is best suited when analysing the vertical structure as well as the interplay between bar component and vertical structure in spiral galaxies.

Additionally in the NIR regime the influence of dust patches and dust lanes is highly reduced compared to the optical regime (extinction at H and $K \approx 0.1 - 0.2$ times that in the visual wavelength regime (Buta & Block 2001)). This effect becomes stronger with longer wavelength. When studying the vertical structure of our sample galaxies it is desirable to minimize extinction by dust. Specially the fitting of profiles (Chap. 4.2) to the vertical light distribution has to be done avoiding any alteration of the distribution by dust lanes or patches. Since the thermal emission increases also with longer wavelength the K -band is best suited to achieve the former described goals. In particular the SSO K_n -band filter is tailored to avoid larger thermal emission at the long wavelength end of the original K -band as well as taking into account atmospheric transmission conditions at the short wavelength edge at the SSO.

2.4 Data Reduction

The data reduction was done according to the standard NIR reduction techniques using the CASPIR reduction package running in Image Reduction and Analysis Facility (IRAF) and provided by the SSO. Apart from the standard NIR reduction steps (bias correction and dark subtraction) the raw data had to be linearized with the CASPIR reduction package procedures since the response of the CASPIR detector array to light is quadratic. It showed up that the sky subtraction was performed best when combining (using the median) five sky frames taken immediately before and after the object frame. Flatfielding was achieved by dividing through a dome-flatfield frame obtained through the combination of 5 dome-flatfield frames taken at the date when the scientific object was observed. The telescope emission was accounted for by subtracting the dome-flatfield frames taken with an apposite lamp switched off from that ones which were achieved with the lamp switched on. A sky-flatfield was not used after some trials using it. The background noise level was higher than in the case using dome-flatfields. Summarizing the reduction process the following procedure was adopted: bias and dark correction for all frames; flatfielding of all frames; sky subtraction of the frames containing a calibration or a scientific object.

Bad pixel masks were not used based on the fact that when combining distinct exposures bad pixels were rejected by the correct setting of the appropriate parameters of the combining algorithm. This was possible due to the dithering pattern (see Chap. 2.2) resulting in a repeated coverage of a galaxy region avoiding the placements of bad pixels on the same spatial location of the observed object.

The mosaicing of the entire images of the galaxies was realized using the offset information contained in the macros used during observation. Due to a telescope drift this position offsets were not sufficient to mosaic the images correctly. In the optical regime mosaicing is facilitated by the frequent presence of numerous stars in the field of view. This fact can be exploited to use stars in the overlap region of each single frame of the mosaic as a fix point when registering the frames. In the NIR regime stars are not as frequent as in the optical so that in a large fraction of the sample not a single star was present in the overlap regions of the single mosaic frames. Therefore, the registrations of the single frames was achieved by checks of the results by visual inspection.

A crucial issue when registering mosaic frames is the correct leveling of the sky background in the overlapping regions. This was achieved by calculating the mode value over the whole overlapping region (including the area of the galaxy) and adding the difference in the calculated value to one of the overlapping frames. Finally, the single frames displaying the complete galaxy, were combined using the median for each pixel calculated on the entire image. For the spatial displacements only linear transformation (IRAF-routine GEOMAP, GEOTRAN) were used so that one single star or, if not present, the galaxy center was used to align correctly the images. When necessary the galaxies were finally rotated to align (maximum a 2°) them correctly with the edges of the image so that the major axis of the galaxy is centered at the central row of the image. For that purpose the outer isophotes were used. Exceptions from that procedure were done, when the outer isophotes clearly did not represent the general orientation of the disk (e.g., warps). At the end each image frame has odd column and row numbers in order to have a central row and a central column.

2.5 Calibration

For the calculation of the extinction correction and the zero-point the following calibration equation was used:

$$K + k_1 + k_2 * xK$$

with K as the literature value, k_1, k_2 as fit parameters representing the magnitude zero point as well as the airmass correction, to correct for the airmass during the observation in that wavelength band. A color term could not be calculated since the objects were observed in the K_n passband only. The frames taken during photometric conditions were used as reference after registration. Subsequently all frames of each observation were combined to one image of the galaxy. After that the combined image was compared to the reference image. For the comparison the inner part of the major axis profile is used, excluding the central few arcseconds where the profile has a sharp peak and therefore the seeing influences the profile most. The reference major axis profile is calibrated in magnitudes with the appropriate instrumental magnitude zero-point. After that the combined major axis profile was fitted to the correspondent reference profile which results in a value for the magnitude zero point to calibrate correctly the combined image. Finally the galactic extinction in the K -band wavelength range was taken into account (see Tab. 2.1) using the values available at NED.

2.6 Seeing and masking

The estimation of the resultant seeing, after all reduction steps, was done by calculating the median of values obtained on distinct selected stars present in the field of view. For each

star the Full-Width-Half-Maximum (FWHM) was determined by fitting Gaussians to three different parts of the stars spatial extension of the intensity. One method was based on a fitting of a two-dimensional Gaussian, the other two on a one-dimensional Gaussian along the x and y-axis on the image. The one-dimensional fitting was necessary when analyzing the vertical structure/profile of each galaxy. There, only the y-axis component of the Gaussian is effectively used and therefore a value based on the two-dimensional fits, including also data on the x-axis, would be incorrect. That is because the two-dimensional fit would not represent precisely the FWHM in the y direction.

When analyzing the galaxy images in relation to their spatial surface brightness properties, stars present in the field of view can strongly alter the obtained results. Therefore, two methods are used to limit the contribution of stars to the surface brightness. With the first method the stars were totally masked out by setting the area covered by the star to a default constant value (-99999) clearly distinguishable from true values obtained by the observations. Frames with stars masked out were used when fitting the VSFBD to enhance the reliability of the fitting procedure (Chap. 4.2). For the analysis summing up the surface brightness along the vertical extension of the galaxy (Chap. 3.2), images with interpolated areas have to be used. The usage of frames with masked stars would have neglected the light contribution originating from the galaxy in that region.

A way to avoid this problem, consisted in replacing the masked region by values which were obtained by the interpolation of the surrounding regions. This turns out to be satisfactory in a large fraction of the galaxy sample. When calculating the values replacing the pixel values contaminated by the stars contribution an annulus with a width of 2 pixels was used, surrounding the area marked for substitution. Only in few cases the width of the annulus was reduced to one pixel. This was done when the gradient was too steep so that a larger region for the calculation of the background would have had the result to reproduce the background at the masked area. Sometimes also the vicinity to the galaxy of another object made it necessary to reduce the area of calculation. The calculation of the values to be inserted was accomplished using a polynomial of third order. This seemed to be the best solution avoiding a too simplistic replacement using a linear interpolation and avoiding the incorrect replacement caused by numerical artifacts when using too many parameters to be fit. In a few cases it was necessary to change the order of the polynomial and reduce it from a third order to a second order one to achieve at least acceptable results. The third order polynomials introduced inexistent small scale structure, so that a more simple approximation through a second order polynomial yielded more realistic results. For the calculation of new values no noise model was assumed so that no artificial noise was added. Both described methods were applied through the procedure IMEDIT in IRAF. The same procedure was used in the unsharp masking analysis (Chap. 3.1).

2.7 Sources of errors in the data reduction

The above described procedure of data reduction has, apart from the classical uncertainties (e.g., imprecise sky subtraction), some further sources of inaccuracy which can influence the analysis based on that data and their results.

As discussed in Chap. 2.4 the quality of registration of the mosaic frames was checked by visual inspection. It has turned out that this is quite accurate. An inspection of the profiles and contours of the galaxies shows that no discontinuities can be found in the profiles and

contours. This is a prove of a rather accurate mosaicing. Nevertheless the applied procedure cannot provide a reproducible method based on objective and quantitative parameters.

Exposures which were not correctly focused show an non-isotropy along the two image axis. Along the x-axis of the image the object is squeezed whereas along the the y-axis the object is elongated. Because of that, stars in images which are not in focus show a diamond shape structure. This fact influences the determination of the FWHM of stars respectively the seeing for that image.

Additionally to the broadening of the stellar radial profiles due to the seeing — affecting also the galaxy — the alignment of the galaxy core to the center of the central pixel of the frame introduces a further smoothing to the image due to the interpolation used for the spatial shift. The additional smoothing increases the FWHM of the order of $0.25''$.

Chapter 3

Morphological Analysis

Although the peculiar shape of galaxies with a B/PS structure has been discussed frequently (see Chap. 1.4) only few studies focused on a detailed morphological analysis exist. Until now only two published studies dealing with the separation from other galactic components of the structure causing the B/PS in the central regions of spiral edge-on galaxies have been published. Shaw (1993) and Lütticke (1996) quantified the B/PS structure through the calculation of an excess luminosity by fitting a galactic disk and a bulge component to the galaxy and subtracting it. The excess luminosity was then compared to the total bulge luminosity. Approaches to quantify the B/PS structure with an isophote shape parameter describing the deviations from perfect ellipses — the a_4 parameter — were used by Combes et al. (1990), Shaw (1993), Lütticke (1996), and Merrifield & Kuijken (1999). Another quantity was introduced with the parameter θ by Lütticke (1996) measuring the angle between the MJA and the line intersecting the galactic center and the maximum of the B/PS distortion. A slightly modified method based on the 25mag/arcsec^2 (B -band) SFB level was presented by Shaw, Dettmar, & Barteldrees (1990). Finally Lütticke (1999) proposed as an additional method the measurement of the depression of the SFB isophotes, characterizing the B/PS structure, at the MNA. That parameter is introduced as an angle (ψ).

Other studies (e.g., Bertola & Capaccioli 1977; Kormendy & Illingworth 1982; Shaw, Wilkinson, & Carter 1993) dealt with the stellar kinematics of the whole region showing a B/PS. In that studies emphasis was put on the issue of cylindric rotation of the bulge region but also in that cases no distinction between the structures from which the analyzed signal originated (bended orbits or disk component) was done.

In Chap. 3.1 an approach characterizing qualitatively the bar-buckling phenomenon is described which in part avoids the analysis of the whole spatial region showing the B/PS region without separation between the different present components. As stated in Chap. 1.4 the formation of the B/PS structure is ascribed to the redistribution of disk material belonging to the bar in the vertical direction. This additional component can be distinguished from the underlying disk component taking advantage of its different characteristic length (the term scalelength would be inappropriate here since no scalelength can be attributed to the bended structure).

In Chap. 3.3 radial surface brightness profiles (RSFBPs) are analyzed investigating the relation between bar B/PS structure, and disk light contribution. RSFBPs profiles are a widely used tool to analyze the different components (e.g., Wakamatsu & Hamabe 1984; Lütticke et al. 2000b) and have been proven to be quite reliable for drawing conclusions

about the B/PS structure and the underlying bar component (Bureau & Athanassoula 2005 and Chung & Bureau 2004).

3.1 Unsharp masking

In contrast to simulations in real galaxies it is not easily possible to disentangle unambiguously the light contribution of different galactic components, like disk, bulge, bar as done in a large number of studies. There is more and more evidence that the structure of disk components in spiral galaxies has been misinterpreted due to low resolution data. Prominent cases are the central bulges of galaxies which are now often unveiled to be physically disks (Kormendy 1993; Erwin, Beltrán, Graham, & Beckman 2003). There is a major problem when analyzing the B/PS structure of the present sample since the overall contribution of the light originating from the disk component covers the light contribution evoked by a B/PS structure. One way of distinguishing the described components is to rely on the fact, that each component has a different characteristic length (e.g., scalelength, scaleheights in the case of a galactic disk) and use image processing techniques to separate this scales and therefore the different components.

3.1.1 Spatial filtering

The technique of unsharp masking is used in image processing for spatial filtering (see Gonzales & Woods 1992) and is realized with spatial filter masks with a predefined geometrical form and size. Spatial filters can be used as *bandpass*, *high-pass*, *low-pass* filters. All three are based on the principle of filtering frequencies of spatial structures in the Fourier domain.

Bandpass filter This kind of filters are used when selected frequency regions of spatial structures have to be detected and removed from the original image.

Low-pass filter In case that low frequencies of spatial structures in the image have to be preserved, low-pass filters are used. Due to the discarding of the high-frequency components, sharp edges are eliminated which results in a blurring of an image.

High-pass filter Contrary to a low-pass filter, a high-pass filter is tailored to remove the low-frequency components. Consequently edges in the light distribution seem to be sharpened. Unsharp masking is based upon this kind of filter.

The masks used by the different filters are realized by dividing the mask area into elements which each have a defined value assigned to. Mathematically the values of the masks elements can be interpreted as weights given to the intensity at the position covered by each mask element. The pixel (p_c) in the center of the region covered by the mask is then replaced by the sum of the products of the element weights (w_j) with the intensity (i_j) of the pixels covered by the mask: $p_c = \sum_{j=1}^j w_j \cdot i_j$. This procedure is done for all pixels of the image obtaining a blurred version of the original one. Finally, the unsharp masked image is obtained by subtracting the blurred image, which contains all low-frequency components, from the original image. The resultant image finally contains only high-frequency components. It is important to emphasize that the technique of unsharp masking enhances existing fine structure but does not introduce them (Malin, Quinn, & Graham 1983). Therefore, each detected structure can be trusted since it cannot be an artefact. However, when analyzing it, care has to be taken not to interpret noise as a real structure.

3.1.2 Application to the galaxy sample

Unsharp masking has been described for the first time by Malin & Zealey (1979) and Malin et al. (1983) in an astronomical context. It has been used since then for the enhancement of faint and small structures like galaxy shells in galaxy mergers (Malin et al. 1983) or small scale structure in the center of spiral galaxies (Erwin & Sparke 2003; Matthews & de Grijs 2004). Contrary to Erwin & Sparke (2003) and Matthews & de Grijs (2004) in this work instead of a gaussian filter a median filter is used to preserve the possibilities of detecting sharp edges, i.e., strong gradients on small spatial extension. The structure caused by the bar–buckling is sharply delimited (as the orbital analysis of Patsis et al. 2002b, suggests) and therefore shows strong gradients. In Appendix C it can be seen that at the edges of the visible X–structure strong gradients are present.

As described in Chap. 3.1.1 the size of the spatial filter has to be specified before applying it to an image. Since the filter size and the spatial structure to be analyzed are correlated, it is a characteristic scale for the structure. Unfortunately there is no concrete scale describing correctly the spatial extension of the structure formed by bar–buckling, when no information about positions of resonances is available. That kind of information is very rare among the observed galaxies. Therefore, for each galaxy a sequence of circular median filters with a radius ranging from $5''$ to $25''$, in steps of $5''$, was adopted to obtain the correspondent unsharp masked images. Based on these results, the scale enhancing best the underlying structure, was selected (see Tab. 3.1) to visualize the morphology (i.e. the best scale can have values intermediate to two adjacent step values). It turned out that the scales can vary largely from galaxy to galaxy. This is not surprising because of two reasons. First, each galaxy has a distinct distance and second, the extension (which is tightly connected to the scalelength of the disk) of the galaxies is not uniform. Therefore, each object has its individual scale at which the unveiled structures are best evidenced.

Further enhancements of the unveiled spatial structures can be achieved by folding i.e., mirroring the image at the symmetry axis parallel to the sides of the image intersecting the galactic center and combining the images. Applying that folding method leads to an increase of the Signal–to–Noise (S/N) ratio. Clearly, the described procedure holds a disadvantage. Structures present only in one quadrant of the image will be manifold and be present in the other quadrants of the image falsifying the morphological analysis. The effect of duplication is most evident when folding a galaxy which is not perfectly edge–on. Spiral arms present in the galaxy and offset of the MJA will be duplicated, forming a pseudo disk with a dip in the SFB on the symmetry axis (Fig. 3.1(b)). Because of this problem, folding is not applied. In contrast to the increase of the S/N it is more important to avoid misinterpretations caused by artefacts.

Since the unsharp masking technique has the characteristic of enhancing sharp gradients, stars present in the images are interpolated over as described in Chap. 2.6. In three cases this was not done (*NGC 4703*, *IC 4767*, *NGC 6722*) because it was not possible to apply the interpolation (even when changing all possible parameters described in Chap. 2.6) without altering severely the morphology of the galaxy. The reasons for the described problems are stars with positions near to or at the central plane of the galaxy. Since at that positions the gradients in the SFB are quite large, the interpolation was not able to reproduce in a correct way the course of the galaxy SFB.

The fluctuations in the background of the original image have a reflex also in the unsharp masked image as can be seen in all galaxies in Appendix C. In the process of the visualiza-

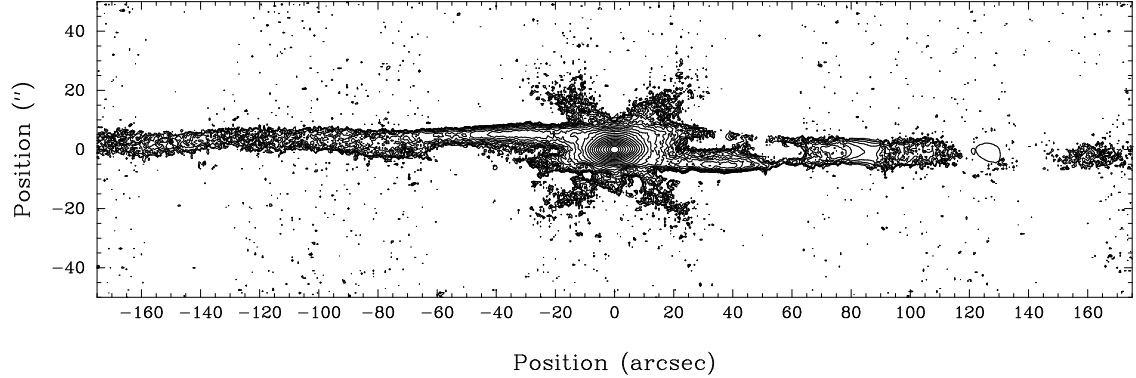
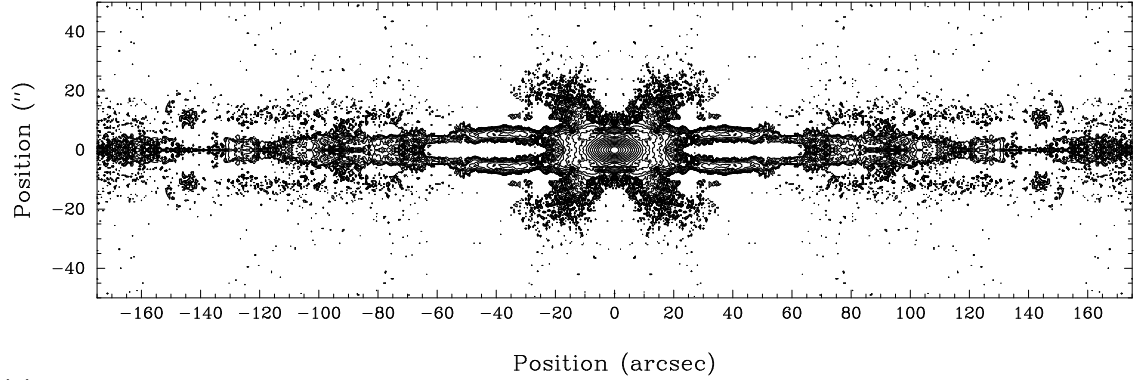
(a) *NGC 5746 without folding*(b) *NGC 5746 with folding*

Figure 3.1: *Effects of using folded images for unsharp masking. In Fig. (a) no folding is applied and the structures are a resultant effect of the unsharp masking technique. Fig. (b) shows the same galaxy but folded before the unsharp masking. Because of the folding algorithm, the galaxy seems to have a disk structure with a deep trough at the equatorial plane, which is not present in reality (see Fig. (a)). Apart from the doubling it can be noticed that the shape of the spiral arm emerging on the left side of the central region of the galaxy in Fig. (a) is strongly changed in Fig. (b). The regions with a lower noise level correspond to overlap regions of the single mosaic frames or in some cases to (circular) regions where foreground stars were masked out.*

tion of the faint structures in the B/PS region, reaching the limiting SFB isophotes, it was not possible to avoid the enhancement of the background level. Regions, where stars were interpolated, can be often recognized by the fact that they don't show any noise. This is a consequence of the omission of any artificial noise creation when interpolating over the stars (see Chap. 2.6).

Table 3.1: Sizes of masks used for each galaxy to create the unsharp masked image created from the K_n -band images. The size is given in units of arcseconds. For each galaxy the size at which the structures enhanced by the unsharp masking are best visible are notified.

Galaxy	size (arcsec)	Galaxy	size (arcsec)	Galaxy	size (arcsec)
<i>NGC 0128</i>	7.5	<i>NGC 3203</i>	7.5	<i>IC 4767</i>	12.5
<i>ESO 151-G004</i>	8.5	<i>NGC 3390</i>	7.5	<i>NGC 6722</i>	7.5
<i>NGC 1032</i>	7.5	<i>NGC 3957</i>	7.5	<i>NGC 6771</i>	8.5
<i>NGC 1381</i>	6.0	<i>NGC 4469</i>	15.0	<i>ESO 185-G053</i>	8.5
<i>NGC 1596</i>	6.0	<i>NGC 4703</i>	8.5	<i>IC 4937</i>	6.0
<i>NGC 1886</i>	8.5	<i>NGC 4710</i>	10.0	<i>ESO 597-G036</i>	8.5
<i>NGC 2310</i>	7.5	<i>PGC 44931</i>	8.5	<i>IC 5096</i>	6.0
<i>ESO 311-G012</i>	7.5	<i>ESO 443-G042</i>	10.0	<i>NGC 7123</i>	6.0
<i>NGC 2788A</i>	8.5	<i>NGC 5084</i>	7.5	<i>IC 5176</i>	8.5
<i>IC 2531</i>	10.0	<i>NGC 5746</i>	11.0	<i>ESO 240-G011</i>	6.0

3.2 Radial surface brightness profiles

For each galaxy (App. C) the RSFBP on the MJA as well as the RSFBP based on the sum of regions above and below the major axis (i.e., the vertically summed surface brightness profile (VSSFBP)) have been analyzed. Summed profiles were produced by the following procedure: Starting from the MJA all pixels with a positive value are summed until the first pixel with a negative value is detected. The occurrence of negative pixel values is due to the fact that sky subtraction had to be done during the image processing (Chap. 2.4). At that point the summation stops. The same procedure is done for the part below the MJA. Both contributions are then summed together. This method is the most practical one and ensures that all the available signal is used. Further it ensures that no contribution from fluctuations of the background is picked up. In the SFB plot profiles tracing an exponential intensity distribution will be represented by a straight line whose slope is fixed by the scalelength of the distribution. All discrepancies from a straight line point to a non-exponential light distribution (e.g., the $R^{1/4}$ -law). Clearly, a disk profile which has a radial SFBD following an exponential law, will not show up as a simple straight line. Instead it will have a convex shape curved towards the center of the galaxy. The additional SFB — compared to a RSFBP with a constant slope — is due to the integration along the sight-of-line of the 3-dimensional disk. Hence, this discrepancy from an exponential distribution does not impede a recognition of other structures or components with extrinsic different SFBDs.

The VSSFBPs are first of all a means of making a rough analysis of the constancy (or variability) of the scaleheight. A VSSFBP extracted on a fixed height (the RSFBP is a profile extracted at the height of the galactic plane) above the galactic plane would confirm the constancy of scaleheights in the galaxy. Any discrepancy of the VSSFBP from the shape of the RSFBP gives therefore useful information about the intrinsic structure of the galaxy. Further, the summed profile has the advantage, in cases where the vertical structure is constant over large radial range, to smooth out fine structure caused by observational effects and surface brightness properties of the observed object. On the observational side the variations in the SN -ratio can have an influence whereas irregular dust patches, asymmetries caused

by dynamical peculiarities (e.g., induced by interaction with another object), and enhanced emission by large and bright star formation regions are possible sources inherent to the galaxy itself. If, besides the previously mentioned scatter due to observational effects, no systematic change is given in the outer parts of the galaxy the VSSFDP has the advantage to bear a higher S/N ratio in the outer parts than RSFBPs at the same radial position. This makes it possible to follow the disk component to positions further out.

In the case of the RSFBP it can give already some insight in the dynamics of the galaxy. Any discrepancy from a pure disk profile, as described above, points to a more complex structure and in some cases to non-axisymmetric components like bars. Furthermore, the central regions of the galaxy can be used to discriminate between different components residing in the overall galactic potential. It is obvious, that the RSFBPs do not reveal the origin and dynamical state (like e.g., the ratio of the velocity dispersion and the main velocity) of the (luminous) matter. But those profiles can assert the current or past presence of different physical processes shaping the galaxies morphology. Hence, for a 'classical' RSFBP of an edge-on disk galaxy a part comprising the outer and intermediate regions of the galaxy dominated by the profile of a galactic disk is expected. This structure is only interrupted in the central region where the presence of the bulge, depending on the special Hubble-type of the object, changes the slope of the SFBD noticeably forming a peak. The work of Wakamatsu & Hamabe (1984) and Lütticke et al. (2000b) focusing on barred galaxies have already shown that the SFBD of edge-on galaxies and especially galaxies showing a B/PS structure are more complex than the model described above. In those cases the SFBD exhibits two other components apart from the parts described above. The first of this components which can be observed immediately beside the central peak when going to larger radial positions is more prominent than the second one. Both are similar in structure but different in strength. The first can be observed either as a flat plateau (in extreme cases also minima in the middle of that plateau) or a very shallow gradient making the structure resembling a shoulder. Regarding the second feature detected further out, only structures resembling a shoulder have been observed since they are shallower. The transition between the first to the second structure and from the second one to the disk profile dominating the outer parts of the SFBD, are rather abrupt. Wakamatsu & Hamabe (1984) have, in their observed object, shown convincingly that the first intermediate region can be attributed to a bar seen side-on and the second one to a lens seen edge-on. The studies of Lütticke et al. (2000b) analyzed a larger sample of edge-on disk galaxies and interestingly only the first intermediate region was detected but no fourth SFBD component was reported. Summarizing it can be stated that the typical barred edge-on disk galaxy has at least a three component structure.

The central SFB peak is canonically attributed to a bulge component. In the past ten years several publications and studies point to the possibility that the central structure of the galaxies is either more complex or dominated by a disky component or a combination of both (for a review of all arguments see Kormendy & Kennicutt 2004). Since in simulations of disk galaxies the possibility of different viewing positions and the disentangling of different galactic components is naturally given, a photometric study of such simulations can help to give insight to the origins of different photometric structures. Bureau & Athanassoula (2005) have undertaken such a study using high resolution N-body simulations of an isolated disk galaxy developing bar instabilities. They followed the temporal evolution of the MJA surface brightness profile in a large number of models. Finally they showed that bar formation and evolution within an (initially) exponential disk is associated with the buildup and continued growth of a dense central region resulting in a central peak (which would normally be identi-

fied with a bulge), and with the formation and gradual flattening of an intermediate region, in addition to the outer exponential disk (see also Athanassoula & Misiriotis 2002; Athanassoula 2003). The central peak extends to 1–1.5 original disk scalelengths while the intermediate region extends to the end of the bar, well beyond the central peak and the B/PS structure. The existence of three SFBP regions is thus normal (and expected) in barred galaxies, but it remains unexplained in classic bulge models.

3.3 Results

3.3.1 Morphological structure

The analysis of the K_n -band images as well as the unsharp masked versions have revealed a large variety of morphological features. Nevertheless it is possible to classify the features in a rough scheme describing the most characteristic properties of the single morphological features. A large part of the studied sample galaxies shows a X shape structure in the bulge region which is best visible in the unsharp masked images. Two main classifications can be distinguished for the X shape structure:

Off-centered X-structure (OX) Following the branches of the X, the ridges do not cross in the center of the galaxy but rather fall short of it. This leads to a '> <' feature labeled an 'Off-centered X-structure (OX)', rather than a true '><'. Prototypical examples are e.g., *NGC 1886*, *IC 2531* and the sample contains 13 galaxies ($\approx 43\%$ of the complete sample) with this kind of morphology.

Centered X-structure (CX) In the case where the branches of the X-structure do cross the galactic center this feature is labeled a 'Centered X-structure (CX)'. The number of galaxies showing this kind of morphology is comparable to the number galaxies harboring an Off-centered X-structure, namely also 13 ($\approx 43\%$ of the complete sample).

Clearly, the classification is not sharply defined and therefore consequently 'transition' objects are among the classified ones. However, this does not affect largely the dichotomy present in the sample objects. This X-structures should not be an inherent characteristic of box shaped SFB distributions but should reflect the orbital structure of the underlying B/PS since its appearance varies from galaxy to galaxy.

Further, local SFB enhancements are a feature detected in many galaxies. As in the case of the X shape also the local SFB enhancements can be grouped in two major classes:

Minor axis extremum (ME) A large part of the galaxies in the sample show a rather narrow and elongated local maximum along the MNA, which is called 'Minor axis extremum (ME)'. This kind of structure is generally only visible in the unsharp masked images of the K -band data on a smaller scale than the that presented in Fig. 3.2. For illustrative purposes only the cases of *NGC 1381*, *NGC 3203* are shown. Furthermore, the structures are very faint and hence difficult to detect. The situation is made worse by the fact that in the unsharp masked images the background variation causes also some structures which are at least in the dimensions similar to the minor-axis extrema presented here.

Secondary maxima (SM) As an important morphological structure local maxima of SFB are detected away from the center along the MJA, labeled 'Secondary maxima (SM)',

in a large part of the galaxy sample. Their importance relies in the fact that their outermost positions coincide with the strong decline of the RSFBP at intermediate radii supposed to be the end of the bar (see below).

Finally, some galaxies can be classified by the presence of spiral arm features (spiral arms (SA)) which are a consequence of the fact that not all galaxies are exactly edge-on. Though, this drawback can be used positively to check the incidence of spiral structure on galaxies with a B/PS structure and consequently for galaxies harboring a bar. The detection of the previously described features in the galaxy sample can be seen in Tab. 3.2.

Table 3.2: *Galaxy features as defined and described in Chap. 3.3.1. The features listed were identified on images unsharp masked on scales ranging from 2.5 to 17.5". A rough estimate of the inclination is also shown. Three different classifications have been used for the inclination ranging from (exactly) edge-on over quasi-edge-on to inclined. This allows a better analysis since according to the inclination it is possible to decide whether the observed features are genuine or a result of the probably large inclination angle.*

Galaxy (1)	Features ^a						Notes (8)
	OX (2)	CX (3)	ME (4)	SM (5)	SA (6)	I (7)	
NGC 128	OX		ME	SM		E	Warped disk ($m = 0$ mode?)
ESO 151-G004	OX			SM	SA	Q	
NGC 1032 [¶]			ME			E	
NGC 1381		CX	ME			E	Upwardly curved CX (∪)?
NGC 1596	OX?		ME			E	
NGC 1886		CX	ME	SM		Q	
NGC 2310		CX		SM	SA	I	Inner ring with outer SM
ESO 311-G012	OX		ME	SM		E	
NGC 2788A		CX	ME?	SM		Q	
IC 2531		CX		SM		E	
NGC 3203	OX		ME	SM	SA	Q	
NGC 3390		CX		SM	SA	Q	
NGC 3957 [¶]		CX	ME	SM		Q	
NGC 4469	OX		ME?	SM	SA	I	
NGC 4703 [¶]			ME	SM		Q	
NGC 4710	OX			SM	SA?	Q	Inner SFB plateau?
PGC 44931		CX	ME?	SM	SA	I	Inner ring with outer SM?

^a OX: Off-centered X-structure; CX: Centered X-structure; ME: Minor axis extremum;

SM: Secondary maxima; SA: spiral arms;

I: Inclination; E — (exactly) edge-on; Q — quasi-edge-on; I — inclined;

[¶] Galaxy belonging to the original control sample of Bureau & Freeman 1999

continued on next page

Tab. 3.2 *continued*

Galaxy (1)	Features ^a						Notes (8)
	OX (2)	CX (3)	ME (4)	SM (5)	SA (6)	I (7)	
<i>ESO 443-G042</i>	OX			SM		Q	
<i>NGC 5084</i> [¶]			ME		SA?	Q	
<i>NGC 5746</i>		CX		SM	SA	I	Inner ring with outer SM
<i>IC 4767</i>	OX			SM		Q	
<i>NGC 6722</i>	OX		ME?	SM	SA	I	see <i>NGC 5746</i> , warped disk?
<i>NGC 6771</i>	OX		ME	SM		Q	
<i>ESO 185-G053</i>		CX?		SM		E	'()'-shaped structure
<i>IC 4937</i>	OX			SM	SA?	Q	
<i>ESO 597-G036</i>	OX		ME?	SM		E	
<i>IC 5096</i>		CX	ME	SM		Q	
<i>NGC 7123</i> [¶]		CX	ME			E	
<i>IC 5176</i> [¶]			ME		SA?	E	
<i>ESO 240-G011</i>		CX?	ME?		SA	I	Inner ring with outer SM

^a OX: Off-centered X-structure; CX: Centered X-structure; ME: Minor axis extremum;

SM: Secondary maxima; SA: spiral arms;

I: Inclination; E — (exactly) edge-on; Q — quasi-edge-on; I — inclined;

[¶] Galaxy belonging to the original control sample of Bureau & Freeman 1999

The analysis of morphological features reveals, that in general galaxies with a B/PS structure harbor a larger wealth of features than galaxies with spheroidal bulge structure. In fact, the unsharp masking technique makes it possible to classify with more precision the investigated galaxies. This can be seen through the fact, that galaxies originally belonging to the control sample but hosting (probably) a bar (as shown by Bureau & Freeman 1999 and Chung & Bureau 2004) do reveal a complex morphological structure (e.g., *NGC 3957*). Nevertheless, the dichotomy between galaxies of the control sample and the other ones is still valid. At least 50% of galaxies with a B/PS structure possess an OX feature and at least 38% a CX feature. Compared to the control sample these values are clearly larger, since only 33% have either an OX or an CX feature. A similar situation can be found when the incidence of Secondary maxima (SM) is analyzed. About 88% of the galaxies with a B/PS structure have SM along the MJA, while only 33% of the control galaxies do have such a structure. For the presence of SAs, the ratios become at least 38% and perhaps zero. However, it is problematic to give large importance to a non detection of SAs when the control sample is rather small. In the case of galaxies showing a ME the situation is more straightforward. Only a little more than half of the galaxies with a B/PS structure (58%) do show a ME structure but all control galaxies do. Summarizing the OX, CX, and SM are preferentially associated with B/PS structures, while ME are found preferentially in the other type of bulges. It has to be kept in mind that this trend is strengthened if the galaxies *NGC 3957* and *NGC 4703* were excluded from the original control sample (used here for comparison) since the studies Bureau & Freeman (1999); Chung & Bureau (2004) and this one find clear hints for complex bulge structures in both galaxies. Some authors e.g., Sandage (1961); Whitmore & Bell (1988) point to the possibility that local maxima of SFB on the MJA (like the observed SM) can result from the presence of obscuring dust filaments. This is also possibly observed in this

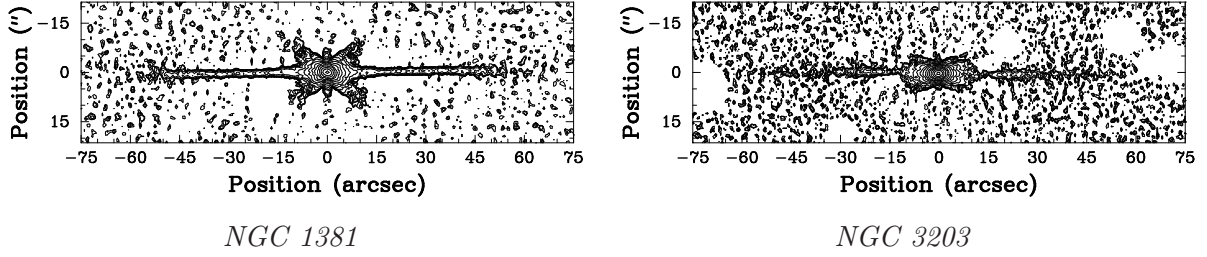


Figure 3.2: K_n -band images of NGC 1381 and NGC 3203 unsharp-masked on a scale of 2.5 arcsec. A long and narrow extremum is clearly seen along the minor-axis of NGC 1381, while a weaker one is observed in NGC 3203. Both features are labeled as a Minor axis extremum (ME). NGC 3203 also reveals bisymmetric elongated maxima slightly offset from the MJA, which are associated with spiral arms (SA) in a nearly but not exactly edge-on disk. Those spirals arms are not as apparent in images unsharp-masked on larger scales.

study but does not influence much the discussed trend since the majority of the cases with SM does not show significant amounts of dust when images from the DSS2 and the K -band are compared. However, the reason and accordingly the formation mechanisms leading to the morphology of the SM will be discussed in Chap. 3.3.2.

3.3.2 Orbital structure of bars and related morphological features

The CX and OX features have the largest vertical extent and are shaped like a smile or a frown. As clearly shown by the orbit superpositions of Patsis et al. (2002b), x_1v_1 orbits seen side-on have a morphology entirely consistent with an Off-centered X-structure. Depending on the model (i.e., mass distribution and pattern speed) and viewing angle, CX features can also be created. The x_1v_3 and x_1v_4 orbit families (bifurcating from the x_1 family at the 3:1 vertical resonance and shaped like a ' \sim ') and the x_1v_5 orbit family (bifurcating at the 4:1 resonance and shaped like a 'w') can also give rise to OX or CX features, depending on the model and viewing angle (see, again, Patsis et al. 2002b). This is also the case for the $z_{3,1}s$ family, which does not bifurcate from the x_1 orbits but is morphologically similar to the x_1v_4 family, although it was present in only one model.

The orbit superpositions of Patsis et al. (2002b) further show that the orbit families described above (as well as higher order families such as x_1v_7 , x_1v_8 and x_1v_9) can give rise to a number of maxima along the MJA, similar to the secondary maxima identified in Chap. 3.3.1. Those maxima generally occur at larger radii than the X features and near (but within) the ends of the bar, often where orbits have loops. An alternative and more straightforward explanation of the observed SM are simply the edge-on projections of inner rings (edge brightening), known to exist in a large fraction of barred disk galaxies and located at the end of the bar (e.g., Kormendy 1979; Buta 1995, but see also Chap. 3.3.5). Inner rings naturally form in gas-rich disks under the influence of bars (e.g., Schwarz 1981, 1984; Byrd, Rautiainen, Salo, Buta, & Crocher 1994), but they also develop in purely dissipationless simulations (e.g., Athanassoula & Misiriotis 2002; Bureau & Athanassoula 2005). Either way, both mechanisms support a relationship to bars, and both mechanisms may coexist. Accretion scenarios producing CX on the other hand, will generally not produce SM along the MJA (even less so systematically located outside of the X feature itself), making them

even less suited for a consistent formation mechanism. Interestingly Patsis, Athanassoula, Grosbøl, & Skokos (2002a) report that strong non-axisymmetric structures like bars are not categorically necessary for the formation of the B/PS regions but it suffices the presence of a slightly deviation from axisymmetry and/or ovals distorted disks (see also Martinez-Valpuesta et al. 2005).

3.3.3 Structures in the surface brightness distribution

Working with the sample of galaxies which was already used for the studies of Bureau & Freeman (1999) and Chung & Bureau (2004) we can reliably compare features detectable on the MJA with processes driven by a bar. Different slopes in the profiles in the outer parts of the galaxy evidence different components of the disk. Specially local SM in the RSFBP on both sides of the galaxy center support the assumption of the interpretation of the plateaus in the radial SFB plots as bar signatures because the plateau is delimited by this maxima (see also the classification Chap. 3.3.1). In the literature that maxima are related to an inner ring whose diameter is fixed by the distance of the two SFB enhancements. Based on that assumption several studies (e.g., van den Bosch & Emsellem 1998) use the positions of the enhancements to determine an upper limit for the length of the bar. Also, in the case where no ring should be present, the enhancements can be interpreted as either the position where spiral arms are parallel to the line of sight, as inner rings, or as the ansae (local enhancements of luminous material) of bars observed in either observational astronomy or (N-body) simulations (see also Chap. 3.3.2). In the first case the position can as well be regarded as a (rough) limit of the bar extension since it is well known that spiral arms start very often where bars do not expand further into the disk. For the second case the situation is even simpler since the ansae are, as described, intrinsically a bar phenomenon.

The present study does not contradict to this view but suggest a more simpler approach. Most of the galaxies showing a SM (cf. Tab. 3.2) have a rather extended SM. From the point of view of the present analysis the extension is far to large to be related uniquely to the interpretations based on other galactic components as described above. Spiral arms and inner rings should appear as a more localized signature in the RSFBP. An alternative explanation based on more simple arguments is the interpretation of the SM as the relict of the bar signature interrupted by the presence of the B/PS structure. If the B/PS structure is taken as the vertical growth of a central part of the bar with a change of the scaleheight of the bar component (see below and Chap. 1.4) then it is quite natural that between the central bulge and the end of the bar a decrease in the RSFBP is present. The reduction of SFB would be simply a result of the depletion of bar material redistributed in the vertical direction and therefore causing a decrease of SFB compared to other bar segments. Hence, more than naming the SFB features at the end of the bar enhancements it is more adequate to speak of intermediate minima in the bar SFB. As the notion 'maximum' would suggest it is not additional material but a *depletion* of material in that regions causing that effects. Apart from this that view is also supported by the fact that the extended SM do not peak in an maximum value but have all along their extension a constant SFB i.e., in the present approach the side-on SFB of the bar. A possible small increase towards the galactic center could be interpreted as LOS effect of the disk SFB contribution still present beyond the bar. Nevertheless, that kind of interpretation does not contradict the other point of views described previously since additional SFB could still be present due to the presence of ansae, rings, and SAs. For that reason the notion of SM will be kept all along this study.

The redistribution of disk material (i.e. stars and to a less degree also gas) in the vertical direction leads to the assumption that the summed SFBP should have the shape of an exponential disk profile all along the MJA reflecting the structure of a typical (exponential) disk. When additionally radial redistribution of material has also occurred (Athanasoula 1992; Friedli & Benz 1993, 1995; Athanasoula & Misiriotis 2002) then the VSSFBP should differ, especially in the central regions of the galaxy, from a genuine exponential disk profile.

As described in Chap. 3.2 for galaxies showing a B/PS structure a comparison of the RSFBP with the VSSFBP can be done resulting in a qualitative description of the scaleheights in that regions. A galaxy with a B/PS structure, whose VSSFBP does not show a plateau but its RSFBP showing one, must have a varying scaleheight in the region where the difference in the shape of the SFBP are present. That can be understood in the picture where the plateau in the RSFBP is interpreted as the signature of a bar. Along the bar the scaleheight of the bar component should be constant if the B/PS wouldn't be taken into account. But since it has been convincingly shown that bar resonances and instabilities lead to variations in the scaleheight, here that effect is consistently observed. The monotonically decreasing course of the vertically summed radial SFBP in the plateau regions reveals that the scaleheight is larger in the inner parts (more precisely in the region of the B/PS structure) than at outer edges of the plateau (see App. D). Clearly, the effect of line-of-sight integration has to be taken into account which increases when approaching the center of the galaxy but in the present sample the formerly described scaleheight variations are the first order effect.

In both cases, RSFBP and VSSFBP, the radial redistribution of material can be recognized. The sharp decrease of SFB at the end of the bar signature in the RSFBP is still observable in the VSSFBP but less pronounced. That hump interrupts the monotonic decrease of the VSSFBP, when starting in the center, typical for an edge-on disk. For most of the galaxies no remarkable change of slope is observable in the regions before and after the hump showing that in both regions the scalelength of the disk is approximately constant. In fact, Pohlen, Dettmar, & Lütticke (2000b) do not report any change of radial scalelength at such high SFB. Generally, the changes or truncations occur in regions further out. The prototype for a genuine disk is the galaxy *IC 5176* which apart its tiny central nucleus exhibits no other components than a disk. For this galaxy it is also possible to observe, unperturbed by other components, the slight inner curvature (observing the SFBP from the outer to the inner regions) caused by the line-of-sight integration in a galactic disk. Therefore, it can serve as benchmark for the other galaxies when detecting distinct structures in their SFBPs.

An exception from the scaleheight change described above can be found for the galaxy *IC 5096*, where the RSFBP and VSSFBP have nearly parallel courses despite the presence of a hump which could be mistaken as a bar signature. At nearly symmetric radial positions on both sides of the center the RSFBP shows a pronounced decrease of SFB. This situation can also be observed in the VSSFBP but less pronounced. What is remarkable about the course of the SFB is that compared to other galaxies with a similar profile (e.g., *NGC 2310*, *NGC 3957*) the region between the central peak and the decrease is extended and with a shallow slope so that the RSFBP is monotonically rising towards the center. A check whether the galaxy has been notified by Bureau & Freeman (1999) and Chung & Bureau (2004) to harbor a side-on bar gives a negative result. An analysis of the PVD has revealed rather the typical signatures of a bar seen end-on. Hence, this galaxy does not coincide with the relation of a RSFBP bearing a plateau or shoulder and the presence of a side-on bar. Further, the analysis of its morphological features (see Chap. 3.3.1 and Tab. 3.2) shows that the detected SM are located at a distance from the SFBP break which corresponds approximately to the distance

of the SM to the galactic center. Such a situation has not been observed in the other galaxies. Even if the positions of the SM are not considered since the SM in the case of *IC 5096* are extremely small and shallow, other explanations have to be found for that decrease of SFB. A first approach could be that the break is caused by the presence of different star formation rates (SFRs) in the disk. From the work of Rossa (2001) and Rossa & Dettmar (2003) it can be seen that in their *R*-band as well as H_α images the same decrease in the RSFBP can be observed. Since both wavelength bands show this feature it could be created by different SFRs in the outer and inner disk region. This is also sustained by the classification of the galaxy as an intermediate to late **Sb** Hubble-type which are known to show extended star formation in the disk. However, it is not clear what could cause the change of the SFR in the two components. If the HI surface density has distinct values it should be connected to some other dynamical (and photometrical) parameter. The second possibility for the described RSFBP is the presence of a lens. Already Bureau & Freeman (1999) emphasize that a lens would cause a similar signature as side-on bars. A strong argument for that interpretation is the continuous rise of the SFBD from the change in the slope to the inner parts. That fact is in case of side-on bars a sign for a weak bar. When the lens is seen as a component having a weaker gravitational influence than a bar as done by Athanassoula (1983) then the interpretation is consistent with the former view. However, the following argument reduces the probability of the presence of a lens. As Kormendy (1979) has shown, the presence of lenses is systematically reduced along the Hubble sequence leading to the result that the observation of a lens in late-type galaxies is strongly improbable. But *IC 5096* is, as mentioned above, classified as an intermediate to late-type galaxy although, in this case as in others, the fact that the galaxy is edge-on has severely complicated the classification.

A further example of such a RSFBP is observed in *NGC 1381*. Also there the bar seems to be shorter than the signature visible in the RSFBP (App. C). The bar extends to ≈ 30 arcsec from the galactic center whereas the signature up to $\approx 45''$. Again, in this case the signature does not show a plateau but rather a shoulder. Contrary to *IC 5096*, this galaxy is classified as an early-type SA0. Although the classification¹ has to be used with caution, the early-type characterization should be correct. Therefore, it is not improbable to observe a lens in such a galaxy. Further, the rather early classification should make strong star formation improbable so that the presence of a lens is less speculative. Interestingly both galaxies suspected to harbor a lens (beside the bar) have an intermediate RSFBP shape which resembles a shoulder. Therefore, the extension of a lens could be distinguished by that of the bar (if the bar is not exactly side-on) when a shoulder instead of a plateau is present. Still, there is an ambiguity concerning the strength of the bar component. At least in the case of *NGC 1381* the bar should be rather strong since the characteristic features of bar are clearly present in the velocity curve (see for a description and a figure Chung & Bureau 2004).

Apart from the case of *IC 5096* and *NGC 1381* galaxies without a detected bar and therefore showing a spheroidal bulge or being more spheroidal as a whole show neither any differences in the slopes of RSFBP and VSSFBP nor any difference all along the SFBD. For all galaxies with a bar which can be classified as one seen side-on — even if the viewing angle does decrease up to $\approx 45^\circ$ — the slope in the region of the bar signature in the RSFBP and VSSFBP do differ. That fact can be seen as a consistent proof that the observed SFB plateaus are highly probable the reflex of the bar.

¹The absence of a bar denoted by the character **A** is not correct as can be seen in Tab. 2.2.

3.3.4 Photometry of barred galaxy simulations

Bureau & Athanassoula (2005) investigated a series of N -body simulations to study the resulting 'photometry' from the simulated galaxies (see Chap. 3.2). A comparison of that work with the result of the observations of the present sample reveals numerous coincidences but also some divergencies. First, the three component structure of simulated side-on observed barred galaxies is confirmed. Apart from *NGC 1596* all galaxies harboring a bar which is not observed end-on do show such a three component structure. This is not surprising since the work of e.g., Wakamatsu & Hamabe (1984) and Lütticke et al. (2000b) already showed a clear relation. Nevertheless, the present study investigates in depth the SFBD of (barred) edge-on galaxies. A typical discrepancy between simulations and observations of real galaxies is evident when the RSFBP of simulated galaxies seen end-on are investigated. The simulated galaxies harboring rather strong bars do have a local minimum in the plateau region. This is not observed in the present sample. Either galaxies have a local minimum but then they are observed from a rather side-on viewing angle (good examples are *NGC 2788A* and *ESO 597-G036*) or they are seen end-on but don't have any local minimum (*IC 5096*).

Further, the extension of the central peak is quite different from that one observed in the sample galaxies. In the case of an intermediate bar the central peak has an extension of $\approx 43\%$ of the bar length as an overall lower limit whereas the strong bar case setting the upper limit of $\approx 71\%$ of the bar length. The peaks in the observed galaxies can reach such high values (as e.g., *NGC 0128*) but there are also some examples which have a much lower value (e.g., *ESO 443-G042* with a value for the peak-to-bar-length percentage of $\approx 20\%$). This is surprising since the simulations do not include star formation and that process would increase the brightness of a component, in this case the central one, so that one would expect that the central peak extensions of the real galaxies do not fall over the simulated galaxies value. In the sample galaxies the central peak is often much brighter than the disk with the SFBD showing huge gradients in SFB. Such a morphology would be in agreement with additional star formation but is missed totally in the simulation where the peaks have shallow gradients whose SFBD can be described by an exponential (Bureau & Athanassoula 2005). Summarizing the discussion of the difference of the central peak morphology in the simulations and the sample galaxies no convincing answer can be given apart the rather vague explanation stating that probably the discussed simulations don't yet describe completely real galaxies.

Another difference between simulations and the sample galaxies can be seen in the case where the inclination of the simulated galaxies is varied. It is true that the sample galaxies should have inclinations of greater than 85° so that no differences between simulation and observation should be detectable. But the galaxy *NGC 5746* is an exception and can therefore be used as a benchmark. The simulations show that for galaxies at an inclination lower than 85° a discontinuity in the RSFBP between the beginning of the central peak and the plateau of the bar signature is observable. This kind of feature is not observable in *NGC 5746*. The RSFBP shows a shallow local minimum but no discontinuity. In Bureau & Athanassoula (2005) the analysis of different inclinations has been done using a strong bar case. Probably this is the reason for the discrepancy between simulations and observations. On the other hand no such extreme SFBD as proposed by Bureau & Athanassoula (2005) has been reported in the observational literature. Thus, probably the real galaxies do have a slightly different galactic potential and different dynamics from that one simulated until now. Anyway, real galaxies don't show such strongly depleted regions like the galaxies in Bureau & Athanassoula (2005) do. Some mechanism seems to prevent the material to leave areas completely depleted

and creating high concentration areas. Interestingly the authors do not report any component resembling a lens. In fact, the strong bar case (but even for all bar strengths) shows a strong stability of the bar component until the end of the simulation. Therefore, if lenses evolve from dissolving bars, at least in those simulations there is no possibility to follow that evolutionary path.

3.3.5 Lenses and inner rings

Studies based on photometry of edge-on galaxies suffered often the drawback of ambiguity when analyzing the SFB plateau at intermediate radii (in the disk region). Lütticke et al. (2000b) based on the results of Wakamatsu & Hamabe (1984) used that plateau to search for bars in galaxies with a B/PS bulge region.

As Wakamatsu & Hamabe (1984) showed, besides the plateau which can be identified with a bar there is also a second shallower plateau present which can be attributed to a lens component (see Chap. 3.2). It became therefore evident that the distinction of both components in the edge-on case is only possible when the bar is not seen completely side-on and the photometry is deep enough to be able to show the steep gradient of the edge of the lens component. Therefore, as Bureau & Freeman (1999) already noted, a plateau in the major axis SFBP cannot be unambiguously related to the presence of a bar in the galaxy. Nevertheless such kind of features in the RSFBPs can still be interpreted as a photometrical signature of a bar for the following reasons: The presence of a bar could be proven through the studies done by Bureau & Freeman (1999) and Chung & Bureau (2004) using either gas kinematics or stellar kinematics independently of photometric data. Comparing the photometrical signatures of the bar and that of the lens a difference between both can be observed. The gradient of decline of the bar signature is more pronounced than that of the lens being more steeper and larger in the case of the bar. Further, the lens signature resembles much more that of a shoulder than that of a plateau Chap. 3.3.3. In late-type galaxies the presence of a lens component is nearly excluded as some studies have shown (Kormendy 1979; Kormendy & Kennicutt 2004, although some late-type galaxies show some oval components but not as strong as lenses).

One prominent case where perhaps a lens is observed could be *IC 5096*. This galaxy shows a clearly visible break in the RSFBP on either sides of the galactic center (see App. C). Nevertheless, the RSFBP shows a structure which resembles strongly this kind of bar signature. Therefore, in this case it could be possible that this is a signature for the presence of a lens even if the available Hubble classification ranks the galaxy within the intermediate-type galaxies. Now, how to distinguish between a 'genuine' bar signature and signs for a lens in a galaxy whose bar is seen side-on? First of all only galaxies of early type can be prone to harboring a lens (as described above) with a considerably probability. Second, not all galaxies which show the aforementioned course of the RSFBP and harboring a bar are exactly side-on. In that cases there could be two signatures. The innermost belonging to the bar and the outer one to the lens, since the bar is always as long as or (seen in projection) shorter than the (nearly axisymmetric) lens. There is no clear case where two symmetric signatures are visible in the RSFBP. One possibility is that both bar and lens signature fall together (for a range of line-of-sight angles close to the side-on case) so that they cannot be distinguished. Further, the coincidence of the SM (when present) with the limits of the bar signature is a clear hint that the signature is not a consequence for the presence of the lens. The lens has no ansae nor does it coexist with inner rings (Kormendy 1979), apart, rare cases which do not influence

the present study because of the elevated number of galaxies in the present sample with SM. On the other hand the above developed argumentation would lead to the contradictory fact, that lenses do not exist at all, which is not the case. This is not really the case because — even if the following argumentation starts from the same point as for the opposite fact — focusing on galaxies with a B/PS structure, leads to the consequence that the sample is biased to objects with a side-on bar. Hence, lenses could be 'hidden' in cases where the bar is seen nearly or close to end-on. Even if the argumentation cannot exclude completely the presence of lenses (especially in cases of early-type galaxies harboring a bar) it can be said quite safely that lens signatures cannot be easily *misinterpreted* as bar signatures.

The presence of inner rings is difficult to proof in an unambiguous way. A distinction of features like spiral arms or 'simple' ansae at the end of the bar and on the other side inner rings is rather difficult (see also Chap. 3.3.2). Even the distinction of the presence of inner rings and the other features depending on the Hubble-type of the galaxies does not lead to clear results. Indeed the most prominent cases of the presence of SM are among intermediate type galaxies (except the *ESO 597-G036* and *ESO 151-G004*, both S0) but also among early-type galaxies the SM are clearly detectable. The discussion given in Chap. 3.3.2 makes further conclusions about the presence and frequency of inner rings in different Hubble-types difficult to impossible. Therefore, the strong separation as done in the literature (Kormendy 1979) can neither be confirmed nor contradicted.

3.4 Central regions of the galaxies

The quantification of the dimension of distinct galactic components based on photometric data and thus on morphological features *without* a computational approach is difficult and can fall short of describing the relevant physical processes involved in the evolution of the different component. This is especially the case if those quantities are not related with other measured quantities. Furthermore, the measurement of all quantities is done by visual inspection and is therefore not completely reproducible. Nevertheless, two of them relating the central bulge region to the disk component will be introduced and discussed to give a first estimate and classification of secular evolution processes. In Chap. 1.3 already an overview about the different possibilities in naming and defining bulges has been given. Therefore, those quantities will be used in the following analysis, with the exception of the central nucleus, which will be introduced later.

Even if the following analysis suffers of the previously described problems a quantification of the observed characteristics can serve as a guideline to work out the relevant physical processes with the help or based on other measured quantities. In fact, the analysis of the RSFBP and VSSFBP can be used for such a study, as Kormendy (1979, page 2) states "... morphology ... is very efficient in *suggesting* the presence and explanation of new phenomena" [emphasis added by the author of this thesis]. Here, it seems to be possible to observe two types of components: i) a more fuzzy defined region where the SFBD departs from the inner extrapolation of the disk light (extended to the inclusion of the flat plateau or shoulder interpreted as bar signature) and ii) the extremely sharply constrained nucleus visible in some of the galaxies (8 out of 30 corresponding to $\approx 27\%$ see Chap. 3.4.3). The first component is difficult to define (photometrically) in a physically correct and unambiguous way. This is also true for the second component but here a typically used parameter, the eccentricity, is taken as a criterion despite the fact that no clear limit value is used to distinguish the two

resulting classifications.

3.4.1 Central bulge region

In the following two quantities describing the central region as well as a normalized SFB level are presented where the disk should dominate over all other components or even be the only component. These two quantities are the galaxy diameter at the 20.5mag/arcsec² the K_n -band for edge-on galaxies (D_{KEO}) and the Central-Surface-Brightness-Peak-Extension (CSFBPE). The D_{KEO} limit is in analogy to the galaxy diameter at the 25mag/arcsec² the B -band (D_{25}) parameter established in the literature as a measure for a galactic radius in the outer regions at the B -band 25mag/arcsec² isophotal level. In the present study using the K_n -band the data is not as deep as allowing to reach a 25mag/arcsec² isophotal level so that an isophotal level of 20.5mag/arcsec² has been selected. Most galaxies of this sample have the last regular isophotes at that SFB. It is worth to mention that the CSFBPE is not meant to quantify the central nucleus (see Chap. 3.4.3) but to give a measure of the extension of the bulge region in general. The analysis of regions with large distance to the galaxy center should assure that no distortion of non axisymmetric components can influence the measurement of the galactic radii. In this context no attempt is done to determine the length of the bar. First, because it is difficult to fix an unambiguous definition of the bar length as seen in the major axis SFB profiles and second it is doubtful if a measurement of it makes sense without knowing the viewing angle of it.

For bars and bulges (in weakly inclined galaxies) Athanassoula & Martinet (1980) have undertaken such an approach relying on quantities like half light radii, disk scale lengths, bar length, and normalized SFB levels (e.g., the D_{25} parameter). There, besides the bar length, all other quantities were fitted. Apart from that work other studies have compared the previously mentioned quantities (e.g., Seigar & James 1998; Erwin et al. 2003) but relying completely on fitted quantities which thus are cleanly reproducible. In Lütticke et al. (2000b) one of the few studies can be found where such kind of analysis was performed also on edge-on galaxies. Unfortunately their study is based completely on visual inspection (without a clear prescription for their measurement of the central bulge region called by them Central Bulge (CBU)). Hence, their results are not reproducible. Nevertheless, the partial overlap of their sample and the present one permits a rough comparison. There is also a large number of studies using weakly inclined objects and applying to them a 2-dimensional decomposition algorithm to extract the main parameters quantifying the underlying structure (e.g., Möllenhoff 2004).

A rough analysis of the different length of the components has shown that the ratios CBU/BPL used in Lütticke et al. (2000b) are not constant around one value but have a rather large range. The galaxy *ESO 443-G042* is a very good example for that, since it is notified in Lütticke et al. (2000b) of possessing a CBU/BPL value of ≈ 1 but this cannot be confirmed by this study. The difference between the CBU and the box/peanut length (BPL) represented perfectly by the X-structure seen in the unsharp masked image is too large. Therefore, it is not possible to achieve a ratio of CBU/BPL around unity. Certainly, the bar fuels and redistributes material to the central regions of the galaxy, but it is rather improbable that such a one-to-one relation between the *inner* bulge region and the *outer* B/PS structure could be supposed. This seems even more improbable if a possible relation of the inner disk region with the presence of x_2 orbits is considered as will be done later. Through this argumentation it could be possible to determine a correlation between the x_2 orbit radial

extension and the B/PS structure but that will be not unity. Nevertheless, it is possible to relate the length of the bulge region and the B/PS with the D_{KEO} parameter introduced in this study to describe the extension of the galaxy.

For the present study we use two quantities based on the K_n -band photometry. The first quantity gives a measure for the extension of the whole galaxy, more precisely for the axisymmetric disk component. For the second quantity another component is chosen which is independent from the viewing angle of the galaxy namely the central SFB peak in the RSFBP. The determination is done as described in the following: As explained above the 20.5mag/arcsec² isophotal level is selected since most of the galaxies do have this contour in the outer parts but still with a S/N level allowing reliable analysis results. In cases where the RSFBP in the outer part — due to the low S/N level — has not a continuous course, i.e., the data points have a large scatter, an average value is taken to fix the radial position. For the central region extension the procedure is similar. First, the central peak is taken into account drawing straight lines with slopes corresponding to the inner steep part of the central peak. There, the most dominant slope is used averaging over small deviations and perturbations of the SFBP. It has to be noted that the region where the central peak fades out into the intermediate plateau is largely avoided since no unique slope can be related to the course of the SFBP. Therefore, only the inner part of the peak is considered. Finally the definite extension of that region is calculated by determining the intersection points of the straight lines and the isophotal level of 20.5mag/arcsec². The choice to apply the measurement as described and not considering for example the position where the central peak fades out into the intermediate plateau is done because of the ambiguity of that positions. As can be seen each galaxy of the present sample has its quite 'individual' photometric characteristics — especially in the intermediate region/plateau — so that a consistent measurement in that areas could not be done. An example for the determination of the CSFBPE and the D_{KEO} can be seen in Fig. 3.3.

When analyzing the ratios of CSFBPE/ D_{KEO} it is remarkable that the difference for galaxies residing in a (compact) group with near (giant galaxy) companions compared to galaxies residing in a region with a lower density of objects is rather pronounced. In the former case the ratios are much higher than in the latter case. As a measure for the Galactic Environment (GENV) the classification of the environment as given by Bureau & Freeman (1999) as well as additionally the classification by LEDA is used. The LEDA classification notifies if the galaxy is part of a 'multiple system' being the most 'extreme' case for high density environments. Chung & Bureau (2004) emphasize (and refer to previous publications discussing the question and the implications of interactions to the internal dynamics of the galaxy like Noguchi 1987; Gerin, Combes, & Athanassoula 1990) the relation of the presence and prominence of the B/PS central region with the environment of the galaxy hosting this structure and take as an example *NGC 0128*, *NGC 6771*, *ESO 597-G036*. Hence, it is probable, that the dynamics of the bar or in general of the galaxy is stronger influenced by the environment than in the low density environment. The interplay between environment and the dynamics of galaxy — and therefore intrinsically of the morphology — can be manifold.

Internal dynamics contribute to the morphology of the bulge region. As the material fueled by the bar to the central regions, the local potential is changed due to the accumulation of the fueled mass. Apart from that, the resonance loci induced by the bar parameters (pattern speed as one of the most important) play a crucial role interacting with the predominant potential structures. Foremost the ILR is of high importance delimiting the maximal (radial) extension of the presence of x_2 orbits which have in comparison to their x_1 counterparts a

much smaller eccentricity reaching the minimum value of 0 for circular orbits. In fact, when analyzing the ionized gas kinematics presented in Bureau & Freeman (1999) strong x_2 signatures can be observed in the PVDs. The classification of strength of the x_2 signatures is done in a relative comparing it with the emission of the disk and bar signature. In the cases of *NGC 0128* and *NGC 4469* nearly no emission can be recognized (in the hardcopy of the publication of Bureau & Freeman 1999) contrary to the (very) bright x_2 signature. The galaxies *ESO 151-G004*, *NGC 6771* do have visible emission but to a much lower degree than the emission originating from the x_2 orbits. All galaxies showing strong x_2 orbits signatures (*NGC 0128*, *ESO 151-G004*, *NGC 4469*, *NGC 6771* do also have a high CSFBPE/ D_{KEO} ratio (see Tab. 3.3). Unfortunately Chung & Bureau (2004) do not make any comment on x_2 orbits in their analysis of the photometry and kinematics nor do they relate any studied observable with this second type of orbits in barred galaxies.

Table 3.3: Analysis of the Central-Surface-Brightness-Peak-Extension (CSFBPE) in comparison with the galaxy diameter at the 20.5mag/arcsec² the K_n -band for edge-on galaxies (D_{KEO}). For galaxies where no reasonable delimitation of the central bulge region was possible no value for the ratio CSFBPE/ D_{KEO} was calculated.

Galaxy	BC ^a	Type ^b	GENV ^c	D_{KEO} arcsec	CSFBPE ^d arcsec	CSFBPE/ D_{KEO}
(1)	(2)	(3)	(4)	(5)	(6)	(7)
<i>NGC 0128</i>	1.0	S0 pec	Gr, M	87.0 ± 3.0	38.0 ± 3.0	0.44 ± 0.04
<i>ESO 151-G004</i>	1.0	S0 ⁰	Gr	68.0 ± 2.0	27.0 ± 2.0	0.40 ± 0.03
<i>NGC 1032</i>	4.0	S0/a	Co?	155.0 ± 2.0	—	—
<i>NGC 1381</i>	2.0	SA0	Cl	134.0 ± 2.0	37.0 ± 2.0	0.28 ± 0.02
<i>NGC 1596</i>	4.0	SA0	Gr	150.0 ± 2.0	34.0 ± 2.0	0.23 ± 0.01
<i>NGC 1886</i>	1.0	Sab	Is	140.0 ± 2.0	21.0 ± 2.0	0.15 ± 0.01
<i>NGC 2310</i>	2.0	S0	Is	179.0 ± 2.0	22.0 ± 2.0	0.12 ± 0.01
<i>ESO 311-G012</i>	2.0	S0/a?	Is	219.0 ± 3.0	45.0 ± 3.0	0.21 ± 0.01
<i>NGC 2788A</i>	1.0	Sb	Cl	150.0 ± 3.0	26.0 ± 3.0	0.17 ± 0.01
<i>IC 2531</i>	1.0	Sb	Cl	285.0 ± 3.0	47.0 ± 3.0	0.16 ± 0.01
<i>NGC 3203</i>	3.0	SA(r)0 ⁺ ?	Gr	128.0 ± 2.0	26.0 ± 2.0	0.20 ± 0.01
<i>NGC 3390</i>	2.0	Sb	Co?	174.0 ± 3.0	40.0 ± 3.0	0.23 ± 0.02

^a Bulge Class (BC): Bulge classification as reported by Lütticke, Dettmar, & Pohlen 2000a

1: peanut-shaped bulge; 1.5: bulge boxy-shaped on one side and peanut-shaped on the other;

2: box-shaped bulge; 3: bulge is close to box-shaped, not elliptical; 4: elliptical bulge

^b Morphological classifications from Jarvis 1986, de Souza & Dos Anjos 1987, Shaw 1987, and Karachentsev, Karachentseva, & Parnovskij 1993.

^c Galactic Environment (GENV): Notes by Bureau & Freeman 1999;

Is: Isolated, Co?: Companions?, Gr: Group, Cl: Cluster;

Lyon-Meudon Extragalactic Database (LEDA) classification 'multiple' (M) for objects belonging to a multiple system.

^d Central-Surface-Brightness-Peak-Extension (CSFBPE)

continued on next page

Tab. 3.3 *continued*

Galaxy	BC ^a	Type ^b	GENV ^c	D_{KEO} arcsec	CSFBPE ^d arcsec	CSFBPE/ D_{KEO}
(1)	(2)	(3)	(4)	(5)	(6)	(7)
<i>NGC 3957</i>	3.0	SA0 ⁺	Cl	153.0 ± 2.0	35.0 ± 2.0	0.23 ± 0.01
<i>NGC 4469</i>	1.0	SB(s)0/a?	Cl	198.0 ± 4.0	41.0 ± 4.0	0.21 ± 0.02
<i>NGC 4703</i>	4.0	Sb	Is	179.0 ± 3.0	33.0 ± 3.0	0.18 ± 0.02
<i>NGC 4710</i>	1.5	SA(r)0 ⁺	Cl	221.0 ± 4.0	73.0 ± 4.0	0.33 ± 0.02
<i>PGC 44931</i>	1.0	Sbc	Is	125.0 ± 2.0	20.0 ± 2.0	0.16 ± 0.02
<i>ESO 443-G042</i>	1.0	Sb	Co	130.0 ± 2.0	14.0 ± 2.0	0.11 ± 0.02
<i>NGC 5084</i>	4.0	S0	Cl	242.0 ± 4.0	—	—
<i>NGC 5746</i>	1.0	SAB(rs)b?	Gr	390.0 ± 6.0	62.0 ± 6.0	0.16 ± 0.02
<i>IC 4767</i>	1.0	S pec	Cl	71.0 ± 2.0	20.0 ± 2.0	0.28 ± 0.03
<i>NGC 6722</i>	1.0	Sb	Is	134.0 ± 2.0	44.0 ± 2.0	0.33 ± 0.02
<i>NGC 6771</i>	1.0	SA(r)0 ⁺ ?	Gr, M	106.0 ± 2.0	40.0 ± 2.0	0.38 ± 0.02
<i>ESO 185-G053</i>	2.0	SB pec	Cl	66.0 ± 2.0	24.0 ± 2.0	0.36 ± 0.03
<i>IC 4937</i>	1.0	Sb	Cl	108.0 ± 2.0	19.0 ± 2.0	0.18 ± 0.02
<i>ESO 597-G036</i>	1.0	S0 ⁰ pec	Gr, M	80.0 ± 1.0	27.0 ± 1.0	0.34 ± 0.01
<i>IC 5096</i>	4.0	Sb	Co?	161.0 ± 2.0	44.0 ± 2.0	0.27 ± 0.01
<i>NGC 7123</i>	4.0	Sa	Is	149.0 ± 2.0	—	—
<i>IC 5176</i>	4.0	SAB(s)bc?	Co?	168.0 ± 2.0	—	—
<i>ESO 240-G011</i>	4.0	Sb	Gr	227.0 ± 3.0	37.0 ± 3.0	0.16 ± 0.01

^a Bulge Class (BC): Bulge classification as reported by Lütticke, Dettmar, & Pohlen 2000a

- 1: peanut-shaped bulge; 1.5: bulge boxy-shaped on one side and peanut-shaped on the other;
2: box-shaped bulge; 3: bulge is close to box-shaped, not elliptical; 4: elliptical bulge

^b Morphological classifications from Jarvis 1986, de Souza & Dos Anjos 1987, Shaw 1987, and Karachentsev, Karachentseva, & Parnovskij 1993 (see also Tab. 2.1).

^c Galactic Environment (GENV): Notes by Bureau & Freeman 1999;

- Is: Isolated, Co?: Companions?, Gr: Group, Cl: Cluster;
Lyon–Meudon Extragalactic Database (LEDAs) classification 'multiple' (M) for objects belonging to a multiple system.

^d Central–Surface–Brightness–Peak–Extension (CSFBPE) (see also the text).

It is also important to note that the largest part of the galaxies with a high CSFBPE/ D_{KEO} are early-type (i.e., lenticular S0) galaxies. Especially for the formation mechanism and history of S0 galaxies it has been proposed that the large B/D present in those galaxies can be due to the fading of the disk (e.g., de Carvalho & da Costa 1987) or due to a reduced scalelength but not due to a lower SFB (Bothun & Gregg 1990). That would be in agreement with the calculated values since this would explain the rather fast decline of the SFB towards the background level in the disk. In that picture only the bar part has kept a SFB similar to the period where it formed without suffering any large scale variation. However, as discussed in Chap. 1.1 the class of the S0 galaxies is difficult to explain through a coherent picture of physical process leading to such a morphology. Furthermore, it has to be explained by what evolutionary process the bar decouples from the SFB of disk and keeps its higher brightness through longer time scales.

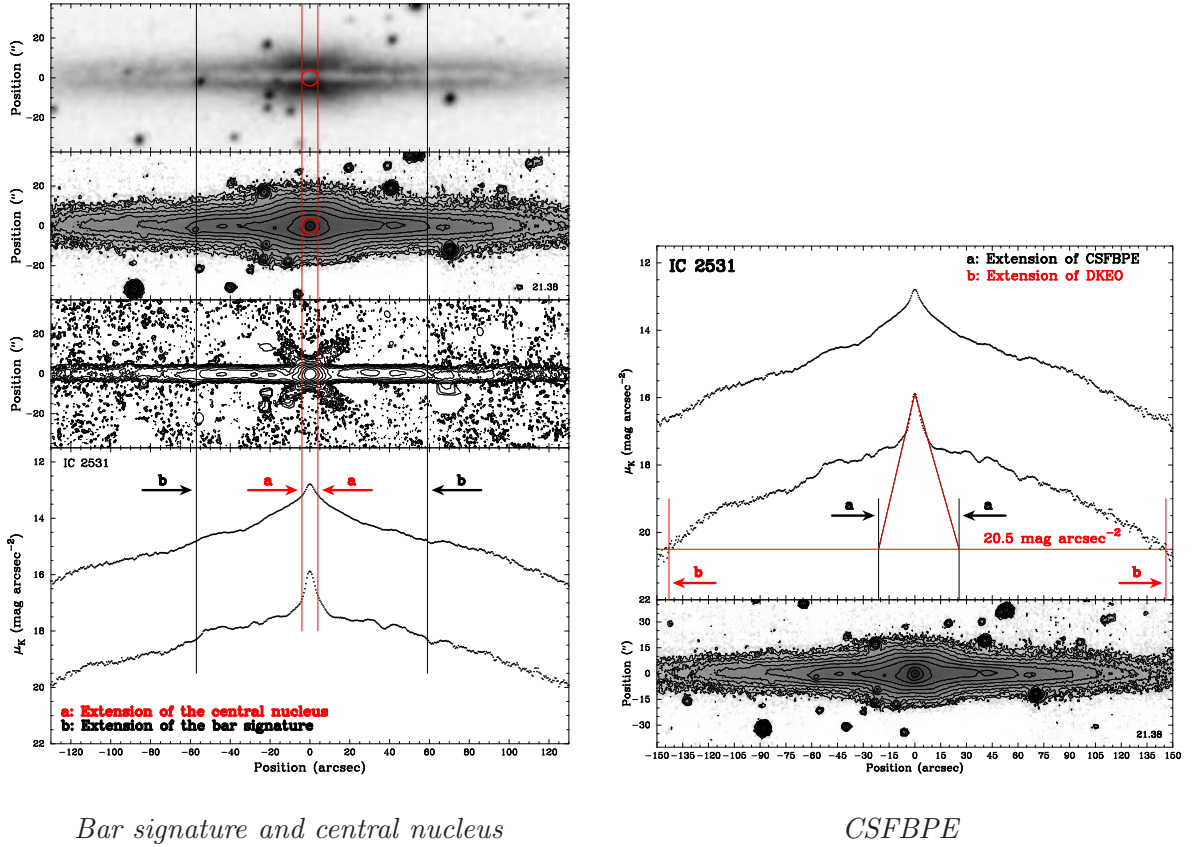
The situation for photometry of barred galaxies is probably much more complicated if the possibility is taken into account that secondary bars may be present in the used sample.

Secondary bars have been analyzed by a large number of authors (e.g., Shlosman, Frank, & Begelman 1989; Friedli & Martinet 1993; Shaw, Axon, Probst, & Gatley 1995; Friedli 1996; Maciejewski, Teuben, Sparke, & Stone 2002; Erwin & Sparke 2002) but in current times Erwin et al. (2003) have made the connection of these kind of structures with bulges and therefore also with the misinterpretation of structures in the center of galaxies. Due to their relative small size, they could appear also as a disk component at the very center.

3.4.2 Mechanisms shaping the inner central regions

Close encounters and minor merger events can trigger or alter conditions for instabilities in the disk of the target (disk) galaxy or inside the target galaxy by transferring large amounts of material (and angular momentum) into distinct components of the galaxy. As shown by Aguerri, Balcells, & Peletier (2001) analyzing N-body simulations depending on the ratio of the masses of the two (or more) galaxies involved in the interaction and subsequently the accretion event the denser part of the satellite galaxy settles in the central (bulge) region of the larger galaxy. From that study emerges that the Sérsic-index n (see Chap. 1.3) is driven from an initial $n = 1$ (exponential) to larger n up to $n = 4$ ($R^{1/4}$ -law). That is only the case when mergers with satellite galaxies comprising approximately the bulge mass of the 'target' galaxy occur. Interestingly the half light radius r_e does not change much in absolute values and when compared to the change of the disk scalelength. For this reason also their B/D does decrease with the increase of the parameter n which is the opposite trend when analyzing SBOs. As one reason for this observation they mention the fact that they did not analyze satellites with intermediate density relative to their high density and low density simulation runs. Further they also propose as an explanation disk evolution effects. The disk scalelength of the original disk becomes larger so that it would be called a 'thick' disk by the point of view of an observer. A further drawback of the work done by Aguerri et al. (2001) is that the analyzed galaxies cannot develop bar-type perturbations. Closely connected to bars are resonances induced by the pattern speed of the bar. These resonances (especially the inner ones) can give a further constraint on the extension of the bulge region (see below).

Aguerri et al. (2001) gave a lower limit to the average number of companions for field spiral galaxies of 1.2 ± 0.3 . The probability and number of accretion events could be noticeable higher in dense environment since the supply for the accretion could be provided by a rather elevated number of dwarf galaxies in those environments. Knierman et al. (2003) have further shown that the dwarf galaxies population in such environments does not diminish monotonically but can be supplied by new members during mergers of giant galaxies forming tidal dwarf galaxies. Although the tidal dwarf galaxies constitute only a small contribution (to the total luminosity function of all groups), they still provide a refreshing of the reservoir of available satellites. Therefore, it is possible to expect minor mergers long time after the formation of the compact groups and not only during the formation period of that kind of groups. According to Pfenniger (1993) the presence of a B/PS structure traces the absence of merging events with objects of more than $\approx 4\%$ of the galaxy mass. Between $\approx 5\%$ and $\approx 10\%$ the B/PS structure is destroyed but not the bar itself which disappears only when mergers with satellites having masses larger than $\approx 10\%$ of the galaxy mass occur. Since some of the sample galaxies are located in merger events or environments where accretion of satellites could have been occurred quite frequently, their morphology can serve as a mass estimation of the involved objects. The observation of a B/PS structure can then be related to an absence of merger events of objects larger than $\approx 4\%$ or alternatively to a recurrent



Bar signature and central nucleus

CSFBPE

Figure 3.3: The left figure illustrates the extension of a typical bar signature and the extension of the central nucleus described in Chap. 3.4.3. On the right side, the figure visualizes the calculation of both entities CSFBPE and D_{KEO} . As can be seen in the case of the determination of the CSFBPE only the innermost parts of the peak are considered trying to average out some small changes and deviations of the SFBD in that area. In both illustrations the galaxy IC 2531 was chosen since it combines all aspects of the described morphology in a clear representation.

mechanism of B/PS structure formation. These are the most probable scenarios since no galaxy with bar signature but lacking a B/PS structure was found. Therefore, that situation compared to the results of Aguerri et al. (2001) corroborate such an evolution history since the masses of satellite galaxies were in same order of magnitude as the limits determined by Pfenniger (1993).

The dissolution of the bar induced by a CMC (as discussed by Shen & Sellwood (2004)) is a further process of secular evolution. However, in that study it is emphasized that the extension of the B/PS region (when seen side-on) does not change (i.e., increase) much when the bar has dissolved. Of even greater influence is the fact, that the bar dissolution mechanism invoked (e.g., Norman et al. 1996) is much less effective as thought before (see Shen & Sellwood 2004). First a rather large mass has to be accumulated in the central galactic regions and second even those larger masses do influence the orbits supporting the bar less effectively than

stated before. Thus, up to the present state, it is dubious if bar dissolution (and subsequent bar renewal) do play a significant role in galactic secular evolution.

3.4.3 Central nucleus

In 8 out of 30 galaxies, as mentioned previously, a small and sharply constrained component is observed which is labeled here central nucleus (the galaxies harboring such nucleus are *NGC 1886*, *NGC 2310*, *IC 2531*, *ESO 443-G042*, *NGC 5746*, *ESO 240-G011*, *NGC 7123*). The most efficient way to detect that component is to analyze the *K*-band contours as well as the contours of the unsharp masked image in the very most center. Coming from larger radii the geometrical forms of the contours are ellipses with a large range of eccentricities resulting in a strong flattening of the disk (see for a description of flattening e.g., Kregel, van der Kruit, & de Grijs 2002). For the 8 galaxies presented here the contours change shape in the innermost radii becoming nearly perfect (concentric) circles. This fact can be interpreted as a signature for the presence of different components since a single disk component has elliptical isophotes. The large flattening of the disk component all along its extension is the reason for that elliptical isophotes (Dalcanton & Bernstein good examples can be seen in 2000, and radial as vertical SFBPs are studied in Matthews, Gallagher, & van Driel 1999; Matthews 2000). A similar method for the determination of such small structure has been used by Erwin et al. (2003). Also Böker, Stanek, & van der Marel (2003) investigate the innermost regions of galaxies. They used a sample of face-on very late-type galaxies to study the connection between inner star clusters and an SFBD.

In their discussion it becomes evident that often a nuclear star cluster can be the explanation for (at least a part of) the light excess compared to the disk component. Although, they refer likewise to a yet unknown component needed for the remaining excess luminosity. The case of a non exponential disk SFBD is further discussed, but again explaining the most central SFB by a star cluster. Additionally Shen & Sellwood (2004) proposed star clusters forming resulting in this sharp SFB peaks as visible in the RSFBPs (see Chap. 3.4.3). The same issue has been analyzed by Athanassoula et al. (2005). Analyzing the innermost region it has to be kept in mind that the seeing has the effect of transforming the central isophotes (whose spatial scale is similar to that of the seeing) into rounder isophotes. In the case of components with a very small extension (a few parsec to some 10^1 parsec, i.e., sub arcsecond scale) the seeing smears out that size into a larger region. Nevertheless, a strong qualitative difference with a morphology present in e.g., *ESO 151-G004* can be stated and used in the further analysis concerning the vertical bulge structure. The present work points to that difference allowing such an analysis.

A good example of a large-scale disk with a small but sharp rise in the SFBD in the innermost region can be observed in the galaxy *IC 5176*. That galaxy has the advantage not to host a large-scale bulge so that it does not influence the SFBD in the central region. As mentioned in Chap. 3.3.4 the discussed structure cannot be found in any simulation analyzed by Bureau & Athanassoula (2005) probably due to the absence of gas in their simulations. The central nucleus described here can be also often observed in color maps created of different optical and NIR images. In such images a central area with a redder color as the surrounding neighboring regions is observable. Probably strong dust concentrations are the source of such a reddening showing that complex dynamics confining dust in such a confined region is at work. Unfortunately the here presented morphology cannot give clear indications whether the described structure has a disk like kinematics or is isotropically hot. The recent

and accumulating claims of central disk detections in disk galaxies (e.g. Falcón-Barroso et al. 2004) feed the presumption that the observed structures are of a dynamically cold disklike nature. Despite the lack of vertical kinematic data the small extension — and consequently low scaleheight — of the innermost structure does not preclude the possibility of a disklike nature of it.

An additional and alternative formation scenario for this innermost structure dating its composition back to the beginning of the formation of the galaxy. Reviewing the formation of the nucleus as the product of a dissipationless collapse in the protogalactic cloud following the scenario of Eggen et al. (1962) but on much smaller scale it is possible to set that formation in the first period of galaxy formation. Several studies (e.g., Carollo et al. 2001) report old stellar populations in that part with emission of light predominantly in the redder wavelength bands (R - and I -band). This certainly leads to the consequence that the large spheroidal bulge component proposed by the model of Eggen et al. (1962) is not a major building block of the galaxy structure (see also Chap. 3.5).

3.5 Conclusions

The morphological analysis has shown a complex vertical structure of for galaxies harboring a (side-on) bar and a B/PS structure. The photometrically distinguishable components are more numerous than that ones predicted by the classical model of a bulge and a disk component. In the literature already a fair amount of studies have worked out that interplay (Wakamatsu & Hamabe 1984; Bureau & Freeman 1999; Lütticke et al. 2000b). The plateau and accordingly the shoulder in the RSFBP of the intermediate galactic regions are consistently related to bar or lens components (see Chap. 3.3.3). The comparison of photometrical and kinematical data indicates that plateaus are related to bars whereas the shoulder is more generally related to lenses or similar components. For the latter case the galaxies *NGC 1381* and *IC 5096* have been discussed as prototypical examples.

The plateau is formed by a depletion of in-plane material at the central positions of the plateau, which is redistributed in the vertical direction. That redistribution results in the B/PS structure. Such a redistribution becomes manifest in a rise in scaleheight at the radial positions of the B/PS structure. A comparison of the RSFBP with the VSSFBP reveals this increase. At positions where the RSFBP exhibits the plateau the VSSFBP has a monotonically rising SFB values in line with a profile of classical exponential edge-on disk (see Pohlen, Dettmar, Lütticke, & Schwarzkopf 2000a, for examples of edge-on disk profiles). Further, the bar components orbits force the in-plane material to redistribute in the radial direction which can be recognized also in the VSSFBP. At positions where the bar ends the VSSFBP shows humps deviating from the normal course of an edge-on disk. Depending on the strength of the bar also the hump in the VSSFBP varies in strength. Apart from the intermediate (bar/lens) region also the innermost region shows some substructure. In $\approx 27\%$ of the sample galaxies a small spheroidal nucleus was detected. The small scaleheight of that component and other investigations focusing on the innermost parts of disk galaxies suggest that the innermost region is dominated by a dynamically cold disklike structure. That would mean that throughout the whole plane of the galaxy evolutionary effects of disks shape the overall morphology of disk galaxies.

As stated in Chap. 1.4 simulations of galactic disks and theoretical formation scenarios for galaxies have proposed a large variety of features to be present in disk galaxies. Although that

surmounts the facts described and discussed by observational studies a detailed analysis as done in this study is missing for simulated objects. Particularly the unsharp masking method described in Chap. 3.1 has not been used so far in the analysis of the results of N -body simulations. A first tentative attempt has been undertaken by Athanassoula (2005) with the same procedure as developed here but adapted to the characteristics of N -body simulations by the author of the present thesis. The unsharp masking technique was used for a simulated galactic disk harboring a strong bar. Interestingly, focusing only on the morphological similarities between structures in observationally obtained and simulated objects can be noted. Either a OX structure, as seen in the galaxy *NGC 4710* as well as a morphology like in *NGC 128*, are detected. The crucial fact is that both structures are visible in the *same* object but under *different* viewing angles (which is possible to achieve in simulated objects). Therefore, it may be well possible that some of the reported morphological structures are due to line-of-sight effects. This possible result would provide a simply structured but effective view to arrange all the different morphologies observed in the inner central part of the galaxy, namely the bulge. Clearly, a large number of distinct simulations has to be analysed to give a definitive answer.

The complexity of the structural components in the inner bulge region show that the monolithic collapse scenario proposed by Eggen et al. in 1962 cannot be applied to all galaxies. In the review of Kormendy & Kennicutt (2004) all observational aspects are collected and discussed which point to complex and differentiated formation mechanisms for disk galaxies and their central regions. Cylindric rotation of the bulge as reported for galaxies showing a B/PS structure and the correlation between bar and B/PS structure as shown in this work — besides other approaches — corroborate the view of secular evolution of the disk as important driver for galaxy morphology and dynamics. The large extent (along the bar) of the bulge region in all galaxies harboring a B/PS structure could indicate an additional process of bulge growth apart from merging or the primordial formation of large bulges. Although it is not straightforward to extrapolate from an edge-on view of a disk galaxy to a probable face-on shape it could well be that the cuboid geometry of the B/PS structure is observed in the elongated central structure inside bars. Prototypical examples are *NGC 175* [SBab(s)], *NGC 1433* [SBb(s)], *NGC 2523* [SBb(r)] presented in Sandage & Bedke (1994), and *NGC 4314* [SBa(rs)] in Castro-Rodríguez & Garzón (2003, their figure 4). At the end of those rectangular components it is possible to recognize unambiguously the bar extending further out showing also a smaller MNA length compared to the other structure. Therefore, the central structure cannot be mistaken by a bar and has to be a distinct component (although this does not mean that it is unrelated to it). Further, a spheroidal structure at the center can be distinguished easily from the other components matching well the typical shape of a canonical bulge. As a consequence it is here proposed to connect the described face-on cuboid structure to the B/PS region seen clearly in the discussed sample galaxies.

Taking into account the described morphology it is difficult to invoke, as the constituent of the classical bulge a spheroidal component with a scalelength in the order of about one tenth of a disk scalelength. The inner region of the galaxy is more likely build up by several components like bars, inner disks, B/PS regions etc. Galaxies which have undergone a major merger could be expected to show a more classical bulge shape but also there, complex substructure can be observed (e.g., van den Bosch & Emsellem 1998; Falcón-Barroso et al. 2004). Hence, the morphology points consistently to a scenario in which bar instabilities and secular evolution play a role of primal importance in the shaping of galactic morphology and especially in the formation of the inner central regions of disk galaxies.

Chapter 4

Vertical Structure

Apart from the investigations on the morphology of galaxies with a B/PS structure, it is also of great interest to characterize the vertical surface brightness distribution and distinguish different components with distinct scaleheights. Contrary to studies about the scalelength of a stellar disk in spiral galaxies a much lower number of publications investigates the vertical surface brightness distribution. Nevertheless, the shape and the underlying physics of the VSFBD is important to understand the structure of the stellar and gaseous disks of spiral galaxies. An important point in that context is the question, whether the scaleheight is constant over the whole disk or if there is an increase towards larger galactocentric distances (often called disk flaring). This is of great importance since that issue is strongly connected with the shape of the potential becoming less profound in the outer parts of the disk. Clearly, when the potential of the galaxies are discussed dark matter plays an important role. Hence, the vertical shape of the disk can give valuable insight also for the correct description of the dark matter halo.

The series of papers by van der Kruit & Searle (1981a,b, 1982a,b) was fundamental for this field. First, an elementary model deducing the function which could describe the VSFBD was developed (van der Kruit & Searle 1981b). Then the calculated functions are applied to observed galaxies with the result that the proposed functions are a quite good approximation of the VSFBD. The subsequent publications enlarge the number of galaxies where that analysis is applied and the approach extend to a three dimensional description of the SFB.

Most other studies following the previously mentioned ones concentrated on single case studies of edge-on galaxies focusing on objects where the small distance to the objects (and their size) favored a detailed study (e.g., *NGC 891*, *NGC 2531*, *NGC 6504*). Among that studies Wainscoat, Freeman, & Hyland (1989) Aoki, Hiromoto, Takami, & Okamura (1991), and van Dokkum, Peletier, de Grijs, & Balcells (1994) should be mentioned discussing the problem of the choice of the fitting functions to applicate. A clear statement could not be given since each galaxy showed individual characteristics preventing the affirmation of a more general picture (see also Chap. 4.1). An analysis detecting different scaleheights along the radial direction of the galaxy is that one of de Carvalho & da Costa (1987) studying the galaxy *NGC 1381*. Interestingly they relate to the main scaleheight variation — noted in the outer parts — to an outer ring with a large vertical scaleheight compared to that one in the inner parts. Although they note a smaller scaleheight variation ($\approx 30\%$) in the disk in the radial domain of the bar/lens component they do not relate this to the B/PS structure despite that they comment on the boxiness of the bulge. Hence, in that case the relation of

the B/PS region (and therefore the bar) and the disk component is not evidenced therefore the correlation between the shape of the B/PS region and disk evolution is not highlighted. Larger samples were analyzed by Barteldrees & Dettmar (1994) where they studied 27 edge-on spirals fitting the scalelength as well as the scaleheight. Also the series of papers by de Grijs & van der Kruit (1996); de Grijs & Peletier (1997); de Grijs et al. (1997); de Grijs (1998) addresses the issue of vertical scaleheight (but mostly in combination with a scalelength analysis). Those studies come to contradictory conclusions. They mainly confirm the constancy of scaleheight with increasing galactocentric radius (de Grijs et al. 1997) but they note also some clear signs of disk flaring detected in de Grijs & Peletier (1997). It has to be emphasized that those distinct results make clear that the subject is difficult to cover and it is difficult to extract unambiguous results. The additional fact, that the VSFBD is probably not a simple one-component function enhances the difficulties of an investigation. The previous doubts can be found across the majority of publications so that the question is far from being solved.

Addressing another aspect of the vertical structure of disks Schwarzkopf & Dettmar (2000b) and Schwarzkopf & Dettmar (2000a) investigated a sample of 110 highly inclined/edge-on disk galaxies. They studied the influence tidal interactions and minor mergers on disk properties and therefore also disk scalelengths and scaleheights. As a result they stated that concerning the vertical scaleheight it does increase (monotonically) in the outer parts for galaxies grouped in their sample of interacting/merging sample. But also perturbations on small and large scales were noted in both the non-interacting/merging as well as the interacting/merging sample. The perturbations were shallower in the non-interacting/merging cases. Reshetnikov & Combes (1997) also analyzed the consequences of interacting and merging on the scaleheight as well as the scalelength of disks in galaxies undergoing such processes. However, they come to a qualitatively different conclusion that within 20% the scaleheight remains constant along the disk of the sample galaxies. An additional driver for VSFBD studies is the discussion about the presence and characteristics of thick disks in galaxies. As an example Pohlen, Balcells, Lütticke, & Dettmar (2004) studied a sample of 8 early type edge-on galaxies to derive surface brightness levels and scaleheights of the thick disk component. Unfortunately it is not clear yet if a thick disk component is an integral part of spiral galaxy structure and how consequently relates to the other components. The (possible) presence of a young disk component (e.g., van der Kruit 1988; van Dokkum et al. 1994) close to the disk midplane does not influence the following approach since the K_n band traces mainly the old stellar population (see Chap. 1.2). It is intriguing that despite the studies carried out on the vertical structure of the stellar disk in edge-on disk galaxies no evidence for a local variation of scaleheight in the inner regions of galaxies was reported. This is much more surprising since galaxies with a B/PS structure are, as seen, quite prevalent among edge-on galaxies, and, as explained in Chap. 3.3.3, a change in scaleheight should have been detected. As will be seen in Chap. 4.2.1 the approaches of previous studies did not allow to detect in an unambiguous way that kind of scaleheight change.

More extended studies in the NIR wavelength regime¹ are still rather rare. Based on Two Micron All Sky Survey (2MASS) data Bizyaev & Mitronova (2002) have undertaken an analysis of edge-on galaxies in the K_s -band concluding that the vertical scaleheight of thin stellar galactic disks is almost independent of radius for galaxies in their sample. However, they state that 2MASS is not sensitive to the very faint parts of the galaxies so that the results are related in the main part to the thin disk. Further, Schwarzkopf & Dettmar (2000a)

¹and especially in the K -band

observed for their study a part of the galaxy sample in the K -band filter. Unfortunately the investigation was not aimed totally to the analysis of possible scaleheight variations in the NIR. Bizyaev & Kajsin (2004) have done an analysis on a (probably) intrinsic different type of galaxies i.e., LSB galaxies. Also there, the authors report no variation of the scaleheight with radial distance from the center of the galaxy. As a slightly different approach studying the vertical scaleheight i.e., the vertical structure of edge-on galaxies some paper focus on color gradients along the VSFBD. One of the most extended and recent studies of vertical color gradients is the work of Dalcanton & Bernstein (2002). They discuss the presence of a thick and old disk component around spiral galaxies differing also in the scalelength of the thin disk. A formation mechanism for this component is still strongly debated. The phenomenon of warps often detected in edge-on galaxies is not addressed in this work (see Chap. 4.3).

4.1 Fitting Functions

Most authors (e.g., Pohlen et al. 2004), fitting the vertical stellar distribution of the disks of spiral galaxies, use the "isothermal-distribution (Isothermal)" describing an isothermal sheet distribution of the stellar. It was originally introduced by Fuchs, Schlickeiser, & Thielheim (1976) and later reexamined and developed by van der Kruit & Searle (1981a,b, 1982a,b) (eq. 4.1). The distribution can be derived by assuming that the old stellar population is locally isothermal.

$$\Sigma_{isothermal}(z) = \Sigma_0 \cdot \text{sech}^2(z/h_z) \quad (4.1)$$

with Σ_0 as the central surface brightness and h_z as the vertical scaleheight.

NIR studies have shown an excess of light over the isothermal model at small distances where the optical photometry is strongly affected by dust absorption (e.g., Wainscoat et al. 1989; Aoki et al. 1991; van Dokkum et al. 1994). Van der Kruit (1988) proposed a more peaked distribution than the isothermal one, the "sech(z)-distribution (Sech(z))" (eq. 4.2) They took into account that near to the plane of the galaxy a deviation of the VSFBD from that one predicted by a locally isothermal disk situation could be present. This can be due to the presence of dynamically cooler stars close to the plane, in contrast to what is expected in the theory (see also Wainscoat et al. 1989)

$$\Sigma(z) = \Sigma_0 \cdot \text{sech}(z/h_z). \quad (4.2)$$

However, in the work of Wainscoat et al. (1989) the authors have argued that the z -dependence of the light in their analysis is more strongly peaked than an isothermal sheet model. That study stated that an exponential-distribution (Exponential) (eq. 4.3) fits much better the observed light distribution

$$\Sigma(z) = \Sigma_0 \cdot \exp(z/h_z). \quad (4.3)$$

But a pure exponential distribution also has as a consequence that the velocity dispersion in the plane of the galaxy should have a sharp minimum. This, though, has so far not been observed in disk galaxies. Fuchs & Wielen (1987) report moderate gradients much smaller than required for the exponential-distribution (see for the required values Bahcall 1984b,a). Thus, the correct description of the VSFBD remains controversial.

Also Aoki et al. (1991), studying the J , H and K -band light distribution in *NGC*891 confirm that the vertical distribution is fitted better by an exponential than by the isothermal sheet approach. Investigations of the Milky Way done by Gilmore & Reid (1983) and Pritchett

(1983) using star counts and by Kent, Dame, & Fazio (1991) using NIR images also determine the exponential distribution as the best fitting one for the vertical structure. As a further approach van der Kruit (1988) has grouped the $\text{sech}(z)$, $\text{sech}^2(z)$, and $\exp(z)$ distributions together resulting in a family of functions — the Generalized Sech (GSec) — based on the Sech(z) function

$$\Sigma_{\text{GSec}}(z) = \Sigma_0 \cdot \text{sech}^{2/n} \left(\frac{n \cdot z}{2 \cdot h_z^{\text{expo}}} \right). \quad (4.4)$$

Here, the shape of the function (expressed by the parameter $2/n$) and the scaleheight (h_z^{expo}) are fitted. The scaleheight is expressed in scaleheight units of the exponential function since in the limes of $n \rightarrow \infty$ the exponential function is obtained with the scaleheight being that one of the exponential distribution. Alternatively the scaleheight for each single distribution shaped by the parameter $2/n$ can be denoted as $h_z = 2/n \cdot h_z^{\text{expo}}$. As can be seen from eq. 4.4 in the case of $n = 1$ and $n = 2$ the $\text{sech}^2(z)$ and $\text{sech}(z)$ are obtained. Further it can be noted that for large values of z the functions of each particular distribution approach each other being in the limit of $z \rightarrow \infty$ indistinguishable. The characteristics of this family of functions is slightly different from the other generalized functions. What distinguishes it from other is the asymptotic behavior of one of the fitting parameters. For the parameter n in the expression $2/n$ used as an exponent for the $\text{sech}(z)$ function the limes towards large values ($n \rightarrow \infty$) results in the shape of the exponential function. This has as consequence that the value for $2/n$ tends in the limes to zero for the description of the exponential function. Furthermore, the exponential function is the more peaked one out of all described by the $\text{sech}^{2/n}(z)$ family (see van der Kruit 1988, their figure 1). That leads to the fact, that VSFBDs more peaked than an exponential can only be described by the same value of $2/n$.

In the case of studies determining the structural parameters of the central regions/bulges of spiral galaxies the utilization of the Sérsic Law (Sersic 1968, eq. 4.5) has gained attraction over the last years (Andredakis et al. 1995; Carollo, Stiavelli, & Mack 1998; Graham 2001):

$$\Sigma_{\text{Sersic}}(r) = \Sigma_e \cdot \exp \left\{ -b_n \left[\left(r/r_e \right)^{1/n} - 1 \right] \right\} \quad (4.5)$$

with r_e the half light radius, Σ_e as the surface brightness at r_e and n the shape parameter of the distribution. As a peculiarity of the Sérsic law there is also one constant b_n depending on n . The advantage of this approach is that it does not fix the shape of the function fitted to the observed distribution but selects the best fitting member of a family of functions. In fact, for the parameter characterizing the shape of the functions a dependence on galaxy type can be observed. That demonstrates that there is a physical basis on using a family of functions rather than simply functions with a fixed shape parameter.

In this thesis primarily the GGau (eq. 4.6) and a GaHe (eq. 4.7) series are used as fitting functions. The exponential, $\text{sech}(z)$, and $\text{sech}^2(z)$ fitting functions are used mainly for comparison and control purposes. As a further generalized approach the GSec is used. It consists of a generalization of the $\text{sech}(z)$, and $\text{sech}^2(z)$ resulting in a family of functions which has as an additional fitting parameter a variable describing the shape (see above). This is similar to the concept of the GGau and GaHe. Also the GSec approach will be used qualitatively and quantitatively but not on the same level as the GGau and the GaHe functions. The reason for that restriction is the fact that due to the structure of the GSec function family the resulting fits are rather instable (see also the equations eq. 4.4).

The Generalized Gaussian (introduced by Athanassoula & Misiriotis (2002), eq. 4.6) is — like the Sérsic Law — a family of functions describing a centrally peaked distribution

with a monotonical fall-off symmetric to the central maximum. They are characterized by 3 parameters: Σ_0 , the amplitude of the distribution which coincides with the central intensity of the vertical surface brightness distribution, h_z , the width of the distribution corresponding to the scaleheight at that point, and λ , the shape parameter. In the case of a Gaussian the parameters have the following values: $\Sigma_0 = \frac{1}{\sqrt{2\pi}\sigma}$, $r_0 = \sqrt{2}\sigma$, and $\lambda = 2$.

$$\Sigma_{\text{GGau}}(z) = \Sigma_0 \cdot \exp\left[-(|z|/h_z)^\lambda\right] \quad (4.6)$$

The equivalence between the Generalized Gaussian and the Sérsic Law is shown in **Appendix B**.

Apart from the Generalized Gaussian, also a set of orthogonal functions — the Gauss–Hermite series — was used as a second method for fitting the observed vertical surface brightness distribution of the galaxies. The Gauss–Hermite series was introduced by van der Marel & Franx (1993) to describe distributions which in first order are described by a Gaussian but have also asymmetric and symmetric deviations from it. Specially when analyzing stellar kinematics GaHe series are used to fit the observed line-of-sight velocity distributions (LOSVDs). In the case of the GaHe series deviations are characterized by higher order terms of the series. For the purpose of this thesis it is sufficient to use terms up to the fourth order since deviations from a Gaussian distribution are measured by the third and fourth order terms. Asymmetric deviations are described by the third order h_3 term whereas symmetric ones by the fourth order h_4 term:

$$\begin{aligned} \mathcal{L}_{\text{GaHe}}(z) = & \frac{\gamma}{\sqrt{2\pi}\sigma} \cdot \exp\left[-\left(\frac{z}{2\sigma}\right)^2\right] \\ & \times \left\{ 1 + \frac{\mathbf{h}_3}{\sqrt{6}} \left[2\sqrt{2} \left(\frac{z}{\sigma}\right)^3 - 3\sqrt{2} \left(\frac{z}{\sigma}\right) \right] + \frac{\mathbf{h}_4}{\sqrt{24}} \left[4 \left(\frac{z}{\sigma}\right)^4 - 12 \left(\frac{z}{\sigma}\right)^2 + 3 \right] \right\} \quad (4.7) \end{aligned}$$

with $\frac{\gamma}{\sqrt{2\pi}\sigma}$ as the central surface brightness of the vertical distribution, σ as the width of the distribution (corresponding to h_z of eq. 4.6 when multiplied by $\sqrt{2}$), and h_3 describing asymmetric deviations as well as h_4 describing symmetric deviations from a Gaussian. As van der Marel & Franx (1993) showed, the GaHe form a linear independent set of functions so that each distribution can be described by that set of functions (see also Chap. 4.2). This fact provides the fitting procedure more stability in determining the appropriate parameters (see also Chap. 4.3.4). The Generalized Gaussian, the Gauss–Hermite series representation, and the Generalized Sech were chosen as fitting functions because contrary to the others presented above, the concrete shape of the VSFBD is not fixed (apart symmetry around a central value and the existence of one global maximum at the center of the distribution). In the case of a Sech(z), Isothermal, or an Exponential-distribution the fitting procedure establishes the best fitting parameters but it does not testify if the fitting functions represent correctly the fitted distribution. Nevertheless each method on its own cannot give an exhaustive answer but only the combined analysis of all methods provides constraints on the correct shape of the VSFBD. The Generalized Gaussian approach e.g., is very well suited to determine the peakness of a given distribution. Furthermore, it has the possibility to fit Gaussian as well exponential functions so that it is possible to judge on this fitting approach what function type (the former or the latter) is present. On the other hand large gradients in the center of the RSFBP are difficult to handle² as will be seen in Chap. 4.3.4. Therefore, the GSec and

²This is the case due to the implementation of the fitting routine used in the present study. Hence, it is an technical issue not a conceptual one.

especially the GaHe approach do contribute to an independent description as the RSFBP is correctly reproduced. Apart from that each method is a benchmark for the other ones to check if some characteristic features are consistently reproduced in the other approaches.

Since the purpose of the analysis is not only to provide arbitrary parameters describing the vertical surface brightness distribution in the observed galaxies but also to give values comparable to that ones determined for simulations by Athanassoula & Misiriotis (2002), the Generalized Gaussian was chosen as primary fitting parameters. Often studies analyzing data obtained by observational astronomy and studies of numerically simulated objects are difficult to compare. It is often the case that each study uses the analysis methods which are best suited for its purpose. Therefore, it can well be the case that a family of functions used to analyze the SFBD of simulated galaxies is not the optimal choice for the investigation of galaxies stemming observational astronomy (for methods analyzing the SFBD of simulated galaxies see also Appendix A).

4.2 Fitting Technique and Parameters

The fitting program works with images in the 'fits' format. In order to avoid perturbation of the fit results by the additional light contribution of foreground stars frames with stars masked out were used as input to the fitting routine. For the purpose of the fitting the background interpolated values replacing the area covered by stars is not precise enough to ensure a correct fitting. When encountered an interpolated region the masked pixels are skipped and therefore not used in the fitting procedure. It has turned out that fitting intensities instead of magnitudes gives better results since in the case of the intensities the higher S/N regions — i.e., the regions around the equatorial plane of the galaxy — are fitted more precisely than in the case of magnitudes (fitting in magnitudes results in giving a higher weight to the outer parts). Apart from this, no special weighting depending on position was applied to the pixel values.

One of the most important differences between the methods mentioned in the literature and the present approach for the determination of the disk scaleheight is the extended spatial sampling of the galaxy. Each column of the digitized image is analyzed independently from the other ones. This enables a detailed analysis of variations along the radial extension of the object. The canonical fitting methods for different components in the galaxy have given valuable results like the discovery of the radial exponential decline in surface brightness of galactic disks. On the other hand fixing the fitting procedure to a global approach i.e., to give results valid for the whole extension of the galaxy resulted in a conglomeration of small but distinct components. Balcells, Graham, Domínguez-Palmero, & Peletier (2003) show that the SFBD of early-type galaxy bulges does not follow a $R^{1/4}$ -law profile but has a shallower SFBD (but see also Scarlata et al. 2004). They blame the seeing which comes along with all ground-based observations to smooth out small scale structure present in the center of the galaxies as e.g., point-like central sources or nuclear disks or bars. But apart from the seeing it is already the assumption that the complete central region is build up by only *one* component which does lead to partly erroneous conclusions. As can be seen in e.g., Erwin et al. (2003) and Laurikainen, Salo, & Buta (2005), additional components, compared to 'classical' ones for structure decomposition in disk galaxies, have to be taken into account. An alternative procedure is that used e.g., by Aguerra, Elias-Rosa, Corsini, & Muñoz-Tuñón (2005) who simply excluded a central region of about twice of the FWHM of their point spread function (PSF).

That method should avoid the fitting of unresolved nuclear components blending with the 'genuine' bulge light. However, all this technical problems could be set in a larger context. Taking another point of view it could be argued, that there is no 'genuine' bulge contribution at all because there is no bulge component as defined in the classical way (see Chap. 1.3). Despite the fact that this study does use only a one-component approach, it is still sensible to small scale variations since it analyzes each token of information (i.e., column) separately.

Another issue influencing the resulting vertical scaleheight consists of the part of the VSFBD used for the fit. Depending on the position and the range used of the VSFBD, different fitting results can be obtained. Therefore, for this study a fitting procedure is implemented which starts at the MJA using a minimum range of $2.5''$ centered around the galactic plane and enlarging the range successively in steps of $1.0''$. Each range is fitted and the resulting fit parameters stored. Through this method a sequence of resulting fit parameters is calculated which are then analyzed for the correct parameter set. No specific outer limits in the vertical direction are defined so that the whole area observed is used for the analysis.

With the above described method each column of the image has not only one set of the used fit parameters but a sequence according to the number of fit ranges used. At that point a parameter set describing the whole VSFBD at that column has to be determined. For each column the 30 calculated fit parameters values are extracted which correspond to the 30 largest fit ranges used. As next step out of that 25 parameter values were selected excluding the 5 parameter values corresponding again to the 5 largest fit ranges. The last 5 values are excluded to avoid perturbations by reduction artefacts at the outer edges of the images. The selected values are used as a data set to calculate the mean value and the standard deviation. The exclusion of the fitting values of the innermost fit ranges is due to the fact that the fit of a low number of pixels is sensitive to any small change. Otherwise the fit would be dominated by the inner data points due to their rather high value compared to the outer regions. Using the part of the outermost 30 fitted values avoids that possible dust lanes and patches near to the equatorial plane — and therefore influencing the first fitting ranges — alter the results of the fitting. In an ideal situation the outer fitted parameter values should be identical because when a sufficient number of column pixels is reached (i.e., a sufficient large fit range) the fitting process should give stable and identical results. This is only the case when no perturbations are present to alter the VSFBD of the galaxy assuming a monotonically decreasing VSFBD. The definition of the radial extent of the galaxy and consequently the region where the fit has to be applied is based on the determination of the first negative intensity value starting from the maximum at the galaxy center. This procedure is done on both sides of the galaxy center using then as limit the larger range ensuring an exhaustive use of the available data.

In the case of the GGau approach 3 free parameters were fitted: the amplitude Σ_0 , the width of the distribution z_0 (in arcseconds) and the shape of the function λ . For the Gauss–Hermite series 4 parameters were fitted: The width of the distribution σ , the value at the central position Σ_0 , the h_3 and h_4 parameters describing the symmetric and asymmetric departures from a pure exponential distribution. Also in the case of the GSec approach 3 parameters were used to fit the VSFBD, i.e., the amplitude Σ_0 , the shape parameter $2/n$, and finally the scaleheight h_z^{expo} . Obviously in the case of fixed shapes like in the case of the Exponential, the Sech(z), and the Isothermal distribution only 2 parameter were used, i.e., the amplitude Σ_0 and the scaleheight h_z .

During the fitting procedure an additional fit parameter was used, apart from the that ones needed to fix the functional shape of the VSFBD. The additional fitting parameter is

introduced for technical reasons in the implementation of the fitting routine. It accounts for the possibility that the VSFBD is off-centered from the MJA i.e., the argument of the fitting functions (z) is replaced by $z - z_0$ with z_0 as the additional fitting parameter. Since the fitted functions have a global maximum and are monotonically decreasing on both sides of the global maximum, correct centering around the maximum of the observed VSFBD has to be assured. This deviation is not listed in the diagrams and tables showing the results. Asymmetries in the observed distributions can arise from inclination effects or dust lanes and patches still visible in the K_n -band. Another source of such is the not correct alignment along the image row defined as central plane. Especially in the outer parts of the galaxy a deviation of the positions of the maximum in the SFB is possible. A prototypical example is *NGC 0128* where one side of the galactic plane is strongly bent. The introduced correction (z_0) is a first order correction. As the case of *NGC 0128* illustrates, a further improvement of the correction would consist in fitting the course of the maximum SFB. The VSFBD is then not represented by the pixel column at that radial position but by the straight line perpendicular to the fitted maximum SFB course. That would need a resampling of the SFB on a different pixel matrix. Since that correction is a higher order effect, this is not applied.

When implementing the fitting program also the convolution of the original intensity distribution of the galaxy by the seeing was taken into account. This is not done by a deconvolution of the data but instead by convolution of the calculated model through a Gaussian representing the seeing. Numerically the convolution is carried out by the calculation of the Fourier transform of the model and seeing function. For that purpose the subroutine 'CONVLV' was used provided by the 'Numerical Recipes in C'. Finally the convolved model is then fitted by the routine and the results used for the next iteration until a stable solution is found. The values of the FWHM of the seeing were determined during the data reduction (see Chap. 2.6).

Further, the fitting procedure takes care of the fact that the pixels of the galaxy image form a grid collecting the light of an area of the galaxy and do not represent the light at one position. That is the reason why the true vertical light distribution is not simply the function value of the model calculated at the center of a pixel but has to be the accumulated light contribution of the galaxy stored in one pixel. Therefore, the comparison during the fitting routine has not be done between the model value at one point and the data but between the integrated values of the model over a pixel and the data value using the trapezoidal interpolation rule.

For the minimization itself the present study made use of the 'MINPACK' package (Moré, Garbow, & Hillstrom 1980; Moré, Sorensen, Hillstrom, & Garbow 1984) freely available on the World Wide Web³. 'MINPACK' is a collection of subroutines developed at the Argonne National Laboratory, Illinois for solving a set of non-linear equations. The subroutine 'lmdif' was suited best for the purposes of this project. It is based on a modified Levenberg-Marquardt algorithm using the forward-difference approximation method for the least square fitting. The fitting functions which have been used require a non-linear approach so that other (and simpler) linear fitting routines could not be used. Hence, all methods are non-linear fitting methods (denoted by the extension 'non-linear' i.e., 'NL'). Initial estimates do not need to be very close to the real values so that the fitting procedure is rather stable against such choices reducing the dependence of technical implementations.

To test the reliability of the minimization routine as well as the whole program, several

³<http://www.netlib.org/minpack/>

tests runs were done with predefined input data in order that it was possible to relate the fit results uniquely to the input data. One of these tests consisted in using artificially created images with the values the pixels set according to the course of a GGau. The parameters characterizing the function were set to depend linearly on the position of the column. As a consequence each column of the artificial fits image has a slightly different surface brightness distribution. The value of sigma starts at 5 pixel and is increased at each successive step by 0.1 reaching its maximum value after 100 steps. For the lambda parameter the same procedure was adopted but starting at a value of 1 and using an increment of 0.02 per step and a maximum value of 3. The amplitude was set to 1 for each case. Through this method the width as well as the shape of the distribution are changed. In the test case a seeing whose function shape follows a Gaussian with a FWHM of 15 pixels was applied. In order to run the test under similar conditions as for the galaxy images the same settings (e.g., a pixel scale of 0.5pix/arcsec) were used. For that test runs an extremely good retrieval of the input parameters through the fitting procedure was achieved. Concerning the concept of the present fitting procedure it has been shown that it is able to determine the parameters of observed objects. Clearly, the disadvantage of low S/N in observed objects cannot be avoided.

The S/N ratio can be improved by an application of a binning of the data in the radial as well in the vertical direction. A vertical binning is problematic since regions which are masked out above or below the galactic plane would influence such a binning and reduce further the available signal to be fitted. Concerning the radial binning several studies do apply such a method for their profiles (see Chap. 4.2.1). As this study aims to use at its maximum the spatial resolution information made available by the data, a binning would have a contrary effect. Nevertheless for each galaxy also a radial binning of 3 and 5 columns (corresponding to a radial spatial resolution of 1.5'' and 2.5'') was applied during the fitting runs. A larger binning would go contrary to the aim of good spatial resolution. Using this binning extend clearly does not increase much the S/N ratio but a larger one (e.g., increasing the S/N -ratio by factor of 5 means a binning of 12.5'') would loose severely information concerning the spatial resolution. At least for the 1.5'' and 2.5'' binning the same qualitative and quantitative results have been obtained.

4.2.1 Analysis methods of other studies

In studies of disk parameters in edge-on disk galaxies the approaches for the determination of the scaleheight are various. Contrary to the scalelength, in the case of the scaleheight, there are much more possible positions for a measurement. The radial extent is by far larger than the vertical one.

As described in Chap. 4 Aoki et al. (1991) have undertaken an analysis of vertical scaleheights in the NIR regime applied on the edge-on galaxy *NGC 891*. Their analysis was based on a few (4) cuts parallel to the MJA on the south western side of the galactic plane. The results point to an exponential as the best fitting function for the VSFBD of the disk. Since the cuts used are well outside the bulge region (*NGC 891* is an object with a prominent B/PS structure) but still not in the outer disk region, they state that the scaleheight is constant along the sampled distance. The fact that *NGC 891* is an object with a B/PS structure makes it probable that the sampled area is dominated by a side-on bar. Therefore, the best fitting function could be a result of fitting the bar region (see Chap. 4.3.3 for a description of the shape of the VSFBD of that component).

In the analysis done by van Dokkum et al. (1994) they examine *NGC 6504* in 6 wavelength bands from the (near) ultraviolet to the near infrared. Also there, as in the previously presented study, they investigated only a few fixed positions (6) spread along the galaxy. It is not clear if the galaxy is barred but its small and spheroidal bulge shape (LEDA classification: Sc) does not imply a side-on bar. Also the presence of a lens is not known but the rather late-type of the galaxy should make this improbable. Hence, especially for the regions outside the bulge region a possible exponential shape of the VSFBD could be detected if present. In fact, in the inner part the profiles are best fitted by an exponential-distribution. However, shifting radially to the outer parts the $\text{sech}(z)$ -distribution does also fit the data points well. For the Isothermal distribution only the outermost profiles can be claimed as satisfying. Nevertheless, they conclude that in the inner to intermediate parts of the galaxy the combination of the stars and dust in the young disk with the light of the thin (old) disk results in an exponential profile. The thin disk should be better fitted by a $\text{sech}(z)$ or $\text{sech}^2(z)$. Again, in this case no complete sampling of the disk has been undertaken.

For a deeper understanding of the formation of S0 galaxies surface photometry was a major topic in de Carvalho & da Costa (1987), investigating the galaxy *NGC 1381*. In their work special attention was paid to an outer ring detected in the observations. The authors applied a decomposition of the different galactic components to subtract the disk component in a second step. Through that procedure the disk parameters scalelength, scaleheight, and central surface brightness were determined. In total they used 9 vertical profiles for their analysis. As the result of a general discussion they state that their assumption for the model of the galaxy (spheroidal bulge, disk, bar, outer ring) fits rather well the data but some localized departures from the observation were still detected. For this galaxy, with the introduction of different components, also different scaleheights were used. But as described in Chap. 4.3.2 the variation of the scaleheight in the region where the B/PS feature is present has been missed.

A slightly different approach using vertical cuts is applied in Bizyaev & Kajsin (2004). They determine the scaleheight by averaging over 10 to 14 vertical cuts at different positions. No special weighting is used since no quantitative variations in the scaleheight are detected. Their sample does not contain any edge-on galaxies with a B/PS structure due to their selection criterion selecting only LSB galaxies. Hence, the assumption of constancy is on first order acceptable since no obvious variations are detected. Nevertheless, other variations due to an intrinsic change of the underlying structure are not analyzed in depth.

At the beginning of a series of papers de Grijs & van der Kruit (1996) have analyzed a pilot sample of edge-on galaxies spanning from early to late Hubble types. That sample was observed in the optical B -, V -, R - and I -band. The determination of the vertical scaleheight was also based on particular positions along the MJA but with a restriction in the vertical range. Especially in late-type galaxies the presence of dust prevents an undisturbed view on the galactic plane. Therefore, an inner region parallel to the galactic plane is excluded and in the outer parts, to avoid a possibly present thick disk component, an outer limit is applied. Through the usage of a more sophisticated approach for the fitting where different functions in combination with goodness-of-fit parameter were used, the complete vertical SFBD was taken into account. For a part of the early-type galaxies in the sample two components were used for the fitting to follow also the thick disk part. The inclusion of a thick disk improved the fit noticeably. Interestingly a comparison between the fits taking into account the complete vertical range and that ones applying exclusively an inner limit (to avoid dust contribution) does not give large distinct results. Further, the authors remark that, concerning the fitting

procedure, the results for the scaleheight obtained by applying an exponential with inner *and* outer limits is a good starting point for a discussion of its behavior. Distinguishing between the three functions described in eq. 4.1 – eq. 4.3 they claim that the exponential and the simple sech function fit the data best. It is worth to note, that the authors pay attention to possible bulge light contribution at large vertical as well as *radial* distances. That is clearly the case if the bulge component is described by an $R^{1/4}$ -law but which in last years (as described previously) is more and more questioned.

The subsequent paper of that series (de Grijs & Peletier 1997) extend the analysis to 48 edge-on galaxies based on the same analysis method as described in de Grijs & van der Kruit (1996). The extraction of positions was managed in that way that a considerable number of profiles were obtained at positions outside of the region where the bulge dominates the other components. In order to avoid possible dust contamination in the case of not perfectly edge-on orientations a distinction between different sides of the plane of the galaxy was adopted. Again, as in de Grijs & van der Kruit (1996), the central plane was not taken into account into the fit excluding a range of $\approx 1.5 - 2.0$ scaleheights starting from the galactic plane. Taking into account a possible influence of bulge light they also tested at which distance from the center the bulge light could be considered to be negligible (i.e., less than 5% of the total light).

A subsequent analysis of the vertical structure (de Grijs et al. 1997) was done in a longer wavelength domain (*I*- and *K*-band). The main focus of that study was on the *K'*-band data in order to use the advantages of that wavelength band as the present study does. As in de Grijs & van der Kruit (1996) also in de Grijs et al. (1997) only at certain positions along the MJA vertical profiles were extracted (in average at ≈ 6 positions). Furthermore, in order to achieve an approximately constant overall *S/N* ratio, the profiles were binned in radial as well as vertical position but it was not applied near to the galactic plane. The same extraction procedure for the profiles as in de Grijs & Peletier (1997) was adopted except that a folding of both sides — above and below the galactic plane — was introduced. In contrast to the previous publications a family of functions was applied to the VSFBD. In a first step, a family of functions equivalent to eq. 4.4 was used. Further, to check the results obtained through the first method, also functions with a fixed shape ($2/n$) parameter were applied. The analysis showed that the 3 parameter fit (including the shape ($2/n$) parameter) are quite reliable indicators of the profiles' shape.

Shaw & Gilmore (1989) introduced a multi-component fit based on the 2-dimensional SFBD of edge-on galaxies. Their aim was to develop a method with which a fitted parameter set could be judged in an objective way. In a first attempt they tried to fit their galaxies with a 2-component approach. As a general result they argued that the $\text{sech}^2(z)$ cannot, as stated by Shaw & Gilmore (1989), be preferred to the exponential one for *NGC 891* because there, no statistically significant distinction based on objective parameters between both can be made. This is an important statement since some more recent studies of the disk parameters still rely on visual inspection and treat the $\text{sech}^2(z)$ distribution as first reference for the VSFBD fitting. In the case of *NGC 4565* the authors opted for a 3-component structure instead of the canonical 2-component one. But they also note that the higher the number of components used the more arbitrary the results can be interpreted, as can be expected.

In a work focusing on flattening and truncations of edge-on spirals Kregel et al. (2002) have chosen a decomposition approach to fix the disk scale parameters relying on the 2-dimensional SFB information. A bulge and disk component were used to fit the spiral galaxy. With that approach clearly an average scaleheight is determined smoothing out local differ-

ences.

For their analysis of the disk scalelength (Pohlen et al. 2000a, Pohlen et al. 2000b, and Pohlen et al. 2004) have made use of a 3-dimensional disk model. Therefore, also a scaleheight was included into their calculations. In that analysis they focused on the large scale structure of the disk component(s) so that for the scaleheight determination variations in the central or intermediate regions are of limited interest. Hence, it is not surprising that even for galaxies overlapping with the sample used in this study no comments on variations or the determination process of the scaleheight are mentioned. It is the global (over the complete extension of the disk and in all parameters) matching of the model with the data that is payed attention to and not the variations in certain regions. Masks or exclusions of galactic regions were not applied to the investigated sample.

Summarizing, two distinct approaches have been applied for the determination of the vertical scaleheight: One method consists in analyzing the scaleheight at some fixed radial positions from the galactic center, with a possible additional averaging over the obtained values. That method is certainly easy to implement and does not take a lot of resources when applied but does not sample completely the galaxy. Moreover, it depends strongly on the positions where the vertical cuts are applied. Often the positions are selected on assumptions or suppositions where some change may occur or some physical mechanisms are at work shaping the VSFBD. This is especially the case when an averaging over the resulting values is done implying a constancy throughout the analyzed region. But through this way a lot of substructure present in the disk can be missed. Additionally to the above described studies also de Carvalho & da Costa (1987); Barteldrees & Dettmar (1994) use this kind of method. The other procedure is based more on the global shape of the disk component fixing the additional parameter of scalelength and central SFB value unambiguously. This method is based on the assumption that there is — in the analyzed region — only one component corresponding to a disk. The advantage of that approach is the usage of a large range of data since the global shape of the disk has to be fitted. However, local changes are not revealed by such a method. Therefore, more complex structures in the disk region are not taken into account and other effects of that complexity may trigger an evolution in the picture of galaxy structure. Besides de Carvalho & da Costa (1987) also de Carvalho & da Costa (1987) follow that method as well as van Dokkum et al. (1994) and the investigations of Schwarzkopf & Dettmar (2000a, 2001).

In the present study this is avoided since the scaleheight is first investigated and then structure models are build out of it. It is clear, that an extended study of scaleheight cannot be accomplished when a global disk model is fitted to the entire disk component. There, the model implies a constant scaleheight for the complete disk component. Also the method of the other types of studies is not suited for the purposes of this thesis since the large variety of morphological structure in barred edge-on galaxies makes it difficult to select only few positions at which a scaleheight analysis is done. Moreover, it is the aim of the present approach to detect possible changes and analyze the areas where such a change takes place. Especially variations in the region of the B/PS structure variations on spatial small scale can and as already shown in Chapter 3.3.3 do appear. The chosen wavelength range for the observation of the presented galaxy sample bears the possibility to fully use the spatial information without excluding areas obscured by dust or dominated by a young star population.

4.3 Results

The usage of one component fitting functions could be generally a problem since it is known that especially early-type galaxies have an additional thick disk component appearing as an envelope around the disk galaxy. In this study it is possible to neglect to first order this component because the data is not sensitive enough to an extended contribution of a thick disk component in the outer parts of the VSFBD. This does not mean that no surface brightness contribution at all originating from the thick disk is observed but its contribution is negligible for the inner parts of the vertical extension which are primarily studied here. Dalcanton & Bernstein (2002) use K_s -band data to generate optical-NIR color maps for their color gradients to analyze possible difference due to thick disk component. They state that their data in the K_s -band reaches $22.5\text{mag}/\text{arcsec}^2$. The present data set has generally a detection limit of about $20.5\text{mag}/\text{arcsec}^2$ in the K_n -band (see Chap. 3.4) which is too high to enable a profound analysis of thick disk components. Only a few objects reach a deeper surface brightness. However, this is not a disadvantage. Nevertheless different components, e.g., the thick disk, can be relevant for the fitting approach. That has to be taken into account in the case they can be distinguished in terms of specific regions in the *radial* extension of the disk component. This is clearly the case for the bar and/or lens showing, as will be discussed in Chap. 4.3.2, different scaleheight characteristics. In fact, a change of scaleheight along the radial direction could be a sign of the dominance in the SFB of distinct components. When dealing with SFBs in spiral galaxies it has been important in the past to take into account also the bulge contribution in the outer (vertical and radial) parts of the galaxy. This was due to the fact that until ≈ 15 years ago the bulge was mainly described by an $R^{1/4}$ -law which is known to give at large r or z a higher contribution than any of the in Chap. 4.1 discussed disk VSFBDs. Since in several studies (see Chap. 1.3) it has been shown that the classical approach of describing the bulge with the $R^{1/4}$ -law is not straightforward (or even not correct) the present study will not consider any influence at large scaleheights of the bulge component.

Another problem for the VSFBD fitting can arise from warping of galactic disks. There, it is probably worthwhile to distinguish between a warping affecting large parts of the visible galactic disk and warping in the outer regions of the disk. The former type of warping is quite strongly connected to interactions. In the present sample some galaxies show the first kind of warping (*NGC 0128* is perhaps the most prominent example). For such cases it is obvious that fitting results obtained in the region(s) affected by the warping are rather less meaningful. Concerning the second type of warping it can be made the assumption that it does not alter the determined fitting values. This is again due to the fact that the used data is not deep enough to follow the galaxy structure up to the regions/radial extensions where this type of warping strongly shapes the galactic disk.

A larger ambiguity can arise in the central regions of the galaxy (but still in the galactic plane). There, blending of light from distinct components but residing in the same location is still possible, actually highly probable. This is the case for the blending of a central component and disk light as well as bar/lens and disk light. A fitting routine taking care of that fact by using a multicomponent fit would not resolve the problem since there is no clearly defined region where the distinct component would be predominant. However, there seems to be a region where some blending is visible. In order to circumscribe the region where this happens it is of advantage to describe the two neighboring areas where it is possible to assert one component as first order contribution to the SFB. The first one is the area of the local

maximum of scaleheight coinciding with the maximum extent of the B/PS structure visible in the photometric panel. The main contribution to the SFB should be a bar component which forms the B/PS structure.

4.3.1 The VSFBD

In general each fitting procedure shows its own characteristics and therefore also qualitatively different conclusions can be drawn based on the different approaches. Therefore, all features visible in all approaches will be presented. Clearly, each feature can have different signatures in the different fitting approaches. In the following mainly the GGau, GaHe and GSec approach will be taken into account when describing qualitatively the scaleheight and the shape parameters. The Sech(z), Isothermal, and the Exponential approach are used when necessary as a comparison. In the case of the latter 3 approaches all described features are less pronounced and differ only slightly between each of the fitted distributions. Therefore, it gives more insight if the generalized fitting functions are discussed primarily. Around the center of the galaxies the courses of the graph representing the fitted parameters are (or should be) symmetric to it. Exceptions are the cases where sources of alteration of the regular SFB are present like irregular dust patches, deformations due to interaction, and locally confined enhanced emission due to star formation. Therefore, it is possible to focus the description just on one side of the galactic center making exceptions only when the deviation of this symmetry can unambiguously be used to gain deeper insight in the dynamics of that galaxy. As a preliminary, all galaxies which are classified as 'I' (inclined, see Tab. 3.2) are excluded from the following discussion. Galaxies which are not exactly edge-on but still classified as 'Q' (quasi-edge-on) can be included in the analysis. This galaxies will deviate only by a few (from 1° to 5°) from an exact edge-on position but can be still used for the study since down to an inclination of 86° the slope of the radial as well vertical SFB profiles does not change (van der Kruit & Searle 1981b).

4.3.2 Scaleheight

The scaleheight in all galaxies shows a characteristic minimum in the center of the galaxy. This can be understood through the fact that in the SFB plots of the galaxies the center is rather bright and has strong gradients in the SFB (see Chap. 3.4.1). The described gradients are not only visible in the radial direction but also in the vertical one so that as a natural consequence a scaleheight variation is expected. Large SFB gradients then translate into small scaleheights. In fact, in the case of the Generalized Gaussian non linear fitting (GGauNL) approach also some discontinuities are detected. This is nearly not the case in the Gauss-Hermite non linear fitting (GaHeNL) approach. A deeper analysis of that can be found in Chap. 4.3.4. Delimiting the described minimum, small local maxima symmetric to the center are visible. This is only true for the galaxies hosting a B/PS structure. Galaxies with a spheroidal bulge component showing no substructure in the unsharp masked images (e.g., *NGC 1032*) do not show such a variation in scaleheight. Such kind of galaxies are *NGC 1032*, *NGC 5084* and *IC 5176* (see Appendix D). It is worthwhile to note that only 3 galaxies out of a sample of 30 show a non varying scaleheight in the regions near to but outside the center. In the framework of the formation scenario of B/PS features this result can be interpreted rather intuitively since the vertical redistribution of material into B/PS region does deplete the region in the galactic region of material. That redistribution has then

the effect of increasing the scaleheight in the considered regions.

Further out the scaleheight is dominated by a slight decrease forming then a plateau at low values or by a clearly defined minimum. Good examples for the extended plateau are e.g., *IC 5096* and for the confined minimum *NGC 2788A*. For radii larger than the extension of the B/PS feature the disk with either a bar or a lens dominates the SFB and therefore also the results for the vertical scaleheight. In general there are 2 categories of profiles. First, 16 galaxies show profiles where there is no plateau but just a minimum which is related to the end of the bar/lens signature in the RSFBP. A prototypical example is *ESO 151-G004* where the clearly detected bar (kinematics, RSFBP) does not have a constant scaleheight along its extension. The other type of signature shows an extended region where the scaleheight stays rather constant (variations of $\approx 10 - 20\%$). As a good example *NGC 1381* can be cited and (partially) *ESO 443-G042* shows the described behavior. In total 10 galaxies of the sample show this kind of scaleheight course. However, it has to be emphasized that the extension of the region with constant scaleheight is much more pronounced in *NGC 1381* which has a more spheroidal bulge and probably a lens component as discussed in Chap. 3.3.3 and Chap. 3.3.5. Interestingly the unsharp masked image shows a clear CX (App. C) probably resulting from a bar which is not completely end-on. Furthermore, *IC 5096* harboring a spheroidal bulge shape and *IC 5176* as a galaxy with the latest Hubble-type in the sample, exhibit also a pronounced region of constant scaleheight. Contrary to that *NGC 1886*, a galaxy with a clear and pronounced B/PS structure, does not show any region of constant scaleheight but a gently decreasing course from the B/PS structure maximum to the end of the bar. If the best examples of a constant scaleheight outside the bulge and accordingly the B/PS structure are considered (*NGC 1381, IC 5096*) it has to be indeed stated that this kind of scaleheight structure is a signature for lens components in accordance with that ones described in Chap. 3.3.5.

In the case of the fixed shape fitting functions (Sech(z), Isothermal, and Exponential) the galaxies, in regions where the other approaches show a marked minimum, harbor a rather shallow minimum. This can be mistaken as a constant scaleheight region. That is a result of the fact that differences primarily intrinsic to the shape cannot be detected. Interpreting that fact as a concrete disadvantage it becomes clear that the fixed fitting functions are not best suited to discuss such characteristics of disk scaleheights. Following this argument it gives the base for a discussion of previous studies using that functions for a description of the shape of the VSFBD. The fixed shape of the functions does not permit to detect intrinsic changes of the shape. In previous studies the focus was set to analyze and discuss the (constancy of the) scaleheight not paying much attention to a possible change of structure in the vertical direction.

The distinction between bar/lens region⁴ and the other (remaining) disk domains can be surprising at the first glance but has in fact a clearly defined base since the scaleheight structure in the disk regions beyond the bar/lens is completely different. Despite the fact, that the S/N ratio does decrease strongly beyond the bar/lens component, it is possible to claim a change of scaleheight and shape of the fitting function beyond the end of the inner component. In all galaxies of the sample the scaleheight increases towards the outermost edge of the galaxy. Whatever kind of component is present in the inner parts, the rise of the scaleheight in the outer part is detected at a position where the scaleheight has reached a minimum (or remained constant) compared to the innermost regions. The possible reasons

⁴In the following the region comprising a bar and/or a lens will be abbreviated with this term.

for that rise will be discussed in Chap. 4.3.8.

It is obvious that the different fitting approaches do have slightly different results (except the GSec approach) compared to each other. As a proof for the consistency of the described fitting procedures, it can be stated that the values for the scaleheight differ *only* slightly. They are rigorously in the same order of magnitudes.

4.3.3 Shape of the VSFBD

Also in the case of the shape parameters a qualitative congruence of the course of the different approaches can be stated. It is clear that a straightforward comparison between the GaHe approach on one hand and the GGau and GSec on the other is not possible. The two parameters describing the shape of the VSFBD in the GaHe approach are qualitatively different to the single parameter in the other two approaches. Even for the GSec and the GGau approach some qualitative differences can be observed. As described in Chap. 4.1 the characteristics of the $2/n$ parameter of the GSec family of functions has an asymptotic behavior for one special shape i.e., when the VSFBD is best described by an exponential function. Nevertheless, a non sophisticated comparison between the GGau and GSec fitting method can be accomplished. Due to its simplicity as first description the course of the shape parameter in the GGau approach is selected and the corresponding features in the GSec approach are compared to it. At the end the characteristics of the shape parameter obtained through the GaHe description are analyzed.

Typically also the shape parameter λ (similar to the scaleheight) has a global minimum in the center of the galaxy. The shape of the innermost central areas are in the case of 22 galaxies of the sample (excluding the galaxies classified as inclined) more peaked than an exponential distribution. This is consistently observed also in the $2/n$ parameter of the GSec fitting functions. In the central region the value of that parameter tends to zero revealing a functional shape of the VSFBD at least as peaked as the exponential one. Shifting to larger galactocentric distances the shape parameter rises on both sides of the galactic center. In the case of the GSec results the values approach a shape near to a $\text{Sech}(z)$ or Isothermal, in some cases also a $\text{sech}^{2/n}(z)$ with a higher exponent. Indeed, this happens in the B/PS structure region and the rise of the value does terminate, reaching a local maximum nearly at the same position where the scaleheight shows a local maximum. Also here, as in the case of the scaleheight, this is expected when the proposed formation mechanism for a B/PS feature is taken into account. The redistribution in the vertical direction of galactic plane material induces a more flat topped VSFBD than in the surrounding areas. Simply, luminous material is taken from the area where the peak in the VSFBD is located and deposited in areas where the usual VSFBD (without an instability forming a B/PS structure) decreases. Interestingly in cases where the shape parameter λ does not exceed values representing an isothermal–distribution⁵ a strong dichotomy of values can be observed. The values at the maxima are either consistent with an isothermal–distribution or a $\text{sech}(z)$ –distribution (see Tab. 4.1). In some cases the values of the $2/n$ parameter do not correspond precisely to that one of a $\text{Sech}(z)$ – or isothermal–distribution but are intermediate. Nevertheless, it is possible to relate them stronger to one or the other distribution; e.g., in some cases one maximum does not represent precisely one of the two proposed distributions but the other does so. Apparently there is a loose correlation between the late–type galaxies and the func-

⁵Either because the galaxy is not exactly edge–on preventing an ”a priori” reliable measurement or because of an intrinsic structure inducing large values.

tional shape described by a $\text{Sech}(z)$. Excluding the galaxies classified as inclined there are 8 galaxies in the range of the Hubble-type **Sb** to **Sc**. Among those galaxies 4 show a functional shape best described by a $\text{sech}(z)$ -distribution whereas 2 of them are best described by an isothermal-distribution. Finally the remaining 2 galaxies were not possible to classify. For early-type galaxies no correlation between the functional shape of VSFBD in the B/PS region and Hubble-type can be stated. Indeed, 3 galaxies have an isothermal-distribution compared to the 2 with a $\text{sech}(z)$ -distribution. The number of galaxies for each bin shows a nearly perfect equipartition of the occurrence of both VSFBDs. In fact 6 galaxies reveal a shape of the VSFBD best described by a $\text{Sech}(z)$ and 6 galaxies with a vertical shape best described by an Isothermal (Tab. 4.1). This corresponds in both cases to $\approx 20\%$ of objects of the used sample (including also the control sample galaxies). As stated it shows up that it is a rather pronounced dichotomy with nearly no case showing a value between the two distributions. An analysis of the literature concerning the shape of the VSFBD does not evidence any statement describing such an observation. Until now there is also no description what kind of shape the VSFBD follows after the B/PS structure has been developed. Further, any correlation between the shape of the X-structure and the presence of any of the functional shapes can be detected. As can be seen in Tab. 4.1 the presence of $\text{sech}(z)$ -distribution and the isothermal-distribution is equally probable for galaxies with a B/PS region. Although the control sample of galaxies without a bar is rather low, it can be stated that an exponential functional shape is not encountered in galaxies without hosting a bar. On the other hand, not all galaxies (of those ones where an analysis makes sense, see above) harboring a bar do show an Exponential functional shape at a position inside the bar component. Indeed, 16 out of 19 galaxies, including that ones where the presence is not unambiguously proven, do have an Exponential functional shape corresponding to approximately 84%. The most probable explanation for the deviation of an 1 : 1 correspondence is the fact, that a part of the galaxies without an Exponential functional shape have a rather short photometrical bar signature like e.g., *NGC 1596*. It is rather strange that both types of functional shapes, the $\text{Sech}(z)$ and the Isothermal can be observed. Further, the fact of an equipartition between both types is a puzzling observation. That could point to a mechanism relating the shape of the VSFBD in the B/PS region with the dynamics of each galactic object.

Leaving the region of the B/PS structure moving further out results in a decrease of the shape parameter λ . There can be 2 different shapes, either the shape parameter stays constant or reaches a local minimum. That situation is comparable with the situation in the case of the scaleheight. In fact there is a relation between the course of the scaleheight and the course of the shape parameter. Both are coupled to each other resulting in the fact, that a constant scaleheight results also in a constant shape parameter and a local minimum in the scaleheight is also present in the shape parameter. Therefore, at this point it is referred to the description of the scaleheight characteristics (Chap. 4.3.2) for the qualitative description of the shape parameter course. Worth to note is the fact, that the value of the shape parameter reaches its local minimum, if present, inside the extension of the photometrical bar/lens signature. Also, if a plateau in the value of the shape parameter is present it extends up to the end of the photometrical bar/lens signature. Beyond that signature the value of the shape parameter does change. In all cases the value of the shape parameter rises to a more flat-topped VSFBD profile. It can be made a distinction between two types of galaxies also in this case (with the exclusion of the galaxies denoted in Tab. 4.1). For one type of galaxies the value does stay approximately constant after a small region in which the rise has taken place ($\approx 23\%$ of the galaxy sample with the best example in *IC 2531*). The other type of galaxies

Table 4.1: This table displays if a galaxy harbors a VSFBD of either a $\text{Sech}(z)$ or a Isothermal functional shape at the positions of the local maxima. In order to have an overview of possible correlations also the Hubble-type as well as the presence and type of a X-structure are given. Galaxies excluded from the analysis are marked by a hyphen (—) or by a question mark (?).

Galaxy	Type ^a	X-structure ^b	Inclination ^c	Distribution shape ^d	
				Sech(z)	Isothermal
(1)	(2)	(3)	(4)	(5)	(6)
NGC 0128	S0 pec	OX	E		•
ESO 151-G004	S0 ⁰	OX	Q	—	—
NGC 1032	S0/a	—	E	—	—
NGC 1381	SA0	CX	E	•	
NGC 1596	SA0	OX?	E	—	—
NGC 1886	Sab	CX	Q	?	?
NGC 2310	S0	CX	I	—	—
ESO 311-G012	S0/a?	OX	E	—	—
NGC 2788A	Sb	CX	Q		•
IC 2531	Sb	CX	E	?	?
NGC 3203	SA(r)0 ⁺ ?	OX	Q	—	—
NGC 3390	Sb	CX	Q		•
NGC 3957	SA0 ⁺	CX	Q		•
NGC 4469	SB(s)0/a?	OX	I	—	—
NGC 4703	Sb	—	Q	•	
NGC 4710	SA(r)0 ⁺	OX	Q	?	?
PGC 44931	Sbc	CX	I	—	—
ESO 443-G042	Sb	OX	Q	•	
NGC 5084	S0	—	Q	—	—
NGC 5746	SAB(rs)b?	CX	I	—	—
IC 4767	S pec	OX	Q	—	—
NGC 6722	Sb	OX	I	—	—
NGC 6771	SA(r)0 ⁺ ?	OX	Q	—	—
ESO 185-G053	SB pec	CX?	E		•
IC 4937	Sb	OX	Q	•	
ESO 597-G036	S0 ⁰ pec	OX	E	•	
IC 5096	Sb	CX	Q	•	
NGC 7123	Sa	CX	E	—	—
IC 5176	SAB(s)bc?	—	E	—	—
ESO 240-G011	Sb	CX?	I		•

^a Classification as in Tab. 2.2

^b Presence and type of X-structure (see Chap. 3.3.1 and Tab. 3.2) A line flags the absence of a X-structure.

^c I: Inclination; E — (exactly) edge-on; Q — quasi-edge-on; I — inclined; (see Tab. 3.2)

^d Shape of the VSFBD. The presence of either a $\text{Sech}(z)$ or an Isothermal is marked by bullet.

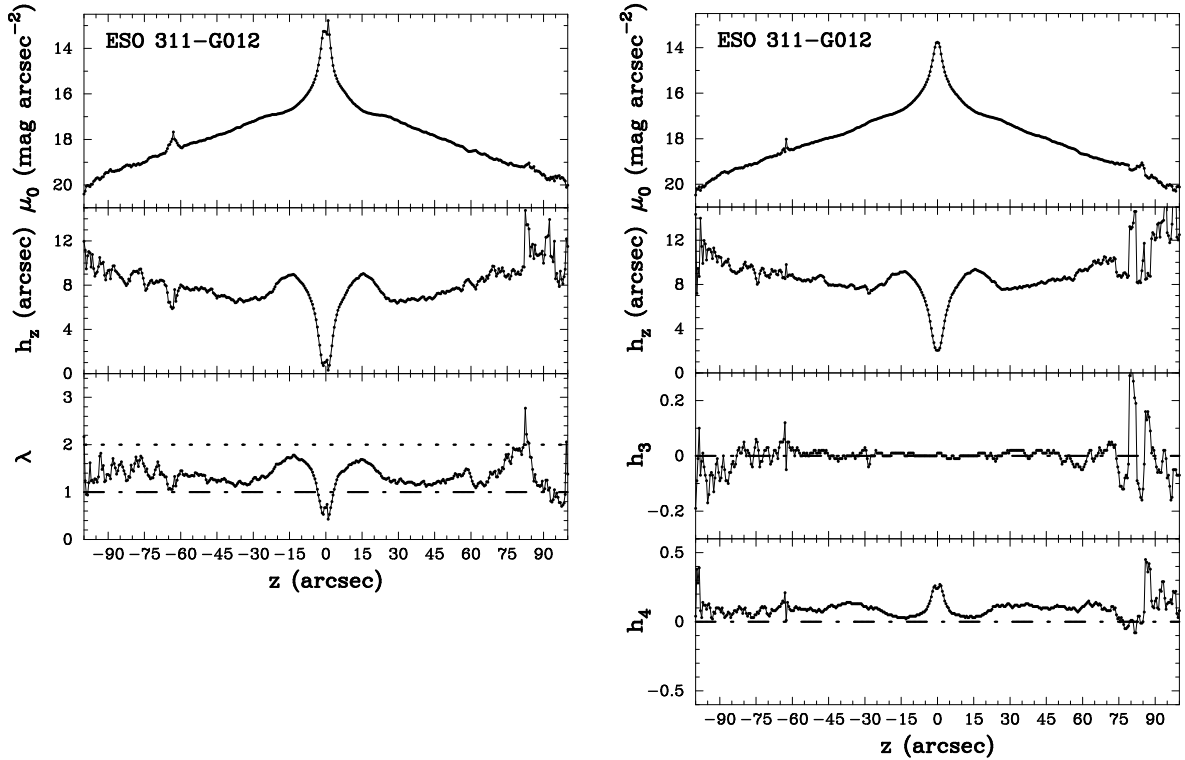
The question mark denotes cases where a clear classification to one of the functions could not be applied.

If no assignment to the two functional shapes could be done at all, it is denoted by a line (—).

show a steady rise of the values of the shape parameter without a subsequent constant region ($\approx 53\%$ of the galaxy sample with the best example in *NGC 1596*). In the latter case it is well possible that the decreasing S/N -ratio can influence the correct measurement. But in the case of an intermediate region of a constant shape parameter value no other technical problem interferes with the determination of the shape parameter values. The reason for the intermediate region of constant shape parameter could well be founded in the presence of a distinct galactic component but a more profound discussion will be given in Chap. 4.3.8.

4.3.4 Fitting the inner central region

Analyzing the results of the Generalized Gaussian fitting it can be observed in the inner central regions preferentially for the fit parameters h_z and λ a discontinuity of the fitted parameter values (see Figure 4.1, innermost $5''$). Due to the characteristic course of the fitted values it could be classified as an internal problem of the fitting routine to converge to the correct value. This is supported by the fact that such kind of problems appear at positions where the gradient of surface brightness is most pronounced, i.e., in the inner central region of the galaxy where the surface brightness reaches its global maximum (compared to the galaxy's surface brightness distribution) with a very peaked center. Further, a comparison of the results of the Generalized Gaussian fitting method and the Gauss–Hermite method for the h_z parameter seems to confirm the conclusions. It can be noted that the course of h_z reaches a minimum at the very center of the galaxy. This can then be used to interpret the fluctuations at the same position in the case of the Generalized Gaussian as a mere technical problem of the fitting routine. However, there are two other facts which make that interpretation of the results less evident. First, there are some cases where the central regions do not have a sharp and distinctive peak but nevertheless a discontinuity in the resulting fitting parameter can be observed. *ESO 151-G004* is a good representative for such a case. Second and more significant is an accurate comparison of the Generalized Gaussian fitting results with the Gauss–Hermite fitting results. In this context it is not consistent to make a comparison between the GGau and the GSec fitting functions since both have the same structure in their approach of describing the observed data. Both are based on a generalization of one special function described by 3 fitting parameters. Therefore, as stated, the comparison will focus on the GGau and the GaHe approach which is based on a different concept. The latter fitting method has only some rare cases (an order of magnitude less than the former method) of discontinuities in the values of h_z and λ and accordingly h_4 (cf. Tab. 4.2). Moreover, the course of the h_4 fitting results shows a regular pattern consisting of two local maxima separated by a local minimum (double-peak structure) in the region where the discontinuity appears. That pattern is in most of the cases symmetric to the center of the galaxy. It is clear that h_4 does not correspond precisely to λ but the two parameters describe qualitatively the changes in the shape of the vertical surface brightness distribution. More precisely, the parameter h_3 is a measure for the *skewness* of the SFBD whereas h_4 can be interpreted as a measure of peakness of the SFBD as characterized by the entity *kurtosis* in context of statistics. A more general comparison of the two approaches to characterize the vertical surface brightness distribution shows further differences which distinguish both. One difference can be observed when analyzing the value of the peak of the radial surface brightness profile. It shows up, that the maximum of the Generalized Gaussian approach is in most cases about 1mag brighter than the peak in the Gauss–Hermite approach. A comparison with the radial surface brightness profiles of the K -band images of Chap. 3 reveals that the Gauss–Hermite

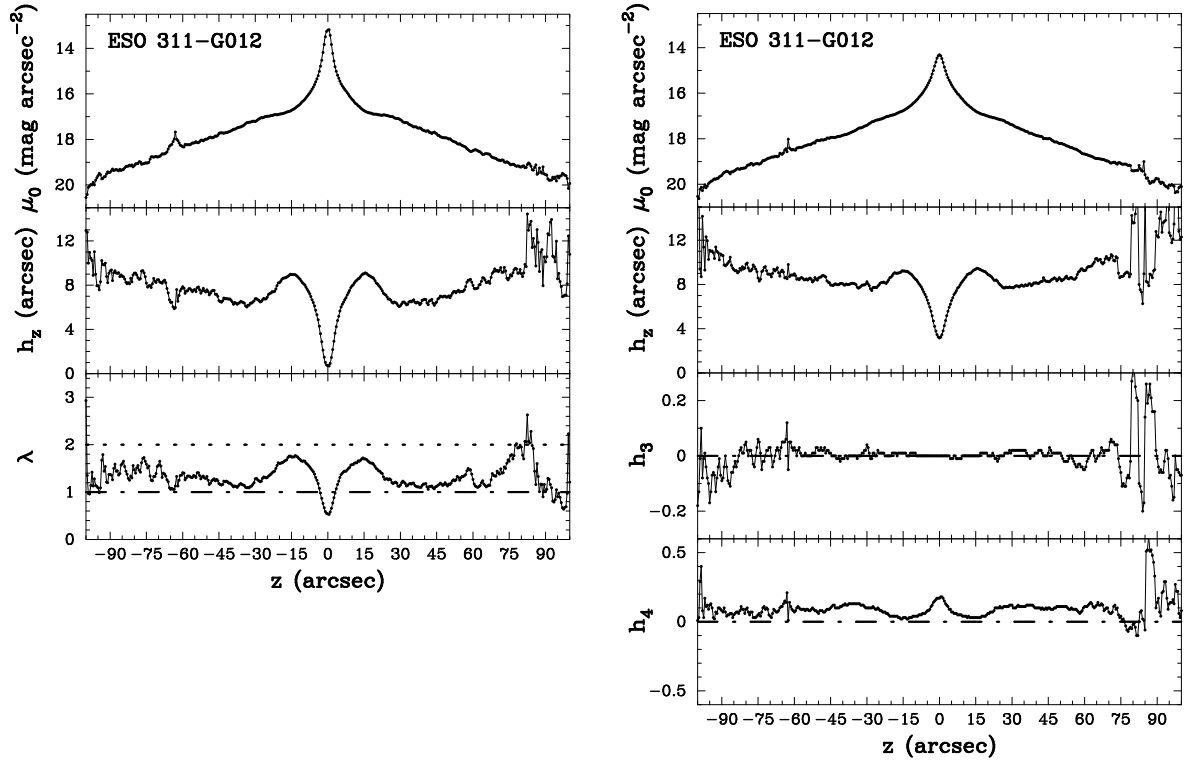


(a) Generalized Gaussian non linear fitting

(b) Gauss-Hermite non linear fitting

Figure 4.1: Fitting results for the galaxy ESO 311-G012 without any masking on the major axis. In Fig. (a) the results for the Generalized Gaussian approach are shown whereas Fig. (b) shows the results for the Gauss-Hermite approach. As described in the text the Generalized Gaussian approach evidences a discontinuity in the inner central region. Opposed to that, the only detectable feature in the discussed area for the Gauss-Hermite approach are the small local maximum of the h_3 parameter in the innermost 5'' and the double-peak structure in the h_4 parameter in the same area.

fitting reproduces better the true peak surface brightness of the galaxy center. The course of the vertical scaleheight h_z is also quantitatively different in both approaches. It exhibits the following behavior: Starting from the galaxy center and going radially outwards it has a (deep) minimum at the center, then rising fast to a local maximum at a position where the ‘shoulder’ or ‘plateau’ (see Chap. 3) of the bar component starts to be observable in the radial surface brightness profile. It then decreases again to some intermediate values in the range between the minimum and the maximum. Depending on each individual galaxy the h_z after the decrease remains nearly constant or rises again slowly (see Chap. 4.3.3). The most pronounced difference between the GGau and the GaHe approach can be seen at the very center of the galaxy. There, the h_z in the Generalized Gaussian approach reaches lower values than the Gauss-Hermite approach. In a lot of cases (e.g., NGC 1032, NGC 2310, NGC 2788A) h_z in the minimum has a value of nearly zero which is clearly not physical as the vertical scaleheight has to be greater than zero. None of the minima of the Gauss-Hermite approach



(a) Generalized Gaussian non linear fitting

(b) Gauss-Hermite non linear fitting

Figure 4.2: Applying a mask to the region around the MJA profile to the galaxy ESO 311-G012 most of the discontinuities in the fitting parameters of the GGau approach disappear. In this case the fitting procedure was done applying a mask of $1.5''$ above and below the MJA so that the innermost area is covered by a $3''$ mask. As a consequence also the double-peak structure in the h_4 plot vanishes proving that it is especially that pattern depending highly of the SFBF in the innermost region. It can be also observed that the peak values of the two approaches used (GGau and GaHe) diminish in comparison with the values without a mask (see Fig. 4.1).

equals to zero even if the values are often very low ($h_z \approx 1''$).

A special case is *NGC 7123*. In the Generalized Gaussian non linear fitting the fitted major axis surface brightness profile exhibits two (nearly symmetric) local minima to the left and to the right of the central peak going radially outwards. Comparing that fitted major axis surface brightness profile with that obtained by the Gauss-Hermite non linear fitting it can be observed that the previously described minima are not present but at their place an outwards shallowly decreasing shoulder appears. This is a large qualitative difference. A closer look at *NGC 7123s* photometric analysis (K -band original and unsharp masked image, App. C) does not give any hint that in the discussed spatial region a complicated structure is visible which could be a reason for the different fitting results. Furthermore, it shows up that the GaHeNL reproduces much better (both qualitatively and quantitatively) the major axis surface brightness profile as that one obtained by the GGauNL.

The above discussed differences in the results of the Generalized Gaussian non linear fitting and the Gauss–Hermite non linear fitting lead to the following conclusion: The Gauss–Hermite approach reproduces both qualitatively and quantitatively better the observed photometric characteristics of the entire galaxy sample. However, this does not mean that the Generalized Gaussian approach cannot be used for an investigation of the scaleheight, but that it has some drawbacks in situations where a large SFB gradient is present. It still gives in a large number of galaxies and galaxy regions valuable information about the vertical scaleheight and shape of the vertical surface brightness distribution. The large discrepancy is only present in the very center of the galaxies and in general for some special cases like *NGC 7123* which have to be examined more closely. Apart from that, all fitted results (major axis surface brightness, h_z , and λ) give the same general trend as well as the same values as in the Gauss–Hermite non linear fitting. Therefore, all three parameters and especially the λ will be used in the analysis.

The reasons for that differences can be the following: The first and strong argument is that the Gauss–Hermite non linear fitting approach is more precise in following the photometrically observed SFB. That can be due to the fact that it uses one more fitting parameter, namely four, compared to the Generalized Gaussian non linear fitting approach. For that reason it has naturally a larger flexibility to account for small scale variations. On the other hand the large(r) amount of fitting parameters could lead to a problem with finding not only the best fitting parameter set in a mathematical point of view (in terms of minimization) but also to get the best fitting result describing correctly the observed surface brightness distribution. Therefore, it has to be focused more on the nature of the fitting function(s). The crucial point is that both enable a fitting of a family of functions but the Gauss–Hermite non linear fitting approach uses an *orthonormal* set of functions whereas the Generalized Gaussian non linear fitting approach uses just one function. Thus, even if the former fitting method does use a truncated set of functions, it is able to follow better the VSFBD without changing strongly the other parameters. As a consequence the Gauss–Hermite non linear fitting is more stable and its results can be interpreted directly as representing the physics behind them.

As discussed previously the large SFB gradients present in the inner central regions cause difficulties to the GGauNL. In order to verify this two tests were run for both fitting approaches, the GGauNL as well as the GaHeNL. In all cases a small region along the MJA of the galaxy was masked out during the fitting procedure. The fitting routine did only take into account the pixels outside a region above and below the MJA delimited by the mask. In the first case a region of 1.5'' above and below the MJA (covering in total a range of 3'') was masked out whereas in the second case a range of 2.5 above and below the MJA was selected resulting in a total range of 5''. In Figure 4.2 as well as Figure 4.3 it can be seen clearly that the masking of the innermost regions as described above eliminate the discontinuity in the values of λ in the GGau approach and lead to a disappearance of the small scale structure detectable in the h_4 parameter of the GaHe approach.

4.3.5 Quantitative description of the VSFBD

Applying a more quantitative description of the mentioned phenomena at least 3 points should be emphasized. Those are the innermost regions of the galaxy, the upper limit of the value of the shape parameter in the inner and intermediate regions of the galaxy (i.e., up the end of a possibly present bar/lens), and the functional shape of the vertical bar SFB. The galaxies *NGC 5084*, and *NGC 7123* are difficult to describe in a consistent way since the

Table 4.2: Table summarizing for each galaxy the characteristics of the radial surface brightness profile and the vertically summed surface brightness profile (VSSFBP) in the inner central regions for the Generalized Gaussian (GGau) and the Gauss–Hermite (GaHe) approach. The presence of a feature is marked by a bullet (●), the absence is denoted by a hyphen (—), and dubious cases by a question mark (?).

Galaxy	Bar class ^a	Extension ^b (arcsec)	Discontinuities		Double–Peak	VSFBD ^c
			GGau	GaHe	GaHe	Exponential
NGC 0128	Bar	—	—	—	—	●
ESO 151–G004	Bar	3	●	—	●	●
NGC 1032	No bar	1	●	—	—	—
NGC 1381	Bar	—	—	—	—	—‡
NGC 1596	Bar	3	●	—	●	—
NGC 1886	Bar	3	●	—	●	●
NGC 2310†	Bar	4	—	—	—	—
ESO 311–G012	Bar	2	●	—	●	—
NGC 2788A	Bar	4	●	—	●	●
IC 2531	Bar	—	—	—	—	—
NGC 3203	Bar	2	●	—	●	●
NGC 3390	Bar?	2	●	●	?	?
NGC 3957	Bar	2	●	—	●	?
NGC 4469†	Bar	3	—	—	—	—
NGC 4703	Bar	4	●	—	●	●
NGC 4710	Bar	—	—	—	—	●
PGC 44931†	Bar	4	—	—	—	?
ESO 443–G042	Bar	3	●	—	●	●
NGC 5084†	No Bar	—	—	—	—	—
NGC 5746†	Bar	3	—	—	—	—
IC 4767	Bar	2	●	—	●	●
NGC 6722†	Bar	—	—	—	—	—
NGC 6771	Bar	2	●	—	—	?
ESO 185–G053	Bar	1	●	—	●	●
IC 4937	Bar	3	●	●	?	?
ESO 597–G036	Bar	1	●	—	●	●
IC 5096	Bar	2	●	—	?	—‡
NGC 7123†	Bar?	—	—	—	—	—
IC 5176	No bar	—	—	—	—	—
ESO 240–G011†	Bar	—	—	—	—	—

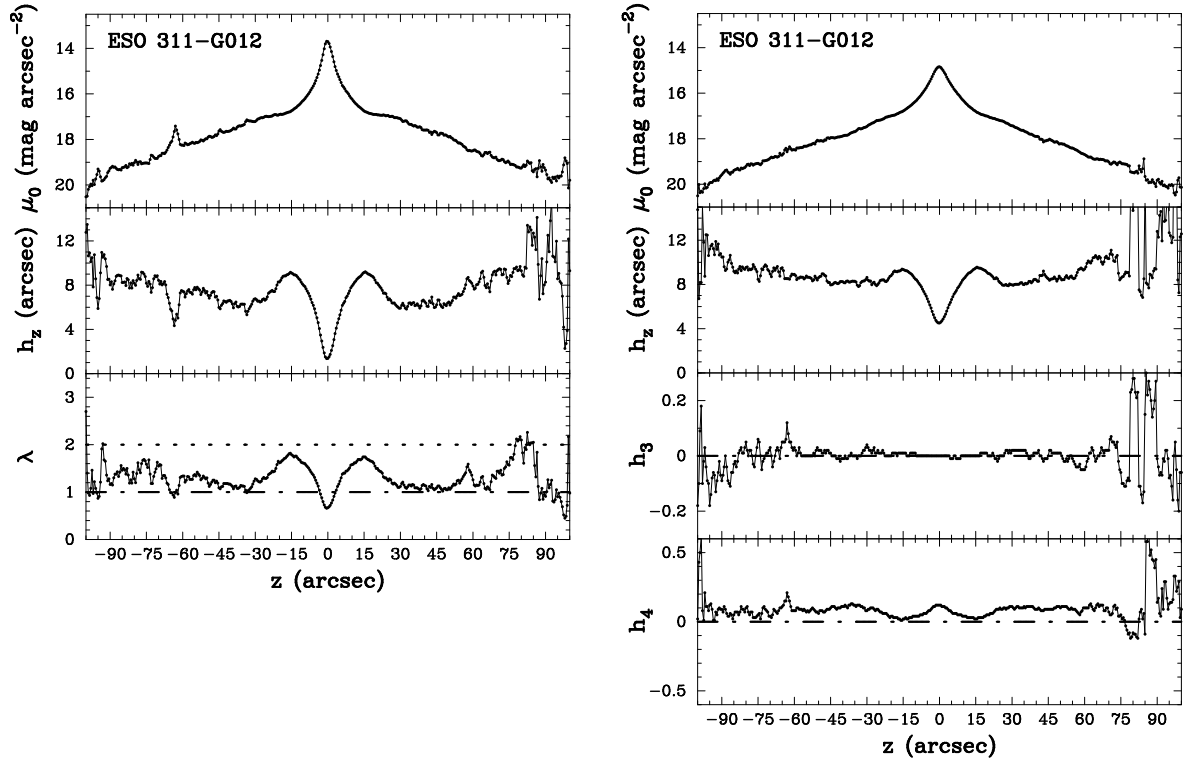
^a Classification as in Tab. 2.2

^b Approximate radial extent of the region where the discontinuities for the λ fitting parameter appear.

^c Galaxies showing in λ a decrease after the local maximum to values of about $\lambda = 1$ (corresponding to an exponential VSSFBP) at the end of the photometric bar signature (if present, see Chap. 3).

† Galaxy excluded from the analysis. Either it is classified as inclined (see Tab. 3.2) or it has some peculiarities.

‡ With high probability the hump visible in the RSFBP is a *lens* signature (instead of a bar, cf. Chap. 3) Therefore, the VSSFBP is not denoted as an exponential.



(a) Generalized Gaussian non linear fitting

(b) Gauss-Hermite non linear fitting

Figure 4.3: Enlarging the masked area on ESO 311-G012 further (compared to that one used for the plots in Fig. 4.2) alters the fitted parameters in the innermost region dramatically. In this case a mask of $2.5''$ above and below the MJA was applied. The peak value of the RSFBP of the GaHe approach differs by about 1mag from the observed one as plotted in Appendix C.

course of the shape parameter is below the value of an exponential functional shape along a large part of the inner region. This is completely different from the other galaxies. In the case of *NGC 5084* such kind of difference seems to be evident since it has a large and bright spheroidal bulge suggesting different dynamics and formation mechanisms than the galaxies with a 'canonical' B/PS region or a small spheroidal bulge (e.g., *IC 5096*). The VSFBD of *NGC 7123* has not been correctly fitted in the GGau approach as can be seen from the fitted RSFBP in Appendix D. Therefore, both have been excluded from the following detailed analysis but *NGC 5084* will be used for a discussion linking together galaxies with a B/PS region and galaxies with a large spheroidal bulge.

A remarking feature is the fact that in the inner regions (i.e., inside the photometrical bar/lens signature) the value of the shape parameter corresponding to a Gaussian is never exceeded drastically. Apart from *NGC 6771* which is the only galaxy marginally surpassing the value corresponding to an exponential functional shape, there is no other object reaching such large values. Clearly the minimum of the difference between the measured value and the Gaussian one is located in the region of the B/PS area. There, as described previously, the

shape parameter values reach a maximum. Further out in the disk, beyond the bar/lens signature, the values representing a Gaussian functional shape are reached or largely surpassed. Anyway, in that regions it is difficult to interpret the results unambiguously since possibly fainter additional galactic components as e.g., a thick disk are present.

A focus should also be put on the presence of a local minimum or plateau inside the bar/lens region as described above. In both cases, minimum and plateau, a value of the shape parameter is reached which corresponds to an exponential functional shape. This is quite remarkable since it relates for the first time a distinct galactic region to the accentuated functional form of an exponential. The value corresponding to an exponential VSFBD shape is reached at the outermost part of the photometrical bar/lens signature in the case if a local minimum is detected. In the plateau case, the exponential VSFBD shape is present already at positions which are nearer to the galactic center but their deviation from the constant value coincides again with the end of the photometrical bar/lens signature. Indeed, the reaching of the exponential shape or the deviations from it at such positions could well be used to mark the delimiters of the bar/lens positions. Here, the analysis of the shape parameter obtained by the GSec approach is of invaluable use. In fact, the GSec does sustain the finding of the exponential functional shape through the detection of equivalent values of the shape parameter $2/n$. The coincidence of the equivalent values with the positions where in the GGau approach exponential values have been detected is nearly identical. Without any doubt a bar/lens component has at its ends an exponential VSFBD shape. As in the case of the scaleheight also here the same examples can be cited i.e., *NGC 2788A* and *IC 5096*.

In the very center of the galaxy the VSFBD does show a much more peaked shape than an exponential distribution. The values go down nearly to zero but it could well be that it does not reflect correctly the original shape since in some galaxies discontinuities like in the scaleheight can be observed (see Chap. 4.3.4). What is possible to say is that the scales and shape parameters observed there are quite different to that ones in the regions outside the center even if the problems of fitting in the GGau approach are taken into account. In fact, the analysis of the results obtained by the GaHe fitting approach show large deviations from a Gaussian towards a sharply peaked distribution. Nevertheless the differences are not as strong as the results from the GGau approach would suggest. Compared to the results of the last years proposing, especially in late-type galaxies, for the bulge component a functional shape with a low Sérsic-index or even with shaped as an exponential functional distribution (corresponding to a Sérsic-index of 1). As discussed, a low Sérsic-index is equivalent to a high value of shape parameter λ in the GGau approach. Hence, the present result could be contradictory to the results found in the literature. However, this is not the case since in the present study, high Sérsic-indices are found for the innermost regions whereas the investigations found in the literature do consider a larger region of about the extent of the distance between the two local maxima found in the shape parameter course. The results of this thesis point to a small and rather sharply defined component in the very center which can be related to the nuclear objects reported e.g., in Scarlata et al. (2004). Further, there seems to be no clear distinction between early- and late-type galaxies concerning neither the peakness nor the ratio between the central peak value of the shape parameter and that one in intermediate bar/lens signature. A good example for that situation are the two galaxies *NGC 2788A* and *NGC 3203*, the first one classified as late-type (Sb) and the second one classified as an early-type (SA(r)0⁺?).

4.3.6 The shape parameter in the GaHe approach

As stated in Chap. 4.3.1 the characteristics of the shape parameter in the GaHe approach are different from the other two fitting methods using a family of functions. Since the h_3 parameter measures just the skewness of the fitted distribution it will not be considered further. Of much more interest is the h_4 parameter measuring indeed the functional shape of the given data distribution. Though measuring only a *deviation* from a Gaussian it gives important information about the functional shape of the VSFBD. First of all the larger the h_4 values are, the more peaked the SFBD is. A value of 0 marks the absence of any deviation from a pure Gaussian distribution, whereas negative values are an equivalent for more flat-topped functional shapes like e.g., a Gaussian.

The general course of the shape parameter is as follows. In the center a global maximum for the value is reached if the outermost fitting results are excluded. About approximately 40% of the galaxies show a double-peaked structure in the center so that there are two maxima both having nearly an identical value. This fact is described in more detail in Chap. 4.3.4. Shifting the focus further out a fast decrease of the shape parameter can be observed until a local minimum is achieved. This minimum coincides almost exactly with the positions of the local maxima of the scaleheight and marks the region where the B/PS structure is strongest pronounced in the photometrical panels. After that, for larger galactocentric distances the value of the shape parameter rises again until a local maximum or region of constant values is reached. That morphology corresponds to that one described with the results of the GGau fitting. Also there either an extremum or a plateau was reached outside the galactic center. In the case of the maximum (as for the minimum in the shape parameter λ of the GGau approach) the position of it is also the delimiting position of the bar/lens signature. Beyond the plateau a decrease of the values can be noted before the measurement becomes strongly noise dominated. Thus, the bar/lens extension is strictly defined. Indeed, as seen in the GGau approach also the end of the plateau of the shape parameter is equivalent to the end of the bar/lens signature. Hence, in other words it can be stated that the deviation of the shape parameter from an exponential value in the outer parts of the intermediate galaxy region is the signature of the end of a bar/lens structure. This fact can thus be used to define a bar length measure in edge-on galaxies based on pure photometrical data. Until now no straightforward measure could be given in photometrical analysis. The congruence of the features observed in the GGau as well as the GaHe approach points to the fact that the vertical structure of the observed galaxies is consistently described.

4.3.7 Comparison with simulations of disk galaxies

Apart from the comparison of the shape of the VSFBD with that one observed in disks of galaxies it is also possible to compare the results obtained here with that ones obtained through N -body simulations. The only study putting some focus on that kind of investigations is the work by Athanassoula & Misiriotis (2002). In their work they fitted their data which were extracted from simulations with the GGau approach. Due to different simulation runs they were able to study the shape of the vertical SFBD on disk galaxies with distinct features. Three main types of galactic disks were used: First, a simulation with a massive halo compared to the other components (massive-halo (MH)) is presented. Second, a disk component which is the dominant one (massive-disk (MD)) inside the typical radii of a disk (several scaleheights) is analyzed. Its dominance can be checked in the rotation curve where

that component shapes the rotation curve all over the inner regions. Finally a model in which a massive bulge potential massive-disk-with-bulge (MDB) was added to the disk and halo component is used. Investigating the parameter values they obtained (Athanasoula & Misiriotis 2002, their figure 10) a rough agreement with the observationally obtained data can be stated. In the case of the scaleheight in all three cases a central minimum can be distinguished delimited by 2 local maxima at the position of the B/PS region. Beyond that maxima the scaleheight decreases constantly. Between the three models a distinction through the prominence of the central minima is possible. The MH model has the most pronounced minimum among the three models. Further, in the case of the MD and the MDB models the maxima of the B/PS region are rather shallow compared with the strong ones in the MH model. In all cases the central minimum has a scaleheight value larger than that one in the outer disk regions. Concerning the shape parameter λ the situation is similar. In the center a minimum is present of which the depth is strongest pronounced in the MD case. Also here the maxima denoting the B/PS region are strongest in the MH model. The outer regions do have larger values for the shape parameter than the inner ones when the simulation has been run for about one Hubble-time.

The largest difference between the simulated galaxies and the observationally analyzed is the central minimum. It is much more pronounced in the galaxies analyzed in the present study compared to the simulated ones. Especially in the MD model the central decrease of scaleheight is hardly detectable whereas in the case of the observed galaxies the central minimum is clearly dominating the central region. Contrary to that, the central minimum studied in the here used galaxy sample is a global one. Further, the constant decrease of the scaleheight in the outer disk regions is completely different to the present observations. In the case of the shape parameter the model resembling best the results obtained in the present study is the MDB model. Although the value of the central minimum is not a global one it is quite pronounced. Another point of interest is the fact that the shape parameter decreases when starting from the B/PS region and shifting further out. Of further interest is the fact that following the previously described decrease a local minimum is formed reaching nearly the value of an exponentially shape distribution. This is remarkable since the values observed in the simulated galaxies are in general much larger compared to those determined from the galaxy sample used here. As stated in Chap. 4.3.5 the shape parameter does not exceed the value of 2, whereas in the simulated cases the limit of 2 can be seen as a lower limit. Only the minima in the outer parts of the MDB model reach lower values. Furthermore, beyond this minimum the shape parameter does increase rapidly as it could be observed in the fitting results of the galaxy sample. However, it has to be said that this feature is observable in simulations ran by over one Hubble-time. Summarizing it can be stated that there is a large disagreement between the simulated galaxies and the observed ones concerning the results for the scaleheight. The situation is much better for the shape parameter especially in the case of the MDB model. That could be a hint to the structure forming in disk galaxies but details will be discussed in Chap. 4.3.8.

4.3.8 Galactic components and the VSFBD

As a major result of this study the observation of an exponential functional shape of the VSFBD in the bar/lens region can be emphasized. This result is to a high probability a real feature present in the observed galaxies since first, there are areas in which a different situation can be found and second three different fitting methods find the same correlation. One

of the important conclusions that can be drawn is that the vertical structure in that areas is not correctly described neither by a $\text{Sech}(z)$ nor by an Isothermal. Indeed, only 2 of the galaxies with an inclination suited for a deeper study do not have an exponential functional shape in at least a part of the intermediate region of the galaxies. Those galaxies are *NGC 1596* and *ESO 311-G012* and both galaxies do harbor a bar. Nevertheless, it seems that the bar/lens region is, at its outermost limits, characterized by an exponential vertical SFBD shape. Bars have been characterized to have an exponential RSFBP profile but a canonical description of its vertical shape has been missing so far. Also for the lens component no clear vertical description has been provided.

Further the double-peak structure observable in the inner central regions of the galaxies revealed by the GaHe approach is intriguing. This approach corroborates the tendency observed in Chap. 3.4.3 of galaxies harboring a central nucleus. However, the fitting approach gives a much more reliable method to detect such features and subsequently quantifying them. In Tab. 4.2 the galaxies with a clearly observable double-peak are notified as well as the fact if an exponential VSFBD is present. The occurrence is strongly correlated. For 12 galaxies showing a double-peak structure also an exponential VSFBD can be observed out of 13 galaxies with an exponential VSFBD corresponding to $\approx 92\%$. The same is true for galaxies harboring a exponential VSFBD (13). Here again 12 corresponding to $\approx 92\%$ do show also a double-peak feature. The determination of the presence of a double-peak structure by the vertical fitting approach provides also a strictly reproducible method for the analysis of the central regions. A comparison with the selection done in Chap. 3.4.3 shows that, apart from the galaxies excluded (see Chap. 4.3.3) only 2 coincide with a detection of a double-peak, whereas the same amount of galaxies was not listed in Tab. 4.2. Definitively the presence of the double-peak structure with the observable sharply delimited central region of small scaleheights in the center points to a small scale structure component. The facts point to some nucleated or disky component as reported by several studies (for a review see Kormendy & Kennicutt 2004). In this context it is important to emphasize the strong correlation between the presence of a double-peak structure and a bar. Indeed, the bar could provide the mechanism to create such kind of structures since as discussed in Chap. 1.2 it can fuel large amounts of disk material into the center. However, it is not clear what would be the fate of such a central structure when the bar would dissolve. Interpreting the strong correlation under this aspect, the central components are dependent on the presence of a bar. Possible dependencies of the strength of the bar with the central component could be worthwhile to investigate but are not possible with the present approach.

The outer parts of the disks where no bar/lens component is present remain problematic. Unfortunately there are no clear results concerning the vertical functional shape but in cases where the disk has a rather large extension (e.g., *IC 2531*, *IC 5176*) it becomes evident that the scaleheight as well as the shape parameter rise in value. In the case of the shape parameter it exceeds the value representing a pure Gaussian. Although it has been argued in this study that the thick disk can be neglected at high z distance from the galactic plane still that component can have an influence at large *radial* distances from the center. At that positions the contribution of the thin stellar disk can drop below that one of the thick disk.

As described in Chap. 4.3.7 the strongest resemblance between simulated and observed galaxies can be found for the simulation of the MDB case. It is interesting that just this internal structure of a disk galaxy leads to the local minima in the outer regions streaking the value of an exponential shape. That feature is one of the most remarkable results of the vertical fitting of the observed galaxies. Clearly, in cases like *NGC 1886* and *ESO 443-G042*

the region representing minimal values form a plateau and not a simple minimum. But those galaxies are also classified as late-type galaxies which have by definition a smaller spheroidal bulge contribution. The fact that prevent a coherent picture is the argument that the positions of the minima are not in agreement with that ones of the galaxy sample used here. When a minimum in the outer part was observed in the galaxy sample it could be clearly related to the end of the photometrical bar/lens signature. That is not the case in the simulated MDB case. There, the position of the minima in the shape parameter value occur far outside the bar extension, at nearly twice the radial position of the bar limit. In fact, the correlation of bar extension and position of the local shape parameter minima (in combination with the exponential shape of the VSFBD) was a major characteristic of that area. A further disagreement between the simulated and the observed objects is the fact that the central minimum is more sharply confined and bearing values which fall below of that ones observed at the limit of the bar extension. A deeper analysis of spheroidal bulge components in simulations is needed, though. The mentioned model was used as simple test case. It has to be investigated how the results change if the parameters determining the shape of the spheroidal bulge are varied. In Athanassoula & Misiriotis (2002) only one parameter set was used. Nevertheless, at the present point it is rather dubious if the observed similarities are a hint to such a galactic structure.

The galaxies *NGC 5084* and *NGC 7123* are morphologically different from the others in sense that they harbor a large spheroidal bulge structure. Although the galaxy *NGC 1032* does also have a spheroidal morphology in the center, it can be distinguished from the other two objects by the fact that the disk component cannot be morphologically distinguished from the bulge part. In *NGC 5084* as well as *NGC 7123* a distinct disk component can be detected sticking out radially from the central spheroidal part. Nevertheless all three galaxies are of nearly the same Hubble class (see Tab. 2.1) which evidences again the difficulties when dealing with galaxies of type S0 (Chap. 1.1). However, *NGC 5084* and *NGC 7123* are farther distinct from each other since the latter exhibits a small photometrical bar signature as well as a X-structure visible in the unsharp masked image whereas the former does not (see Tab. 3.2). The results of the fitting of the VSFBD unveil for the both objects an incorrect reproduction of the fitted RSFBP obtained through the GGau approach. Thus, the results of the GGau approach cannot be used in this discussion. A remarkable feature in both cases is that the maximum at the very center of the galaxies is in fact a local one, since the values of the shape parameter in the intermediate region are higher. Actually, in the case of *NGC 5084* the shape parameter does not reach values constituting a local maximum but a local minimum. This could be due to problems in the fitting process since the scaleheight in all other fitting approaches except the GGau one do show constant values. Further, the GSec approach does also exhibit a non correctly fitted RSFBP in the very center. Therefore, for both cases a local central maximum can be observed. The course is similar to that one observed in galaxies with a B/PS structure. As a consequence the central part is less strongly peaked than the intermediate region. Furthermore, also in those galaxies with a large spheroidal bulge component a structure with the same characteristics as the B/PS structure is present. That fact in combination with the presence of a B/PS structure in *NGC 7123* points probably to a scenario where the large spheroidal structure has covered the B/PS morphology. Such a point of view suggest that the large spheroidal structure has been formed out of completely different formation mechanism than that one leading to a B/PS structure. Since both galaxies are classified as S0s or intermediate between a S0 and a Sa it would not be improbable because formation scenarios explaining the shape of S0s explicitly consider

accretion or merger events. In that picture *NGC 7123* would be an important object showing different mechanisms forming the central regions of galaxies at work.

4.4 Conclusions

The fitting of the VSFBD has given a large amount of information concerning the substructure of galactic components like a bulge region and a disk. Morphological entities like the photometrical bar signature can be related in a consequent way to changes in the slope of the course of the different shape parameters defined by the distinct fitting approaches. Also the inner regions like the innermost central regions show clear signs of substructure as was presumed in Chap. 3.4.3. The presence of a double-peak in the course of GaHe the shape parameter in the innermost region does strongly suggest a small scale component which is closely related to the presence of a bar. As e.g., Erwin et al. (2003) argue such kind of component should have a kinematical signature similar to that one of a cold disk. However, if the two peaks are taken as the limiting edges of such a disky structure it is not possible to assign to the whole bulge region characteristics of a disk. The extension of central component is of one order of magnitude smaller than the typical B/PS structure (see e.g., *NGC 2788A*). Furthermore, the observed extension of such a structure is constantly of the same size compared to the B/PS structure in all galaxies. Therefore, it cannot be line-of-sight dependent as the B/PS structure is. This also sustains the view of the central component's shape obeying azimuthal symmetry.

For the bar (and/or lens) component the presence of an exponential VSFBD, at least at the limits of the structure, has been observed. The shape defined by the other two functions proposed for the description of the disk VSFBD have been detected unambiguously only in the B/PS region. That is almost surprising since both are still used equally to describe the vertical structure of galactic disks. Relying on the results of the fitting of the VSFBD it can be stated that the exponential-distribution is clearly 'preferred' in the bar region. The presence of an additional component in the outer parts (i.e., the thick disk) is suggested by the change of values in all the approaches relying on generalized functions. This is not possible to observe in the approaches using a fixed functional shape of the VSFBD. There, the results rather suggest an approximate constancy of the scaleheight all along the extension of the disk. Therefore, the claims arguing for a constancy of the disk scaleheight should be discussed also by this aspect. However, it is difficult to quantify in a more precise way the parameters describing the outer thick disk components since the resulting fit parameters in that regions are rather noisy.

As has been discussed the exponential-distribution as a functional description for the VSFBD is, at least in the intermediate regions of the galaxies, the most appropriate one to describe the vertical structure of galactic components having disk-like characteristics as e.g., a low average-velocity-dispersion-to-rotational-velocity ($\bar{\sigma}/V_R$) ratio. In Chap. 4.2.1 the rough overview over publications dealing with the functional shape of the VSFBD has revealed that in a number of cases the Exponential functional shape is best suited for a description of the investigated disk property. Furthermore, de Grijs et al. (1997) clearly state: "It is well-known from optical observations that many disk galaxies show a universal, exponential behavior of the vertical luminosity away from the galaxy planes." Although considering the fact that optical observations are often obscured heavily by dust at locations around the plane of the galaxy, it is surprising that the Sech(z) and Isothermal approach are

still considered in an equal manner. The present study reports functional shapes obeying to the $\text{sech}(z)$ -distribution and isothermal-distribution only in the B/PS region which is rather confined compared to the whole extension of the disk. Thus, it is here proposed to use the Exponential approach as that one describing the characteristics of the vertical SFB in disk galaxies. In any case that should be correct for the intermediate regions of disk galaxies.

The analysis has shown the qualitative difference of the scaleheight and the functional shape of the VSFBD in the B/PS region from other areas of the galaxy. In all cases the scaleheight in the B/PS region is nearly doubled in comparison to the local minima in the bar/lens component when present. Further the functional shape of that region is transformed from a peaked to a flat-topped one. This is a strong argument for the interpretation of the B/PS structure as a result of vertical redistribution of disk material. The scaleheight increase can thus be seen as a local 'heating' of the disk material. Indeed about a half of the sample galaxy harboring a B/PS region do show either a $\text{sech}(z)$ -distribution or a isothermal-distribution functional shape at the positions where the B/PS is most prominent. However, this study cannot shed light on the reason why both distributions are present on an equal level and why the VSFBD does adjust to those functional shapes and why the rest of the sample does not follow any of both.

Up to now three main mechanisms for the heating of the thin stellar disk are known. They are based on the process of a steady increase of the vertical velocity dispersion of stars within the thin disk. The main process is 'heating' of stars through the scattering off of giant molecular clouds (GMCs) (Spitzer & Schwarzschild 1951, 1953; Lacey 1984) which happens rather isotropically. Spiral density waves can also contribute by a small amount to vertical heating (Carlberg 1987; Jenkins 1992) but not as strong as the discussion of Dalcanton & Bernstein (2002) suggests. In fact, (Carlberg 1987 as well as Jenkins 1992) come to the conclusion that the estimation of the amount of vertical heating through spiral density waves do contribute only a vanishing part to it. The low efficiency of the latter mechanism is also suggested by the results of Gerssen, Kuijken, & Merrifield (1997) analyzing the ratio of vertical to radial velocity dispersion in the disk. A further scenario changing the scaleheight is proposed by Toth & Ostriker (1992). They argue that infalling satellites can heat in the vertical direction the disk of the target galaxy. That mechanism is reviewed and analyzed with a semi-analytical mechanism by Benson, Lacey, Frenk, Baugh, & Cole (2004) who argue that sub halos of dark matter whose orbits pass through the target galaxy disk do increase the vertical velocity dispersion. The authors address further the issue of the spatial extension of disk heating by satellites passing through or near the disk. They argue that the encounter with a satellite does frequently trigger global modes of the disks which have the ability to redistribute the deposited energy over the whole disk. Interestingly they come to the conclusion that mechanism of vertical disk heating can contribute a comparable amount to that caused by GMCs. In the observational study of Schwarzkopf & Dettmar (2001) the same correlation is emphasized. The authors detected that interacting or merging galaxies were found to harbor disks systematically ($\approx 50\%$) thicker than those of non-interacting galaxies.

Since the present results show a variation of the disk scaleheight with radial distance from the galactic center bar buckling can be regarded as a further vertical disk heating mechanism. But this statement has to be restricted since the bar buckling and the formation of a B/PS structure are *local* phenomenon with respect to the galactic disk. It would be interesting to observe how this 'heated' disk region would evolve if the bar sustaining it would dissolve. The bar destruction/dissolution scenario with a possible subsequent renewal of the that structure has been often discussed but until now no observational imprint or evidence has been reported

(see also Chap. 1.2). Therefore, it would be a promising project to look in detail for structures tracing dissolved bars.

Interpreting the results of the fitting of the VSFBD as done in Chap. 4.3.8 the galaxy *NGC 7123* would be an important object for the study of the different mechanism shaping the central region of a galaxy. Indeed, the parallel presence of a B/PS structure signature and a large spheroidal bulge component does evidence two of the possible bulge formation scenarios, namely through secular evolution (the B/PS feature) and through accretion of material or merger of two galactic objects. In that picture the accretion/merger could have happened before the formation of the B/PS structure or after it. Considering the former scenario it is important to understand if the disk of the galaxy is still dynamically cold enough to develop a bar instability and subsequently a B/PS structure. That prerequisite could be possibly fulfilled if, apart from the growth of the central region, the disk is supplied with dynamically cold material through accretion in the outer parts of the galaxy as described by e.g., Reshetnikov & Combes (1997). The heated disk material belonging to the target galaxy would then form a thick disk component (often observed in early-type galaxies, see e.g., Pohlen et al. 2004) whereas the dynamically cold gas would form a young disk susceptible to instabilities leading to a bar. On the other hand a formation of the central spheroidal component with a B/PS structure already present does imply that the accretion/merger event takes place in a non violent manner at least not to influence much the orbits making up the bar, so that the B/PS structure is not destroyed. Simulations considering satellite infall (e.g., Berentzen, Athanassoula, Heller, & Fricke 2003) and a growth of a central mass concentration (e.g., Athanassoula et al. 2005) have been done but a consistent parameter study is not available to make a clear statement under which conditions a B/PS structure does stay stable or is disrupted. A clear answer cannot be given here but the results are coherent with the view that the structure and forming history of disk galaxies is very variegated by far from being monolithic and simply structured.

Chapter 5

Summary and outlook

5.1 The bar–buckling scenario

The formation of B/PS structures and the evolution of the bar dynamics are closely connected when following the argumentation of the bar–buckling scenario. Despite the fact, that the evolution of a B/PS structure is not necessarily bound to the occurrence of the bar–buckling instability it can still be seen as the basis of the B/PS structure formation (see Chap. 1.4). As described in Chap. 1, the bar–buckling scenario is independent of special conditions in order to evoke the B/PS structures. This is in contrast to the concurring merging/accretion scenario where in fact very special parameters out of a large possible parameter space have to be fulfilled to result in such an observed structure. The different characteristics which each B/PS structure shows are easily explained by the bar characteristics of the galaxy.

In this thesis the bar–buckling scenario was strengthened and enriched by new aspects. A first clear evidence is the presence of Secondary maxima (SM) along the galaxies major axis as described in Chapter 3.3.1 and Chapter 3.3.3. The formation of such a structure is coherent with the assumed bar evolution picture: the depletion of bar material at radially smaller positions than the SM and the redistribution of the material into the vertical direction is the central process in the scenario based on bar thickening. In fact, the depletion coincides with the positions of the largest prominence of the B/PS structure. Further, the comparison of the RSFBP with the VSSFBP does corroborate this view. Analyzing the VSSFBP it can be observed that no SM are detected in such profiles corresponding to a typical exponentially decreasing SFBD of an edge–on disk. Hence, the material missing in the central part of the disk is deposited at larger distances from the plane, more precisely in the B/PS structure, as the comparison of galaxies with a SM and their VSSFBP shows. Out of 23 galaxies with a SM along the MJA, 21 show the described morphology of the VSSFBP corresponding to a percentage of approximately 91%. From the analysis it also emerges clearly that the B/PS structure is positioned clearly within the bar signature described in Chapter 3.3.3. That is not a counter–argument to the bar–buckling scenario but can be understood well within the orbital calculation approach for bars in galactic disks. The calculations of Patsis et al. (2002b) do indeed show that the stellar orbits sustaining a B/PS structure are part of the stellar orbits describing a 3–dimensional barred disk.

Also the prominent X–structure visible in the unsharp masked images of the galaxies with a B/PS structure does fit coherently in the described picture. It is not a structure inherent to a boxy shaped SFBD but is related to the underlying 3–dimensional orbits of galactic bars. A

comparison with the plots presented by Patsis et al. (2002b) shows a good agreement with the morphology of the X-structures presented there and that ones observed in the galaxy sample of this thesis. From that approach it follows immediately that the material which populates the orbits constituting the B/PS structure is then missing in the galactic plane since it is originally part of the bar structure. Therefore, the argument that the B/PS structure cannot be a thickened bar because it is shorter than the bar is not valid; the B/PS structure is part of the bar which has thickened.

In order to provide a comparable morphological analysis for observationally obtained data, Bureau & Athanassoula (2005) have applied diagnostics similar to that one used in this thesis for N -body simulations. The results of that analysis have been compared and discussed in Chapter 3.3.4. Two major arguments should be reconsidered here. First, there is a large agreement between the morphology and the measured density along the MJA of their galactic disks and the equivalent profiles (e.g., the RSFBP) in this work. The different shapes of the central regions in the galaxy (spheroidal or B/PS structures) of the present sample are mostly coherently reproduced by varying simulation parameters like the bar strength or simply the inclination or the amount of the line-of-sight angle measured with respect to the bar major axis. Again, the variety of the morphological features visible in the galaxies of the discussed sample fit well and coherently into the bar-buckling scenario. Second, the major discrepancy between observations and simulations was detected in the innermost regions of the galaxy where the objects provided by the observational side show a much larger and sharply confined SFB peak at the center (see also Chap. 5.3). In the simulations radial redistribution of luminous material along the bar is observed but it is not sufficient to build up a component in the very center with such a strong SFB gradient as reported here. This can probably be due to the nature of the numerical approach lacking a dissipative component such as gas that could be transported into the innermost regions and then form there new stars.

Finally, the observation of the presence of radial breaks of the SFB in the VSSFBP fits well in the bar secular evolution model. The breaks can be interpreted as signatures of the radial redistribution of disk material and of angular momentum. Contrary to a monotonically decreasing SFB of a pure disk component the VSSFBP shows some breaks at positions which coincide with the kinematical signatures found by the analysis of ionized gas and stellar absorption lines (Bureau & Freeman 1999; Chung & Bureau 2004).

Although the observation of the B/PS structure in face-on galaxies is technically difficult or to the present date still infeasible (see e.g., Debattista, Carollo, Mayer, & Moore 2005) also some morphological features/arguments can be used to identify such structures. As described in Chapter 3.5 some images of face-on barred galaxies do have a structure which could be coherent with the picture of a bar which suffered bar-buckling and developed a component positioned well inside the bar diameter but with the main symmetry axis parallel to it.

5.2 The vertical structure of barred galaxies

The analysis in Chapter 4.3 has revealed a large variety of shapes of the VSFBD and scaleheight ranges present in the different components of the disk galaxies. As already pointed out in Chapter 3.3.3 there is a scaleheight variation along the bar component. In fact, as described in detail in Chapter 4.3.2 the scaleheight increases strongly compared to the center and the outer bar region reaching in some cases values as twice as the values observed in the outermost bar region. The local maximum of the scaleheight in the central regions does coincide with

the positions where the B/PS structure is morphologically most prominent. Also, the values of the shape parameters, describing the functional shape of the VSFBD, show coherently a variability with a local extremum at nearly the identical positions as the scaleheight maximum. This fact does corroborate additionally the proposed model of B/PS structure formation relying on bar instabilities. Indeed, in that picture the scaleheight in the B/PS region is a natural consequence of the vertical redistribution of disk material. Other formation scenarios (e.g., accretion or merging scenarios see Chap. 1.4) should not show such a strong enlargement of the scaleheight. Furthermore, in an accretion scenario where the material sustaining the B/PS is *added* to the already existing one in the disk (and not *redistributed* from it) could possibly lead to such a flat-topped functional shape but with the same maximal central SFB as the adjacent regions of the bar. Since no material would be subtracted to the bar, there should be no diminishment of the SFB along the MJA contrary to the observation of the SM originating from disk material depletion. The scenarios invoking a satellite triggered bar formation cannot be seen as an alternative way, since the B/PS structure formation is attributed then to the evolution of the bar component.

The variety of the VSFBD shapes is also visible in the outer regions of the galactic bar. Approximately 84% of the barred galaxies exhibit an Exponential functional shape inside the photometrical bar signature, according to the GGau approach. Such kind of correlation is shown for the first time with a large galaxy sample. Additionally the GaHe approach does support this and reveals a region of constant shape parameter h_4 . The end of that signature does correspond with the limits of the photometrical bar signature. At larger radial distances than the extension of the bar component no clear results can be reported apart from a tendency of an increase of the scaleheight and functional shapes being more flat-topped as the isothermal-distribution. In the case of the scaleheight such observations are reported in the literature but in a rather low number (e.g., de Grijs & Peletier 1997). Apart from such a view also the possibility of the presence of a thick disk has to be considered, reminding the fact that a large part of galaxies are of early-type. With decreasing SFB of the thin disk component the thick disk's share of the overall SFB does increase noticeably.

A deeper analysis of the VSFBDs shape in the region of the B/PS structure has unveiled an interesting dichotomy of the shape parameter values based on the fitting results of the GGau approach. In fact, as described in Chapter 4.3.3 and shown in Table 4.1 the cases where the galaxy inclination allows a thorough analysis two possible functional shapes are observed, the $\text{Sech}(z)$ and the isothermal-distribution. The exponential-distribution is not detected at all in that regions. A correlation between Hubble-type and the preferred presence of one of the two functional distributions is not detected. Further, the lack of the exponential-distribution in such regions was not expected, as the other regions dominated by the bar component do show such a shape. Nevertheless, the observation of the $\text{sech}(z)$ -distribution and the isothermal-distribution favors the view that such kind of distributions are in some way related to the processes shaping the vertical structure of galactic disks. Here, they are related to a defined process in the evolution of bars, i.e., the formation of a B/PS structure. Summarizing the last arguments a probable evolutionary path could consist in the view that galactic disks have, after they are settled, a VSFBD obeying an exponential-distribution. During the evolution of other components related to the disk their vertical functional shape can evolve to a less peaked distribution like other disk heating processes suggest.

5.3 The central regions of disk galaxies

Besides the characteristics of the B/PS structure the central region of the galaxies shows interesting substructure. First, the small scaleheights in the center detected in the data values of the GGau scaleheight measurement as well in the GaHe approach is remarkable. The surrounding B/PS region does show scaleheights larger than that ones detected in the other disk components but towards the center it decreases dramatically to minimal values. Also the shape parameter of the GGau approach does reach minimal values in that region in concordance with the local maximum in the GaHe representation. Studies on early-type galaxies repeatedly report such low values but not investigations on late-type galaxies (see for a review Kormendy & Kennicutt 2004). However, those studies focus on the large scale bulge region, whereas the discussed structures are seen in the innermost parts of those bulge regions. The dramatic change in scaleheight and the different shape compared to the surrounding structure does point to a distinct component residing in the center of those disk galaxies. In Chapter 4.3.6 the presence of a double-peak feature in the course of the VSFBD was discussed. The symmetry of such a feature shows that its detection is not an artefact created by the fitting process. All such features have an maximal spatial extension of $\approx 5''$ and are hence very sharply confined and small compared to the other galactic components discussed in this study. Such structures may be well related to that ones reported more and more frequently in the literature during the last 5 years. Central star cluster or small scale bars are probably the origin of such kind of components (e.g., Erwin & Sparke 2002; Erwin 2004). Those components, and especially the second one, do point to a close connection to large scale bars to fuel the center with stars and cold gas. The link of those double-peaks observed in the VSFBD analysis to a bar component, is given by the strong correlation between the presence of a double-peak structure and the presence of a bar (Tab. 4.2 and Chapter 4.3.8). Therefore, that innermost structure can be viewed as tightly connected to a large scale bar. This result strengthens the argument that the bar plays an essential role in shaping the overall morphology of a galaxy.

Since the bar is effective in shaping the overall bulge region as well as the innermost center (see above) also the shape of the central surface brightness peak and its corresponding region can be influenced by the bar. Bureau & Athanassoula (2005) reported a spatially rather extended central peak in their simulations. This has not been observed consistently in this work but some early-type galaxies show similarities in SFB to simulated galaxies harboring a strong bar. As has been shown in Chapter 3.4.1, the analysis of the CSFBPE/ D_{KEO} ratio reveals a slight tendency towards large ratios for early-type galaxies, although some objects with a typical early-type galaxy morphology e.g., *NGC 2310* have a diverging value. Taking into account the possibility that the proposed measure is a quantity simply reflecting the fact of a high B/D ratio, it has to be considered that in the present case not the whole bulge region was taken into account. Furthermore, the result would fit well in a picture of early-type galaxies being in a farther evolved state compared to late-type galaxies in the sense that the bar fueled a large amount of disk mass into the center. Such process would then form the central disks described e.g., in Athanassoula (2005). Those disks have not to be confound with the smaller structures detected in the very center as described above (see also Scarlata et al. 2004). The latter components are probably also seen in early-type galaxies as the results of Tab. 4.2 suggest. Indeed, among the galaxies where a double-peak was detected, several early-type objects were present.

A possible correlation between the values of the CSFBPE/ D_{KEO} ratio and the environ-

ment in which the galaxies can be found could not be proven, although a weak trend for galaxies with large $CSFBPE/D_{KEO}$ values being present in high density environments is observed. Possibly the ratio is not well suited to make an analysis discussing the galactic environment but also the classification describing the density of the surrounding objects has to be improved to allow a thorough investigation.

5.4 Secular evolution in barred disk galaxies

The accumulating evidence of the past years that bars do have a role of primal importance in galaxy evolution is sustained further through the results of this work. In fact, the morphological study in Chapter 3 has shown that the observed features in the unsharp masked versions of the K_n -band imaging can be interpreted well and coherently in the framework of 3-dimensional orbit calculations of galactic bars. Also the results obtained by the fitting of the VSFBD in Chapter 4 support the bar thickening model. Further, the two approaches of this thesis, the morphological analysis using unsharp masked images and the RSFBP, as well as the approach describing the VSFBD by a fitting procedure do show a large variety of substructure in the 'classical' bulge and disk components. The efficiency of the secular evolution processes at work in disk galaxies can be observed very well in late-type galaxies. There, the B/PS structure, from a morphological point of view, constitutes the whole bulge component. Indeed, most of the SFB present in the inner regions of the galaxy is dominated by the thickened part of the bar. Only a spatially very small and confined component does also contribute to the SFB in the center. This can be seen in an illustrative manner in the galaxies *NGC 1886* and *ESO 443-G042* where the extended photometrical bar signature visible in the RSFBP is just interrupted by a sharp and marginally extended peak at the center of the galaxy. That is quite different from the much broader central peak in early-type galaxies as, e.g., *ESO 151-G041* (see App. C).

Apart from the weak correlation of galaxies with a large $CSFBPE/D_{KEO}$ value (typically early-type objects) and a dense galaxy environment, no other correlation depending on the Hubble-type of the objects could be claimed. In fact, the presence of a double-peak structure as well as the dichotomy of the vertical functional shape in the B/PS structure can be observed in all equally well. The weak trend seen in the higher number of cases where, in late-type galaxies, at positions of the B/PS structure, the VSFBD is shaped like a $\text{sech}(z)$ -distribution, is opposed to the missing of any trend in the case of early-type galaxies. However, the results of this study do not give a complete answer to the aspect whether the central region i.e., the bulge region of early-type galaxies can be formed with all their characteristic parameters also by the dynamical evolution of the bar component. From the point of view of the occurrence of bars in disk galaxies this could be in fact the case since the frequencies of bars are very high (Chap. 1.2.1) or following some authors are probably present in all disk galaxies (Seigar & James 1998). The morphology of late-type galaxies, as discussed above, can suggest an evolution from Sd to Sbc objects, though.

Studying edge-on galaxies it was not possible to analyze the average velocity dispersion in the central regions, which in combination with the observation of the disk's maximal rotation velocity could have given better insight into the dynamics present in such regions. Therefore, it is not possible to give a statement about the precise dynamical conditions in the central regions of early-type galaxies harboring a B/PS structure. The fact that early-type galaxies show a higher $\bar{\sigma}/V_R$ ratio compared to late-type ones is crucial to the understanding of bulge

formation, though. Nevertheless, this study could show that in late-type galaxies the same processes connected to the presence of a bar are at work as in early-type galaxies. In fact, features detected in later-type galaxies are also widespread in earlier Hubble-type objects. Although secular evolution cannot explain completely the large bulge components in early-type galaxies (e.g., the problem of a high $\bar{\sigma}/V_R$ ratio) it provides an important evolutionary path for galaxies.

5.5 Outlook

The presented study of disk galaxies has corroborated the view that several galactic components can be distinguished in each object. Whilst the structure connected to the bar present in the galactic disks could be analyzed in depth in this thesis, other components have to be reobserved with other or improved methods of observational astronomy. Progress in understanding the dynamics of galactic disks is also strongly driven by the analysis of simulated objects provided by numerical astrophysics. Thus, the transfer of the methods used here to numerical simulations will give a strong improvement of the processes at work in the evolution of galactic disks.

As shown in Chapter 4.3.2 and observable in Appendix D, the regions beyond the bar signature show an increasing scaleheight towards larger radii. The same is valid for the course of the VSFBD in a large number of galaxies. However, the precise shape of the VSFBD of that outermost regions and accordingly components as, e.g., possibly a thick disk could not be determined. In fact, the large variations of the obtained fitting parameters seem to point to an insufficient SN -ratio in that area. Therefore, it would be desirable, that deeper images of the galaxy sample could be reanalyzed with the here presented methods.

It is clear that results coming from observational astronomy should be compared with N -body simulations to gain deeper insight in the physical processes involved. Therefore, such an extensive investigation should be also applied to several galaxy disk models harboring a bar and a B/PS structure. Of special interest is, in that case, the correlation between the parameter set defining the simulated disk and the morphology of the disk components as well as the VSFBD. Such an extended study is still lacking in the literature. First attempts based on the methods and results developed in this thesis have been described in Athanassoula (2005). Further the vertical fitting approach was tackled as is described in Appendix A. A lot of work is still needed, though. The initial concept to extend the analysis done in Athanassoula & Misiriotis (2002) could not be pursued since the VSFBD in the B/PS region of the simulated disks shows much more complex substructure than in the observations (see App. A.1). As discussed in Appendix A.3 the GaHe approach used in this thesis could give a further driver to push forward such kind of investigations.

Since the NIR K_n -band images show the luminosity emitted by the dominant stellar population in mass, the SFBD is a tracer of the underlying potential governing the dynamics of the object (see Chap. 1.2.1). That allows a direct determination of the gravitational potential and a construction of a dynamical model under the assumption of a constant mass-to-light ratio (M/L ratio) and an isotropic dispersion tensor. Emsellem, Monnet, & Bacon (1994a) have developed a method using a multi-gaussian expansion approach to build photometrical and kinematical models of stellar systems based on photometrical information (imaging). They have shown the viability of that approach analyzing images resulting from an observation based on optical wavelength filters of the central regions in *NGC 4594* (Sombrero

Galaxy Emsellem, Monnet, Bacon, & Nieto 1994b). Further, van den Bosch & Emsellem (1998) applied the same approach successfully to the barred S0 galaxy *NGC 4570* observed in the optical *V*-band. Based on the potential the characteristic parameters for a bar as a function of the cylindrical radius R could be determined. Finally, the usage of the detection of a ring in the very center of the galaxy and the assumption of the ring's position at the ILR leads to the determination of a possible bar pattern speed of about 350 km/s. In fact, the determination of the bar pattern speed in galaxies is in general problematic, especially in edge-on galaxies. The progress doing that analysis with the galaxy sample used here would consist in the possibility of correlating morphological features and changes in the shape of the VSFBD presented here with the kinematical analysis published in Bureau & Freeman (1999) and Chung & Bureau (2004). Such an enlarged parameter set on barred galaxies would result in an improvement of a *coherent* picture of the processes involved bar secular evolution.

In Chapter 4.4 it was discussed that the formation of the B/PS structure can act as a mechanism for disk heating. The observation of the SFB of a galaxy does not give information about velocity dispersion in that object. Velocity dispersions in the vertical and radial direction of galactic disk can give valuable information on the evolution of that component. Measurements of velocity dispersion in all three dimensions are feasible as, e.g., Gerssen et al. (1997) have shown. Apart from the results presented in this thesis also Benson et al. (2004) state that the importance of disk heating by (satellite-triggered) bars and whether the heating caused by such a component is local or global is poorly understood. The extreme inclination of the galaxies of the here analyzed galaxy sample makes a future measurement of the vertical velocity dispersion impossible. However, the N -body simulations used to compare the observational data with, do offer the possibility to investigate that question in depth. It is evident that such simulations cannot comprise all aspects of disk heating since an important part is presumed to result from scattering off stars from molecular clouds. Nevertheless, the influence of a bar component on disk heating can be focused in an optimal way.

The presented results show that an unambiguous proof for bar destruction and renewal is needed. A large number of arguments discussing the evolution of disk galaxies invokes such kind of process and some numerical studies using N -body simulations (e.g., Bournaud & Combes 2002; Bournaud et al. 2004) do report such evolution. On the other hand the N -body simulations used by Athanassoula discussed in a number of publications (e.g., Athanassoula 2003; Bureau & Athanassoula 2005) do not report any bar dissolution or renewal. Clearly, the former approach does include replenishment of cold gas material to the disk component by accretion in the outer parts, whereas the second one analyzes isolated galaxies, but an overall coherent picture is lacking. Bearing in mind the discussion about disk heating it is eventually possible, after a thorough analysis of that phenomenon, to use the irreversibility of such an evolution to detect in unbarred galaxies, dynamical signatures of a former B/PS structure.

Appendix A

Alternative methods

A.1 Vertical analysis in simulated disks

The analysis of the VSFBD of observationally studied galaxies has led to the development of several fitting approaches. However, in the case of N -body simulations the data describing the density distribution of the disk galaxy is stored and visualized in a completely different way than observational data. Simulations have the advantage to provide all necessary kinematical information describing the objects which form in their galactic disk. Therefore, distinct analysis methods have been developed. That situation leads to the problem that results obtained by the different approaches are difficult to compare preventing a straightforward interpretation. In the following a trial for providing an universally applicable method is presented. However, the analysis of the properties of that approach is not meant to be complete but can serve as guidance if the method is (re)considered.

As described in Chap. 4.1, Athanassoula & Misiriotis (2002) have investigated their simulations through the fitting of a family of functions to the VSFBD. That method is a suited starting point to apply it on simulations and observations of disk galaxies. In that work Generalized Gaussian of the following form were used: $\Sigma_{gg}(z) = \Sigma_0 \exp(-(z/z_0)^\lambda)$, with z_0 as a scaleheight and λ as a shape parameter, to fit the vertical extent of their simulated disks. Since the purpose is to compare the K_n band observations with the N -body simulations, the GGau approach was applied to the galaxy sample as was described in Chap. 4 but also tentatively to the simulations. Even if Athanassoula & Misiriotis (2002) have already used that approach to analyze simulations, a discussion of the applicability to simulations has to be undertaken. What is also important to note, is that the here described substructure is also present in the data used for the investigations shown in Athanassoula (2005). Since that study aimed to a more global view, such a problem in the B/PS region was not discussed in detail. However, the analysis of that data resulted in the decision that in an investigation aiming particularly to the understanding of the formation of the B/PS region, an improvement to the analysis methods is needed. Further, there are some differences between the fitting of GGau to simulations and the application to the observations. Particularly in the observational case no absolute scale can be used to fix the positions of each pixel whereas in the N -body case simulation units are the natural units for a spatial measure which is common to all simulations. In general the fitting procedure for N -body simulations is affected by the problem that the S/N level is not appropriate enough to justify an acceptance of the fitting results as best physical fit to the data. An increment of the S/N by binning of data points is

not viable since this results in a heavy loss in spatial resolution. Further it turned out that in areas where the S/N level is sufficient, complex vertical morphology is detected which can intrinsically not be fitted by functions like the described GGau. An example of such a case can be seen in Fig. A.1.

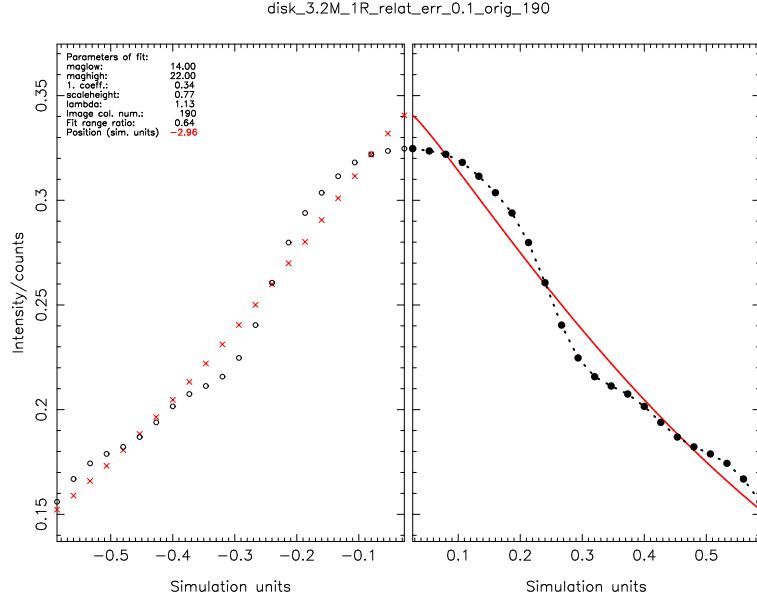


Figure A.1: Vertical cut through a simulated, symmetrized disk with $3.2 \cdot 10^6$ particles showing the density distribution. The cut has been done at -2.95 radial scalelength from the center defined by the momentum of inertia of the disk. On the left panel the lower part of the disk (with the galactic plane as the symmetry plane) is shown. The data points are marked by circles, whereas the crosses show their fitted values. On the right panel the density distribution and its fit of the upper disk part are plotted. Data points are shown with black, filled circles and the fitted function is represented by the solid line. As can be seen in the right panel, the fit does not account for the complex structure present but rather minimizes exclusively the differences between the model distribution and the data.

A.2 Variance and Kurtosis

In order to be independent from this shortcomings, methods not based on assumptions about the form of the vertical profiles, were developed. After the analysis of statistical methods the statistical quantities "variance" and "kurtosis" calculated using the pixel position with respect to the galactic plane and its intensity/magnitude value are proposed as a measure to describe the VSFBD of the simulated disk galaxies. This allows to rely only on data without any kind of assumptions.

$$\text{Var}(x_1, \dots, x_n) = \frac{1}{N-1} \cdot \sum_{j=1}^N \left(\frac{x_j - \bar{x}}{\sigma} \right)^2 \quad : \quad \text{Variance} \quad (\text{A.1})$$

$$\text{Kurt}(x_1, \dots, x_n) = \left[\frac{1}{N} \cdot \sum_{j=1}^N \left(\frac{x_j - \bar{x}}{\sigma} \right)^4 \right] - 3: \quad \text{Kurtosis} \quad (\text{A.2})$$

In eq. A.2 the last term, -3 , assures that by calculating the kurtosis for data points of a normal distribution, i.e., a Gaussian distribution, a value of 0 is obtained. In the case that the value of the kurtosis is negative, the data points used originate from a distribution which is more flat-topped than a normal distribution; for positive kurtosis values the underlying distribution is more peaked than a normal distribution. The implementation of the calculations is not straightforward. In the N -body case only 'existing' particles and accordingly positive surface densities contribute to the two described quantities and no intrinsic 'background' signal influences the values of both variance and kurtosis. In the observational case the situation is quite different. In each observation of a galaxy an intrinsic background is present and therefore the final reduced image frame shows a background level which has only on **average** a value of 0. Locally it can oscillate around this average value in the range of its standard deviation (STDDEV). Also small local deviations from an uniform planar surface are possible. Primarily the statistical fluctuations (STDDEV) in the background alter heavily the values of the calculated variance and in particular the kurtosis.

This fact becomes evident focusing on the mathematical definitions of both. Each addend in the sum of the variance is a power of the difference of data point position and the average position value. The exponent of this expression is 2. Therefore, data points in the outer parts of the frame contribute much more to the variance than the innermost ones. Analyzing the kurtosis the situation is much more accentuated since the exponent of the power of the difference term is 4.

As a first approach avoiding that drawbacks it was tried to discard regions with a background contribution and accordingly to stop the calculation of the statistical quantities when the background level is reached. For each analyzed object the background level has to be determined as well as the appropriate STDDEV. Thereafter, only values larger than the background plus the STDDEV (i.e., contributions to the brightness by real sources) will be considered. The disadvantage of this method is its dependency on individual properties of the observed object and the transparency conditions during its observation. Further, the calculation of the background's STDDEV cannot easily be automatized since regions without any contribution of other sources as the night sky have to be searched. An approximate value for the background is determined by calculating the mode of the pixels' value distribution but the appropriate STDDEV cannot be determined using that method.

Equivalently, to supply a background value and the STDDEV it is also possible to use a lower (faint) limit for the surface brightness just above the noise. Also this method is heavily depending on the individual object and the quality of the observational data. In the case of the simulations a similar but less influential effect emerges. There, single particles whose positions are far from the equatorial plane can alter strongly the value of the calculated quantity so that it is no more a valuable measure of the distribution for the majority of the particles. A possible way to avoid this is to detect the outermost particles and exclude them from any calculation of the variance and kurtosis. Then also in the case of the simulations the problem of finding a stable and globally valid criterion determining which limit (position of particles to be excluded) should be applied arises.

A.2.1 Varying the exponent of the variance and kurtosis

Due to the previously described problems it is not possible to apply the calculation of the variance and the kurtosis as done for the N -body results in the same way also to the observations. The present approach consists in modifying the definition of both statistical quantities changing the exponent. The new definition has to fulfill the criterion of sensitivity characterizing the vertical extent of the galaxy (see eqs. A.3 and A.4). To maintain the characteristics of the variance and the kurtosis the ratio between the exponent of both quantities p_{kur}/p_{var} has to result in a value of 2. The constant $\mathcal{C}(p_{kur})$ in the modified definition of the kurtosis has to be calculated for each selected p_{kur} so that the value of the kurtosis is 0 for a normal distribution, i.e., a Gaussian distribution (see also the description of eq. A.2).

$$\text{Var}(x_1, \dots, x_n) = \frac{1}{N-1} \cdot \sum_{j=1}^N \left(\frac{x_j - \bar{x}}{\sigma} \right)^{p_{var}} \quad : \quad \text{Variance} \quad (\text{A.3})$$

$$\text{Kurt}(x_1, \dots, x_n) = \left[\frac{1}{N} \cdot \sum_{j=1}^N \left(\frac{x_j - \bar{x}}{\sigma} \right)^{p_{kur}} \right] + \mathcal{C}(p_{kur}) \quad : \quad \text{Kurtosis} \quad (\text{A.4})$$

Several tests were run to select the appropriate value for the exponents. Further, artificial noise was added to the distributions to test the validity of the adopted selection in cases of deviations from ideal distributions. The tests were done using distributions based on GGaus in the parameter range $z_0 = 0.5$ to 7 and $\lambda = 0.5$ to 6 which corresponds to a range of $n = 0.16$ to 2 in Sérsic plots.

The first test runs were focusing on the selection of the new exponents of the variance and kurtosis. It is evident that from the definition of the two statistical measures (see for the kurtosis eq. A.4) a lowering of the exponent in the sum reduces the influence of statistical fluctuations on the result of the calculation. Though, with a lower exponent also the responsivity of the kurtosis as a statistical measure is reduced concerning slight changes in the analyzed distribution (namely changes in λ). That effect emerges clearly for distributions depending on high λ values (e.g., $\lambda \geq 3$, see Fig. A.2).

Since a stronger responsivity of the kurtosis for large values of λ has to be avoided, it was opted for an exponent of 1.1.

A.3 Perturbed distributions

Simulations of astrophysical objects have the advantage to be analyzable in every aspect and from each needed position. Further, simulations do not suffer the presence of dust lanes or patches impeding a complete analysis of those regions. Since this is not the case in the observed data of real galaxies, it has to be accounted for this possibilities. An important problem is the influence of dust on the surface brightness and hence on the resulting profiles. Despite the fact that the observations were accomplished in the NIR K_n -band minimizing the effect of dust, a residual influence of dust lanes cannot be excluded. In such cases the dust lanes have, at the equatorial plane of the galaxy, i.e., in the peak of the surface brightness profile, its biggest effects lowering noticeably the level of brightness. Therefore, it was tried to model this effect by changing artificially the inner parts of the tested model distribution and by including a perturbation. This was done first through a reduction of the maximum value of the distribution at the center (Σ_0) defined by the fraction f so that $\Sigma_{0,perturb.} = f \cdot \Sigma_{0,orig.}$.

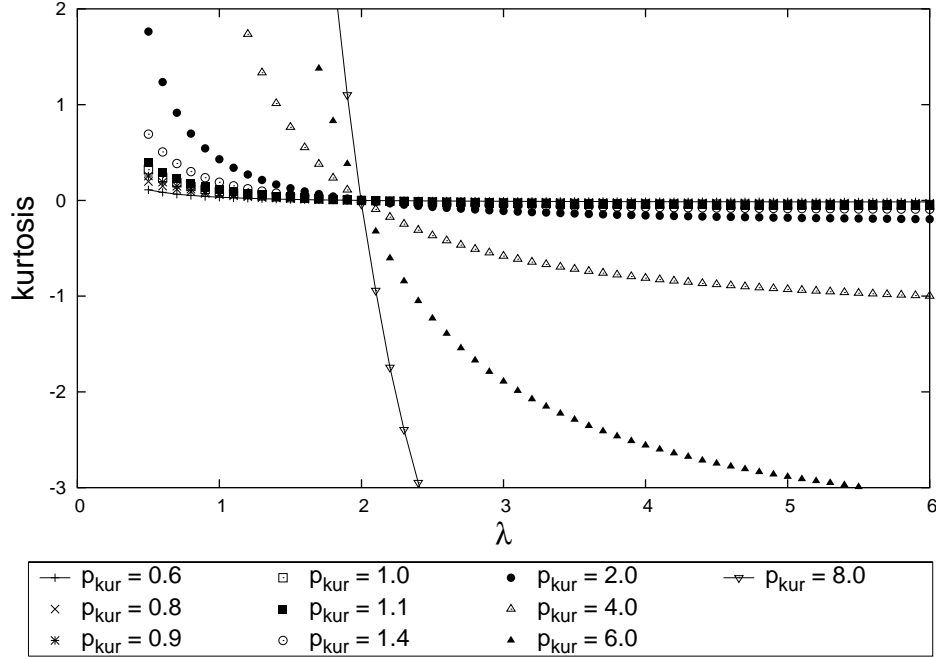


Figure A.2: Diagram showing the kurtosis defined with different exponents p_{kur} as a function of distributions with varying λ . The plotted functions show different behavior in distinct parts of the used λ range. At high λ s nearly no variation is detectable in the kurtosis value even for changes in λ of one order of magnitude.

Further the extension of the altered area, which is symmetric to the center, was fixed by setting limits in absolute units. Within the area of perturbation the deviations were calculated by replacing the original course of the distribution with a straight line whose parameters were determined by imposing the intersection with two predetermined points. These points were the central one with the maximum deviation and the point defined by the maximum spatial extension of the perturbation as the value of the first coordinate and its proper value fixed by the original distribution at that value of the abscissa. In the case of the central maximum (Σ_0) two maximal deviations from the original value were adopted; a fraction of $f = 0.8$ and $f = 0.9$. The spatial extension of the perturbation is independent from the adopted scale-length of the distribution and amounts to the fixed values of $x_{limit} = 0.05, 0.1, 0.15, 0.20, 0.40$ absolute length units. Examples of such kind of distributions can be seen in Fig. A.3. In Fig. A.4 and Fig. A.5 the changes of the variance and accordingly the kurtosis depending on the spatial extension of the perturbation are shown. Comparing both graphs (e.g., Fig. A.4(a) and (b)) it can be seen that both alterations (change of the maximal central value and change of the spatial extension) influence the results of the variance and accordingly the kurtosis calculation to the same degree. Analyzing the graphs of the variance representing the calculated values for the perturbation with the largest extent (0.4 length units) this becomes clear. The difference between the case of $x_{limit} = 0.4$ and $x_{limit} = 0$ for $\Sigma_{0,perturb.} = 0.9 \cdot \Sigma_{0,orig.}$ (Fig. A.5(b)) has approximately the same value than the change of the variance value when using $\Sigma_{0,perturb.} = 0.8 \cdot \Sigma_{0,orig.}$ instead of $\Sigma_{0,perturb.} = 0.9 \cdot \Sigma_{0,orig.}$ (considering for both the

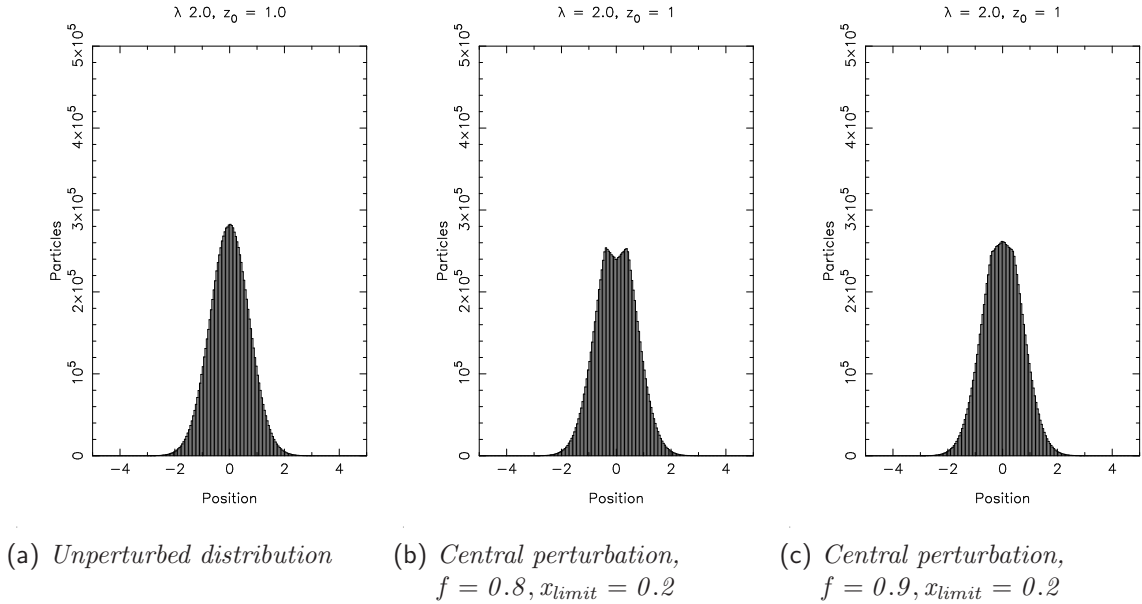


Figure A.3: Here a comparison between original unperturbed and perturbed distribution is shown. In (a) the original distribution with $\lambda = 2.0, z_0 = 1.0$ is plotted. The other two distributions show different perturbations at the center with a fixed spatial extension for the perturbed region. (b) This distribution was created with the following input parameters: $\lambda = 2.0, z_0 = 1.0, f = 0.8, x_{limit} = 0.2$. (c) The here visualized distribution was created with the following input parameters: $\lambda = 2.0, z_0 = 1.0, f = 0.9, x_{limit} = 0.2$. As can be seen, the central parts change not only in shape but also the peak value is altered. In the case of (b) the central region is completely different to the original distribution shown in (a). Nevertheless, this alteration does not influence much the calculation of the variance and the kurtosis (see Fig. A.4, Fig. A.5).

case $x_{limit} = 0$). Also in the case of the kurtosis the alteration of the central value and the change of the perturbation's spatial extension contribute in the same order of magnitude to the variation of the values (see Fig. A.5).

As a second way to simulate noise the shape of the test distributions were changed by redistributing the number of particles in each bin (i.e., the number of particles in a bin represented by the course of the distribution) randomly to other bins. The maximum range of this redistribution was dependent on the scalelength z_0 of the distribution. The following values for the maximal redistribution length were adopted: $c_{noise} = 0.1, 1.0, 2.0, 6.0 \cdot z_0$ (e.g., see Fig. A.6).

When converting simulations into pseudo CCD images a typical scale conversion of 1 disk scalelength per 50 pixels was applied. This then results in the case of $z_0 = 1$ (scalelength) in an extension of $c_{noise} = 5, 50, 100, 300$ pixels for the chosen maximal redistribution length.

From the test it can be seen that in the case of high noise values ($c_{noise} = 6.0 \cdot z_0$) there is a clear departure from the unperturbed distribution case for nearly all analyzed values of the exponents (e.g., Fig. A.7 and A.8). In Fig. A.7 the results of the variance calculation using perturbed GGau distributions are shown. Already at low values for the exponent (≈ 0.7), the

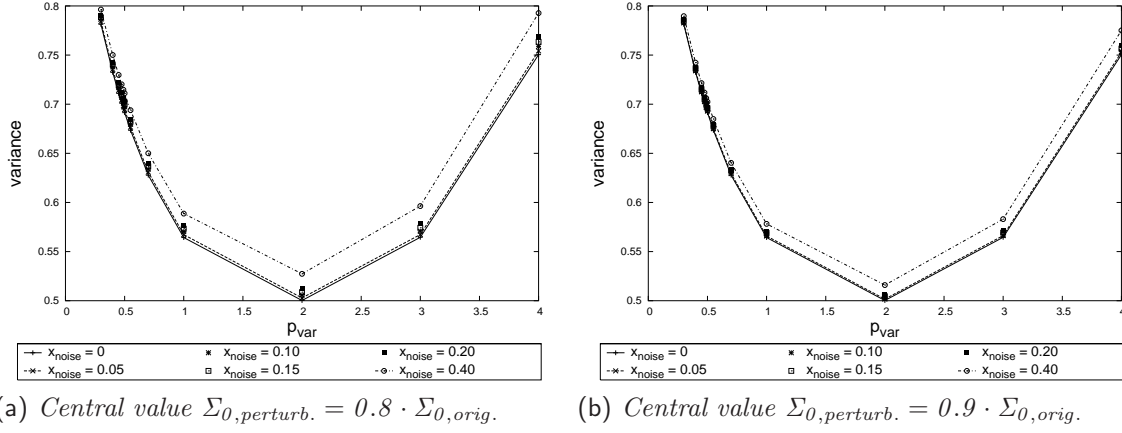


Figure A.4: Variance as a function of the varying spatial extension of the perturbation. In each diagram all test runs for the spatial extension of the perturbation are shown ($x_{\text{limit}} = 0.05, 0.1, 0.15, 0.20, 0.40$ in absolute length units). The solid line represents the original, unperturbed distribution, whereas the dashed-dotted line shows the strongest perturbed distribution ($x_{\text{limit}} = 0.40$). All other tested distributions range between those two.

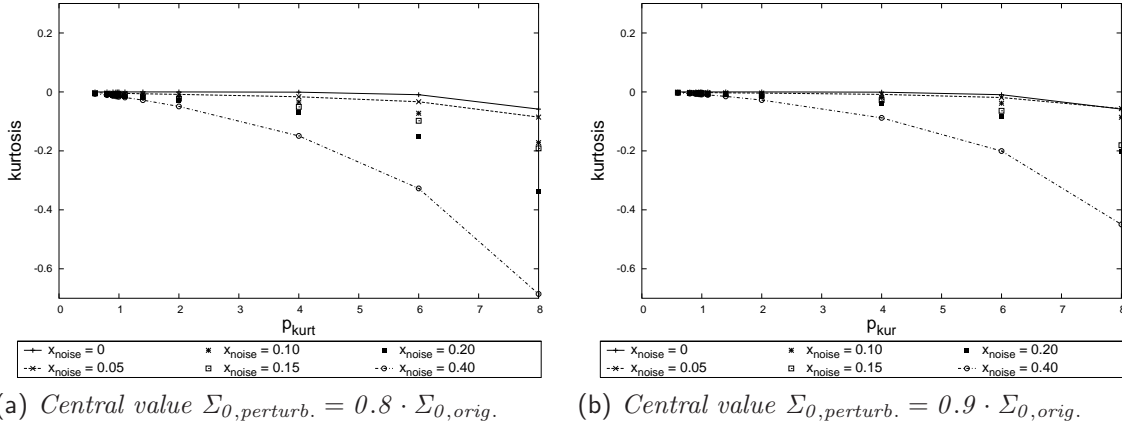


Figure A.5: Kurtosis as a function of the spatial extension of the perturbation (see also Fig. A.4).

deviation of the variance calculated from the highly perturbed distribution, compared to the variance based on the original distribution is quite large ($\approx 100\%$). The deviations between the values of the kurtosis based on the original distribution and the perturbed one show the same trend as in the case of the variance. For exponents larger than 1 (which correspond to exponents ≈ 0.5 in the case of the variance) a deviation of $\approx 100\%$ can be observed.

A comparison with plots showing the same analysis but different values concerning the noise perturbation in the center (change of the central value and extension of the perturbed

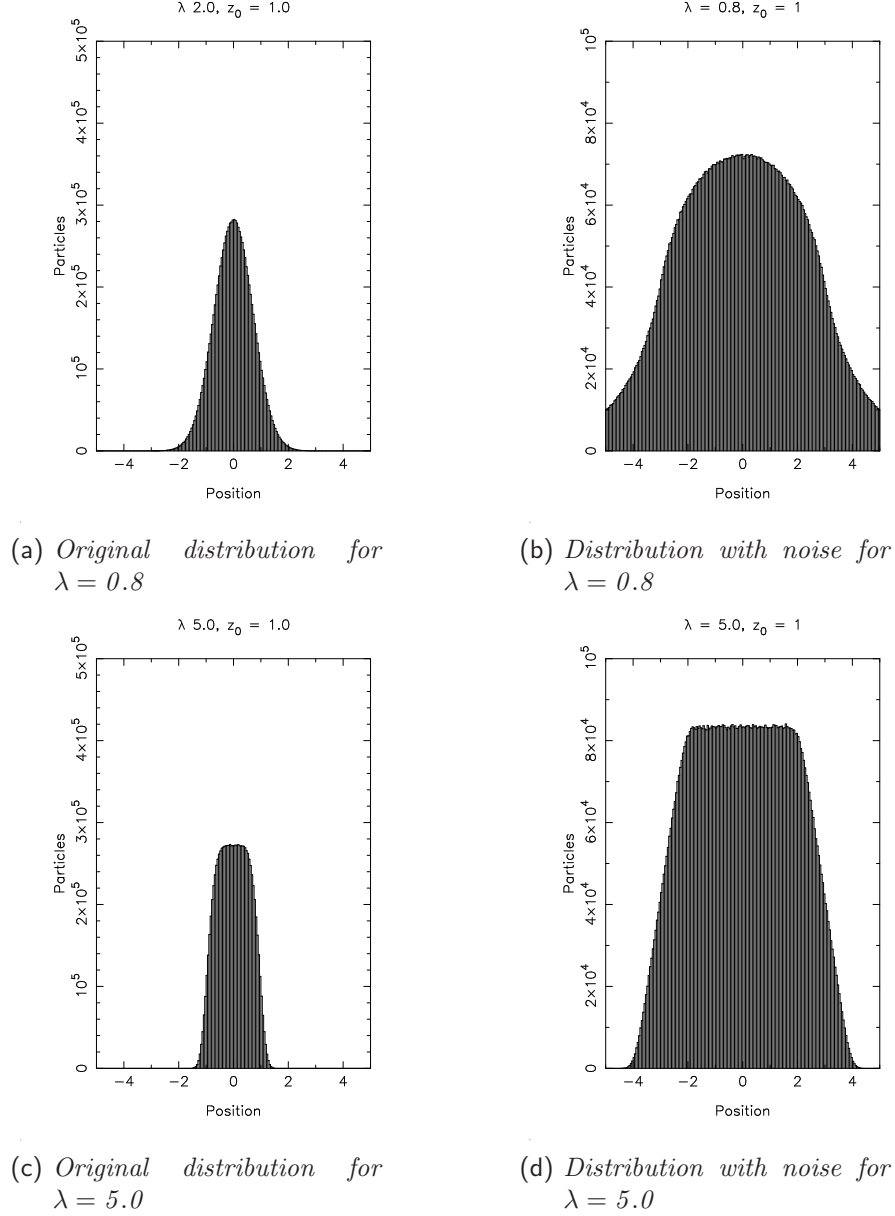
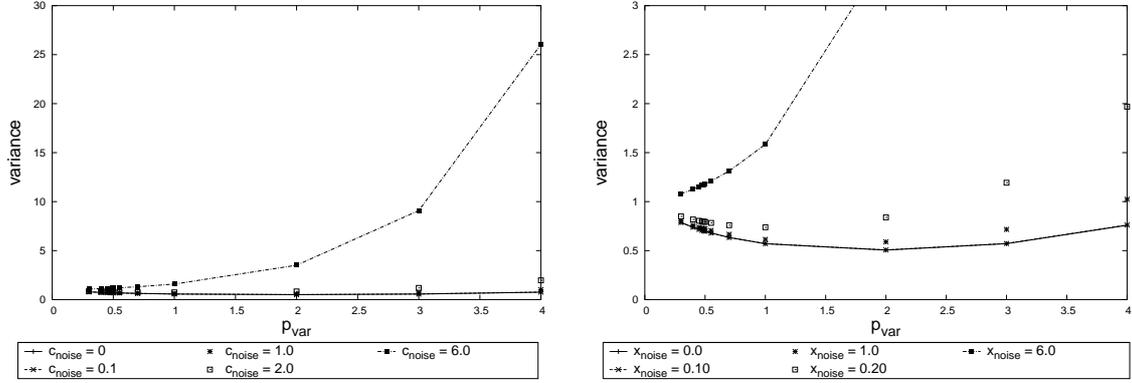
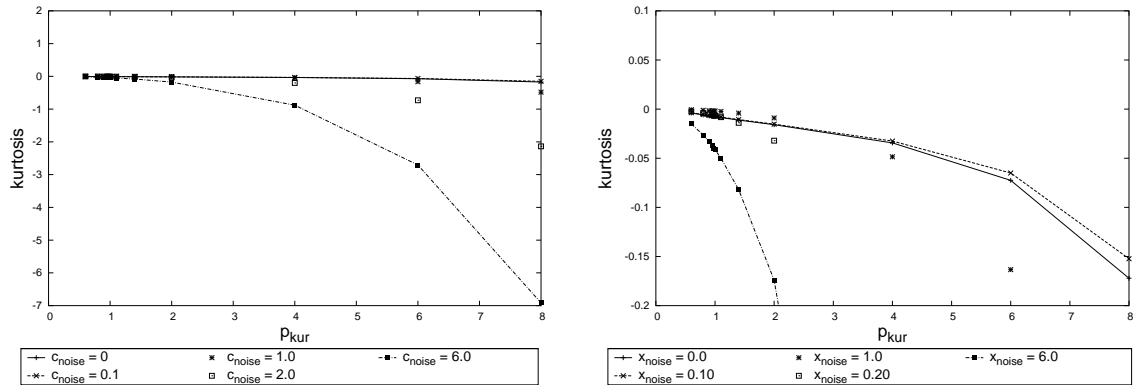


Figure A.6: As an example for the random redistribution of particles two analyzed distributions are shown, with on the left side the appropriate original distributions (Fig. (a) and Fig. (c)). In both altered cases the maximum redistribution length $c_{noise} = 6 \cdot z_0$ was chosen to emphasize the large effects this type of noise induces. Specially in the case of $\lambda = 0.8$ the characteristic of the original distribution (a sharply peaked central region) has altered to the contrary, i.e., to a slowly rising flat plateau. (b) The shape parameter λ is set to 0.8 (d) Here the shape parameter λ is set to 5.0.



(a) Analysis of the stability of variance calculation (b) Enlarged view of a part of (a)

Figure A.7: Analysis of the stability of the variance calculation under the influence of noise in the underlying distribution. The parameters used for the analyzed distributions are: $z_0 = 1.0$, $\lambda = 2.0$; spatial extension of the central perturbed region: 0.1; deviation from original distribution at the center: 20%; max. redistribution range of particles: $c_{noise} = 0.1, 1.0, 2.0, 6.0 \cdot z_0$; exponent used for calculation of the variance: 0.5 to 4. The solid line represents the values determined for the original distribution whereas the dashed-dotted line shows the values calculated using the most disturbed distribution. Starting at exponent values of ≈ 0.7 the calculation of the variance of the strongly disturbed distributions shows qualitatively distinct results than less perturbed distributions as well as the original one. For an enlarged view of a part of the region with low exponents see Fig. A.7(b).



(a) Analysis of the stability of kurtosis calculation (b) Enlarged view of a part of (a)

Figure A.8: Analysis of the stability of kurtosis calculation under the influence of noise in the underlying distribution. For details see Fig. A.7.

region) evidences that the major deviation of the calculated values compared to values obtained using unperturbed distributions is caused by noise, redistributing randomly particles to other positions. This analysis strengthens the choice to use the value 1.1 as exponent for the kurtosis since it is not too sensitive for changes in the ideal course of the analyzed distributions caused by noise sources.

The previously discussed tests are valid for the aspect of reducing the statistical quantities' sensitivity with respect to values far from the center of the data distribution (as well as at the center) with values strongly different from the surrounding data points. Now, also the other 'side' of the problem should be focused. Indeed, the problem is to find also a value for the exponent which is still sufficiently sensitive to detect most distributions present in the simulations correctly. A statistical measure which is robust under the aspect of outliers but insensitive to most of the smoothly decaying distribution is useless for the present purposes. That aspect is largely time consuming to cover and therefore in the framework of this thesis it was opted to first develop a high quality method to describe the VSFBD of objects obtained by observational astronomy rather than to continue on this topic. The effort to do both would have surmounted the time allocated for the project, especially under the aspect of analyzing as soon as possible the observed galaxy sample. In fact, the investigations done in Chap. 4.3.4 have shown a possible and reliable alternative to the GGau approach. The GaHe approach could provide a means of describing the large amount of substructure visible in Fig. A.1 based on the characteristic that the GaHe approach uses an orthonormal set of functions. However, it is clear that the number of terms used for the fitting process should be increased to account for additional structure. That possibility and the continuation of the previously presented method could be done in a subsequent project distinct from this thesis.

Appendix B

Conversion of the Sérsic Law to Generalized Gaussians

The description of the galaxies' vertical surface brightness profiles with Generalized Gaussians is equivalent to the description with the Sérsic Law widely used for the fitting of radial profiles of disk galaxies. For comparison also a canonical Gaussian is shown.

$$\text{Sérsic Law} \quad : \quad \Sigma_s(r) = \Sigma_e \exp \left[-\kappa(n) \left[(r/r_e)^{1/n} - 1 \right] \right] \quad (\text{B.1})$$

$$\text{Gaussian} \quad : \quad \Sigma_g(r) = \frac{1}{\sqrt{2\pi}\sigma} \exp \left[-\frac{1}{2} \left(\frac{r}{\sigma} \right)^2 \right] \quad (\text{B.2})$$

$$\text{Generalized Gaussian:} \quad \Sigma_{gg}(r) = \Sigma_0 \cdot \exp \left[-(|r|/r_0)^\lambda \right]. \quad (\text{B.3})$$

The parameters characterizing the functions and used as fitting parameters are the following:

Sérsic law	Generalized Gaussian
r_e : the half light radius	r_0 : the scale factor of the function
Σ_e : surface brightness at r_e	Σ_0 : the central surface brightness
n : the power law index with κ depending on n	λ : the shape parameter

To establish relations between the parameters of Generalized Gaussians and the Sérsic Law will be rewritten in a different way. First the central surface brightness in both profiles is calculated:

$$\Sigma_s(0) = \Sigma_e \exp(\kappa) \quad (\text{B.4})$$

$$\Sigma_{gg}(0) = \Sigma_0. \quad (\text{B.5})$$

Using the result of equations B.4 and B.5 it follows:

$$\Sigma_s(r) = \Sigma_0 \exp \left[-\kappa(r/r_e)^{1/n} \right]. \quad (\text{B.6})$$

The formula can be further simplified by introducing the following new variables

$$\lambda = 1/n, \quad \rho = \kappa(r/r_e)^\lambda \Rightarrow r = r_e(\rho/\kappa)^{1/\lambda} \quad (\text{B.7})$$

$$\text{and} \quad dr = r_e/(\kappa^{1/\lambda}\lambda) \cdot \rho^{\frac{1}{\lambda}-1} d\rho. \quad (\text{B.8})$$

B. CONVERSION OF THE SÉRSIC LAW TO GENERALIZED GAUSSIANS

and using them in equation B.6:

$$\Sigma_s = \Sigma_0 \exp(-\rho). \quad (\text{B.9})$$

To get a relation between the power law index n and κ the fact that half of the total flux F_{tot} is reached at the radius r_e can be used. Therefore first it has to be integrated to infinity to determine the total flux F_{tot}

$$F_{tot} = \int_0^\infty \Sigma_s dr = \int_0^\infty \Sigma_0 \exp(-\rho) dr \quad (\text{B.10})$$

$$= \Sigma_0 \frac{r_e}{\kappa^{1/\lambda}} \int_0^\infty \rho^{\frac{1}{\lambda}-1} \cdot \exp(-\rho) d\rho \quad (\text{B.11})$$

$$= \Sigma_0 \frac{r_e n}{\kappa^n} \int_0^\infty \rho^{n-1} \cdot \exp(-\rho) d\rho. \quad (\text{B.12})$$

with reintroducing n through $\lambda = 1/n$. The form of the integral is related to the gamma function $\Gamma(x)$

$$\Gamma(x) = \int_0^\infty t^{x-1} \cdot \exp(-t) dt \quad (\text{B.13})$$

and therefore the expression for the total flux F_{tot} can be given as

$$F_{tot} = \Sigma_0 \frac{r_e n}{\kappa^n} \cdot \Gamma(n). \quad (\text{B.14})$$

The calculation of half of the total flux includes the same steps as before but using a different upper integration limit, which corresponds to the half light radius r_e

$$\frac{F_{tot}}{2} = \Sigma_0 \frac{r_e n}{\kappa^n} \int_0^\kappa \rho^{n-1} \cdot \exp(-\rho) d\rho, \quad \text{with } [\rho]_{r_e} = \kappa. \quad (\text{B.15})$$

The former integral can be solved by using the incomplete gamma function

$$\gamma(a, x) = \int_0^x t^{a-1} \cdot \exp(-t) dt. \quad (\text{B.16})$$

Equation B.15 can then be rewritten with B.16 as

$$F_{tot} = \Sigma_0 \frac{2r_e n}{\kappa^n} \cdot \gamma(n, \kappa). \quad (\text{B.17})$$

Now equation B.14 can be used to write an equation depending only on the parameters n and κ :

$$\Gamma(n) = 2\gamma(n, \kappa) \quad (\text{B.18})$$

It is not possible to solve equation B.18 analytically but only with numerical methods. Some authors have calculated approximations to the relation between κ and n , which in part are determined by analyzing the numerical results for a fixed range in n (e.g., $n > 1$). Here three of them are listed: Caon et al. (1993); Ciotti & Bertin (1999); Balcells, Domínguez-Palmero, Graham, & Peletier (2001)

B. CONVERSION OF THE SÉRSIC LAW TO GENERALIZED GAUSSIANS

$$\text{Caon et al. (1993)} \quad : \quad \kappa = 2.17 n - 0.355 \quad (\text{B.19})$$

$$\text{Ciotti \& Bertin (1999):} \quad \kappa = 2 n - \frac{1}{3} + \frac{4}{405 n} + \frac{46}{25515 n^2} + \mathcal{O}(n^{-3}) \quad (\text{B.20})$$

$$\text{Balccells et al. (2001)} \quad : \quad \kappa = 1.9992 n - 0.3271 \quad (\text{B.21})$$

The conversion of parameter values determined by fitting Generalized Gaussians to values of parameters used in the Sérsic Law is then straight forward. For the formula presented by Ciotti & Bertin (1999) (expansion to the 2nd order of n) this results in:

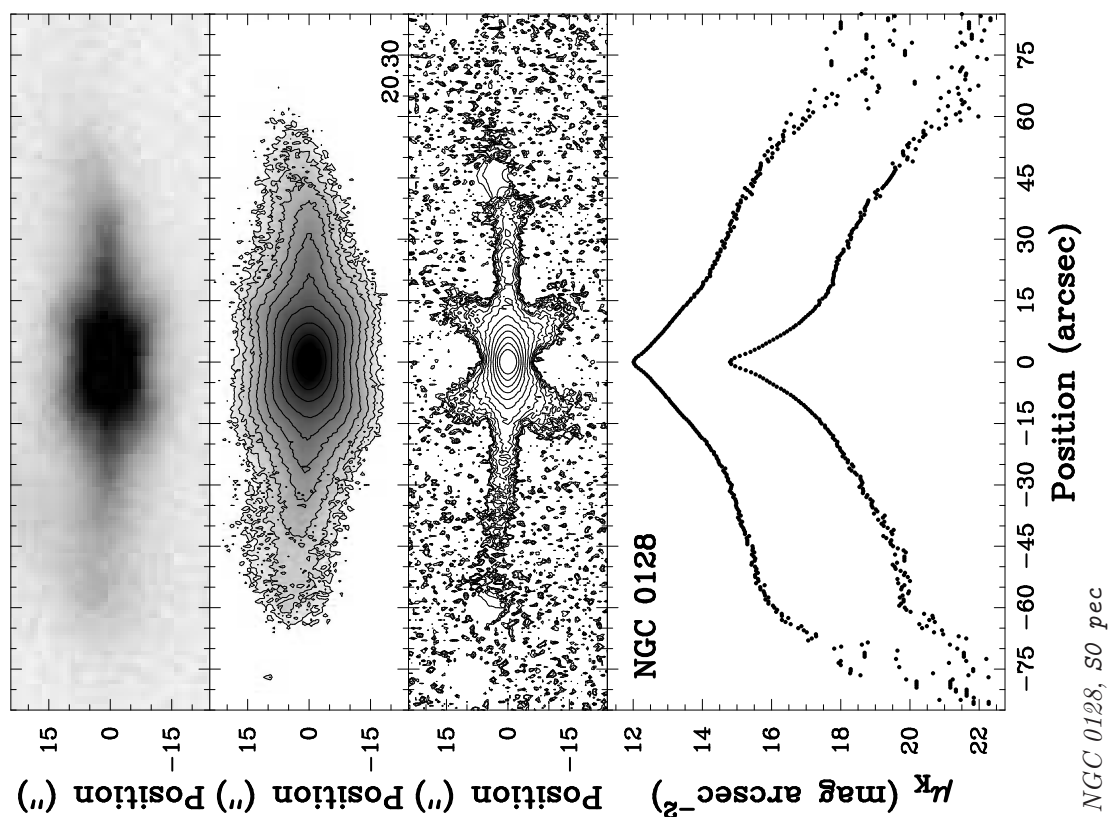
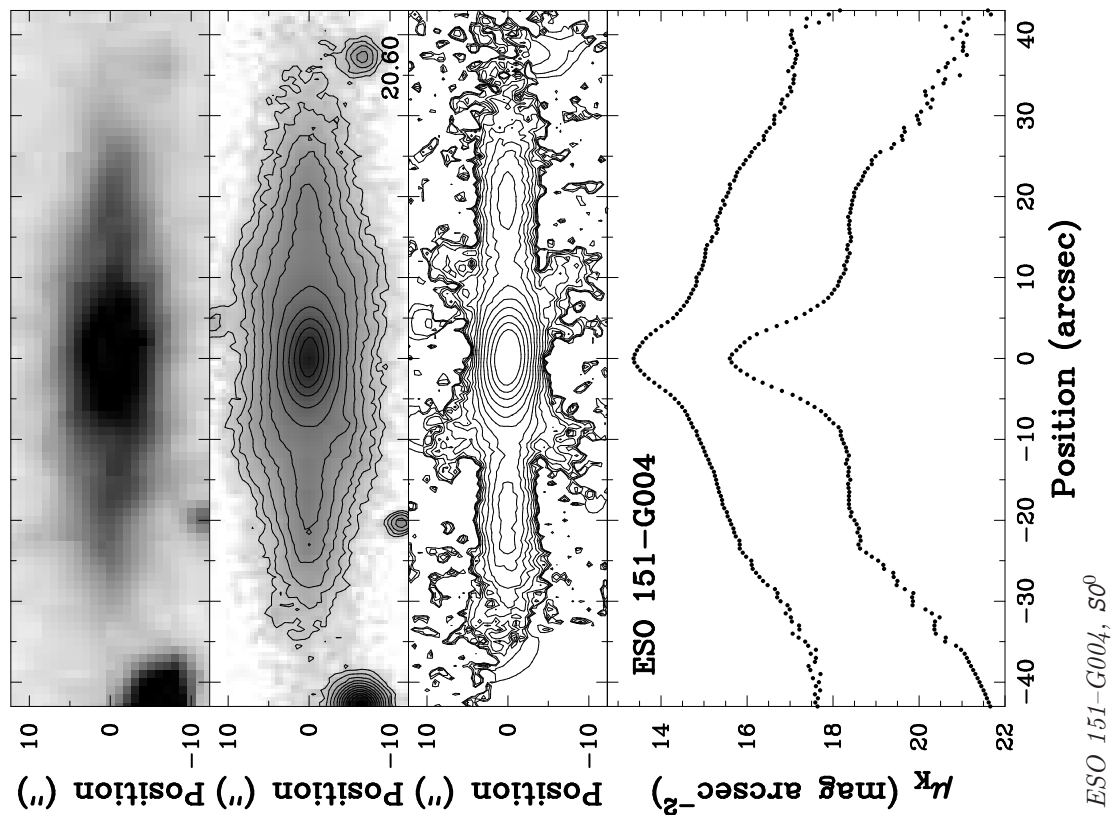
$$n = \frac{1}{\lambda}, \quad \kappa = \frac{2}{\lambda} - \frac{1}{3} + \frac{4\lambda}{405} + \frac{46\lambda^2}{25515}, \quad r_e = r_0 \cdot \kappa^{\frac{1}{\lambda}}, \quad \Sigma_e = \frac{\Sigma_0}{\exp(\kappa)}. \quad (\text{B.22})$$

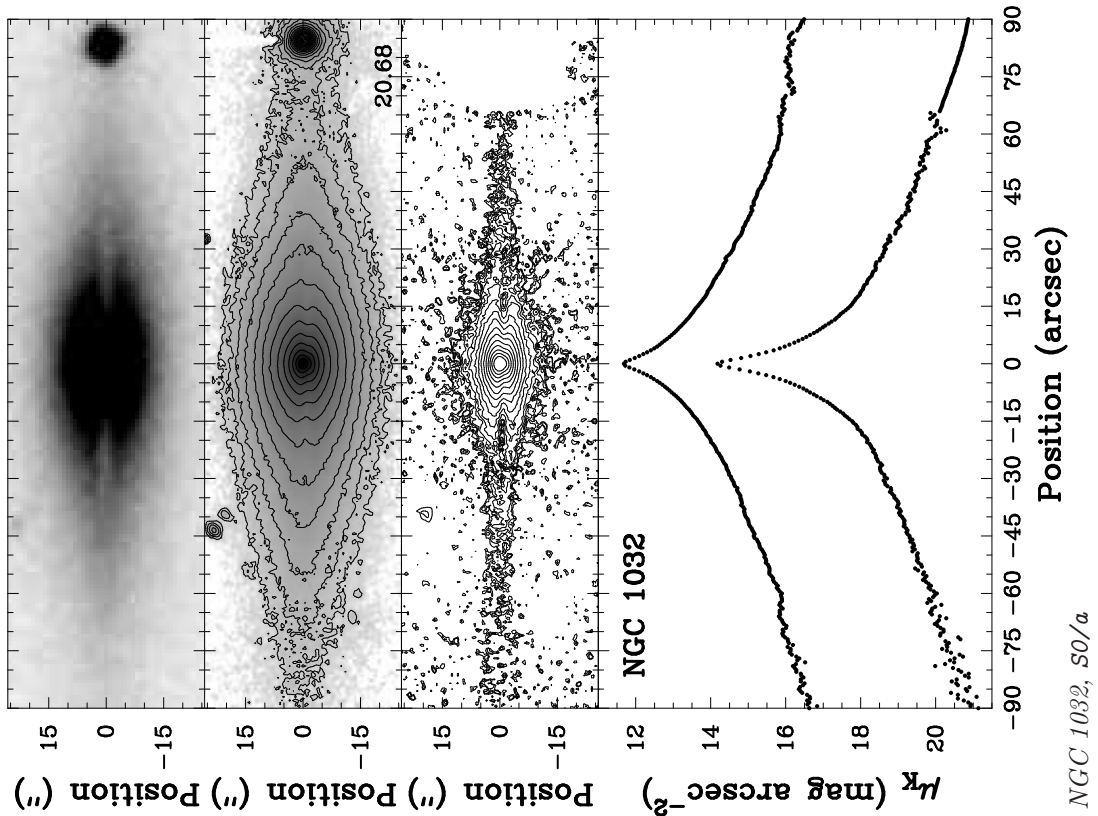
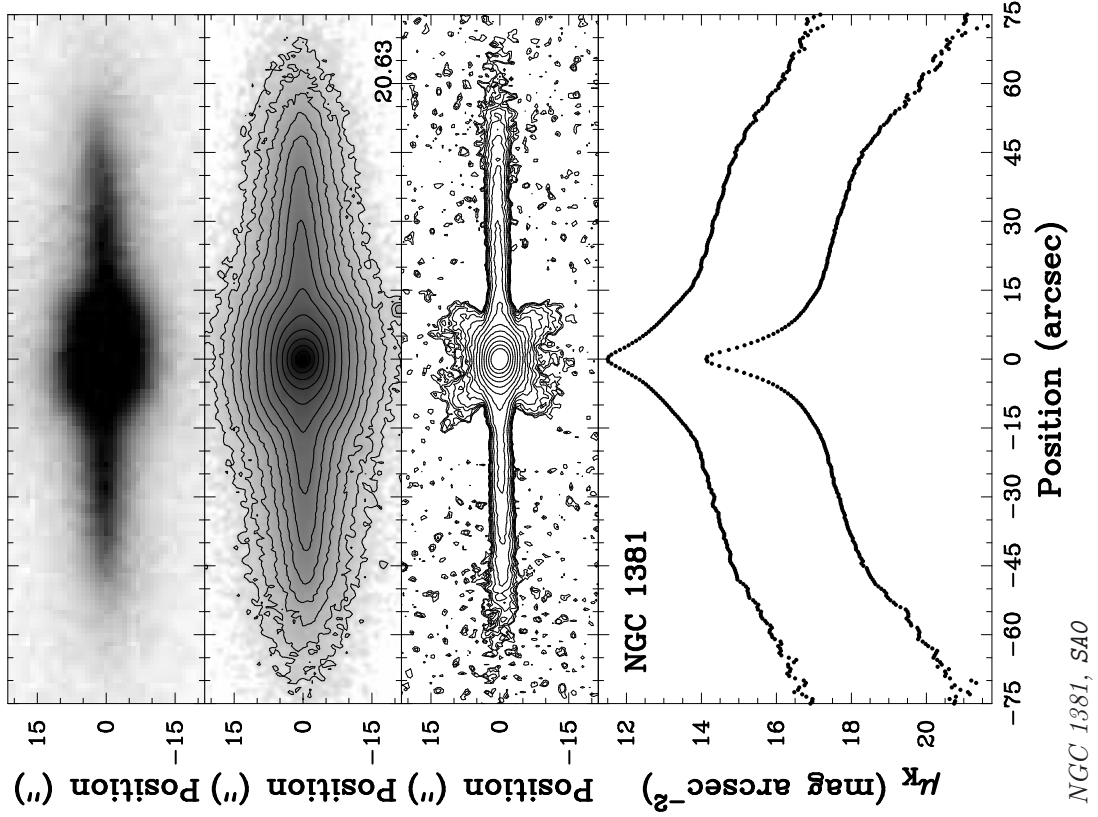
Appendix C

Photometry of the sample galaxies

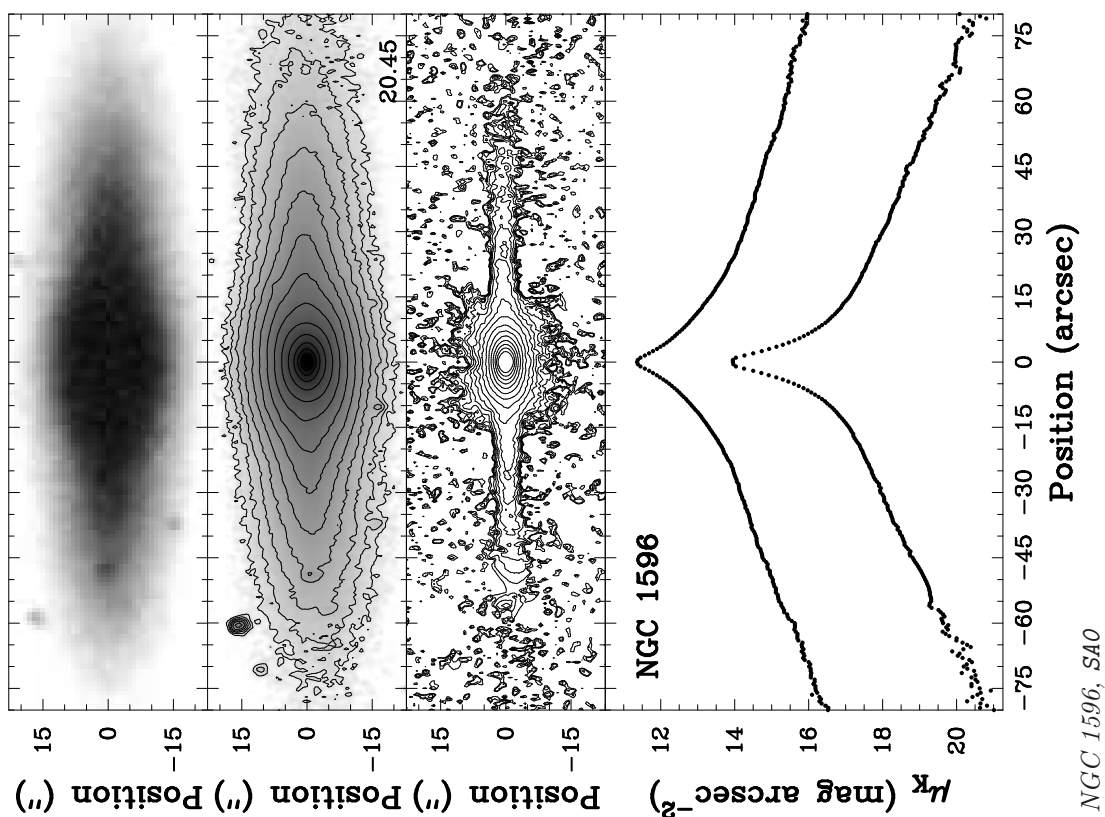
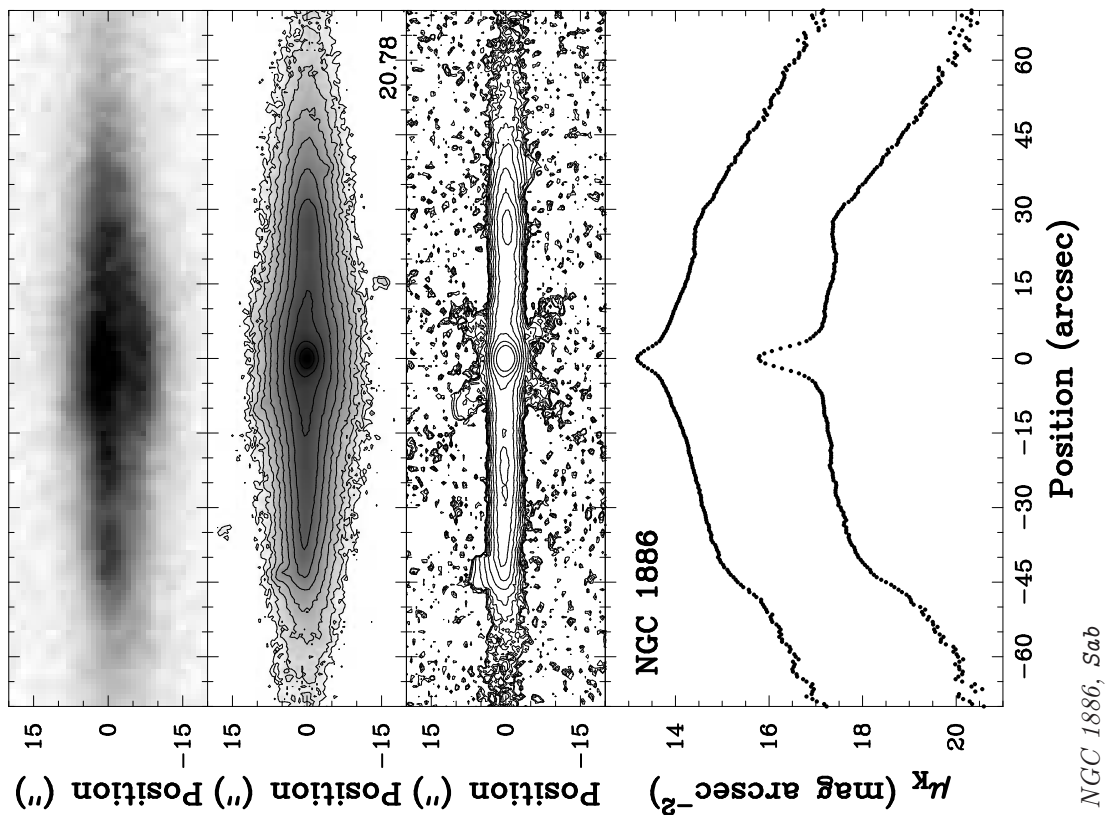
Here the R -band, K -band, and unsharp masked K -band images as well as surface brightness plots for each individual galaxy are presented. At the top of each panel a greyscale DSS2 R -band image is shown. Below of that a greyscale K -band image observed at the SSO is plotted with the superposition of surface brightness isocontours starting from the brightest level and plotted at an interval of 0.3 mag. The lowest level was determined in such a way that it reaches the noise of the background and its value is written in the lower right corner of the image. In the third panel a surface brightness isocontour image of the unsharp masked K -band image is shown. It is based on the K -band image with background interpolated stars. For the isocontours the same settings as for the K -band image were chosen. In some cases large background noise visibility was taken into account to enhance small structure. At the bottom a surface brightness profile of the galaxy major axis as well as surface brightness profile representing the vertically summed surface brightness is shown in units of magnitude/arcsec² and plotted along the radial direction. The lower profile is the major axis profile whereas the upper one is the vertically summed profile. Below of each panel the galaxy name and the classification type (see Tab. 2.2) are given. The galaxies are sorted by increasing right ascension.

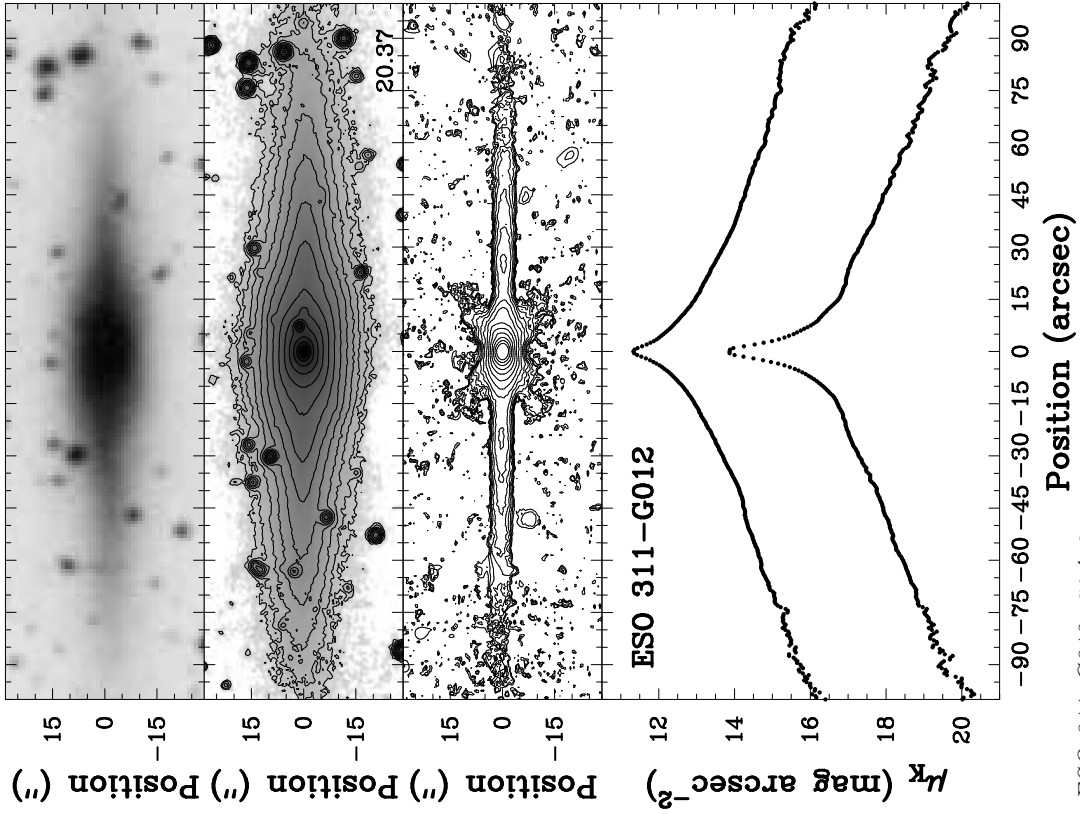
C. PHOTOMETRY OF THE SAMPLE GALAXIES



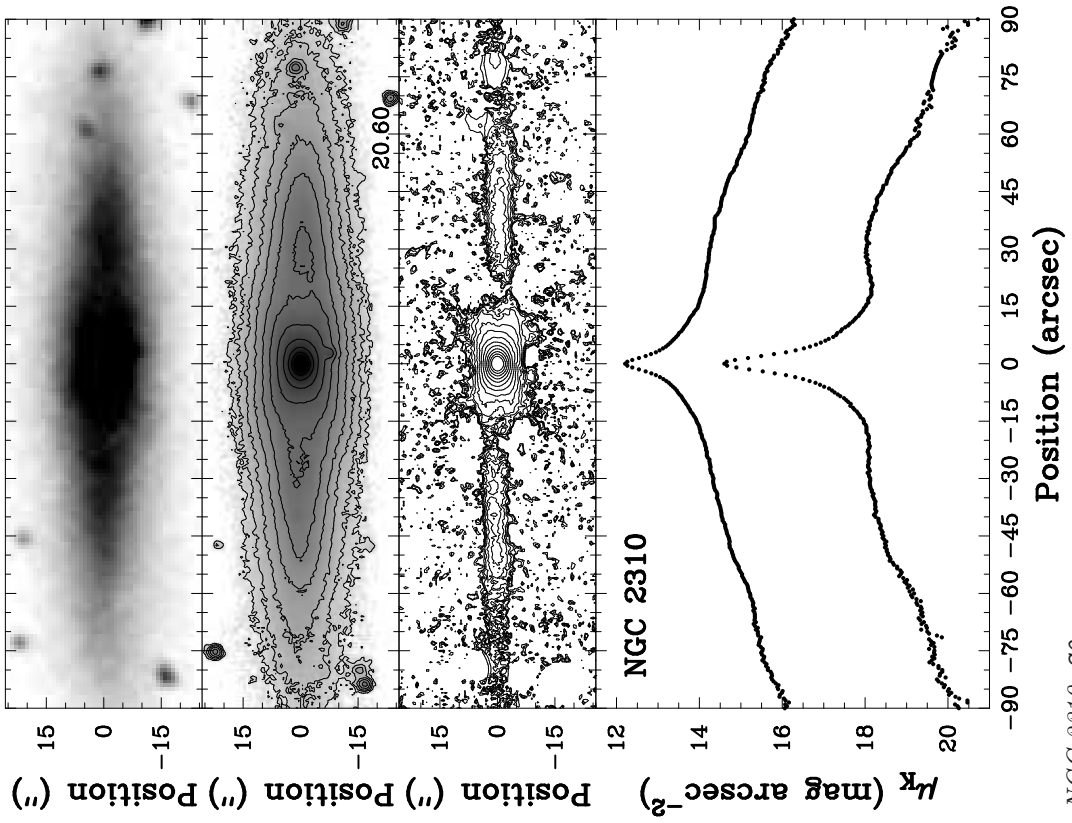


C. PHOTOMETRY OF THE SAMPLE GALAXIES



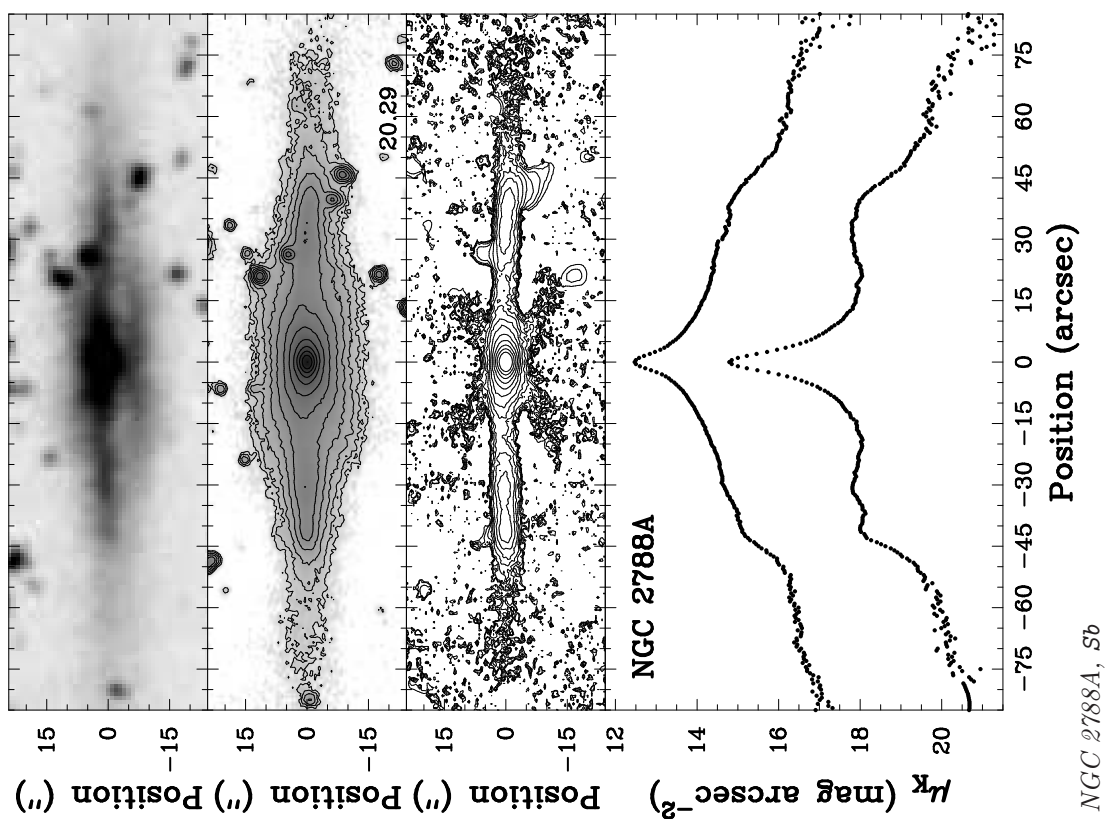
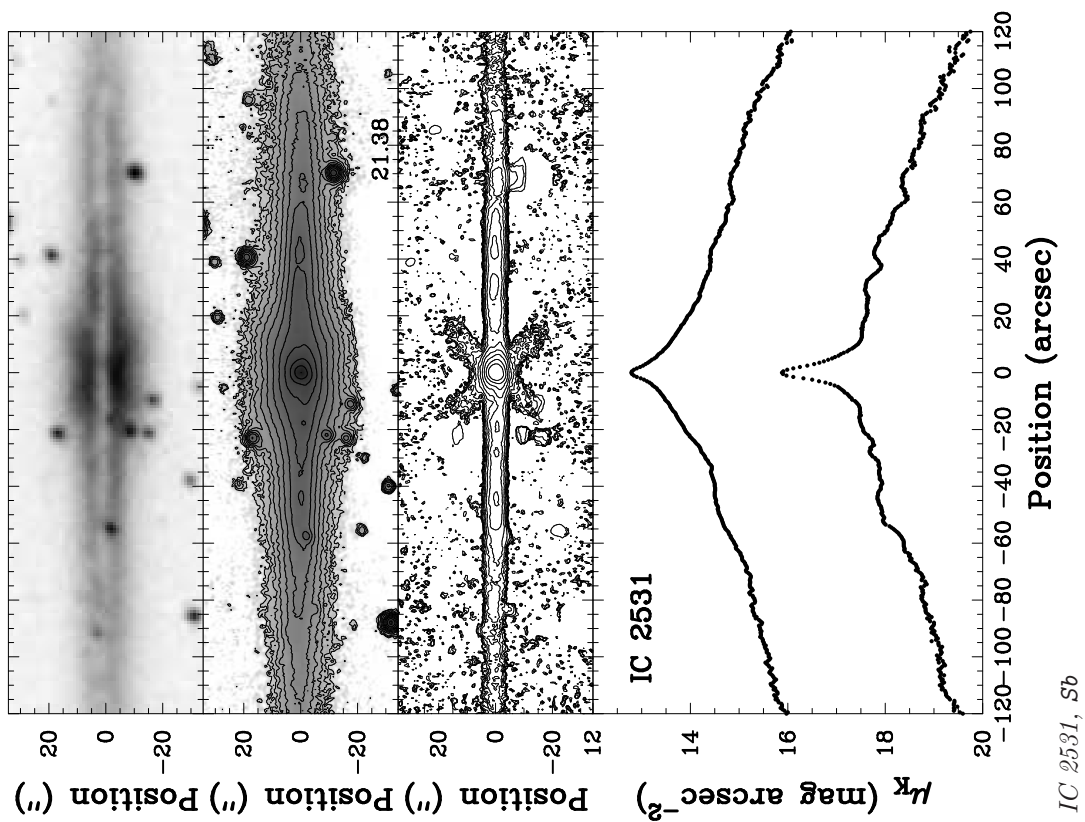


ESO 311-G012, $S_0/a?$

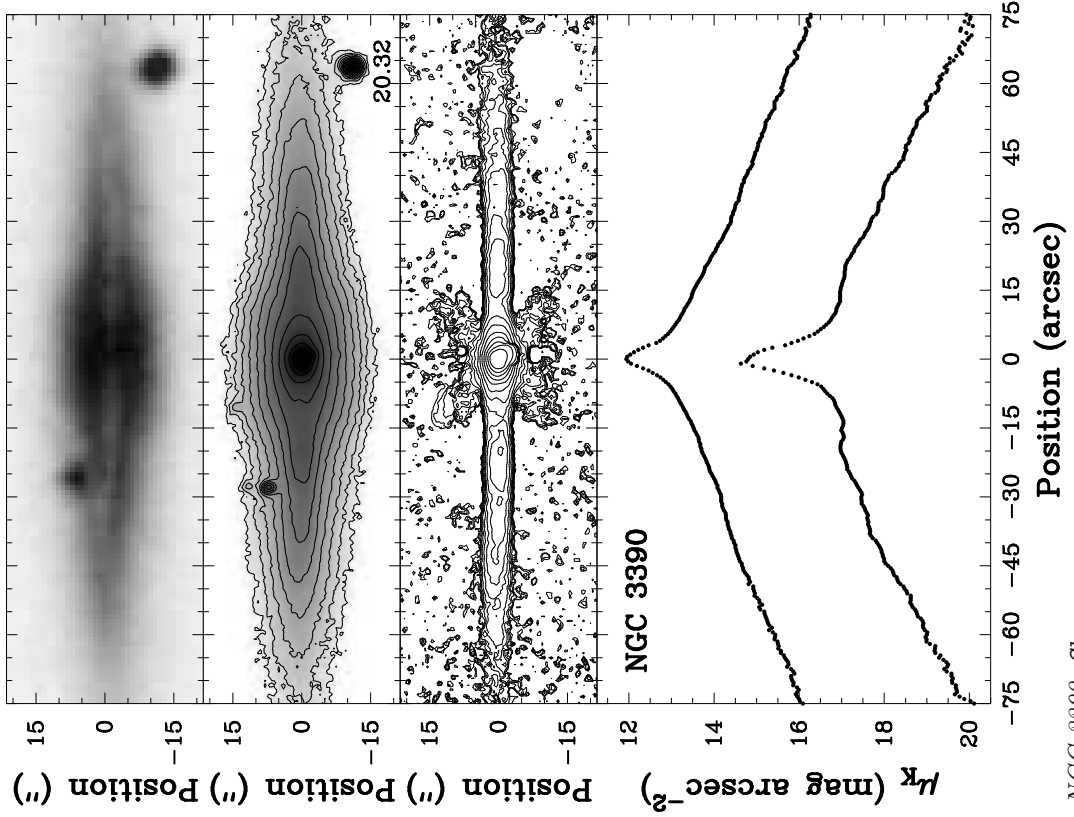


NGC 2310, S_0

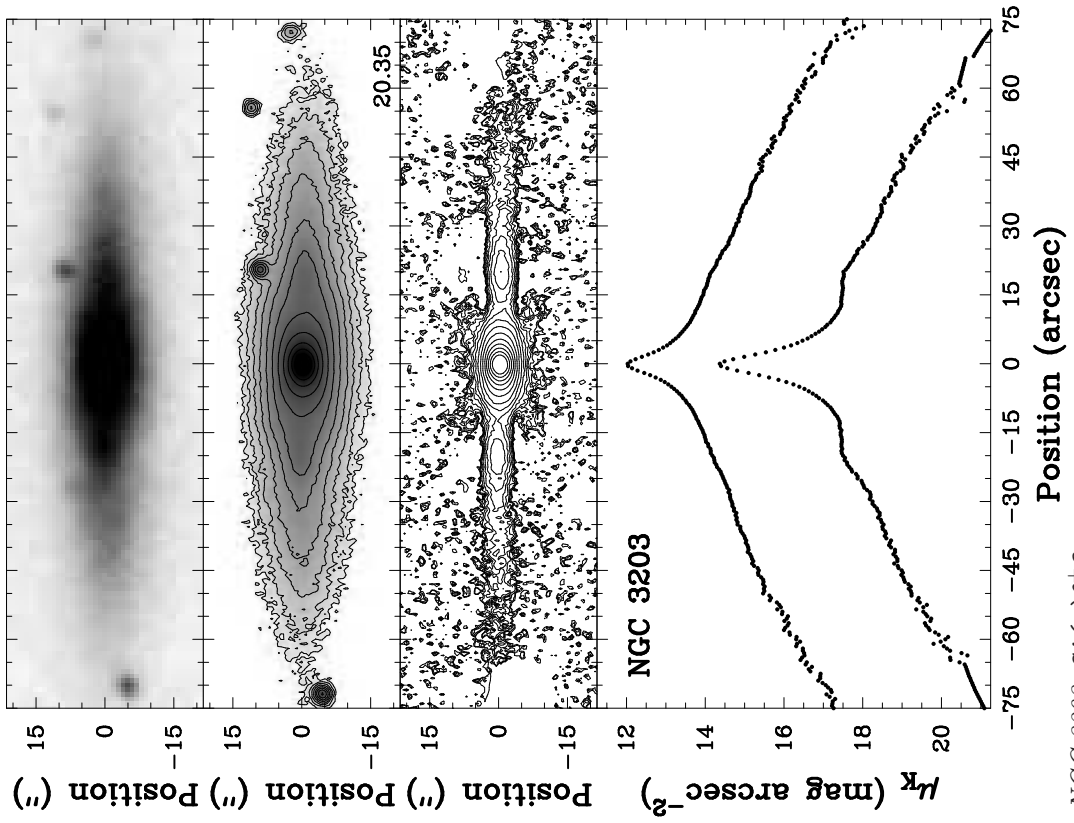
C. PHOTOMETRY OF THE SAMPLE GALAXIES



C. PHOTOMETRY OF THE SAMPLE GALAXIES

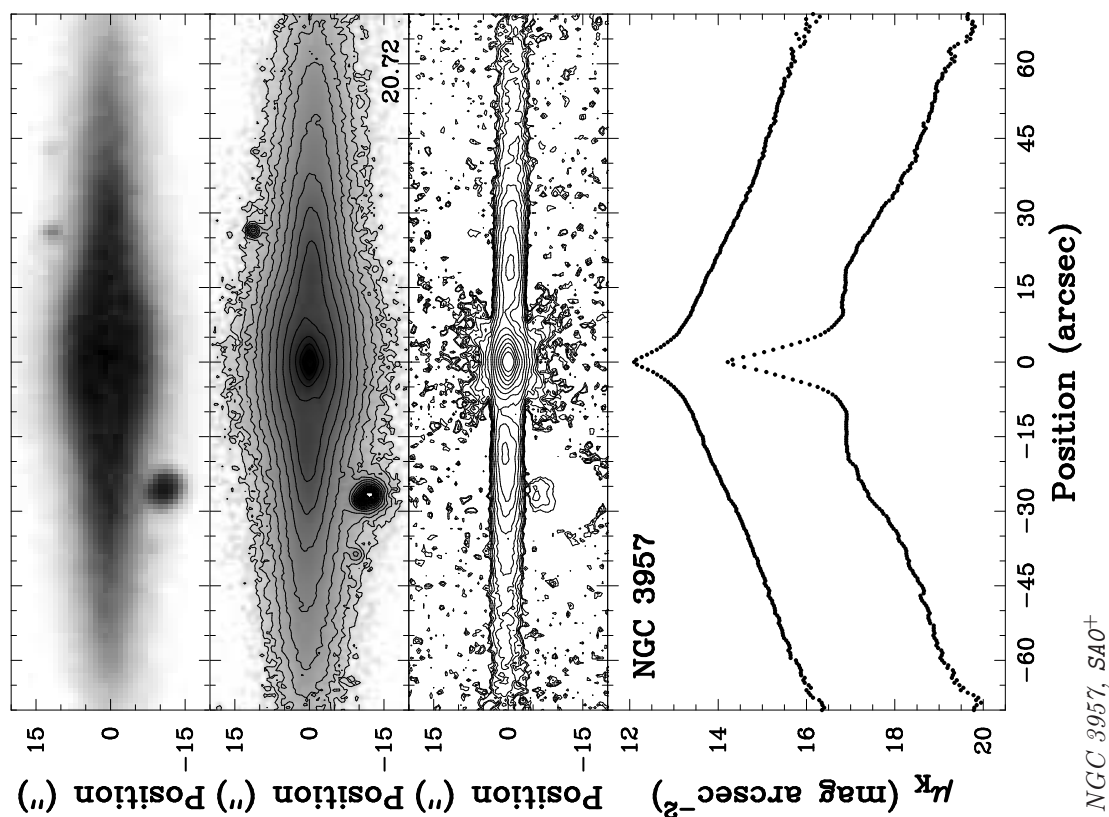
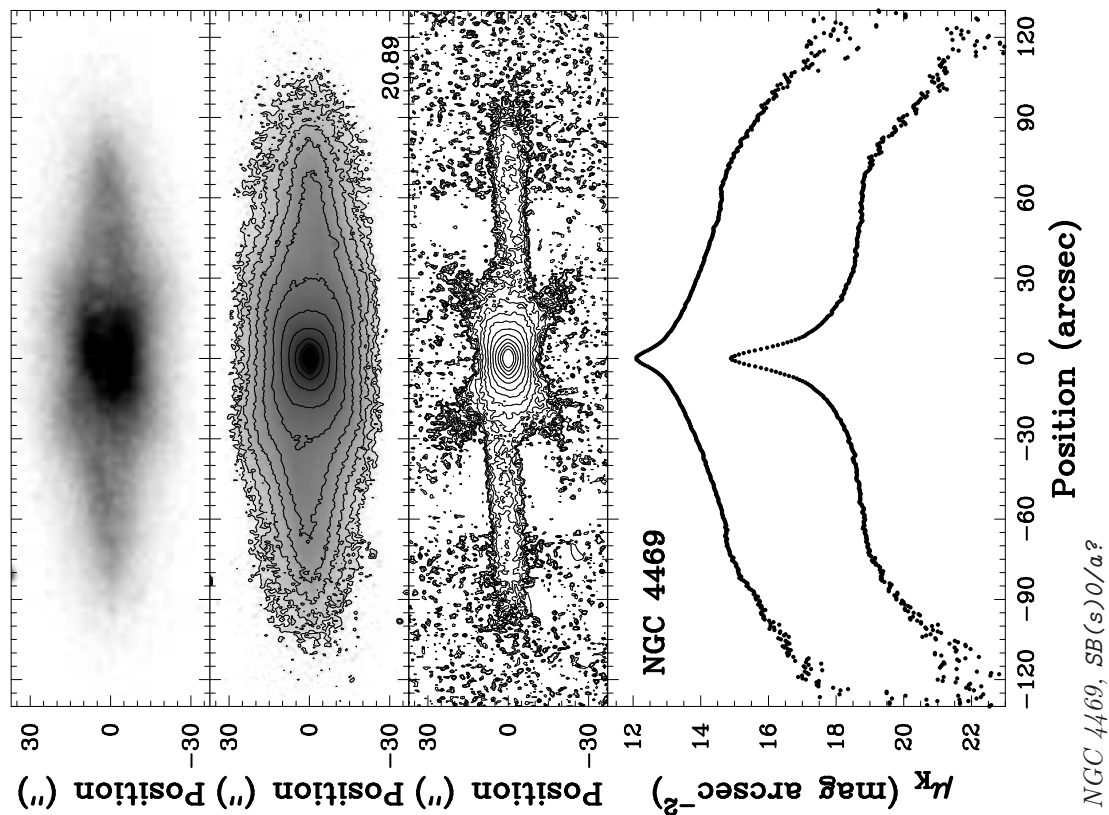


NGC 3390, Sb

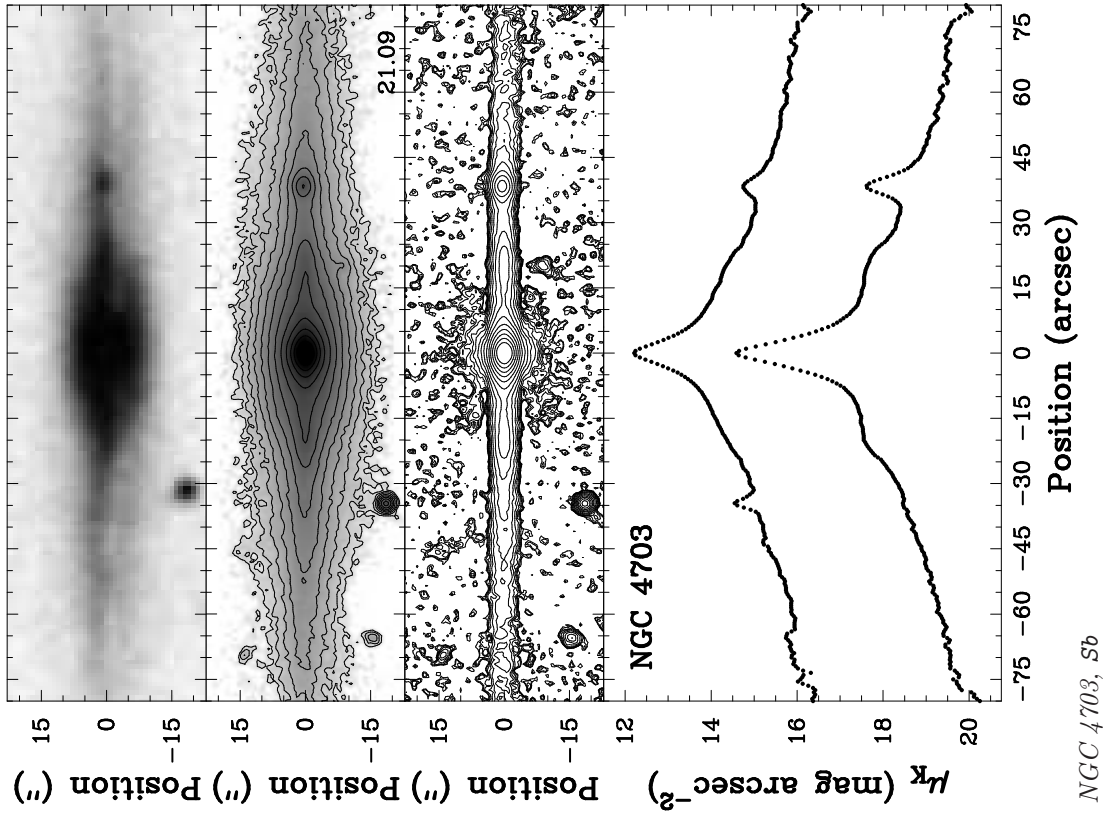
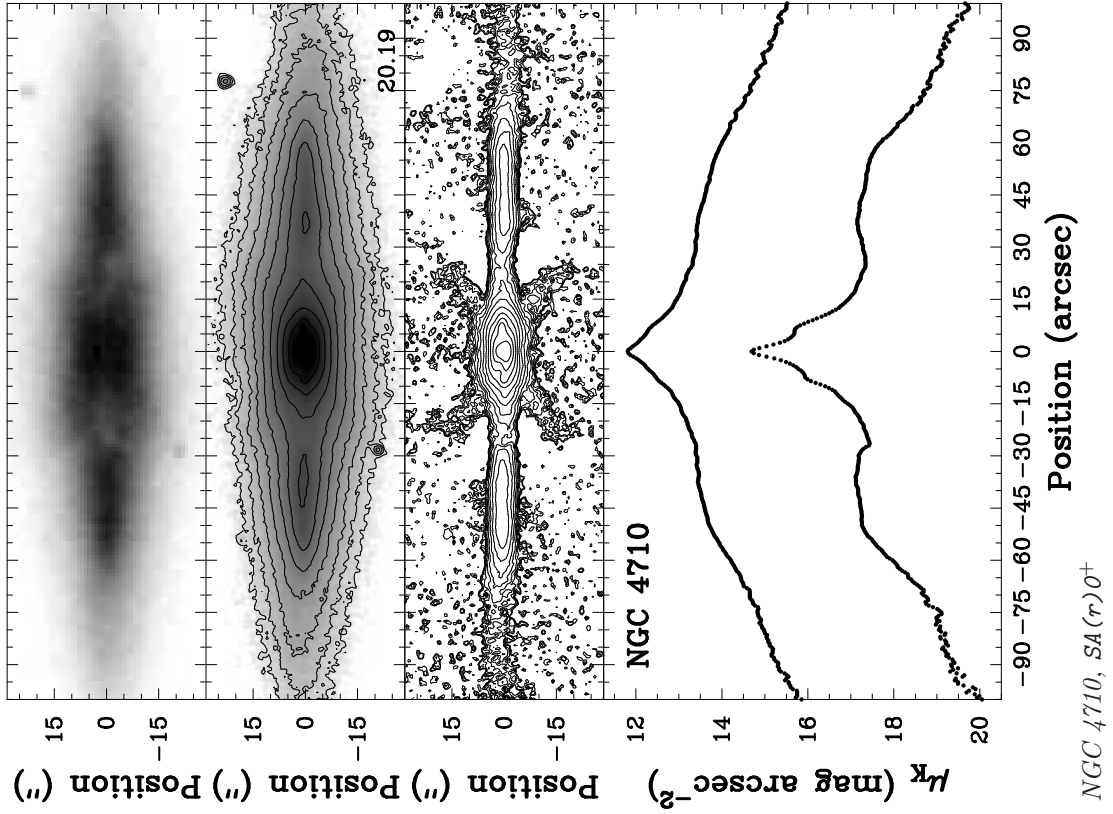


NGC 3203, SA(r)0⁺?

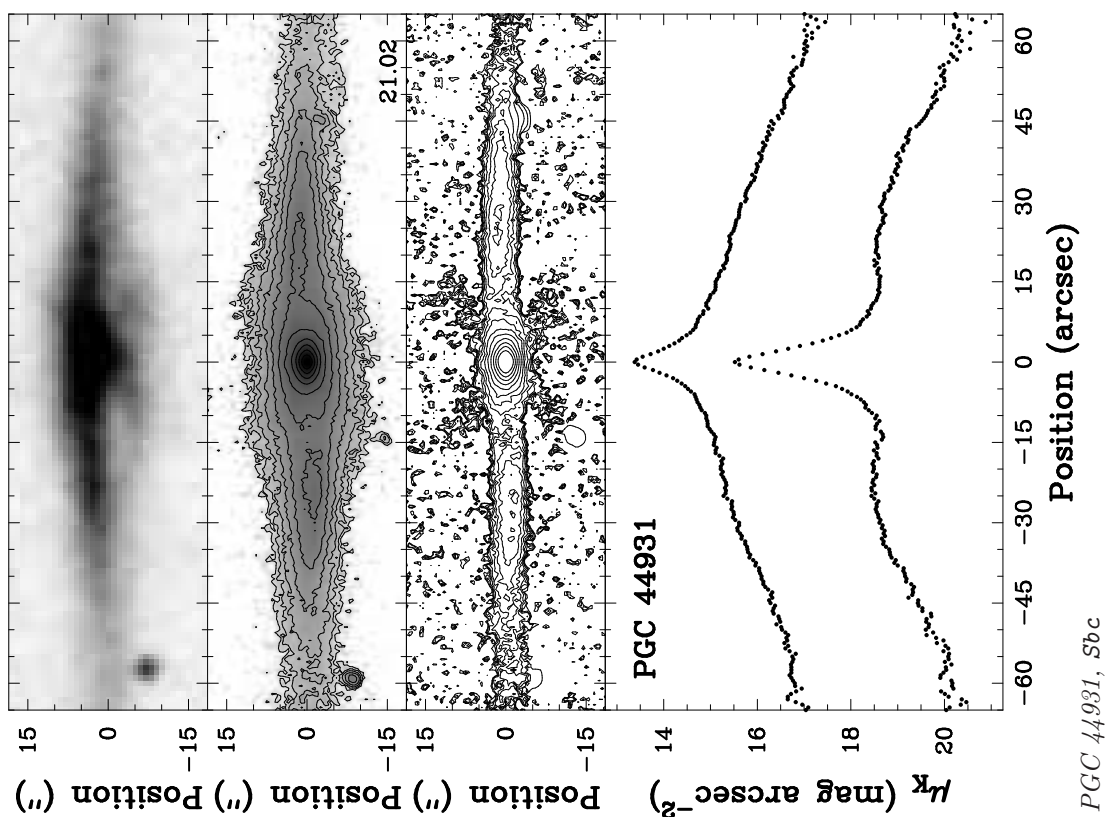
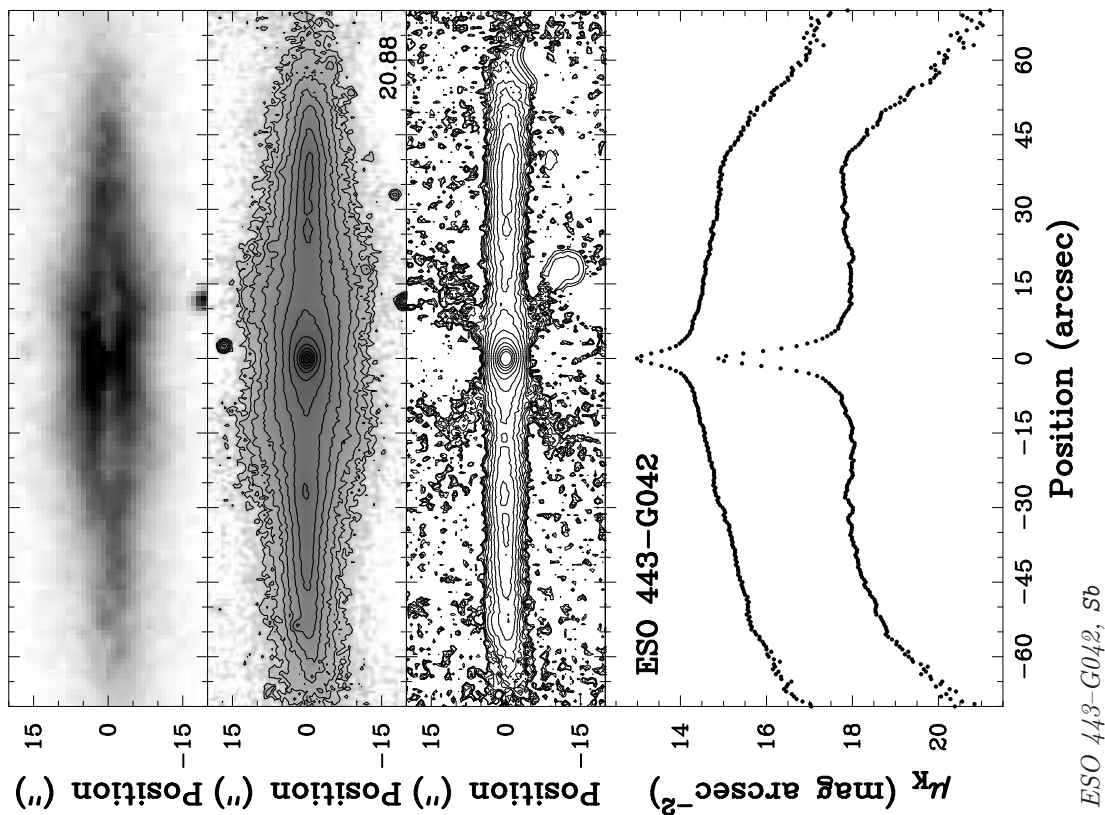
C. PHOTOMETRY OF THE SAMPLE GALAXIES

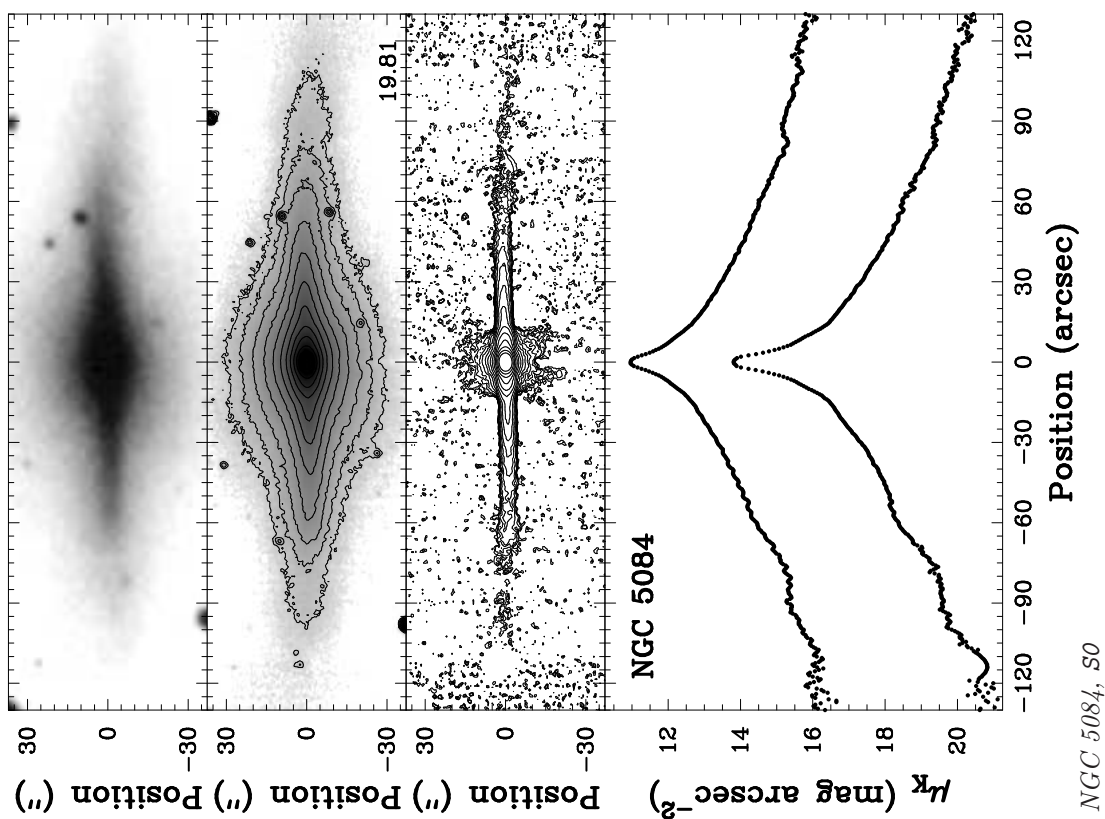
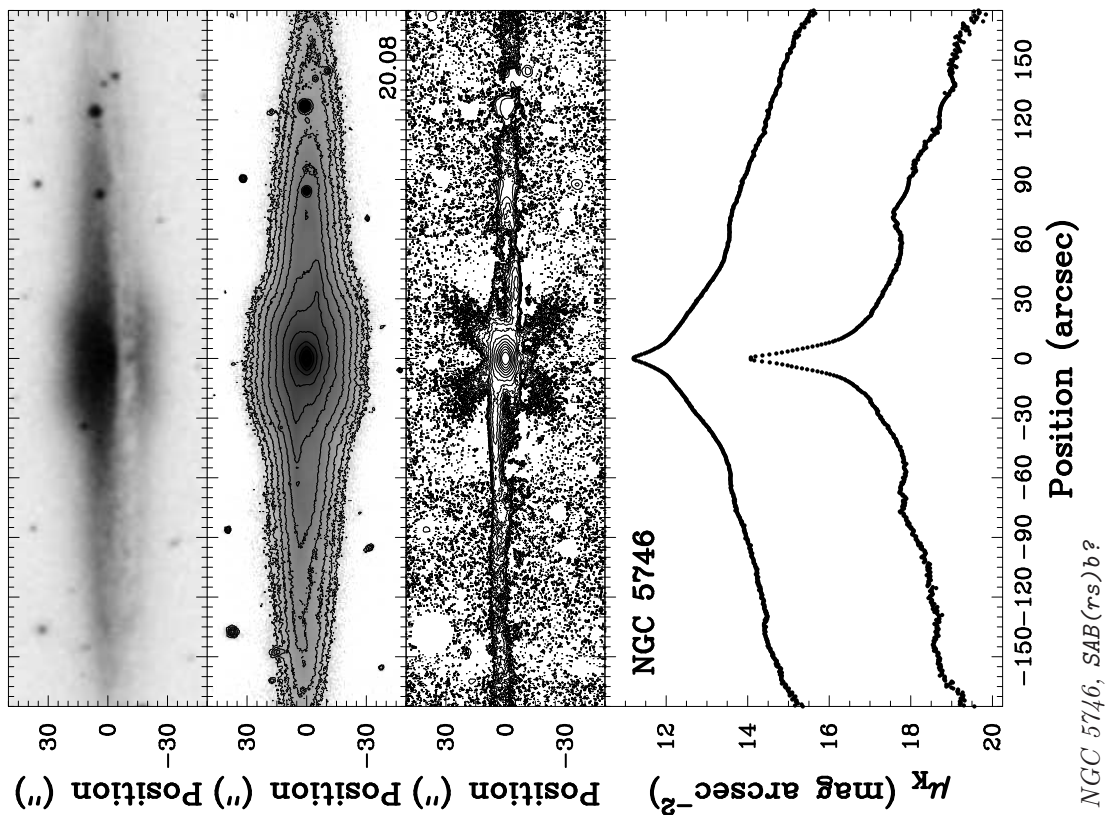


C. PHOTOMETRY OF THE SAMPLE GALAXIES

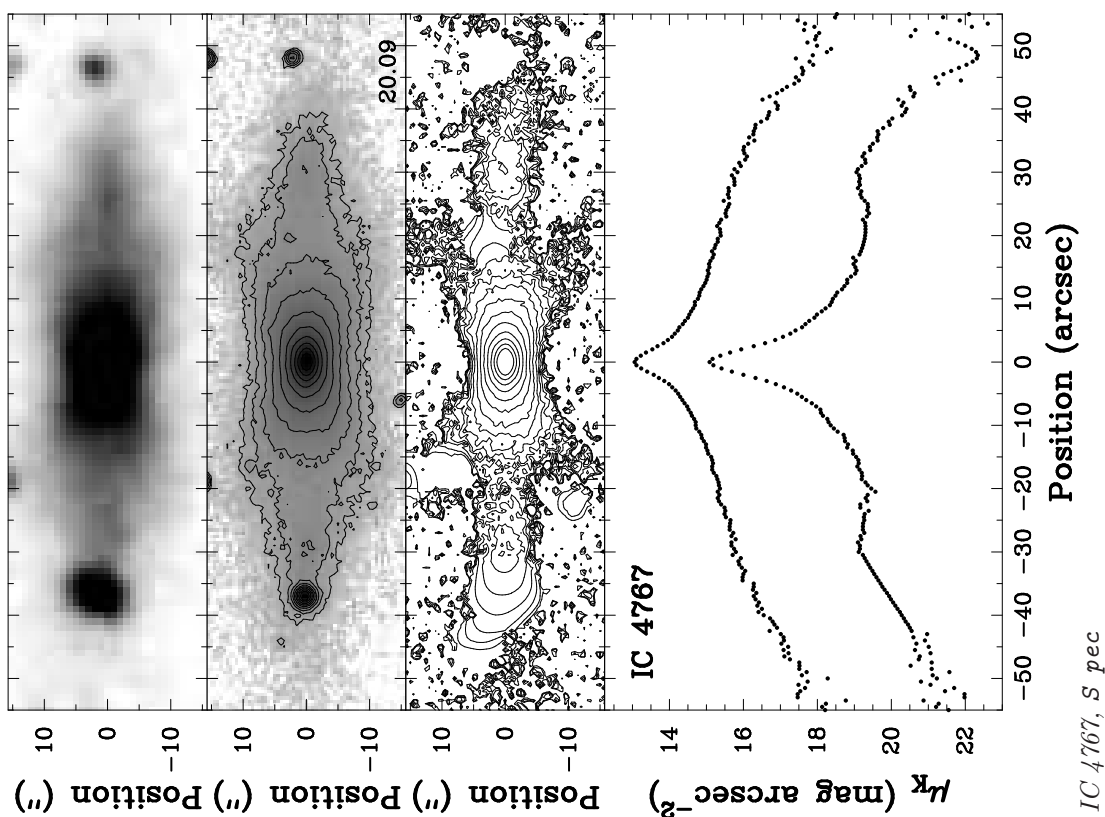
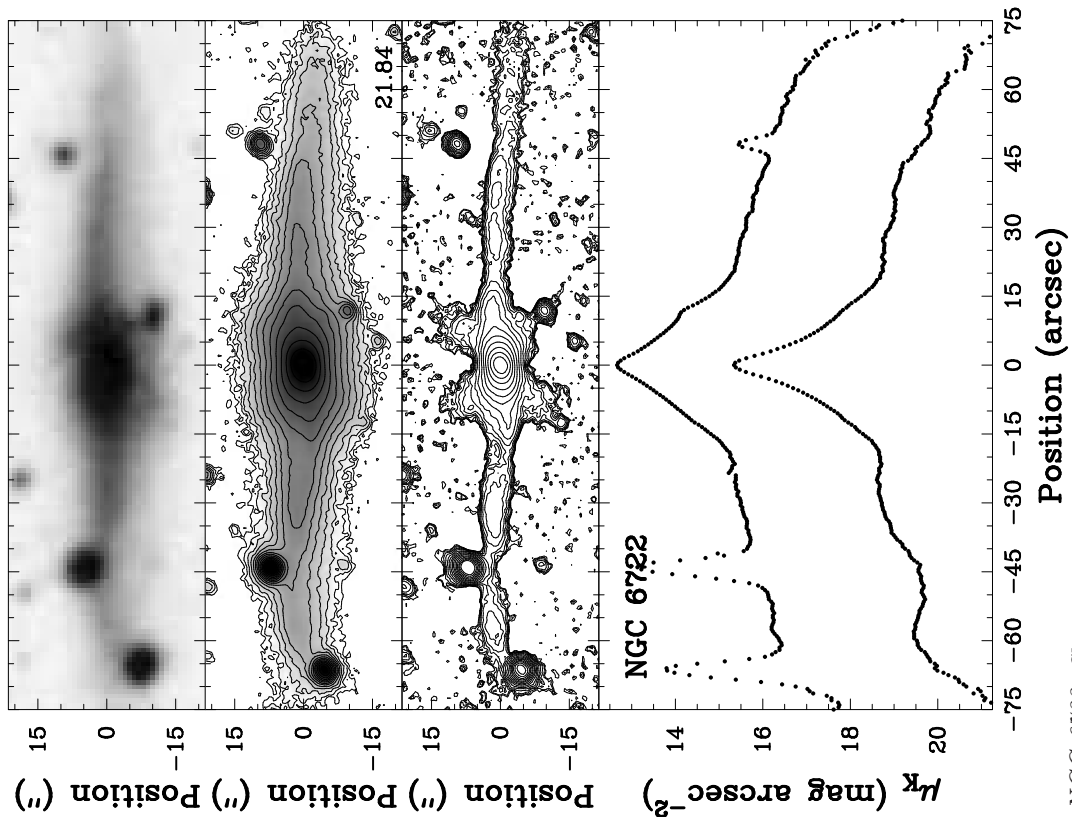


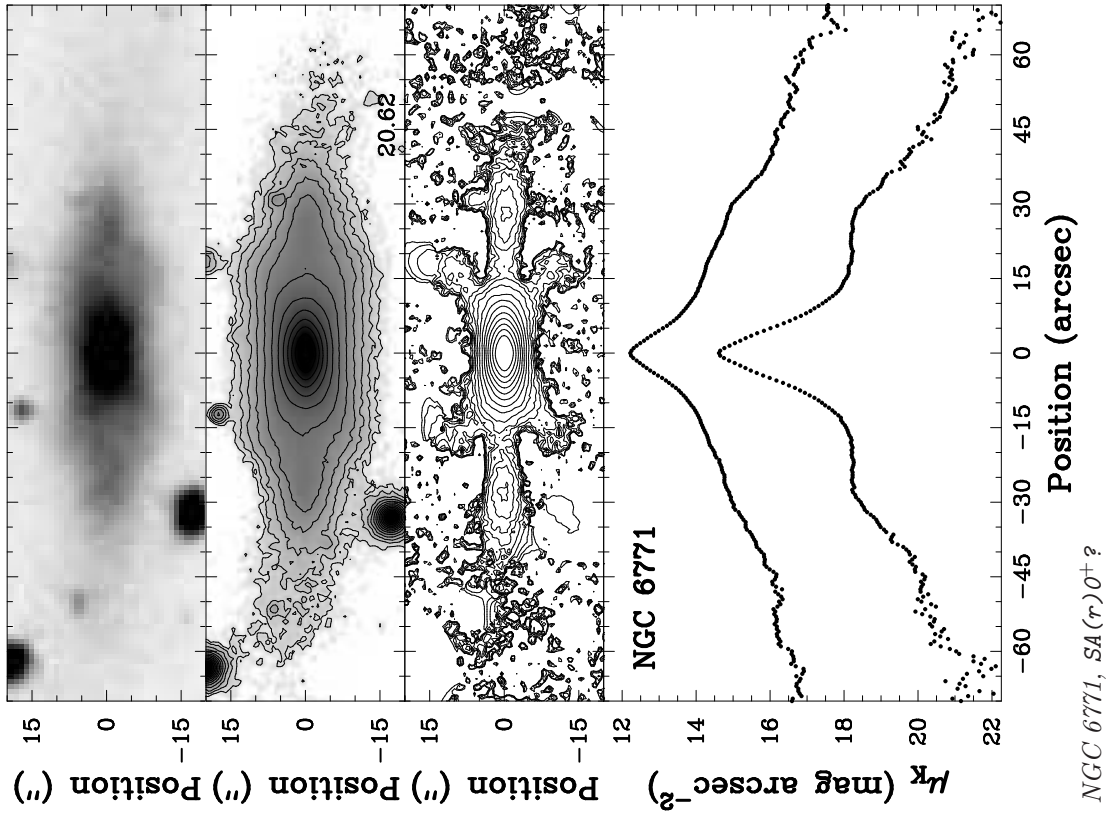
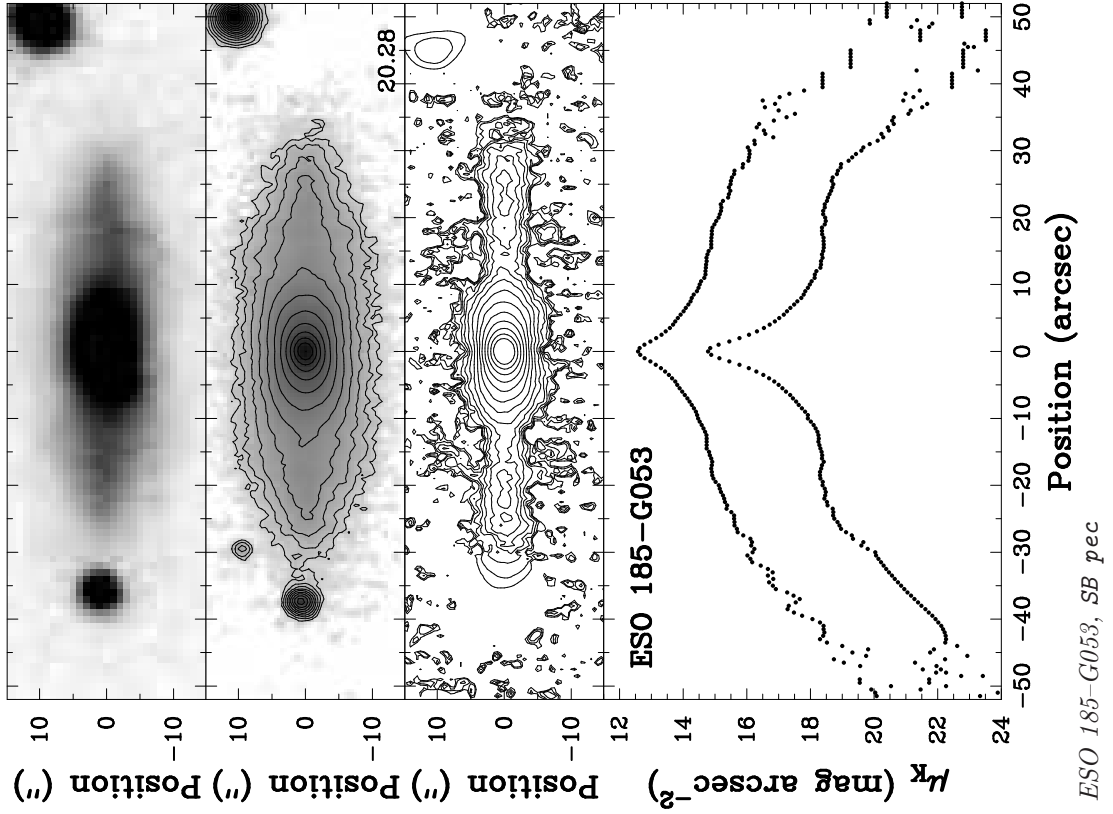
C. PHOTOMETRY OF THE SAMPLE GALAXIES



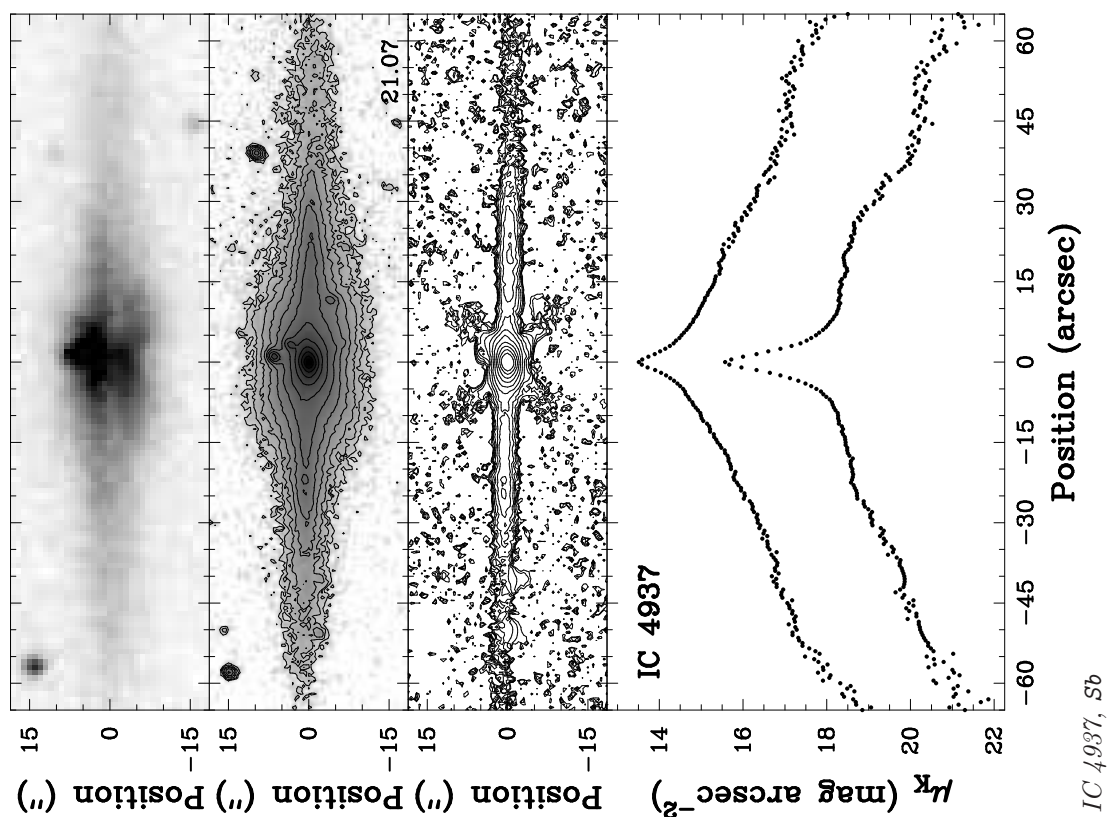
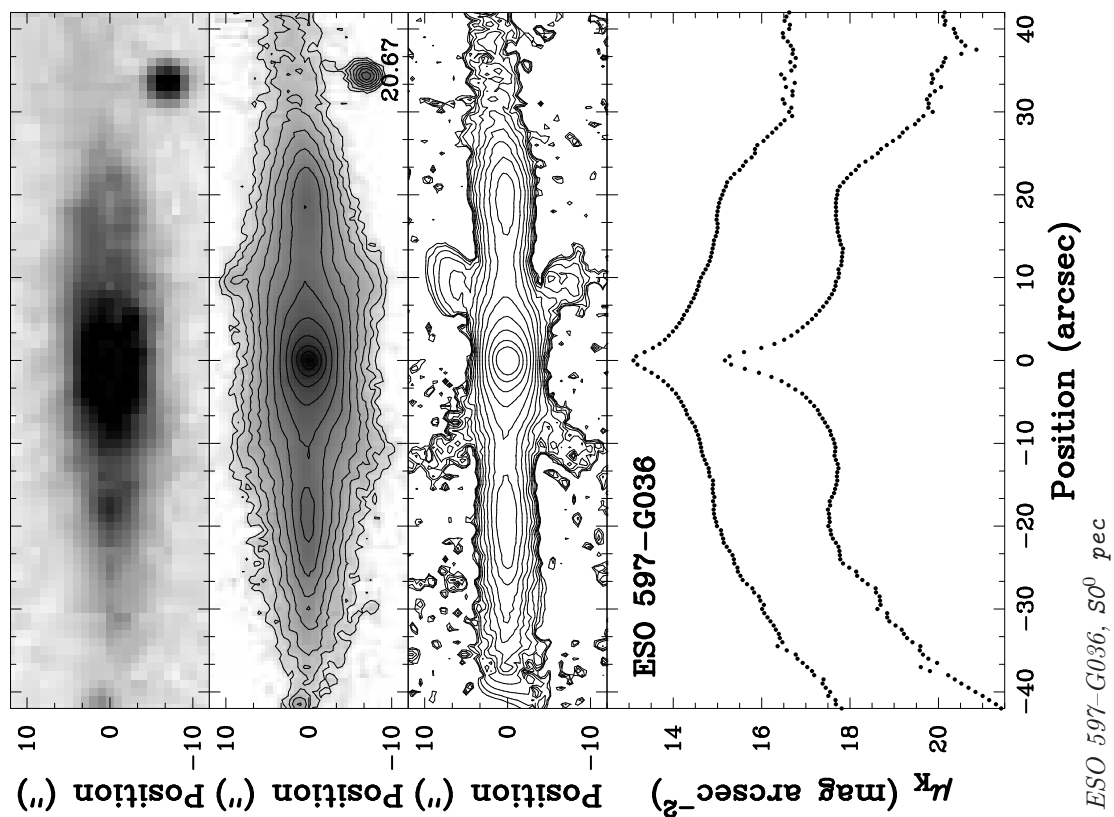


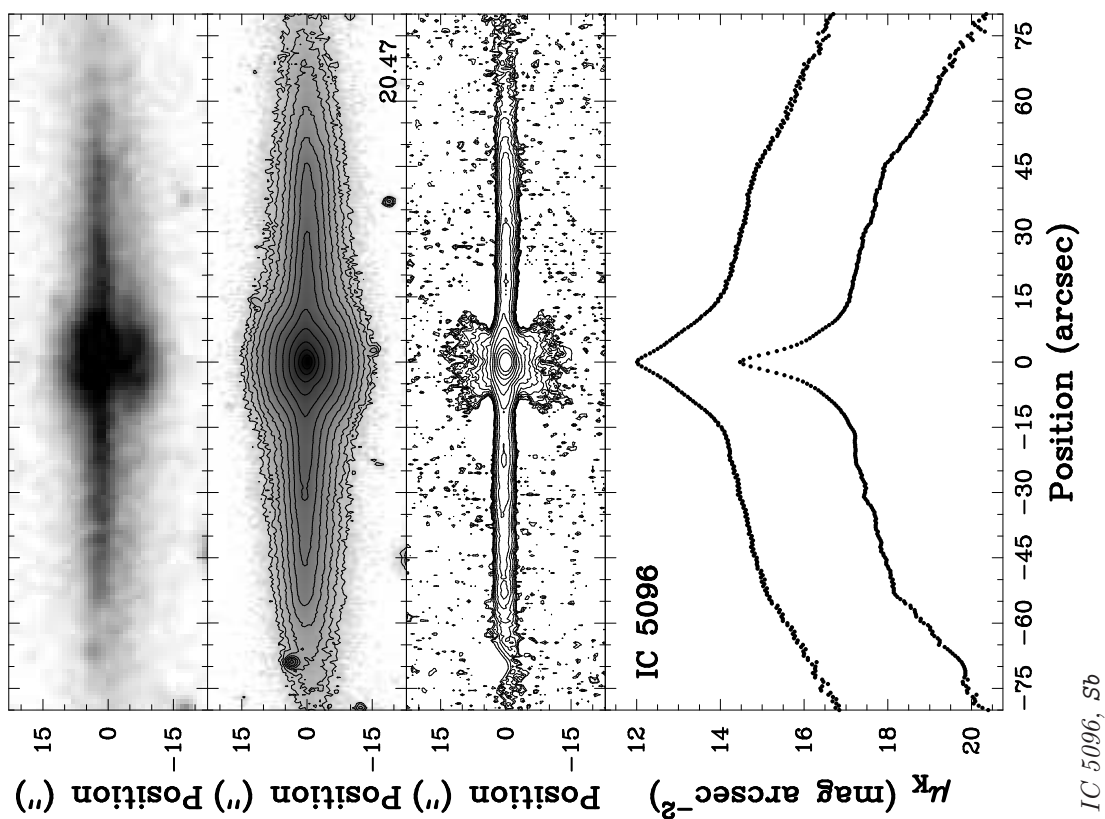
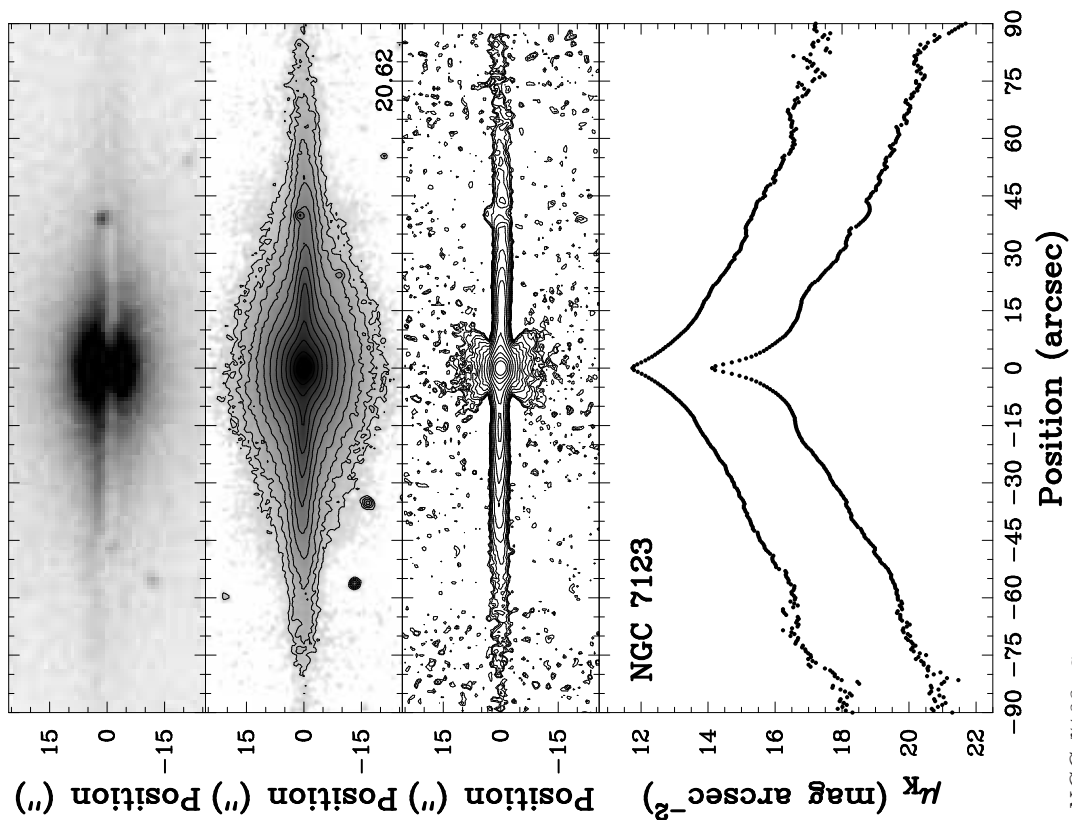
C. PHOTOMETRY OF THE SAMPLE GALAXIES



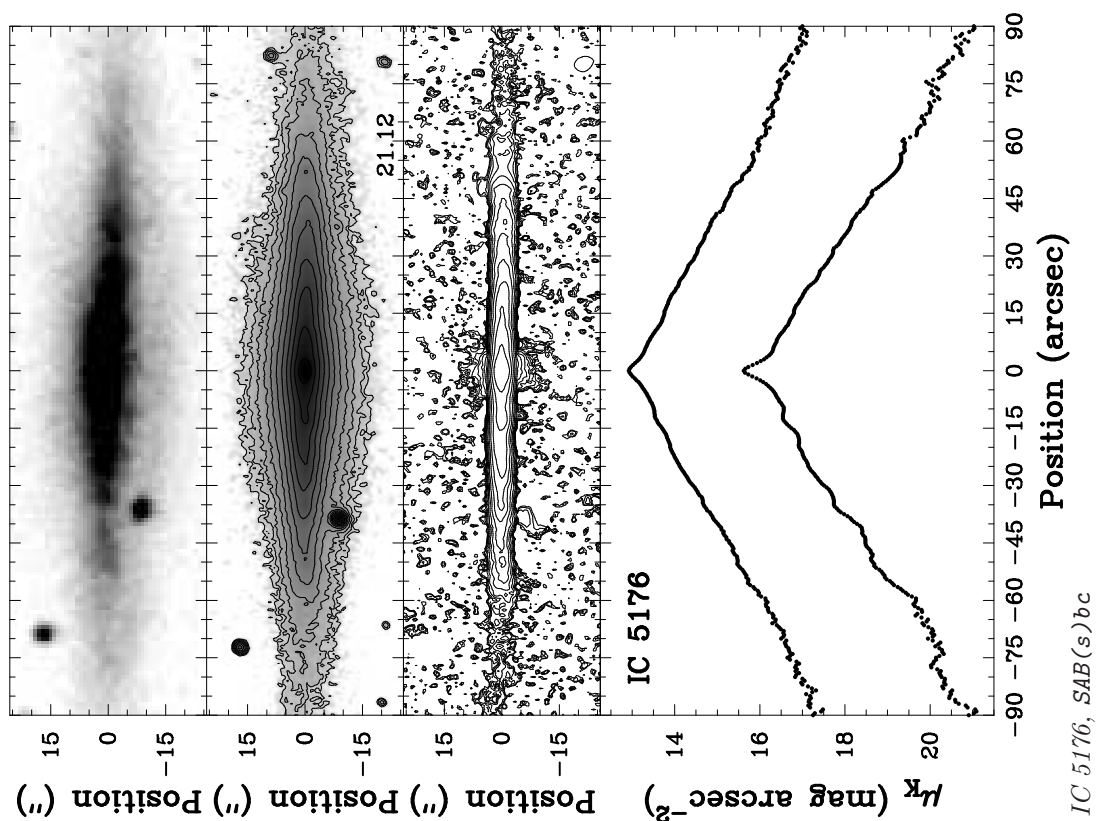
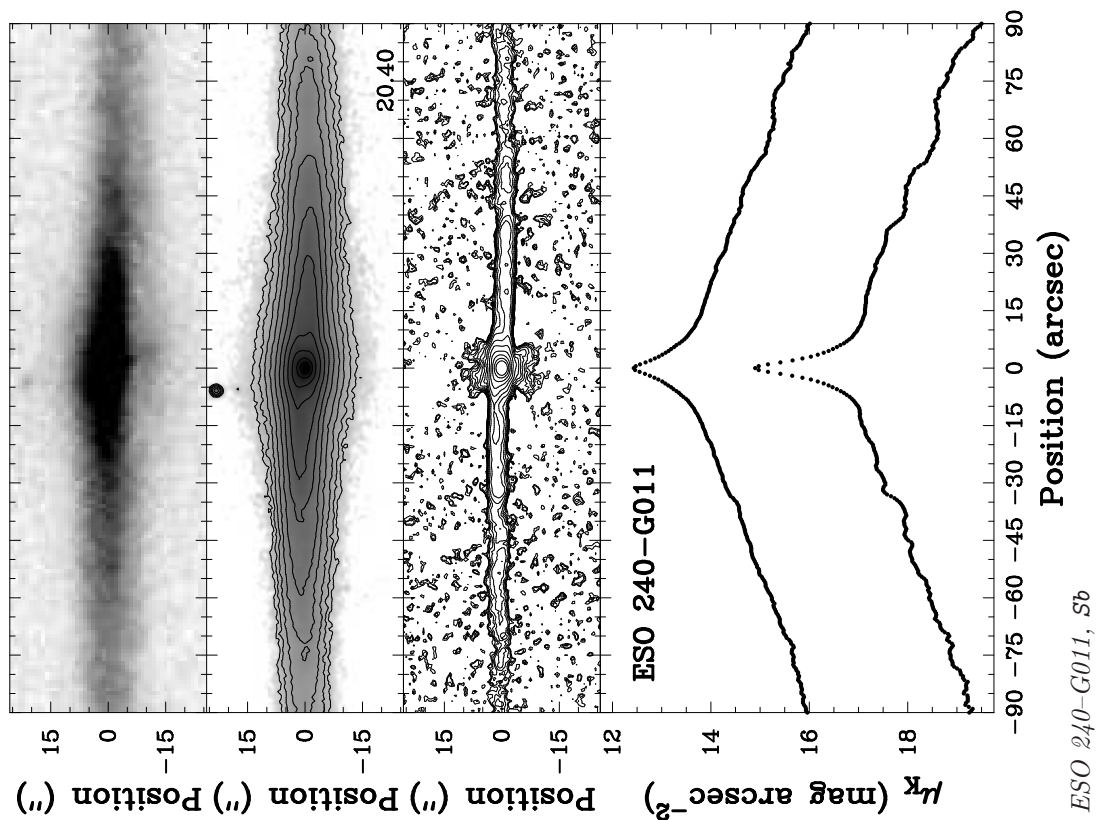


C. PHOTOMETRY OF THE SAMPLE GALAXIES





C. PHOTOMETRY OF THE SAMPLE GALAXIES



Appendix D

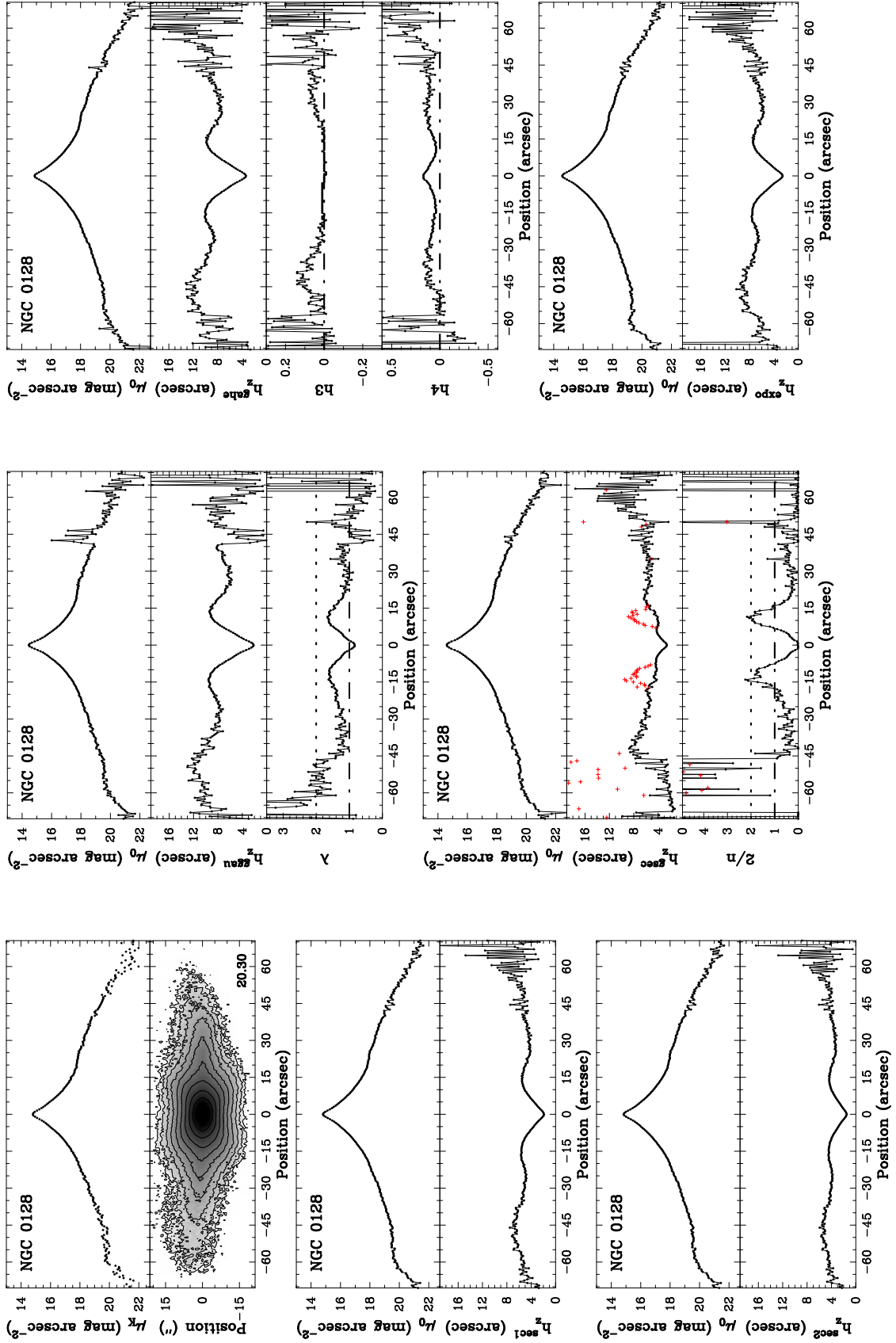
Results of the VSFBD fitting

On the following pages the results of the vertical fitting process are displayed in diagrams for each type of fitting function. All diagrams of a galaxy are shown on one page. At the upper left corner a small overview of the SFBD on the major axis and the K -band image with overplotted isophotes are shown. Further down in that column the results of the usage of the simple $\text{sech}(z)$ and the isothermal $\text{sech}^2(z)$ function as fitting functions are displayed. In the second column the GGau and below of it the GSec approach are shown. Finally in the third column the GaHe and at the bottom the exponential-distribution approach are visualized. The range of the fitting values displayed is chosen in such a manner that the obtained values of nearly all galaxies fit in the panels. Each data point resulting from the fitting procedure is represented by a filled circle and all data points are connected by a straight line to each other in order to form a smooth course. In cases where no meaningful data value was obtained during the fitting process a fixed value was assigned to that position being largely outside the displayed range. Therefore, the line connecting that point to the surrounding ones was left apart. For the GSec approach a second set of data points was printed into the panel of the scaleheight and into that one of the shape parameter. That is due to the special structure of the family of functions grouped in the GSec approach. It is the possibility of an alternative definition for the scaleheight, described in Chap. 4.1, including the shape parameter which leads to a second representation of the fitted values. For the values of the shape parameter larger than 1 also the value of the entity $h_z = 2/n \cdot h_z^{\text{expo}}$ was plotted marked by crosses. The adopted restriction was introduced to limit the alternative representation only to the central part where the SN -ratio is high and avoiding confusion in the outer parts where the data points are spread over the whole value range. In the case of the GGau, GaHe, and GSec approach also lines of constant shape parameter value have been overplotted to the data points. That has been done to facilitate the comparison of the data values with some known distributions. The plot of the shape parameter (λ) in the GGau approach has two distinct lines at a value of $\lambda = 1$ corresponding to an exponential-distribution and at $\lambda = 2$ corresponding to a gaussian distribution. Also in the plot of the GSec approach the panel of the shape parameter has two constant lines, at $2/n = 1$ representing a $\text{Sech}(z)$ and at $2/n = 2$ representing the isothermal-distribution. In the case of the GaHe a perfectly symmetric distribution is marked by a value of 0 in the panel of the h_3 parameter as well as a pure Gaussian is denoted also by a value of 0 in the panel of the h_4 parameter.

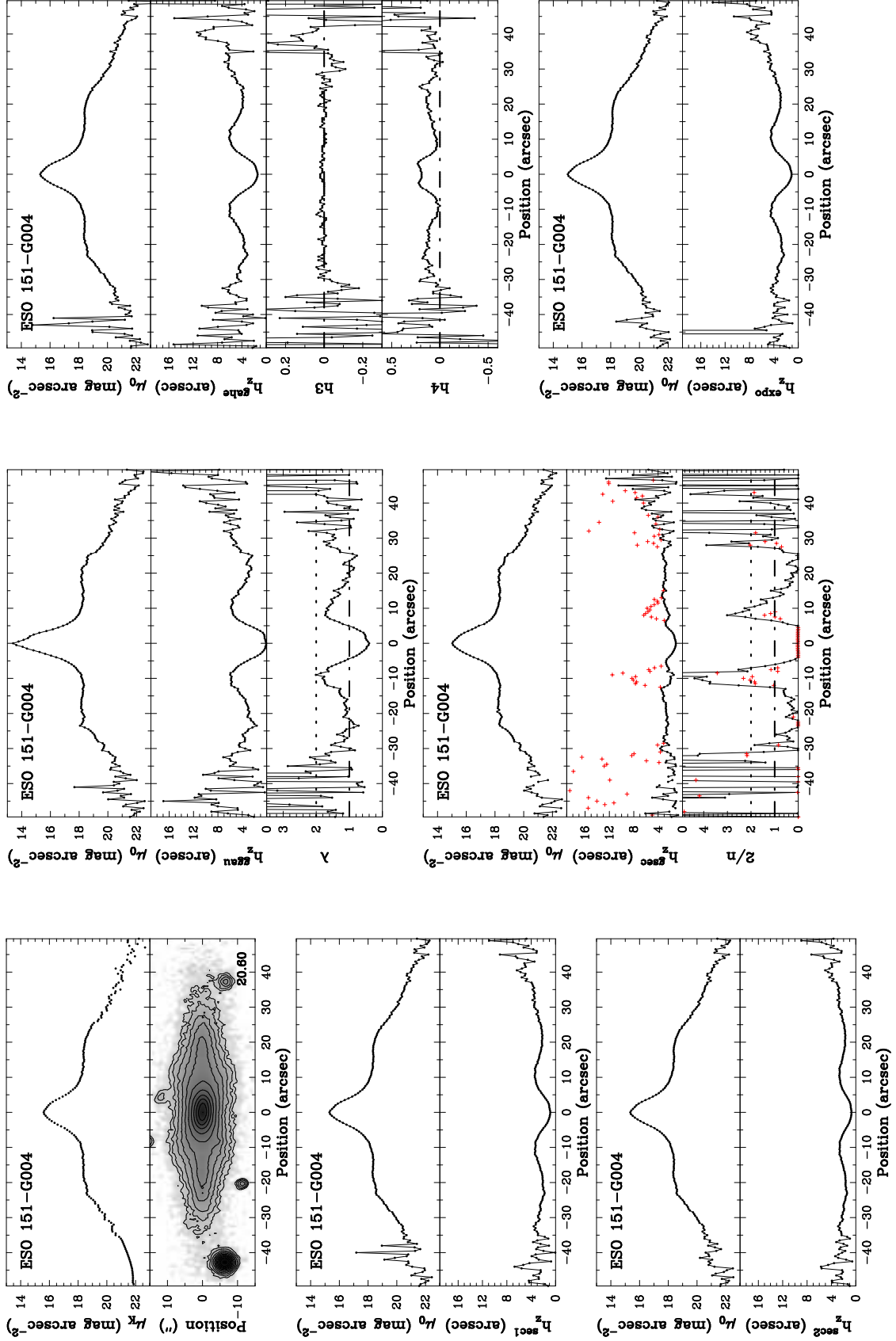
The displayed radial range is set for each galaxy individually in order to show the complete disk region. Thus, it is possible to compare the results of the different distributions also in

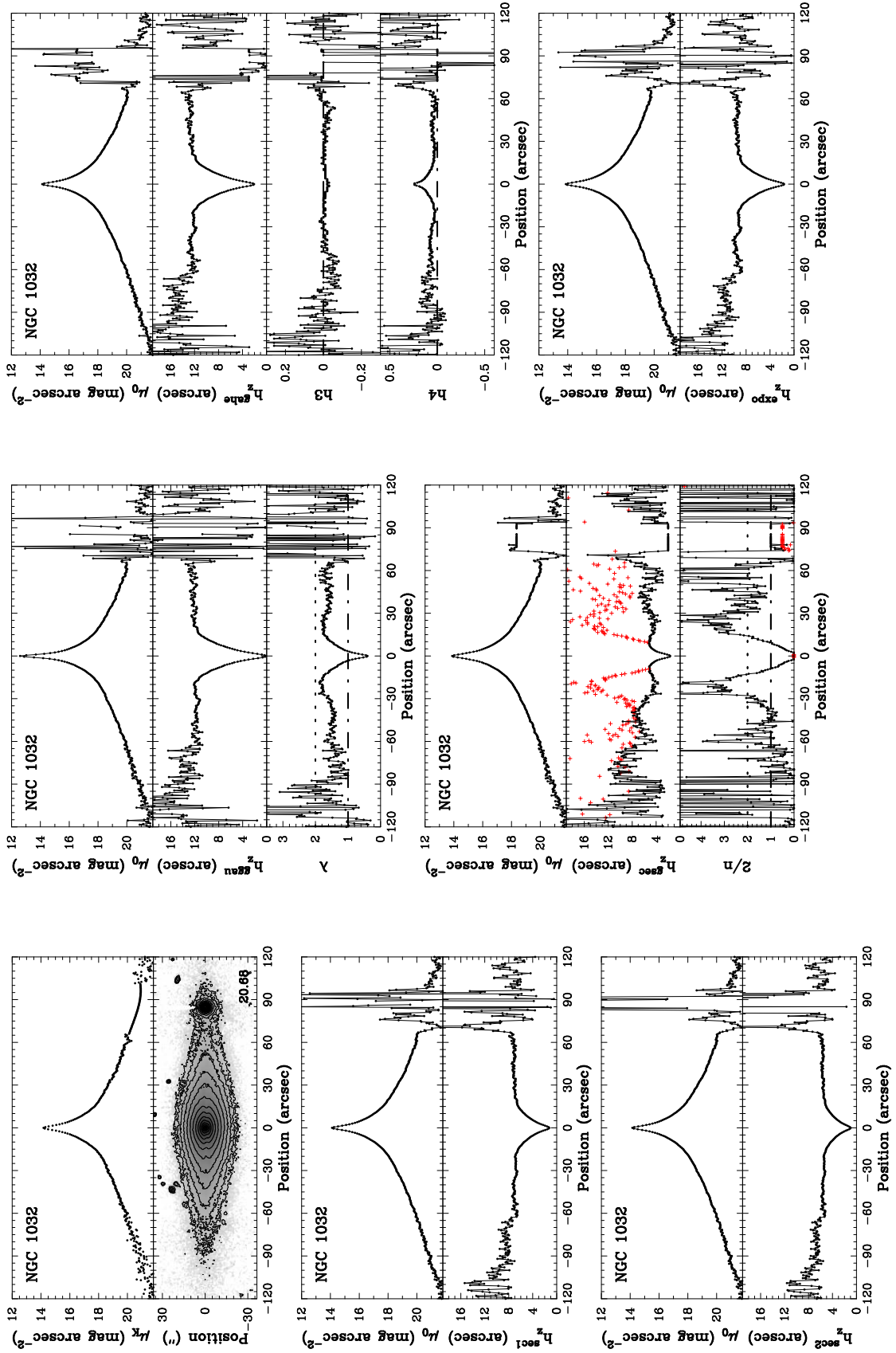
D. RESULTS OF THE VSFBD FITTING

the disk region. This is useful with respect to the question what kind of fitting approach fits best the VSFBD in pure disk components. Although in the literature a tendency towards an Exponential can be stated, the other two approaches (Sech(z) and Isothermal) are still in use.

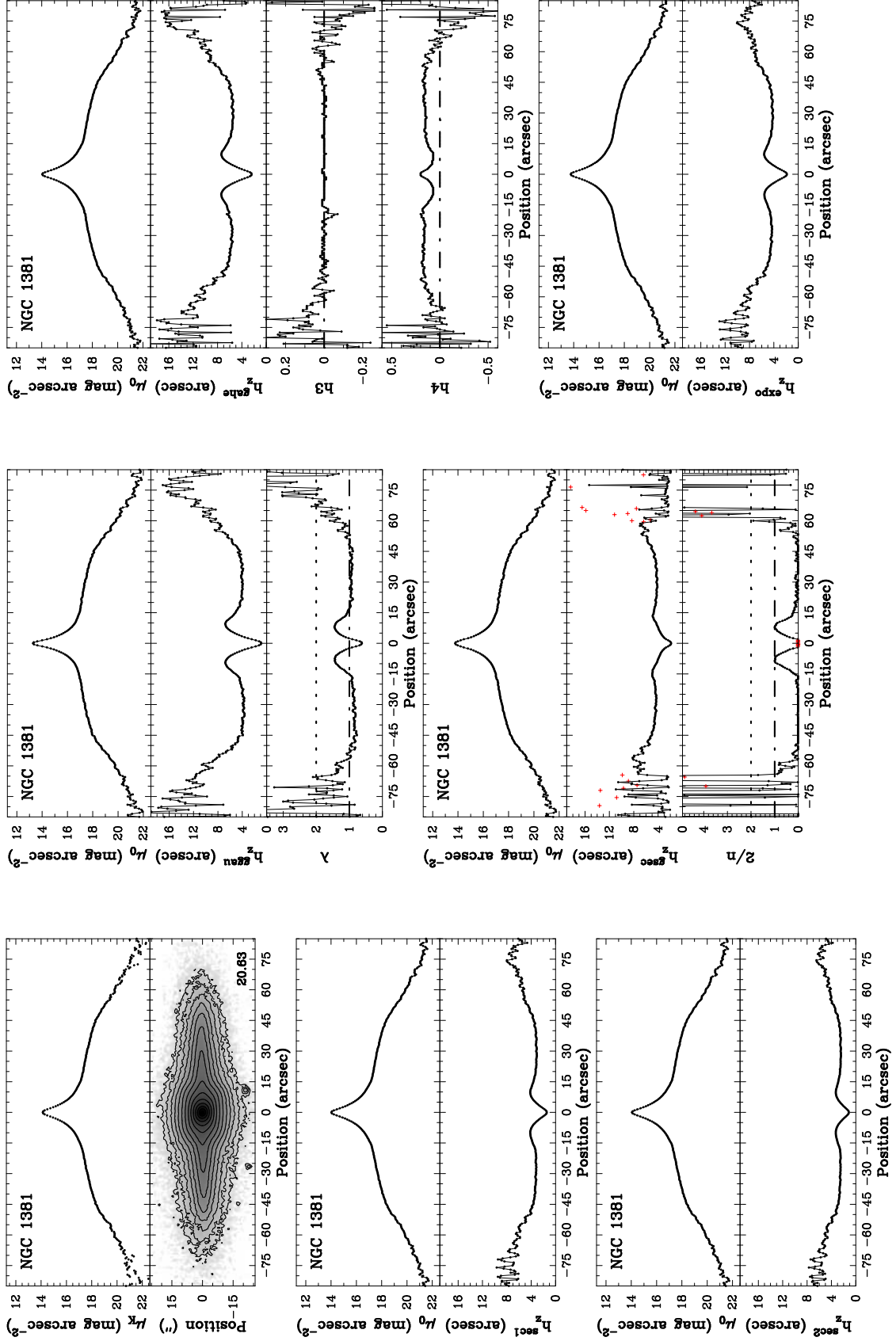


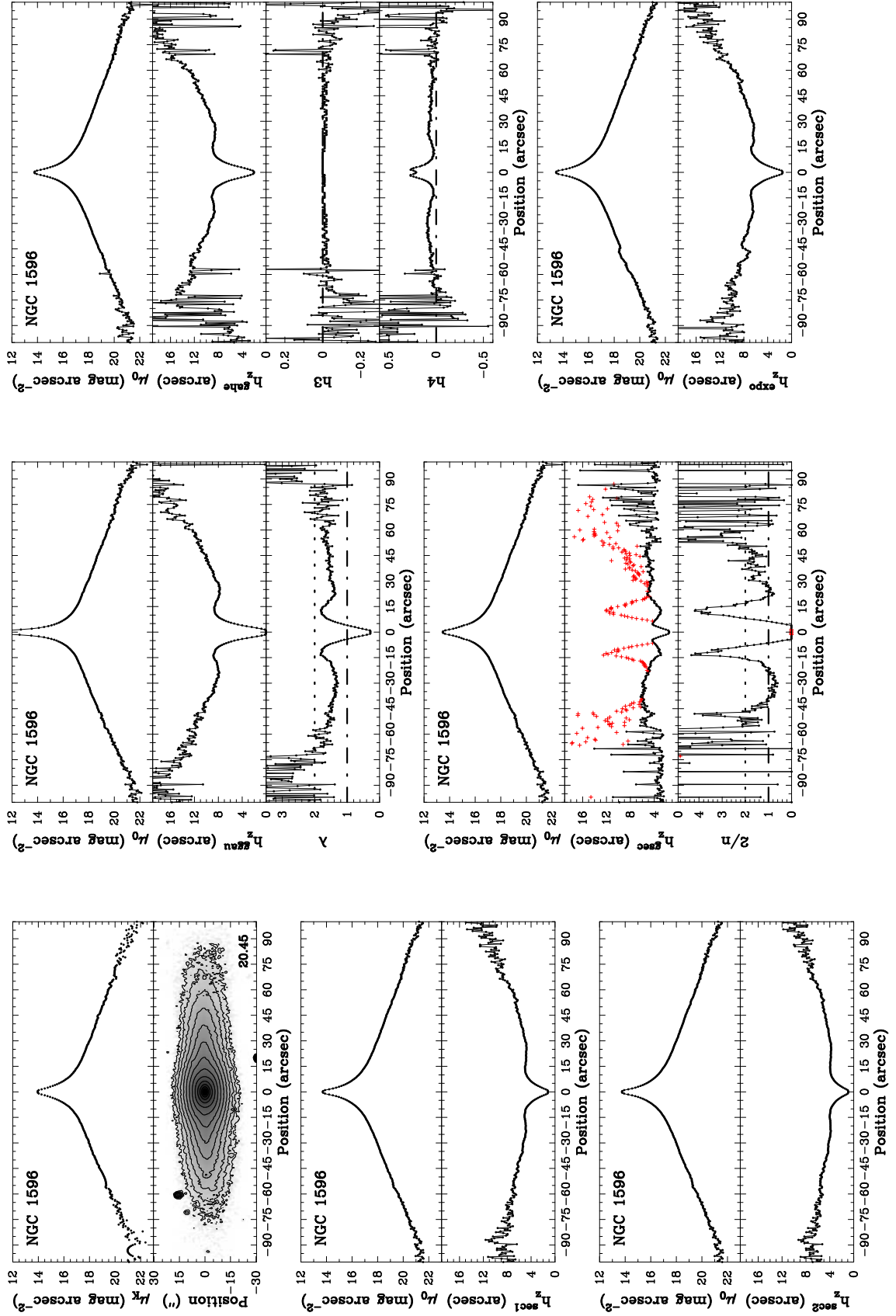
D. RESULTS OF THE VSFBD FITTING



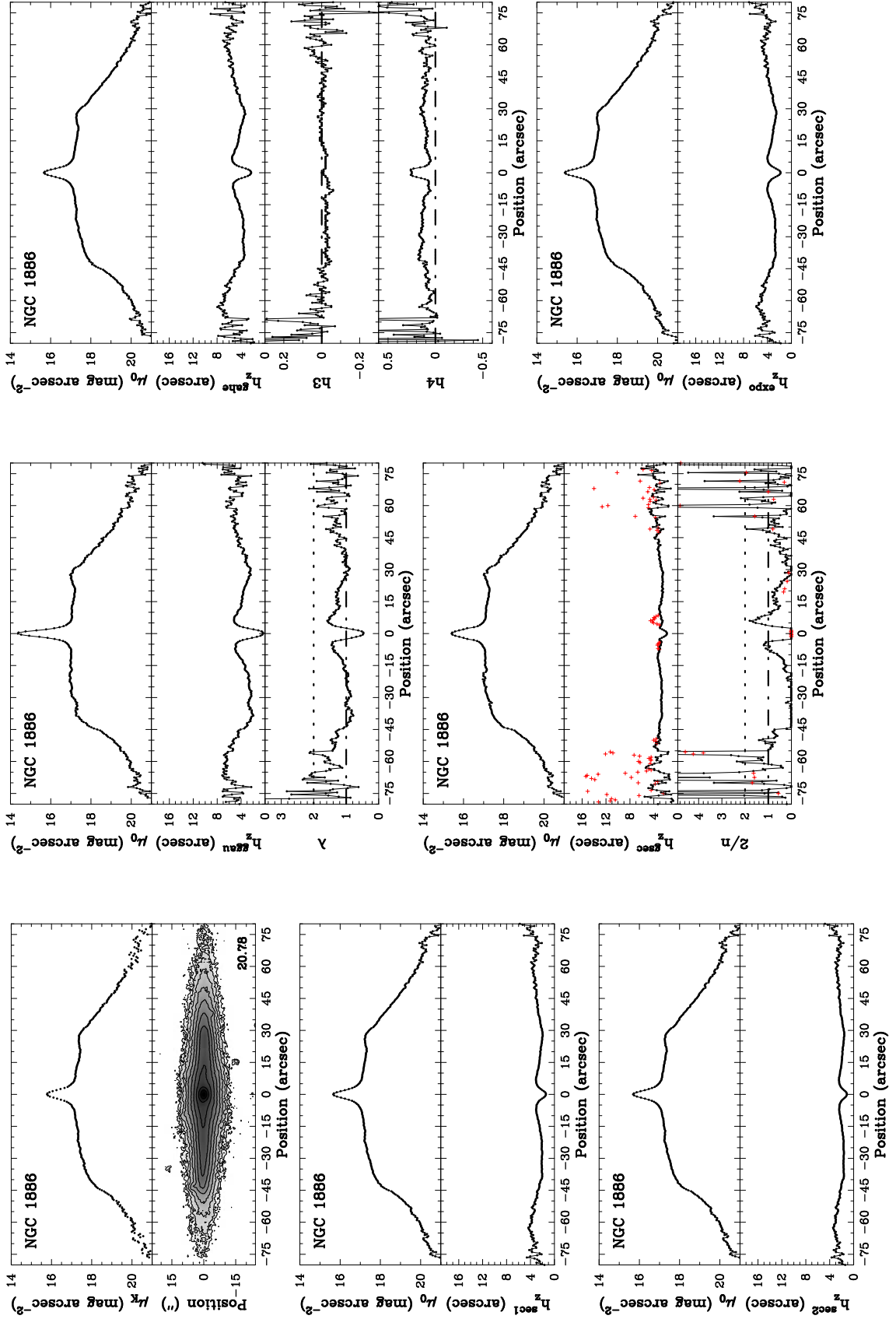


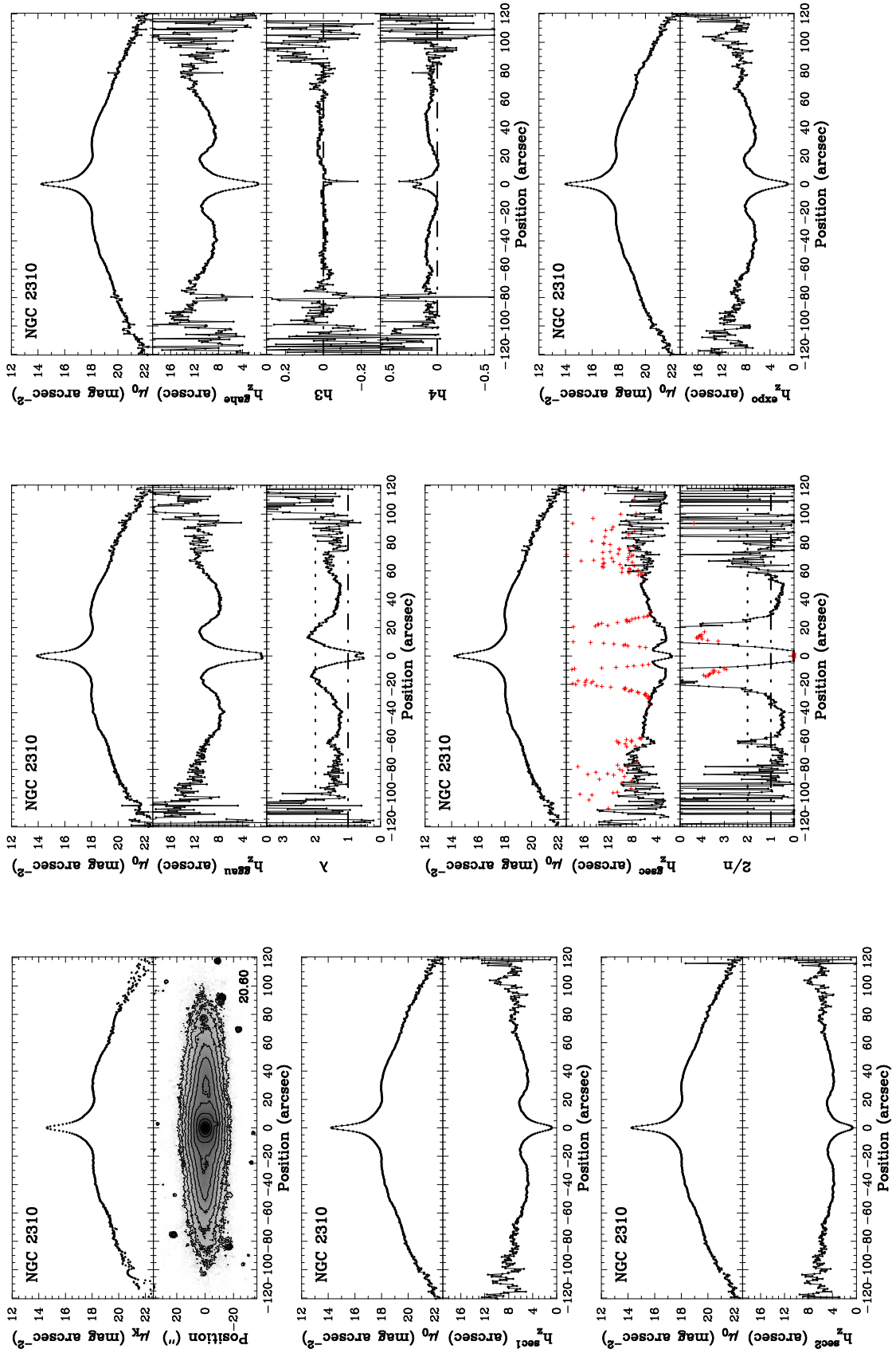
D. RESULTS OF THE VSFBD FITTING



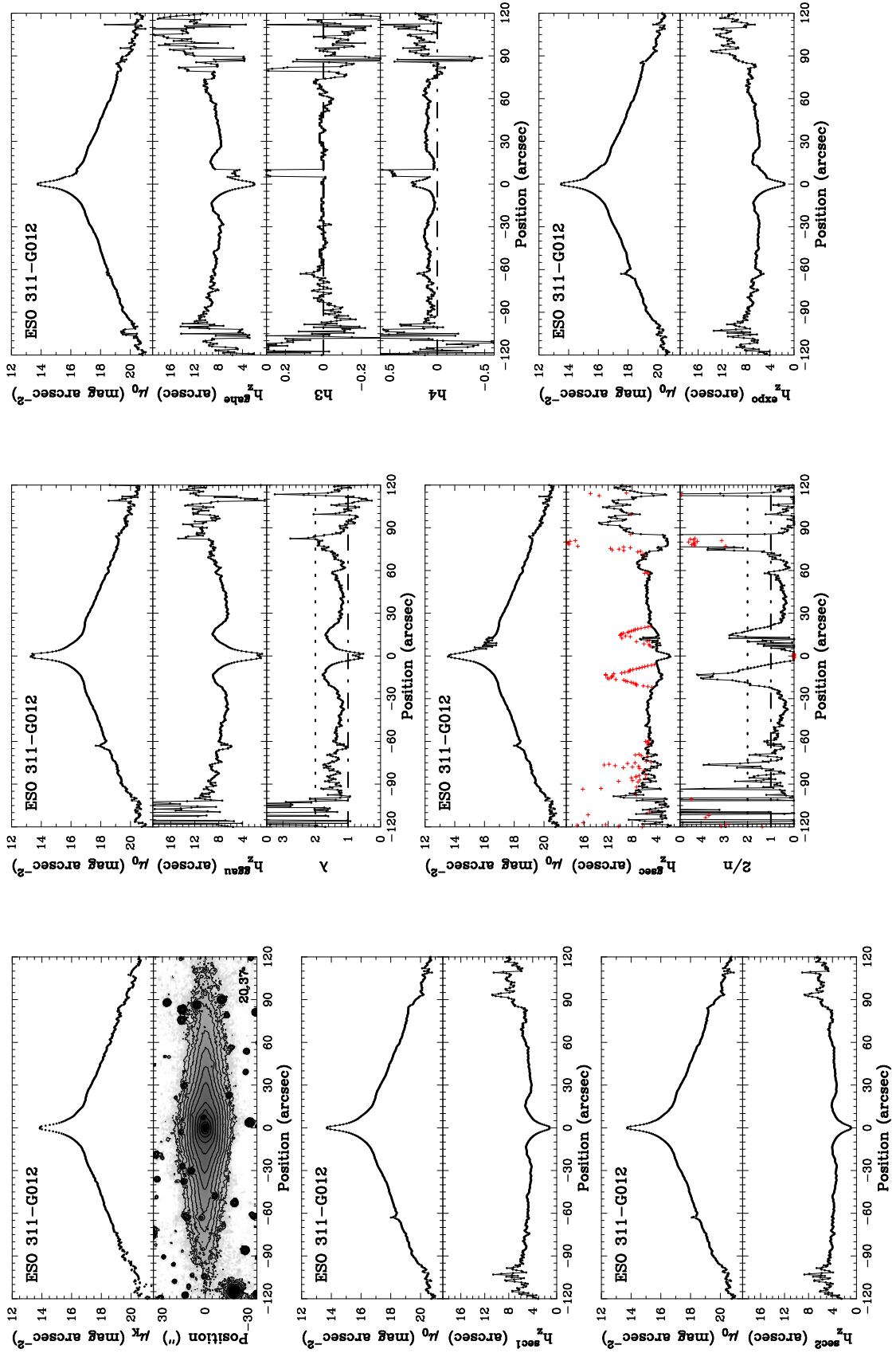


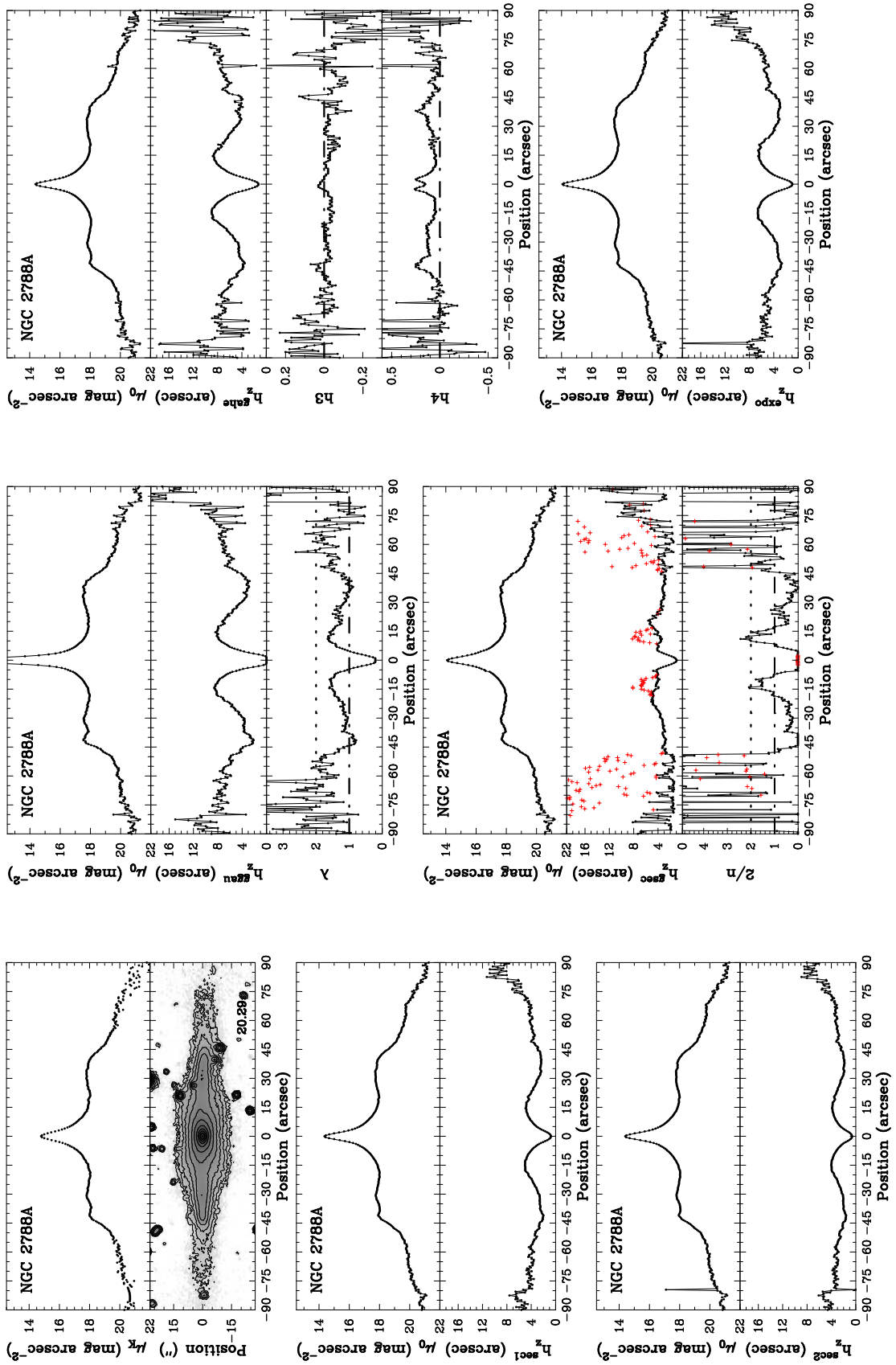
D. RESULTS OF THE VSFBD FITTING



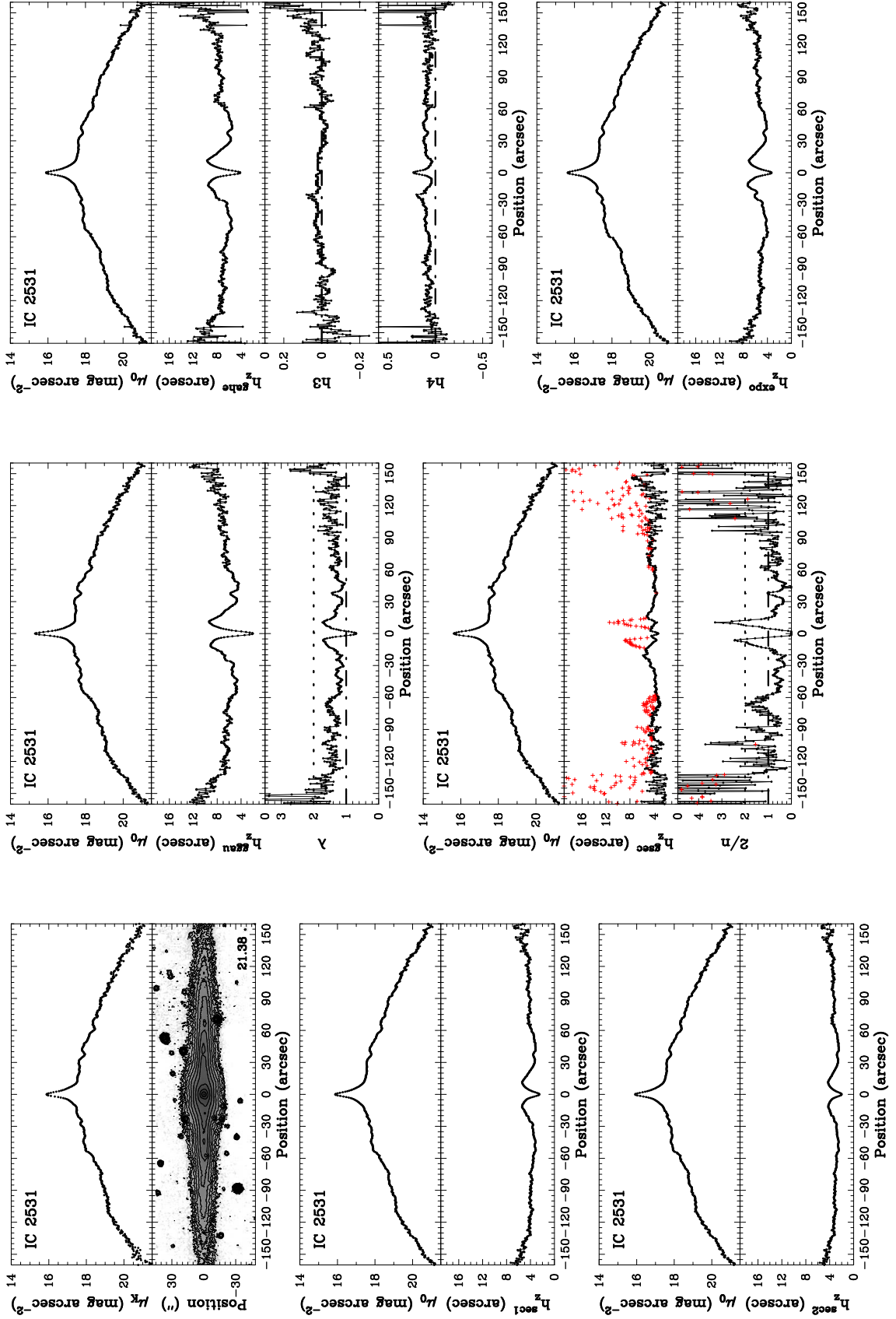


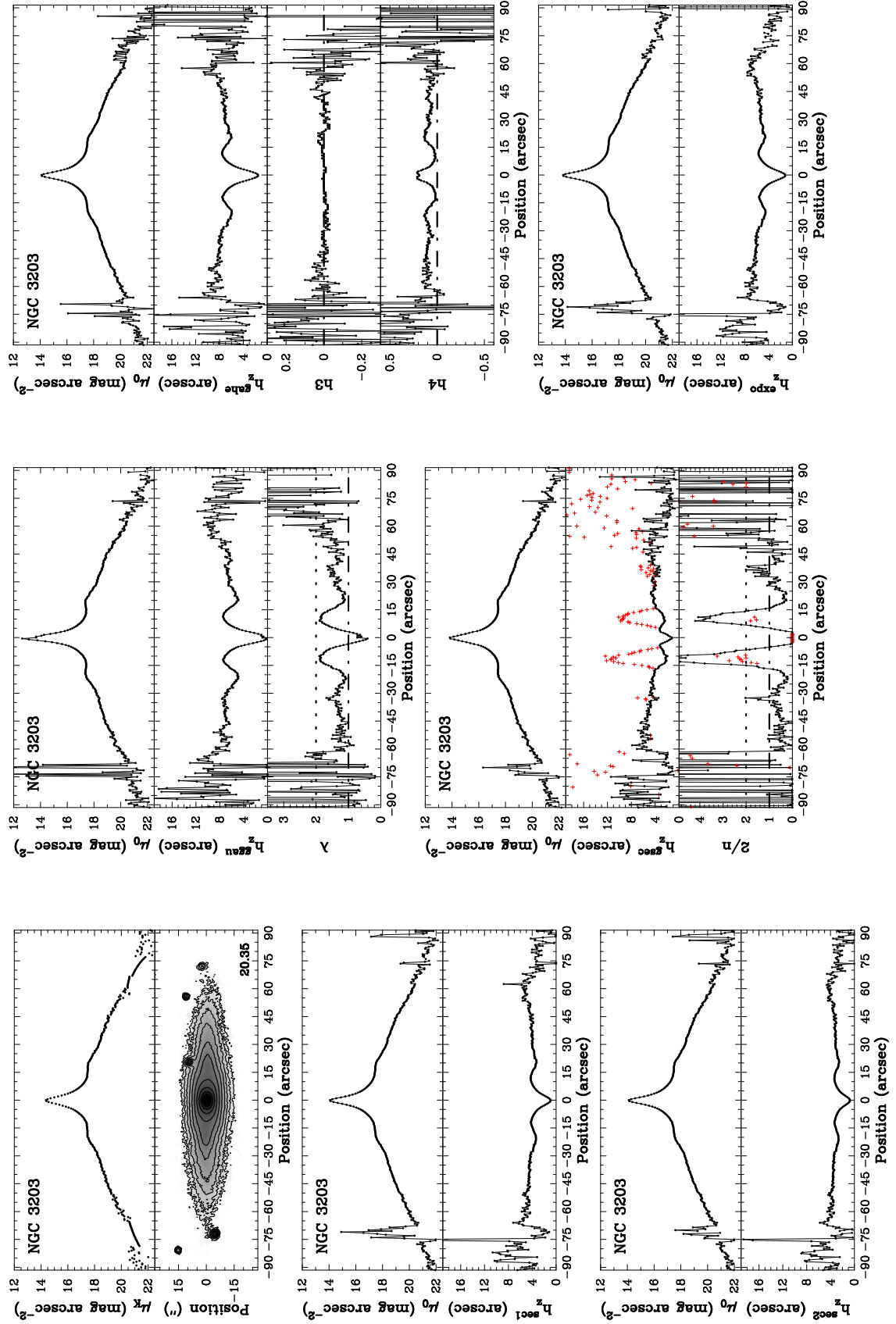
D. RESULTS OF THE VSFB D FITTING



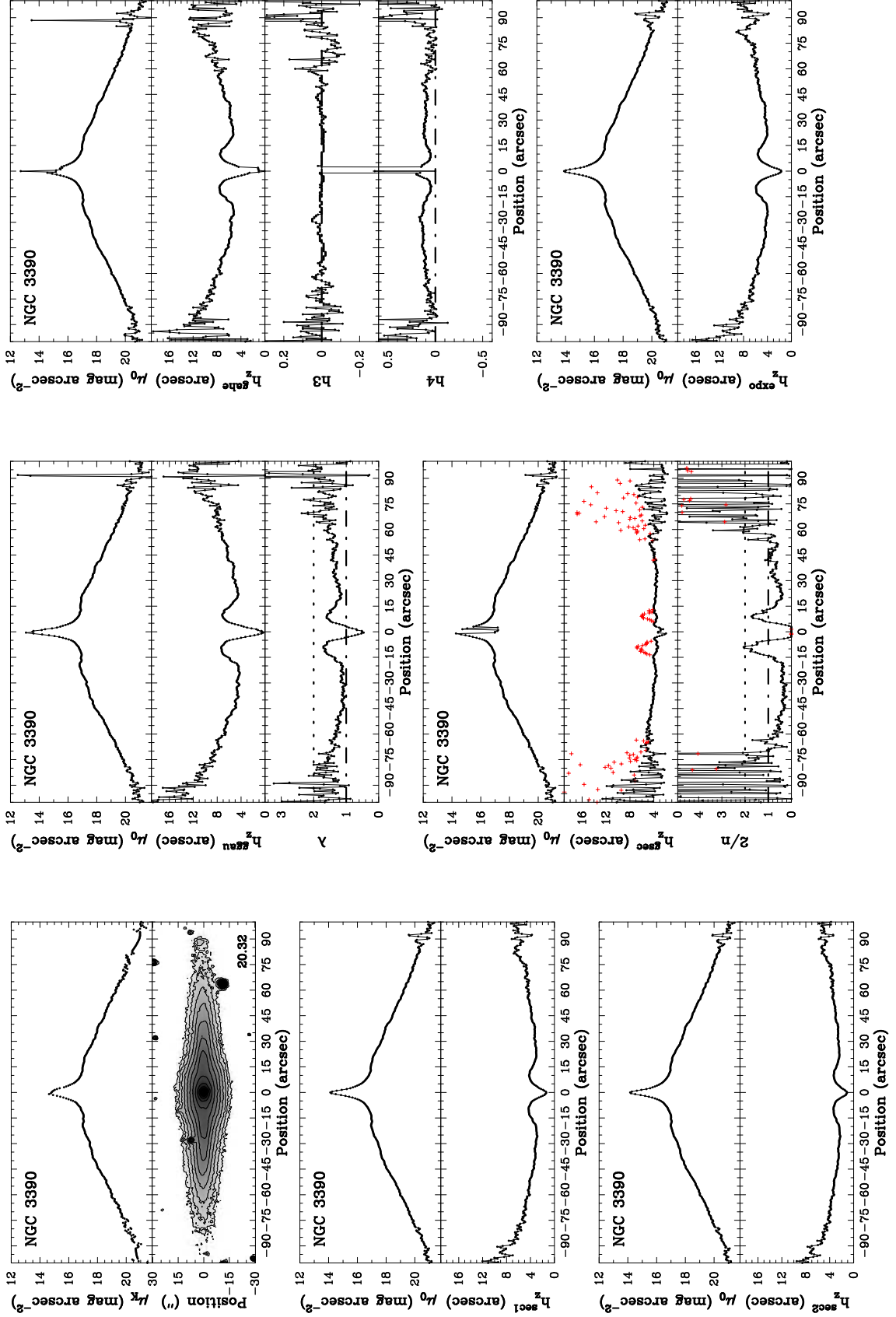


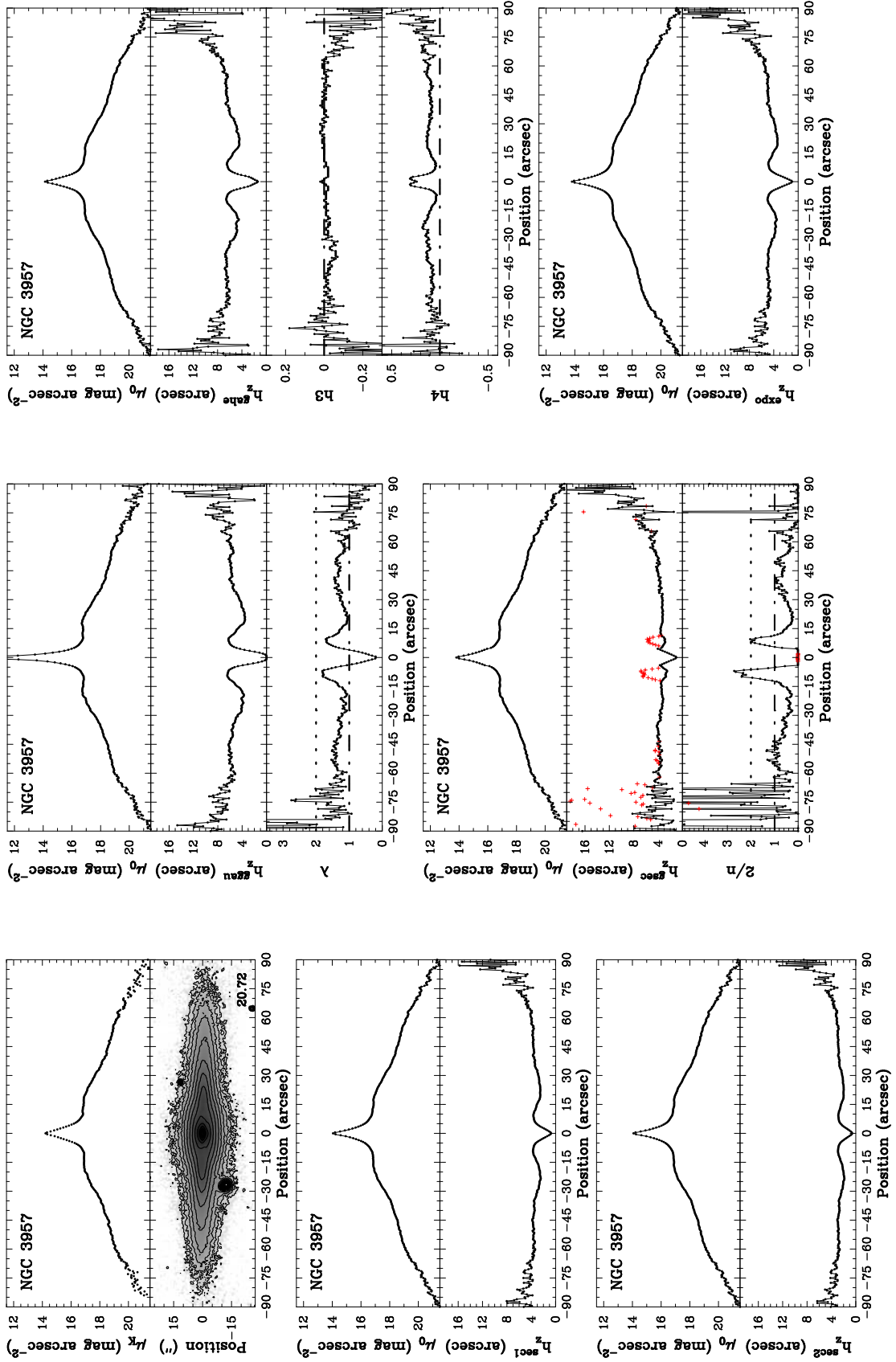
D. RESULTS OF THE VSFBD FITTING



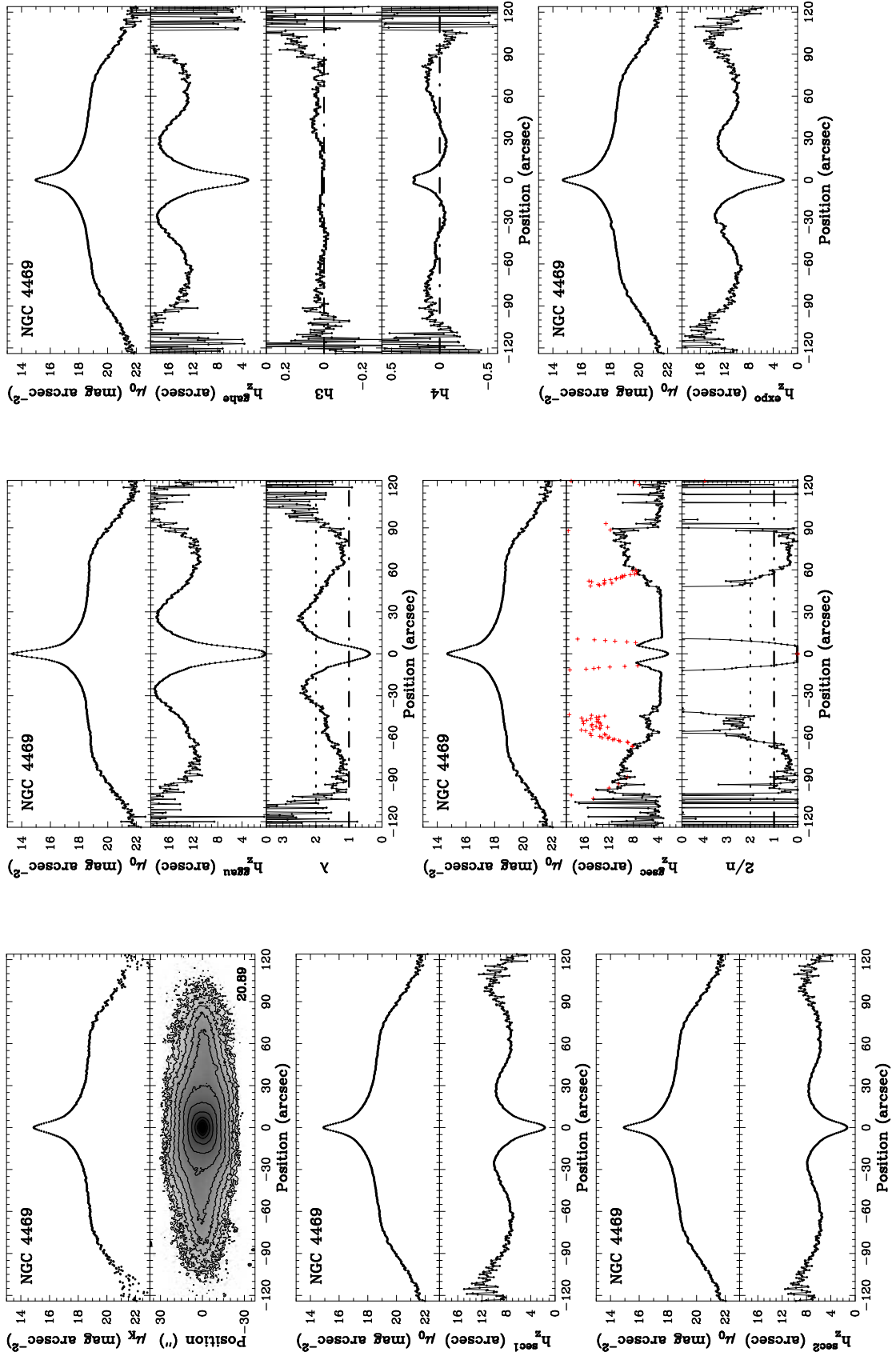


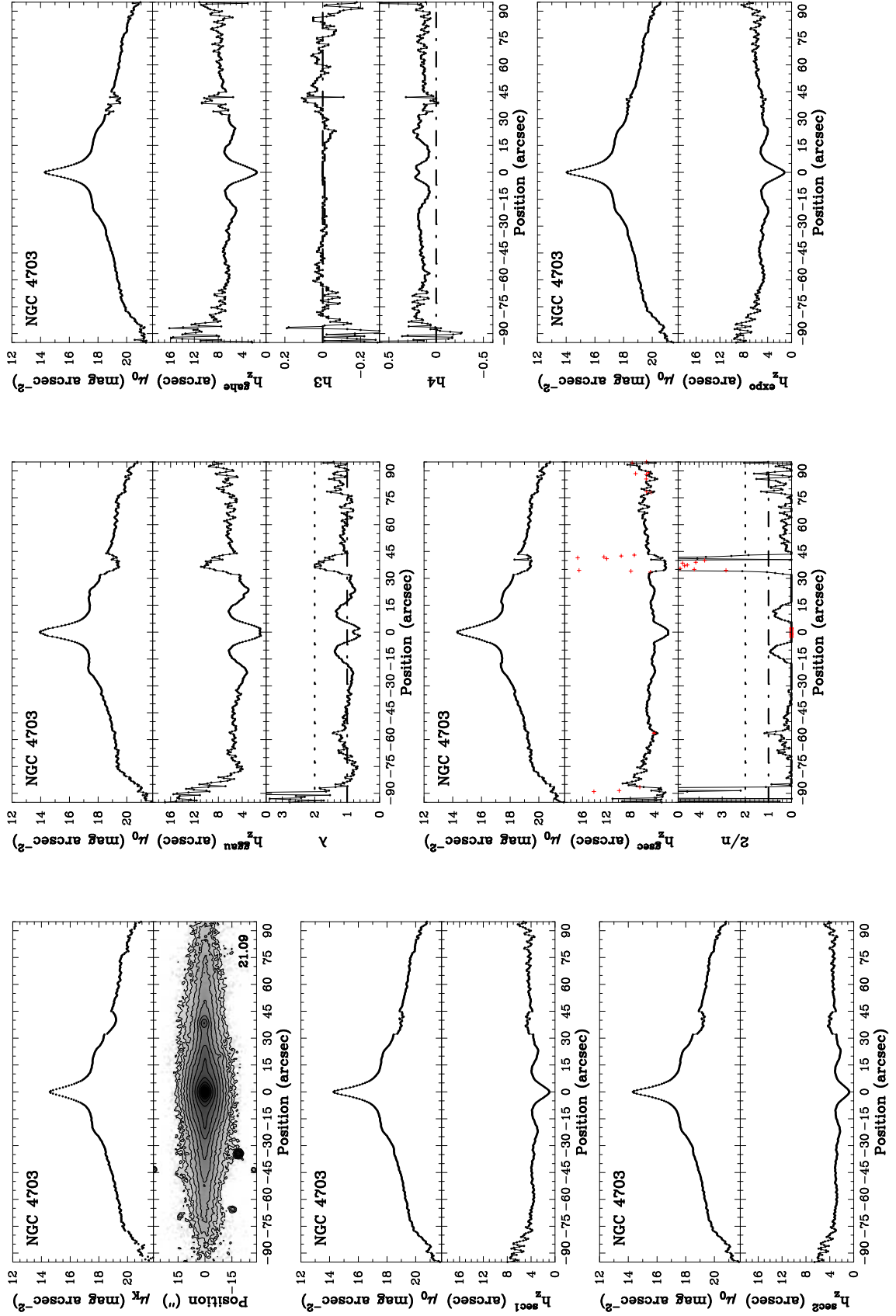
D. RESULTS OF THE VSFBD FITTING



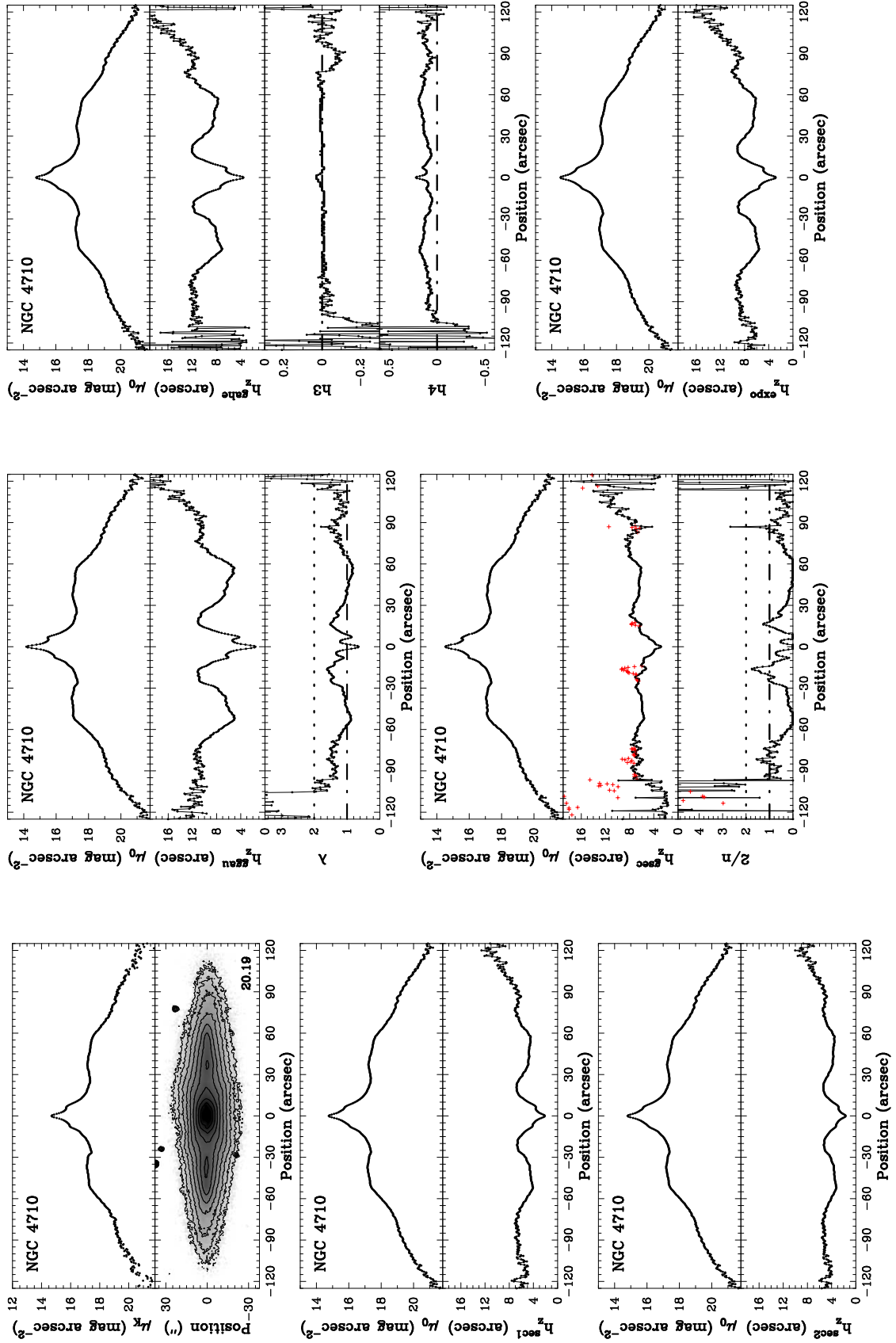


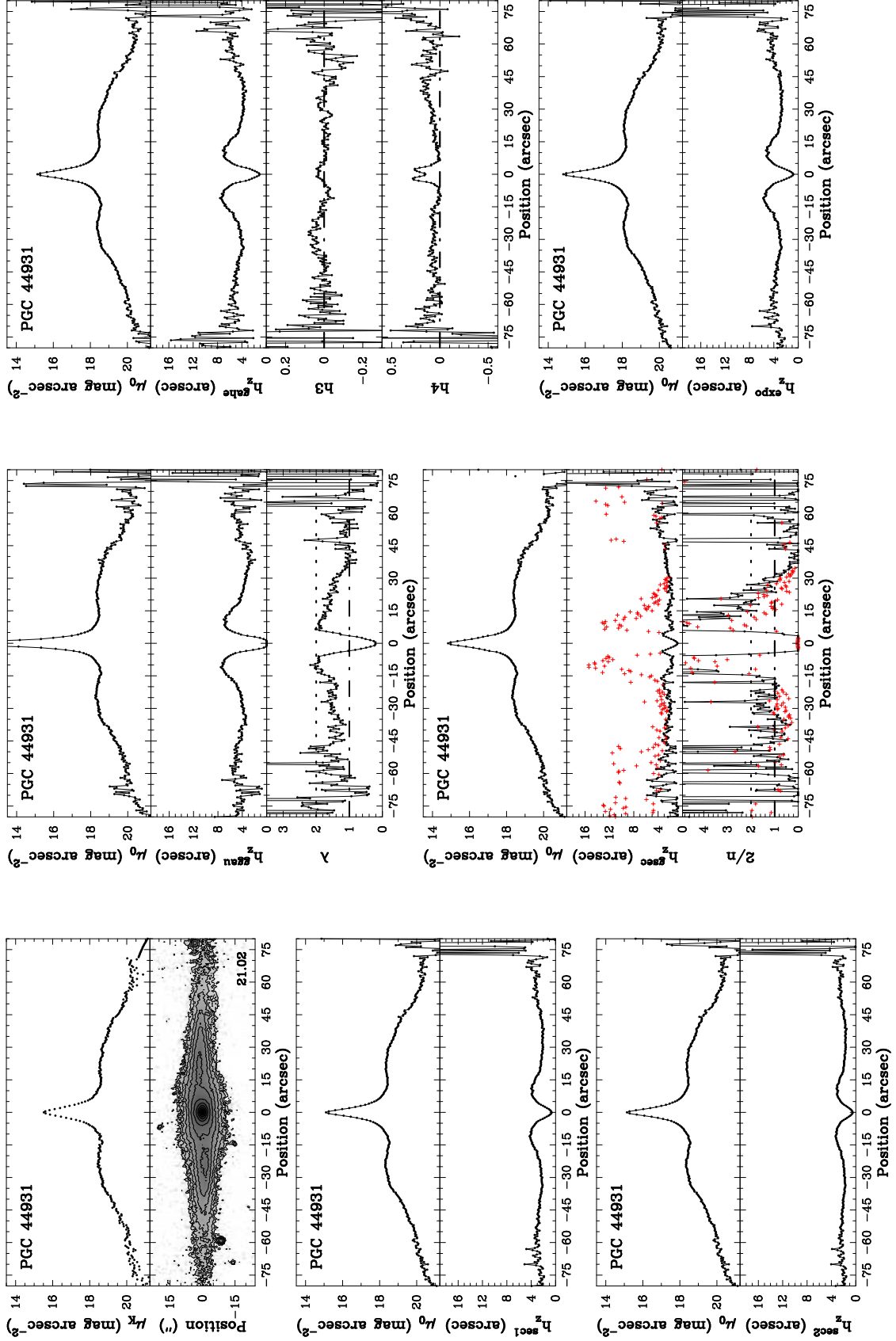
D. RESULTS OF THE VSFBD FITTING



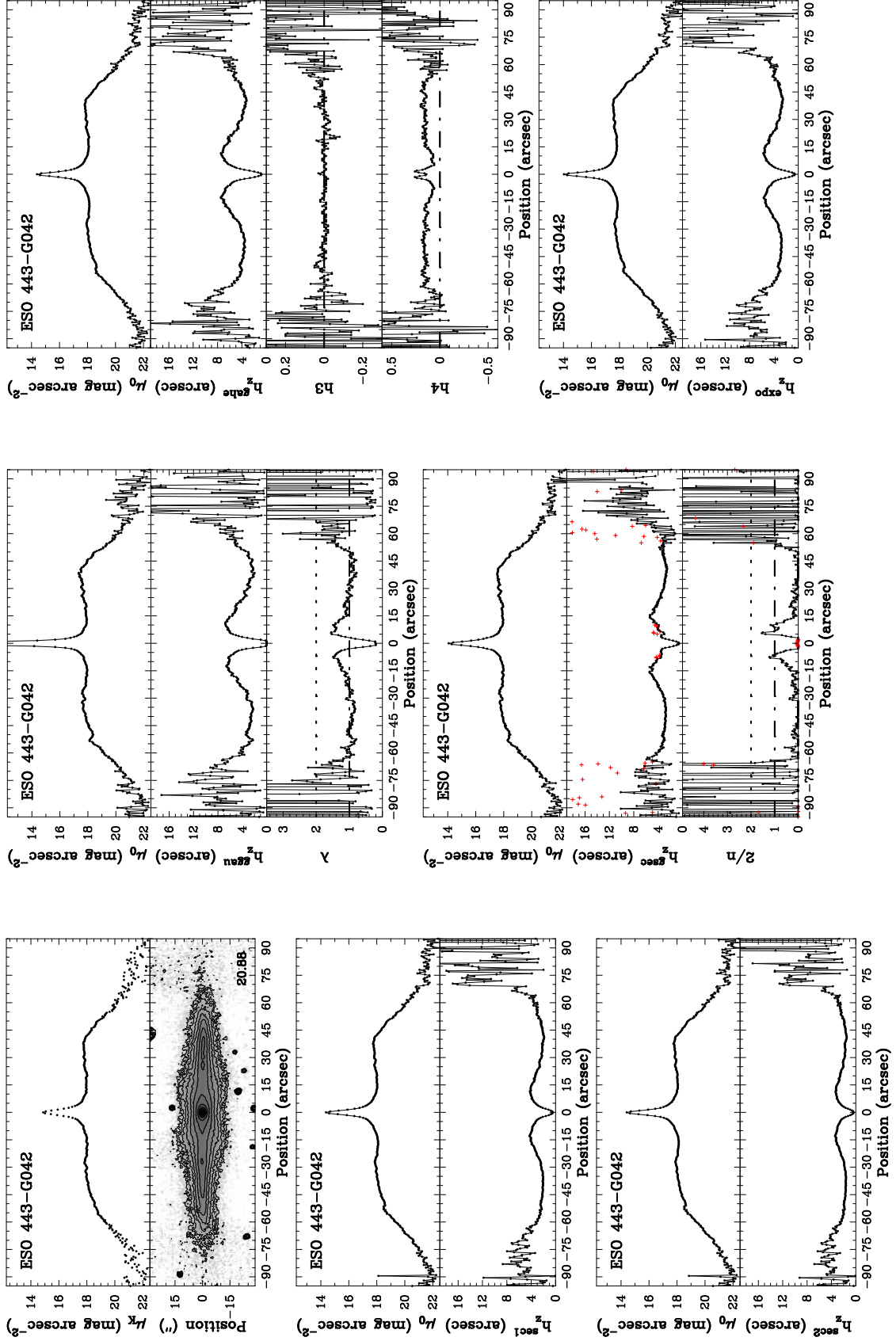


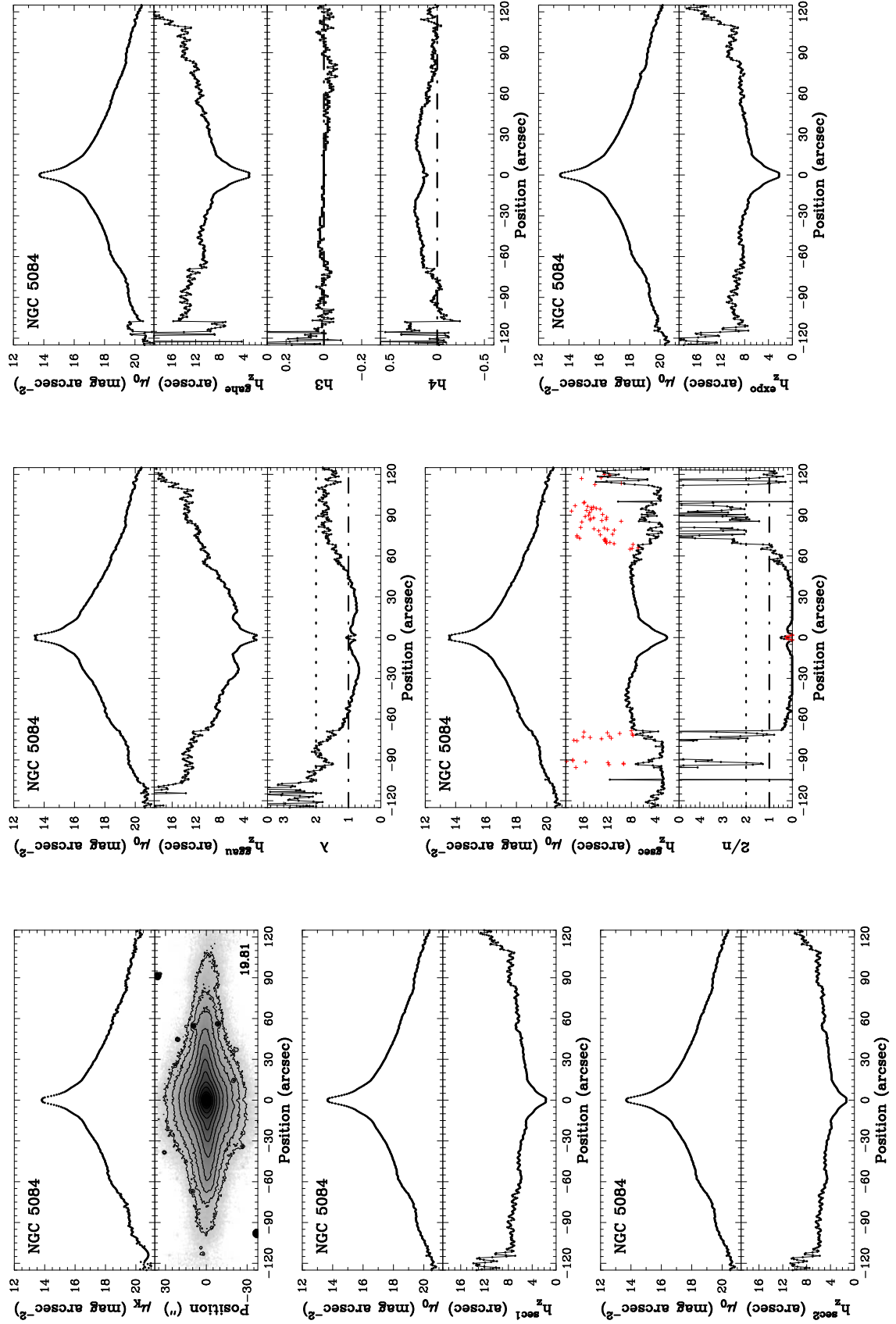
D. RESULTS OF THE VSFBD FITTING



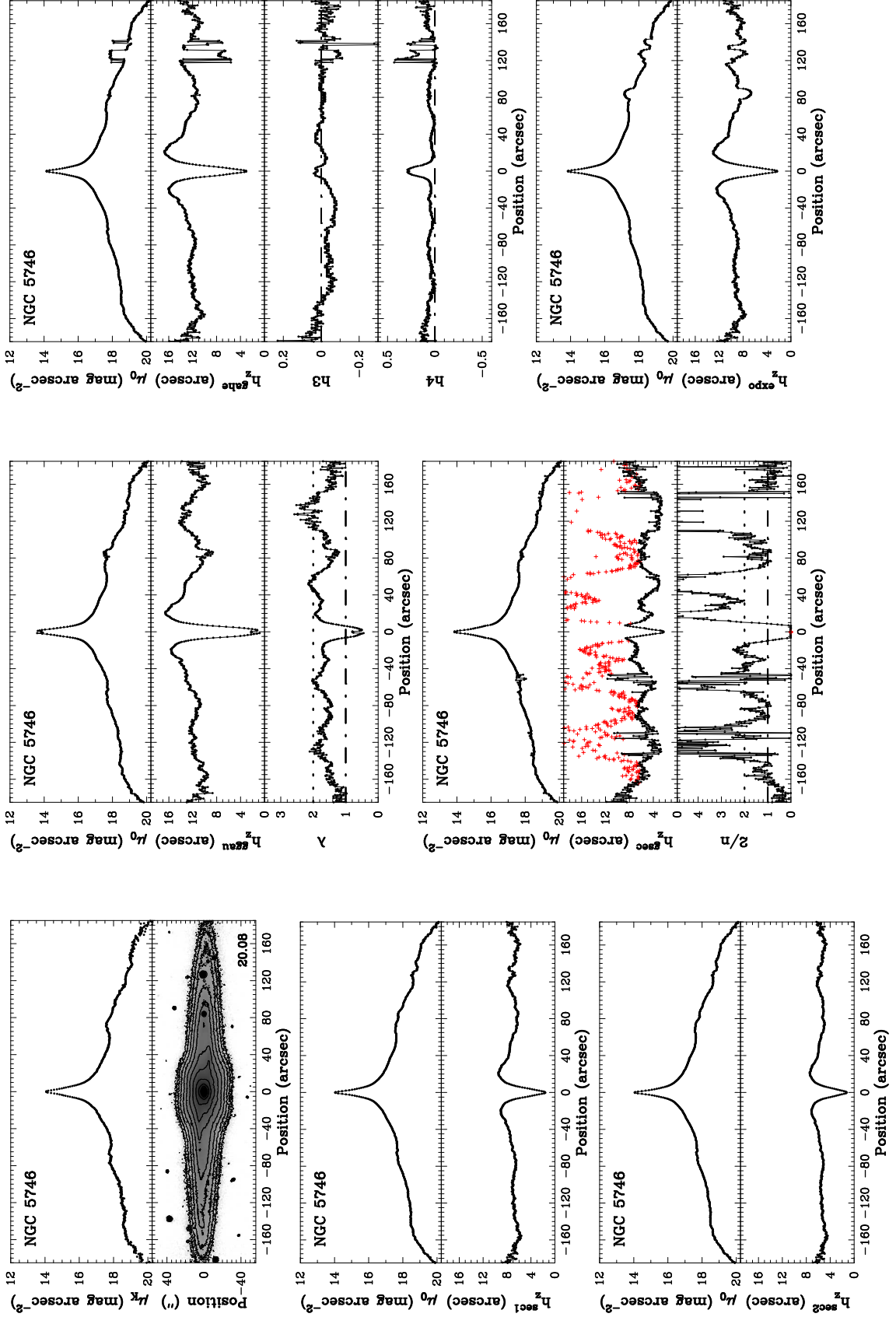


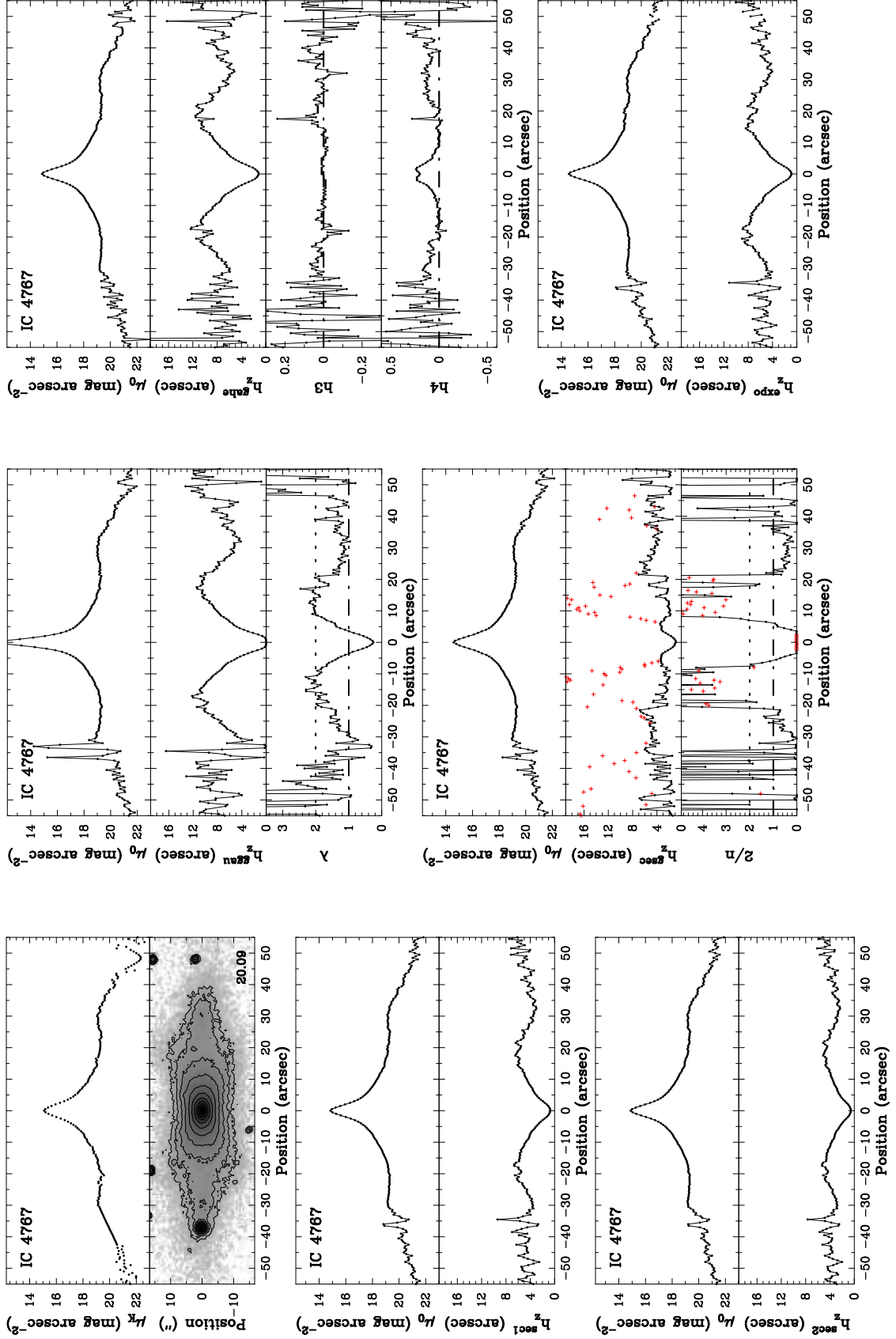
D. RESULTS OF THE VSFB D FITTING



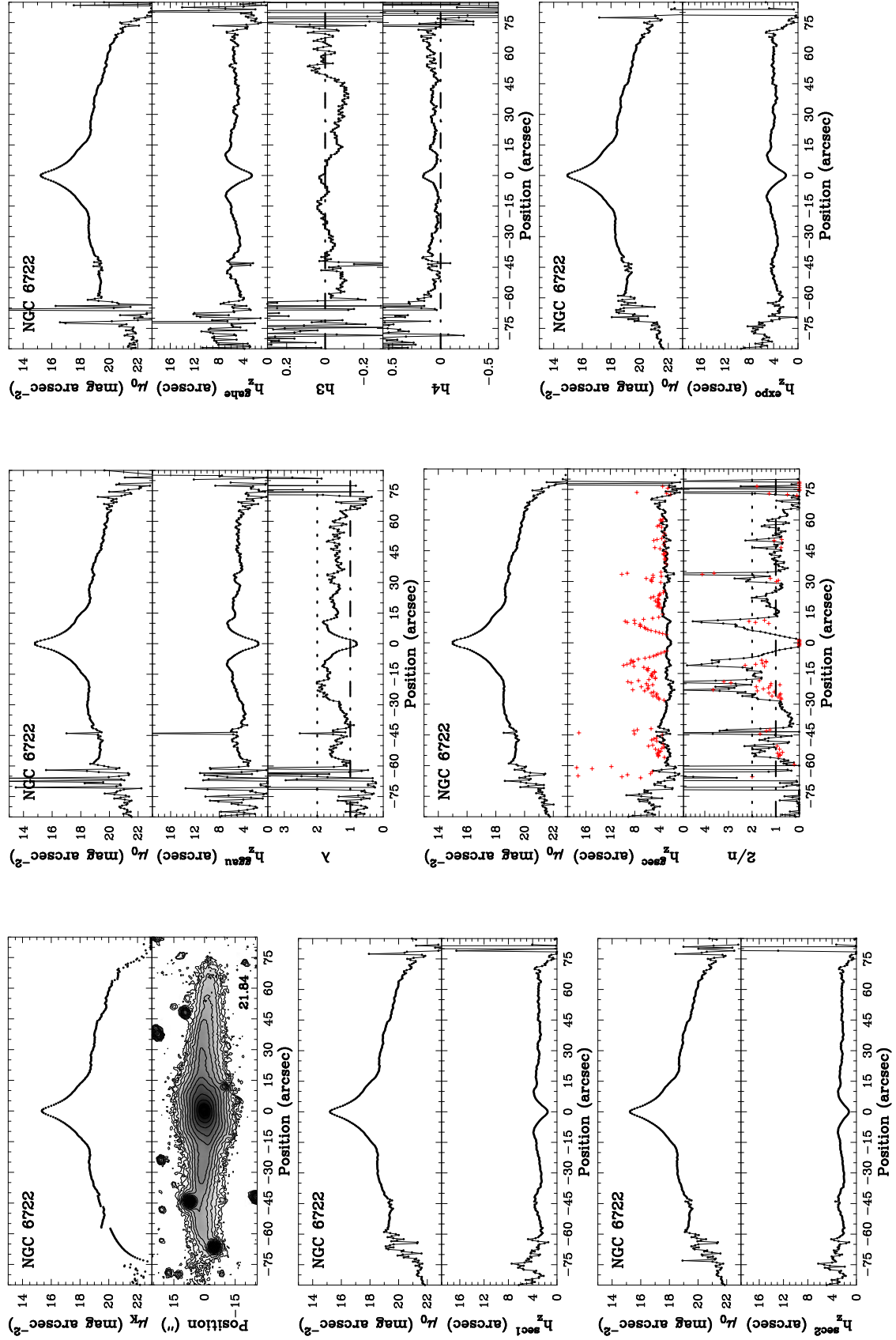


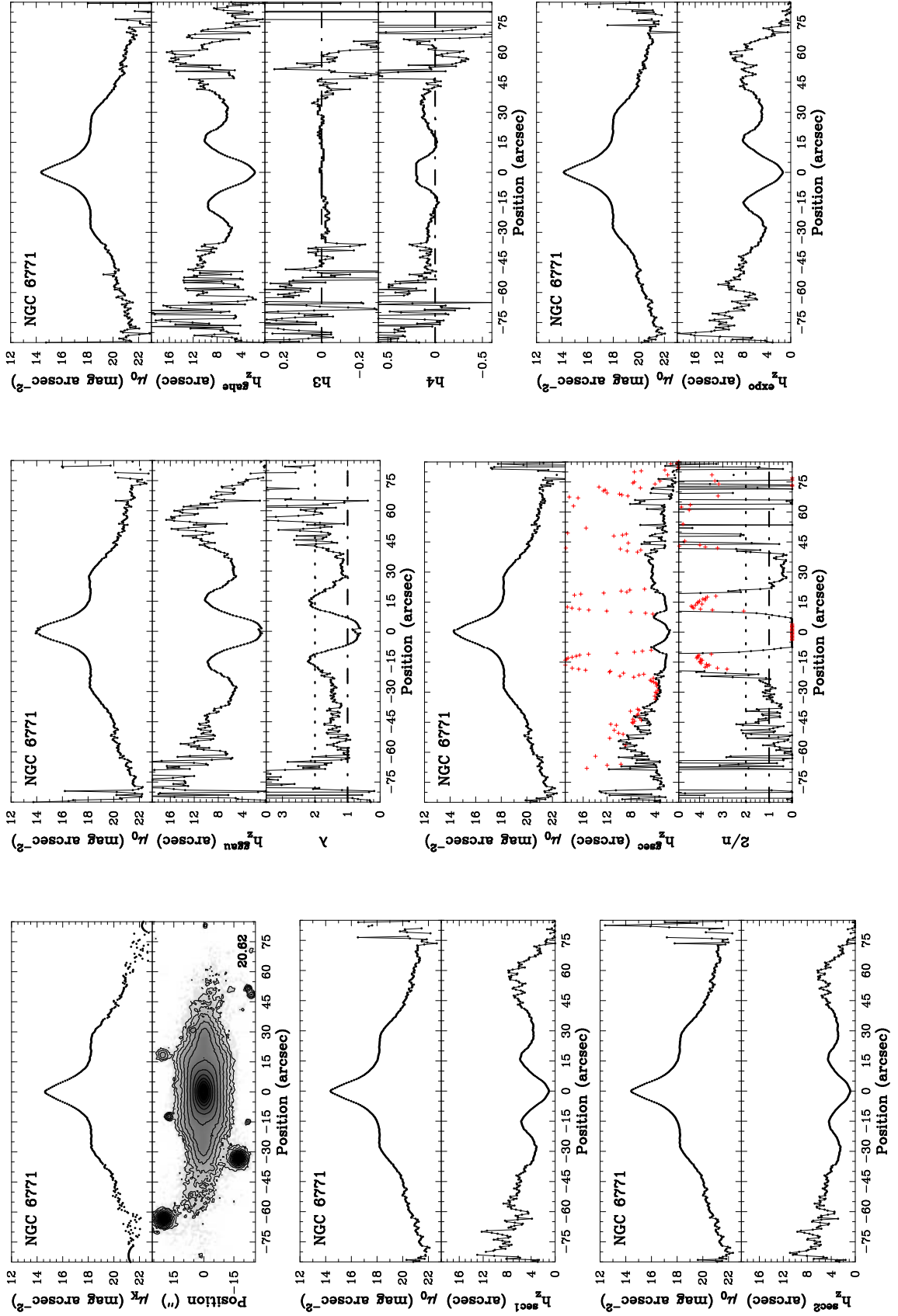
D. RESULTS OF THE VSFBD FITTING



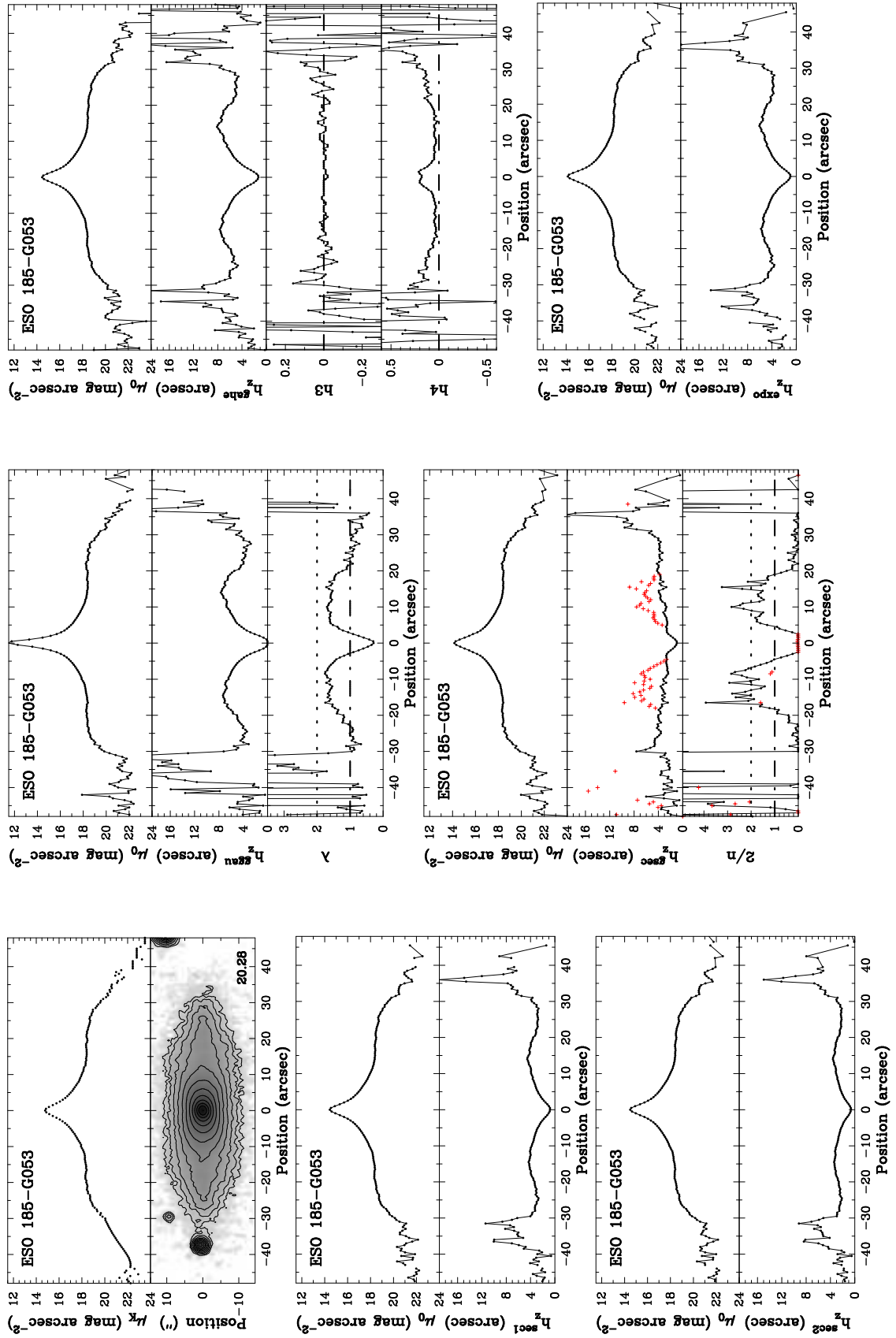


D. RESULTS OF THE VSFB D FITTING

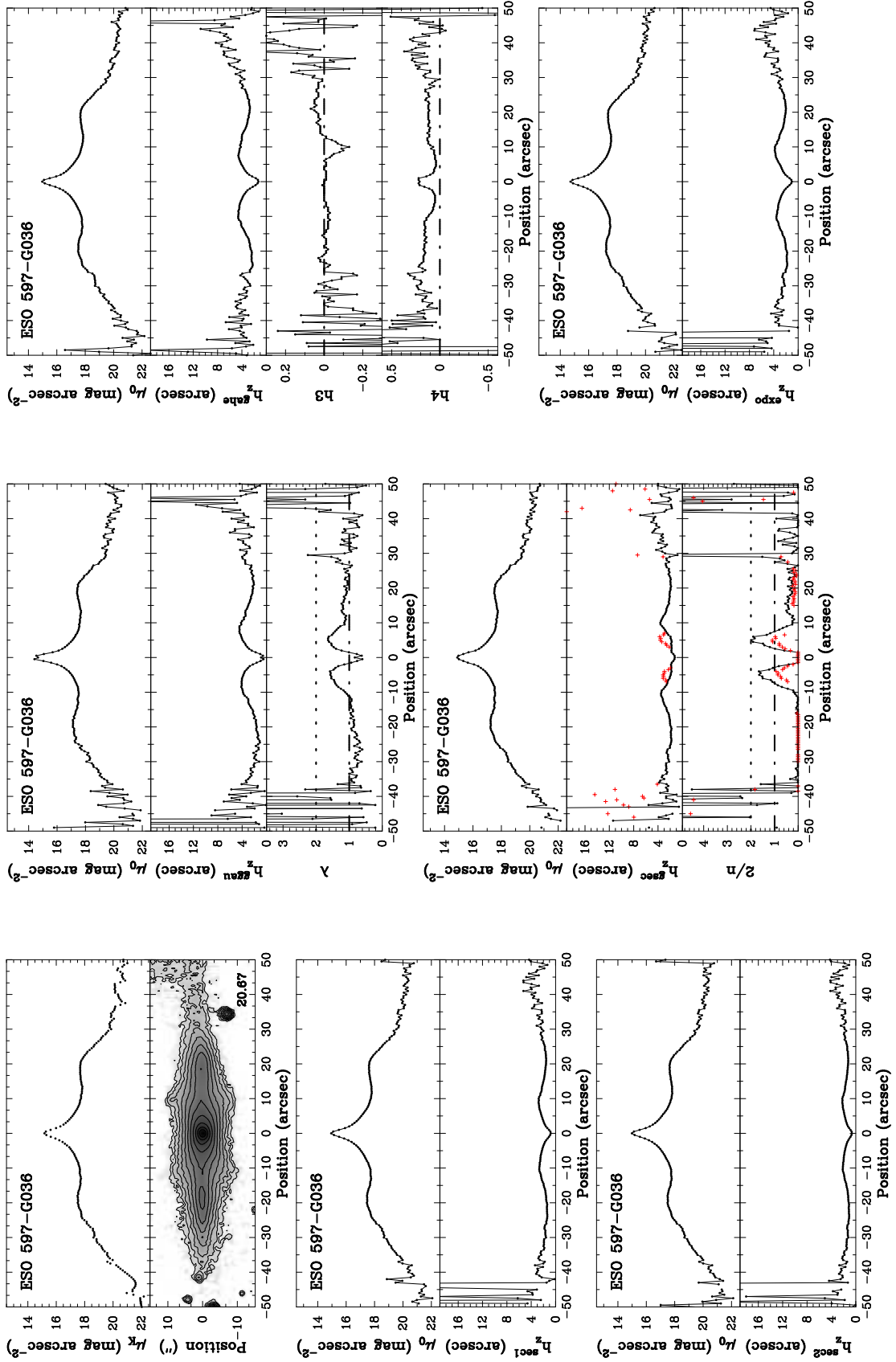


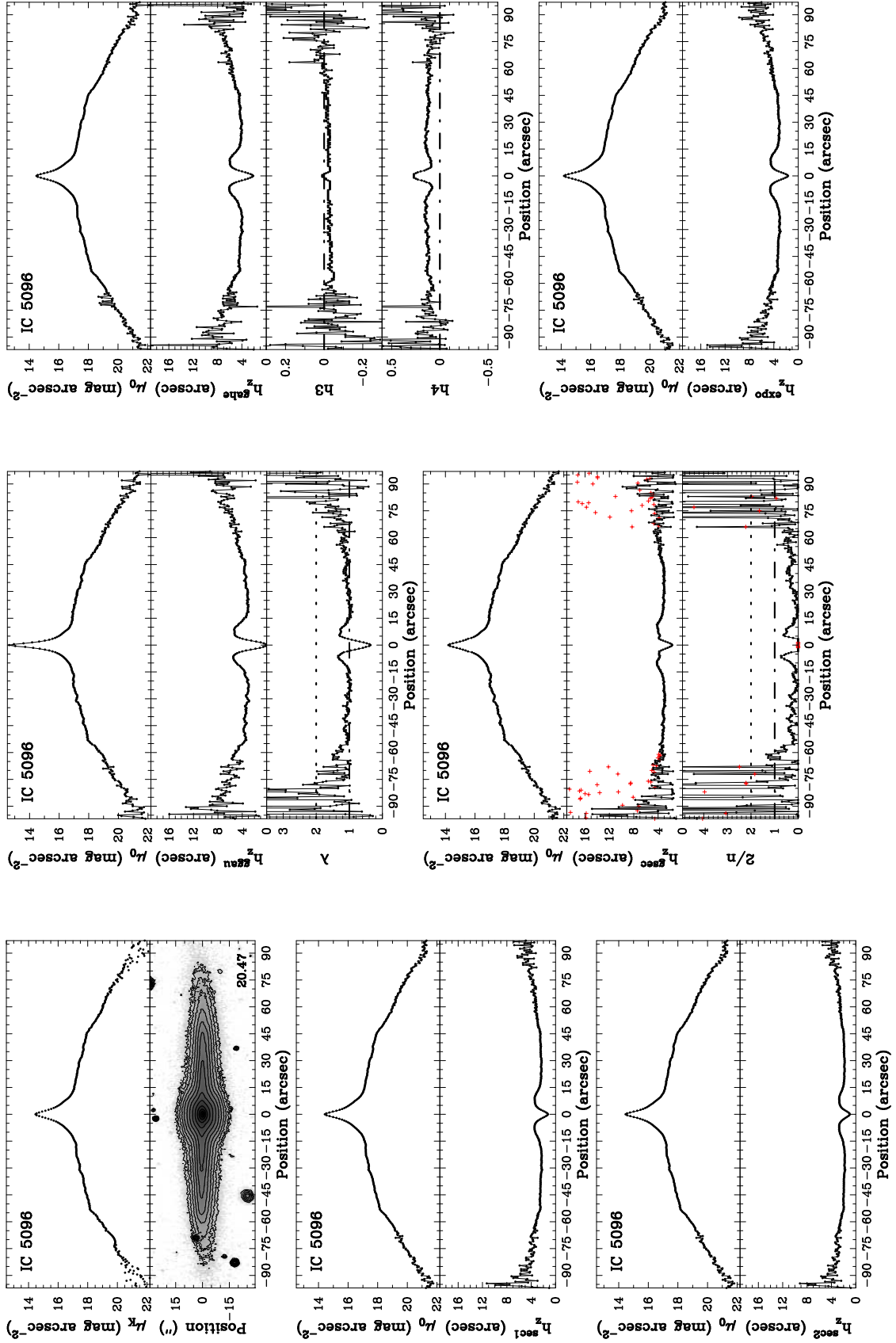


D. RESULTS OF THE VSFB D FITTING

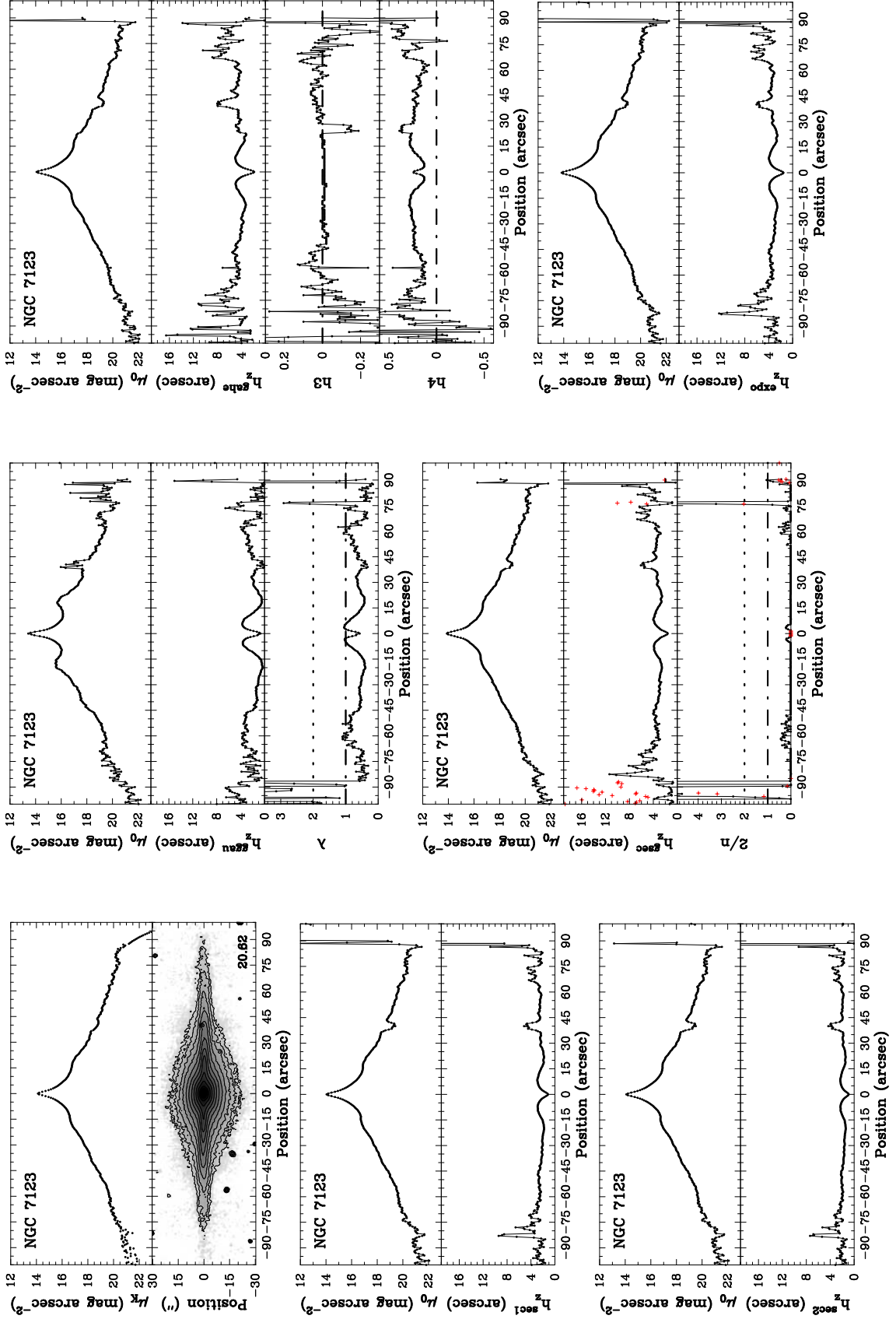


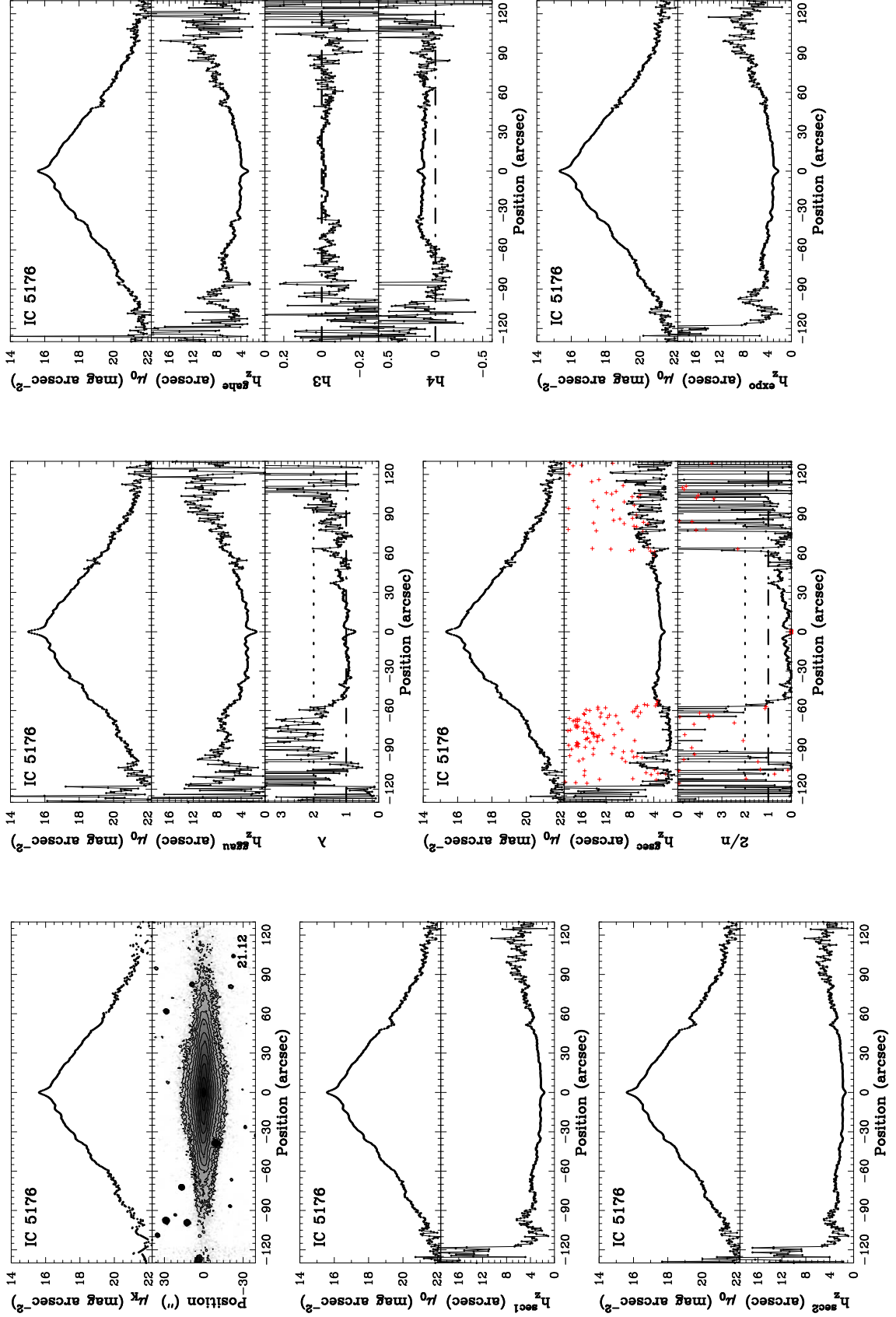
D. RESULTS OF THE VSFBD FITTING



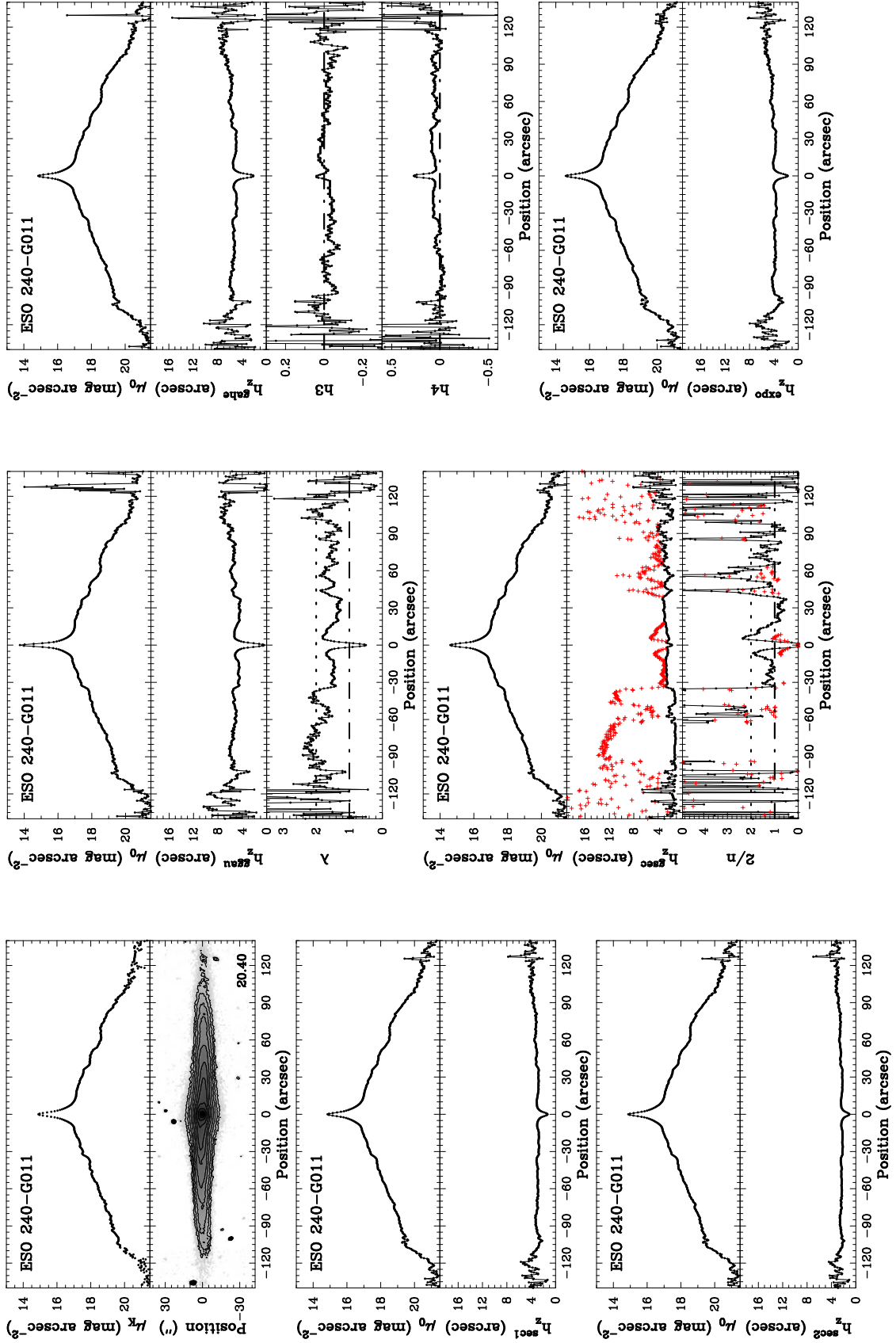


D. RESULTS OF THE VSFBD FITTING





D. RESULTS OF THE VSFB D FITTING



List of used abbreviations

2MASS	Two Micron All Sky Survey
BC	Bulge Class
B/D	bulge-to-disk luminosity ratio
BPL	box/peanut length
B/PS	boxy or peanut shaped
CASPIR	Cryogenic Array Spectrometer/Imager
CBU	Central Bulge
CCD	Charge Coupled Device
CMC	Central Mass Concentration
CR	Corotation Resonance
CSFBPE	Central-Surface-Brightness-Peak-Extension
CX	Centered X-structure
D_{25}	galaxy diameter at the 25mag/acrcsec ² the B -band
D_{KEO}	galaxy diameter at the 20.5mag/acrcsec ² the K_n -band for edge-on galaxies
DSS2	Digital Sky Survey 2
DSS	Digital Sky Survey
Exponential	exponential-distribution
FOV	field-of-view
FWHM	Full-Width-Half-Maximum
GaHeNL	Gauss-Hermite non linear fitting
GaHe	Gauss-Hermite
GENV	Galactic Environment
GGauNL	Generalized Gaussian non linear fitting

GGau	Generalized Gaussian
GMC	giant molecular cloud
GSec	Generalized Sech
ILR	Inner Lindblad Resonance
IRAF	Image Reduction and Analysis Facility
LEDA	Lyon–Meudon Extragalactic Database
LOSVD	line-of-sight velocity distribution
LOS	line-of-sight
LSB	low surface brightness
MDB	massive–disk–with–bulge
MD	massive–disk
ME	Minor axis extremum
MH	massive–halo
MJA	major axis
<i>M/L ratio</i>	mass-to-light ratio
MNA	minor axis
NED	NASA Extragalactic Database
NIR	near–infrared
OB	O and B star
OLR	Outer Lindblad Resonance
OX	Off-centered X–structure
PSF	point spread function
PVD	position–velocity diagram
<i>R^{1/4}–law</i>	de Vaucouleur–law
RSFBP	radial surface brightness profile
SA	spiral arms
Sech(<i>z</i>)	sech(<i>z</i>)–distribution
Isothermal	isothermal–distribution
SFBD	surface brightness distribution

ABBREVIATIONS

SFBP	surface brightness profile
SFB	surface brightness
SFR	star formation rate
$\bar{\sigma}/V_R$	average-velocity-dispersion-to-rotational-velocity
SM	Secondary maxima
S/N	Signal-to-Noise
SSO	Siding Spring Observatory
VSFBD	vertical surface brightness distribution
VSSFBP	vertically summed surface brightness profile

Bibliography

- Abraham, R. G., Merrifield, M. R., Ellis, R. S., Tanvir, N. R., & Brinchmann, J. 1999, *MNRAS*, 308, 569
- Aguerri, J. A. L., Balcells, M., & Peletier, R. F. 2001, *A&A*, 367, 428
- Aguerri, J. A. L., Elias-Rosa, N., Corsini, E. M., & Muñoz-Tuñón, C. 2005, *A&A*, 434, 109
- Andredakis, Y. C., Peletier, R. F., & Balcells, M. 1995, *MNRAS*, 275, 874
- Aoki, T. E., Hiromoto, N., Takami, H., & Okamura, S. 1991, *PASJ*, 43, 755
- Araki, S. 1985, Ph.D. Thesis
- Athanassoula, E. 1983, in *IAU Symp. 100: Internal Kinematics and Dynamics of Galaxies*, 243–250
- Athanassoula, E. 1990, *New York Academy Sciences Annals*, 596, 181
- . 1992, *MNRAS*, 259, 345
- . 2002, *ApJL*, 569, L83
- . 2003, *MNRAS*, 341, 1179
- . 2005, *MNRAS*, 358, 1477
- Athanassoula, E. & Bureau, M. 1999, *ApJ*, 522, 699
- Athanassoula, E., Lambert, J. C., & Dehnen, W. 2005, *MNRAS*, 363, 496
- Athanassoula, E. & Martinet, L. 1980, *A&A*, 87, L10
- Athanassoula, E. & Misiriotis, A. 2002, *MNRAS*, 330, 35
- Bahcall, J. N. 1984a, *ApJ*, 287, 926
- . 1984b, *ApJ*, 276, 169
- Balcells, M., Domínguez-Palmero, L., Graham, A., & Peletier, R. F. 2001, in *ASP Conf. Ser. 249: The Central Kiloparsec of Starbursts and AGN: The La Palma Connection*, 167
- Balcells, M., Graham, A. W., Domínguez-Palmero, L., & Peletier, R. F. 2003, *ApJL*, 582, L79

- Barteldrees, A. & Dettmar, R.-J. 1994, *A&AS*, 103, 475
- Benedict, G. F., Howell, D. A., Jørgensen, I., Kenney, J. D. P., & Smith, B. J. 2002, *AJ*, 123, 1411
- Benson, A. J., Lacey, C. G., Frenk, C. S., Baugh, C. M., & Cole, S. 2004, *MNRAS*, 351, 1215
- Berentzen, I., Athanassoula, E., Heller, C. H., & Fricke, K. J. 2003, *MNRAS*, 341, 343
- Bertola, F. & Capaccioli, M. 1977, *ApJ*, 211, 697
- Bettoni, D. & Galletta, G. 1994, *A&A*, 281, 1
- Binney, J. & Petrou, M. 1985, *MNRAS*, 214, 449
- Bizyaev, D. & Kajsin, S. 2004, *ApJ*, 613, 886
- Bizyaev, D. & Mitronova, S. 2002, *A&A*, 389, 795
- Böker, T., Stanek, R., & van der Marel, R. P. 2003, *AJ*, 125, 1073
- Bothun, G. D. & Gregg, M. D. 1990, *ApJ*, 350, 73
- Bournaud, F. & Combes, F. 2002, *A&A*, 392, 83
- Bournaud, F., Combes, F., & Jog, C. J. 2004, *A&A*, 418, L27
- Bournaud, F., Combes, F., & Semelin, B. 2005, *MNRAS*, 364, L18
- Bureau, M. & Athanassoula, E. 2005, *ApJ*, 626, 159
- Bureau, M. & Freeman, K. C. 1999, *AJ*, 118, 126
- Buta, R. 1995, *ApJS*, 98, 739
- Buta, R. & Block, D. L. 2001, *ApJ*, 550, 243
- Byrd, G., Rautiainen, P., Salo, H., Buta, R., & Crocher, D. A. 1994, *AJ*, 108, 476
- Caon, N., Capaccioli, M., & D'Onofrio, M. 1993, *MNRAS*, 265, 1013
- Carlberg, R. G. 1987, *ApJ*, 322, 59
- Carollo, C. M., Ferguson, H. C., & Wyse, R. F. G., eds. 1999, *The formation of galactic bulges*
- Carollo, C. M. & Stiavelli, M. 1998, *AJ*, 115, 2306
- Carollo, C. M., Stiavelli, M., de Zeeuw, P. T., Seigar, M., & Dejonghe, H. 2001, *ApJ*, 546, 216
- Carollo, C. M., Stiavelli, M., & Mack, J. 1998, *AJ*, 116, 68
- Castro-Rodríguez, N. & Garzón, F. 2003, *A&A*, 411, 55
- Chung, A. & Bureau, M. 2004, *AJ*, 127, 3192

BIBLIOGRAPHY

- Ciotti, L. & Bertin, G. 1999, *A&A*, 352, 447
- Combes, F., Debbasch, F., Friedli, D., & Pfenniger, D. 1990, *A&A*, 233, 82
- Combes, F. & Sanders, R. H. 1981, *A&A*, 96, 164
- Contopoulos, G. 1980, *A&A*, 81, 198
- Dalcanton, J. J. & Bernstein, R. A. 2000, *AJ*, 120, 203
- . 2002, *AJ*, 124, 1328
- Davies, R. L., Efstathiou, G., Fall, S. M., Illingworth, G., & Schechter, P. L. 1983, *ApJ*, 266, 41
- de Carvalho, R. R. & da Costa, L. N. 1987, *A&A*, 171, 66
- de Grijs, R. 1998, *MNRAS*, 299, 595
- de Grijs, R. & Peletier, R. F. 1997, *A&A*, 320, L21
- de Grijs, R., Peletier, R. F., & van der Kruit, P. C. 1997, *A&A*, 327, 966
- de Grijs, R. & van der Kruit, P. C. 1996, *A&AS*, 117, 19
- de Souza, R. E. & Dos Anjos, S. 1987, *A&AS*, 70, 465
- de Vaucouleurs, G. 1959, *Handbuch der Physik*, 53, 275
- de Vaucouleurs, G. 1974, in *IAU Symp. 58: The Formation and Dynamics of Galaxies*, 335
- de Vaucouleurs, G., de Vaucouleurs, A., & Corwin, H. G. 1976, 2nd reference catalogue of bright galaxies containing information on 4364 galaxies with reference to papers published between 1964 and 1975 (University of Texas Monographs in Astronomy, Austin: University of Texas Press, 1976)
- Debattista, V. P., Carollo, C. M., Mayer, L., & Moore, B. 2005, *ApJ*, 628, 678
- Debattista, V. P. & Sellwood, J. A. 2000, *ApJ*, 543, 704
- Eggen, O. J., Lynden-Bell, D., & Sandage, A. R. 1962, *ApJ*, 136, 748
- Emsellem, E., Monnet, G., & Bacon, R. 1994a, *A&A*, 285, 723
- Emsellem, E., Monnet, G., Bacon, R., & Nieto, J.-L. 1994b, *A&A*, 285, 739
- Erwin, P. 2004, *A&A*, 415, 941
- Erwin, P., Beltrán, J. C. V., Graham, A. W., & Beckman, J. E. 2003, *ApJ*, 597, 929
- Erwin, P. & Sparke, L. S. 2002, *AJ*, 124, 65
- . 2003, *ApJS*, 146, 299

- Eskridge, P. B., Frogel, J. A., Pogge, R. W., Quillen, A. C., Berlind, A. A., Davies, R. L., DePoy, D. L., Gilbert, K. M., Houdashelt, M. L., Kuchinski, L. E., Ramírez, S. V., Sellgren, K., Stutz, A., Terndrup, D. M., & Tiede, G. P. 2002, *ApJS*, 143, 73
- Falcón-Barroso, J., Peletier, R. F., Emsellem, E., Kuntschner, H., Fathi, K., Bureau, M., Bacon, R., Cappellari, M., Copin, Y., Davies, R. L., & de Zeeuw, T. 2004, *MNRAS*, 350, 35
- Fridman, A. M. & Poliachenki, V. L. 1984, *Physics of gravitating systems - Vol.1: Equilibrium and stability; Vol.2: Nonlinear collective processes: Nonlinear waves, solitons, collisionless shocks, turbulence. Astrophysical applications* (New York: Springer, 1984)
- Friedli, D. 1996, in *ASP Conf. Ser. 91: IAU Colloq. 157: Barred Galaxies*, 378
- Friedli, D. & Benz, W. 1993, *A&A*, 268, 65
- . 1995, *A&A*, 301, 649
- Friedli, D. & Martinet, L. 1993, *A&A*, 277, 27
- Fuchs, B., Schlickeiser, R., & Thielheim, K. O. 1976, *ApJ*, 206, 589
- Fuchs, B. & Wielen, R. 1987, in *The Galaxy*, ed. G. Gilmore & R. Carswell, 375
- Gerin, M., Combes, F., & Athanassoula, E. 1990, *A&A*, 230, 37
- Gerssen, J., Kuijken, K., & Merrifield, M. R. 1997, *MNRAS*, 288, 618
- Gilmore, G. & Reid, N. 1983, *MNRAS*, 202, 1025
- Gonzales, C. & Woods, R. E. 1992, *Digital Image Processing* (Addison-Wesley Publishing Company)
- Graham, A. W. 2001, *AJ*, 121, 820
- Grosbøl, P., Patsis, P. A., & Pompei, E. 2004, *A&A*, 423, 849
- Hasan, H. & Norman, C. 1990, *ApJ*, 361, 69
- Hasan, H., Pfenniger, D., & Norman, C. 1993, *ApJ*, 409, 91
- Hohl, F. 1971, *ApJ*, 168, 343
- Hohl, F. & Zang, T. A. 1979, *AJ*, 84, 585
- Hubble, E. P. 1926, *ApJ*, 63, 236
- . 1936, Yale University Press
- Hunt, L. K., Pierini, D., & Giovanardi, C. 2004, *A&A*, 414, 905
- Impey, C. D., Wynn-Williams, C. G., & Becklin, E. E. 1986, *ApJ*, 309, 572
- James, P. A. & Seigar, M. S. 1999, *A&A*, 350, 791

BIBLIOGRAPHY

- Jarvis, B. J. 1986, *AJ*, 91, 65
- Jenkins, A. 1992, *MNRAS*, 257, 620
- Karachentsev, I. D., Karachentseva, V. E., & Parnovskij, S. L. 1993, *Astronomische Nachrichten*, 314, 97
- Kent, S. M., Dame, T. M., & Fazio, G. 1991, *ApJ*, 378, 131
- Knapen, J. H. 1999, in *ASP Conf. Ser. 187: The Evolution of Galaxies on Cosmological Timescales*, 72–87
- Knierman, K. A., Gallagher, S. C., Charlton, J. C., Hunsberger, S. D., Whitmore, B., Kundu, A., Hibbard, J. E., & Zaritsky, D. 2003, *AJ*, 126, 1227
- Kodaira, K., Watanabe, M., & Okamura, S. 1986, *ApJS*, 62, 703
- Kormendy, J. 1979, *ApJ*, 227, 714
- Kormendy, J. 1993, in *IAU Symp. 153: Galactic Bulges*, 209
- Kormendy, J. & Illingworth, G. 1982, *ApJ*, 256, 460
- Kormendy, J. & Kennicutt, R. C. 2004, *ARA&A*, 42, 603
- Kregel, M., van der Kruit, P. C., & de Grijs, R. 2002, *MNRAS*, 334, 646
- Lütticke, R., Dettmar, R.-J., & Pohlen, M. 2000a, *A&AS*, 145, 405
- . 2000b, *A&A*, 362, 435
- Lacey, C. G. 1984, *MNRAS*, 208, 687
- Laurikainen, E., Salo, H., & Buta, R. 2005, *MNRAS*, 362, 1319
- Lütticke, R. 1996, Master's thesis, Ruhr-Universität Bochum
- . 1999, PhD thesis, Ruhr-Universität Bochum
- Maciejewski, W., Teuben, P. J., Sparke, L. S., & Stone, J. M. 2002, *MNRAS*, 329, 502
- Malin, D. F., Quinn, P. J., & Graham, J. A. 1983, *ApJL*, 272, L5
- Malin, D. F. & Zealey, W. J. 1979, *S&T*, 57, 354
- Martinez-Valpuesta, I., Shlosman, I., & Heller, C. 2005, *ArXiv Astrophysics e-prints*
- Matthews, L. D. 2000, *AJ*, 120, 1764
- Matthews, L. D. & de Grijs, R. 2004, *AJ*, 128, 137
- Matthews, L. D., Gallagher, J. S., & van Driel, W. 1999, *AJ*, 118, 2751
- Matthews, T. A., Morgan, W. W., & Schmidt, M. 1964, *ApJ*, 140, 35
- Merrifield, M. R. & Kuijken, K. 1999, *A&A*, 345, L47

- Miller, R. H. & Prendergast, K. H. 1968, *ApJ*, 151, 699
- Möllenhoff, C. 2004, *A&A*, 415, 63
- Moré, J. J., Garbow, B. S., & Hillstrom, K. E. 1980, Argonne National Laboratory Report ANL, 74
- Moré, J. J., Sorensen, D. C., Hillstrom, K. E., & Garbow, B. S. 1984, in *Sources and Development of Mathematical Software*, ed. W. J. Cowell
- Morgan, W. W. 1958, *PASP*, 70, 364
- . 1959, *PASP*, 71, 394
- . 1962, *ApJ*, 135, 1
- Noguchi, M. 1987, *MNRAS*, 228, 635
- Norman, C. A., Sellwood, J. A., & Hasan, H. 1996, *ApJ*, 462, 114
- Patsis, P. A., Athanassoula, E., Grosbøl, P., & Skokos, C. 2002a, *MNRAS*, 335, 1049
- Patsis, P. A., Skokos, C., & Athanassoula, E. 2002b, *MNRAS*, 337, 578
- . 2003, *MNRAS*, 342, 69
- Peletier, R. F. & Balcells, M. 1996, *AJ*, 111, 2238
- Pfenniger, D. 1984, *A&A*, 134, 373
- . 1985, *A&A*, 150, 112
- Pfenniger, D. 1993, in *IAU Symp. 153: Galactic Bulges*, 387
- Pfenniger, D. & Friedli, D. 1991, *A&A*, 252, 75
- Pohlen, M., Balcells, M., Lütticke, R., & Dettmar, R.-J. 2004, *A&A*, 422, 465
- Pohlen, M., Dettmar, R.-J., Lütticke, R., & Schwarzkopf, U. 2000a, *A&AS*, 144, 405
- Pohlen, M., Dettmar, R.-J., & Lütticke, R. 2000b, *A&A*, 357, L1
- Pritchett, C. 1983, *AJ*, 88, 1476
- Raha, N., Sellwood, J. A., James, R. A., & Kahn, F. D. 1991, *Nature*, 352, 411
- Rautiainen, P., Salo, H., & Laurikainen, E. 2005, *ApJL*, 631, L129
- Reshetnikov, V. & Combes, F. 1997, *A&A*, 324, 80
- Rhoads, J. E. 1998, *AJ*, 115, 472
- Rossa, J. 2001, Ph.D. Thesis
- Rossa, J. & Dettmar, R.-J. 2003, *A&A*, 406, 505

BIBLIOGRAPHY

- Sandage, A. 1961, *The Hubble Atlas of Galaxies* (Washington, D.C.: Carnegie Institution of Washington, 1961)
- Sandage, A. & Bedke, J. 1994, *The Carnegie atlas of galaxies* (Washington, DC: Carnegie Institution of Washington with The Flintridge Foundation, 1994)
- Scarlata, C., Stiavelli, M., Hughes, M. A., Axon, D., Alonso-Herrero, A., Atkinson, J., Batcheldor, D., Binney, J., Capetti, A., Carollo, C. M., Dressel, L., Gerssen, J., Macchetto, D., Maciejewski, W., Marconi, A., Merrifield, M., Ruiz, M., Sparks, W., Tsvetanov, Z., & van der Marel, R. P. 2004, *AJ*, 128, 1124
- Schwarz, M. P. 1981, *ApJ*, 247, 77
- . 1984, *MNRAS*, 209, 93
- Schwarzkopf, U. & Dettmar, R.-J. 2000a, *A&AS*, 144, 85
- . 2000b, *A&A*, 361, 451
- . 2001, *A&A*, 373, 402
- Searle, L. & Zinn, R. 1978, *ApJ*, 225, 357
- Seigar, M. S. & James, P. A. 1998, *MNRAS*, 299, 672
- Sersic, J. L. 1968, *Atlas de galaxias australes* (Cordoba, Argentina: Observatorio Astronomico, 1968)
- Shaw, M. 1993, *MNRAS*, 261, 718
- Shaw, M., Axon, D., Probst, R., & Gatley, I. 1995, *MNRAS*, 274, 369
- Shaw, M., Dettmar, R.-J., & Barteldrees, A. 1990, *A&A*, 240, 36
- Shaw, M., Wilkinson, A., & Carter, D. 1993, *A&A*, 268, 511
- Shaw, M. A. 1987, *MNRAS*, 229, 691
- Shaw, M. A. & Gilmore, G. 1989, *MNRAS*, 237, 903
- Shen, J. & Sellwood, J. A. 2004, *ApJ*, 604, 614
- Shlosman, I., Frank, J., & Begelman, M. C. 1989, *Nature*, 338, 45
- Skokos, C., Patsis, P. A., & Athanassoula, E. 2002a, *MNRAS*, 333, 847
- . 2002b, *MNRAS*, 333, 861
- Spitzer, L. J. & Schwarzschild, M. 1951, *ApJ*, 114, 385
- . 1953, *ApJ*, 118, 106
- Toomre, A. 1966, ref. no. 66-46, 111
- Toth, G. & Ostriker, J. P. 1992, *ApJ*, 389, 5

- Tremaine, S. & Weinberg, M. D. 1984, *ApJL*, 282, L5
- van Albada, T. S. 1982, *MNRAS*, 201, 939
- van den Bergh, S. 1960a, *ApJ*, 131, 558
- . 1960b, *ApJ*, 131, 215
- . 1960c, *Publications of the David Dunlap Observatory*, 2, 159
- . 1990, *ApJ*, 348, 57
- van den Bosch, F. C. & Emsellem, E. 1998, *MNRAS*, 298, 267
- van der Kruit, P. C. 1988, *A&A*, 192, 117
- van der Kruit, P. C. & Searle, L. 1981a, *A&A*, 95, 116
- . 1981b, *A&A*, 95, 105
- . 1982a, *A&A*, 110, 61
- . 1982b, *A&A*, 110, 79
- van der Marel, R. P. & Franx, M. 1993, *ApJ*, 407, 525
- van Dokkum, P. G., Peletier, R. F., de Grijs, R., & Balcells, M. 1994, *A&A*, 286, 415
- Wainscoat, R. J., Freeman, K. C., & Hyland, A. R. 1989, *ApJ*, 337, 163
- Wakamatsu, K.-I. & Hamabe, M. 1984, *ApJS*, 56, 283
- Whitford, A. E. 1978, *ApJ*, 226, 777
- Whitmore, B. C. & Bell, M. 1988, *ApJ*, 324, 741

Acknowledgments

This research has made use of several astronomical databases: the NASA Extragalactic Database (NED) operated by the Jet Propulsion Laboratory, California Institute of Technology, under contract with the National Aeronautics and Space Administration, the NASA's Astrophysics Data System (ADS) Bibliographic Services, as well as the Online Digitized Sky Survey 2 (DSS2) server at the ESO/ST-ECF Archive produced by the Space Telescope Science Institute through its Guide Star Survey group. Further the use of the Lyon-Meudon Extragalactic Database (LEDA) is acknowledged.

I thank the Deutsche Forschungsgemeinschaft for funding a scholarship of the Graduiertenkolleg "The Magellanic System, Galaxy Interaction, and the Evolution of Dwarf Galaxies" during the Phd thesis project. The collaboration with researchers at the Observatoire de Marseille-Provence in France was made possible by the funding of the Deutscher Akademischer Austausch Dienst (DAAD).

I would like to express my gratitude towards my supervisor Prof. Dr. Ralf-Jürgen Dettmar for providing me the opportunity to work at the Astronomisches Institut der Ruhr-Universität Bochum on a strongly evolving topic of extragalactic astrophysics. I am furthermore deeply indebted to Dr. Martin Bureau and Dr. Evangelia Athanassoula for the possibility to start a collaboration with them and to share their knowledge and data for this Phd project. The extensive discussions with them and Dr. Albert Bosma at the Observatoire de Marseille-Provence, France improved this thesis noticeably.

During my first approach to extragalactic photometry it was of great help to have an experienced observer, like Dr. Michael Pohlen, as an office-mate. His knowledge was of great advantage in data reduction. I would like to thank him further for the very good working atmosphere in our office facilitating the progress of this thesis project. Special thanks also to Dr. Daniela Vergani during her time in Bonn for the informative discussions about bulge formation.

I am further greatly indebted to Dr. Torsten Elwert with whom I have begun my physics studies and shared my time as Phd student. The instructive and enlightening discussions with him as well as his encouragements were of invaluable help for me during the last years. I thank him also for the careful reading of the thesis draft. It was also a pleasure to share with him the tea breaks in the afternoon.

Special thanks also to Dr. Marcus Jütte and Eva Manthey for the insightful discussions with them about the structuring of different chapters of the thesis and the reading of part of the thesis draft. A great pleasure and source of motivation were the talks with both about a large variety of topics concerning science and scientific working. I also appreciated much their encouraging words when problems were obstructing the fluent developing of my thesis project.

During the time at the institute I had the opportunity to appreciate the constructive

suggestions of my colleagues. I would like to thank Volker Knierim for the enlightening discussions about the physical process involved in bulge formation and about possible observational projects. My programming style took large benefit from the experience and knowledge of Kai Polsterer. Further I thank Dr. Susanne Hüttemeister for the enlightening discussions about physical processes involved in bar formation, Dr. Dominik Bomans for the informative discussions on galaxy formation, and Prof. Dr. Wolfhard Schlosser for illustrating different approaches to scientific problems. I am much obliged to the persons who take care of the computer systems at the institute, Tim Falkenbach and Olaf Schmithüsen, fixing rapidly problems with my network access. Further I would like to thank Lutz Haberzettl who helped me with L^AT_EX 2_ε as well as Dominik Rosenbaum sharing with me his experience about administrative aspects of the thesis writing. Special thanks to Dr. Elvira Krusch and Clemens Trachternach for the careful reading of parts of the thesis draft as well as Janine van Eymeren for the informative discussions about strategies to solve problems in the workflow. For general discussions concerning astrophysical processes I would like to thank Prof. Dr. Yuri Shchekinov, Volker Heesen, and Dr. Ralph Tüllmann. I would further like to thank Dagmar Münstermann for her help in administrative questions as well as Klaus Weissbauer for the nice chats between long periods of work which gave me the possibility to relax.

During my sojourn at the Observatoire de Marseille–Provence, France I had the possibility to know a lot of interesting people. I am very grateful to Jean–Charles Lambert, administrating the computer systems, helping me with the installed software. A special thanks to Mrs. Annie Laval who took care of the administrative aspects of my stay in Marseille. My abilities in Fortran and C programming improved strongly with the help of my office–mates Leonardo Sandoval and Ingo Berentzen. Apart from the work it was also a pleasure to share the free time with Leonardo and Ingo as well as Jorge Villa and Mark Gilles. Particularly, listening to and talking about music of the last 40 years with Leonardo and Jorge was very nice. A great support during that time was also the hospitality offered to me by my cousins Michel, Sylviane, Laurine, and Manon. It was fun to stay together.

Finally, I want to thank all those people who made this thesis possible with their persistent encouragement and help in difficult times. Cordial thanks to my friend Bernward Mezger who was all the time beside me with encouraging words when things went difficult. I am very grateful to him that he always had time for me when I needed help. Special thanks to Helga and Werner Oevenscheid who sustained me on my way through school and university. Without practicing the german language with Helga Oevenscheid during my years in the kindergarten and primary school I would have had much greater problems in achieving the requirements for an academic graduation. I would also like to thank Erika and Uwe Elwert for their encouragement during the last two years of my thesis as well as Jochen Lindemann during the last year of my thesis.

I am deeply indebted to the team of doctors and nurses and to the staff personal of the WZfPP clinic in Bochum who helped me to recover from my health problems. Among the doctors I want to thank Christoph Barthel who, with his competency and humor, showed me to approach problems with more serenity and to trust in my own abilities.

Last but not least, I am grateful to all my relatives and parents for their trust and patience during the time of my Phd project. The frequent talks with them gave me the opportunity to take different points of view when focusing on organizational problems of my Phd project. Especially my parents, Grazia and Leonardo Aronica, gave me with their supporting love the force to master the problematic times during my Phd thesis. Without them this thesis would not have been possible.

Curriculum Vitae

Personal data:

Name: Giuseppe Agostino Aronica
Date of birth: 15.04.1975
Place of birth: Lüdenscheid (Germany)

Education:

1981 – 1985: Grundschule Breitenhagen, Altena
(Elementary school)

1985 – 1994: Burggymnasium, Altena
(High school)

June 1994: Abitur at the Burggymnasium in Altena
(High school diploma)

Oct 1994 – Apr 1999: Undergraduate student of physics at the
Ruhr-Universität Bochum (RUB)

May 1997: Vordiplom in physics at the RUB
(Intermediate diploma)

May 1999 – May 2000: Diploma thesis at the Institut für Theoretische
Hadronenphysik at the RUB
Title of the diploma thesis:
"Twist-4-Korrekturen zu Gross-Llewellyn-Smith-Summenregeln
im Instanton-Vakuum"
Thesis supervisor: Prof. Dr. K. Goeke,
second referent: Prof. Dr. W. Glöckle

June 2000: Diploma in physics (RUB)

Sep 2000 – present: Phd student at the Astronomisches Institut der
Ruhr-Universität Bochum
Title of the phd thesis:
"The vertical structure of thickened bars in disk galaxies"
Thesis supervisor: Prof. Dr. R.-J. Dettmar,
second referent: PD Dr. S. Hüttemeister
Jan 2001 – Dec 2003: Phd scholarship granted by the
Deutsche Forschungsgemeinschaft through the
Graduiertenkolleg "The Magellanic System, Galaxy
Interaction, and the Evolution of Dwarf Galaxies"

May 2002 – present: Collaboration with Dr. M. Bureau at the Physics department
of the University of Oxford, UK and Dr. E. Athanassoula
at the Observatoire de Marseille-Provence, France

